AD NUMBER

AD161231

NEW LIMITATION CHANGE

TO

Approved for public release, distribution unlimited

FROM

Distribution authorized to DoD only; Administrative/Operational Use; OCT 1954. Other requests shall be referred to Wright Air Development Center, Wright-Patterson AFB, OH 45433.

AUTHORITY

USAF HQS 88ABW, 88CG/SCCMF ltr, 17 Mar 2006

AD NUMBER

AD161231

CLASSIFICATION CHANGES

TO

unclassified

FROM

secret

AUTHORITY

General Declassification Schedule

SECRET

AD

161231

FOR

MICRO CARD

CONTROL ONLY

Armed Services Technical Information Agency

ARLINGTON HALL STATION; ARLINGTON 12 VIRGINIA

SECRET

"NOTICE: When Government or other drawings, specifications or other data are used for any purpose other than in connection with a definitely related Government procurement operation, the U.S. Government thereby incurs no responsibility, nor any obligation whatsoever; and the fact that the Government may have formulated, furnished, or in any way supplied the said drawings, specifications or other data is not to be regarded by implication or otherwise as in any manner licensing the holder or any other person or corporation, or conveying any rights or permission to manufacture, use or sell any patented invention that may in any way be related thereto."

MX-2276

ATEGIC WEAPON SYSTEM

CONTRACT NO. AF33(616)-2419

REPORT NO. D143-945-011

BELL Aircraft CORPORATION

25 OCTOBER 1954

SECRET

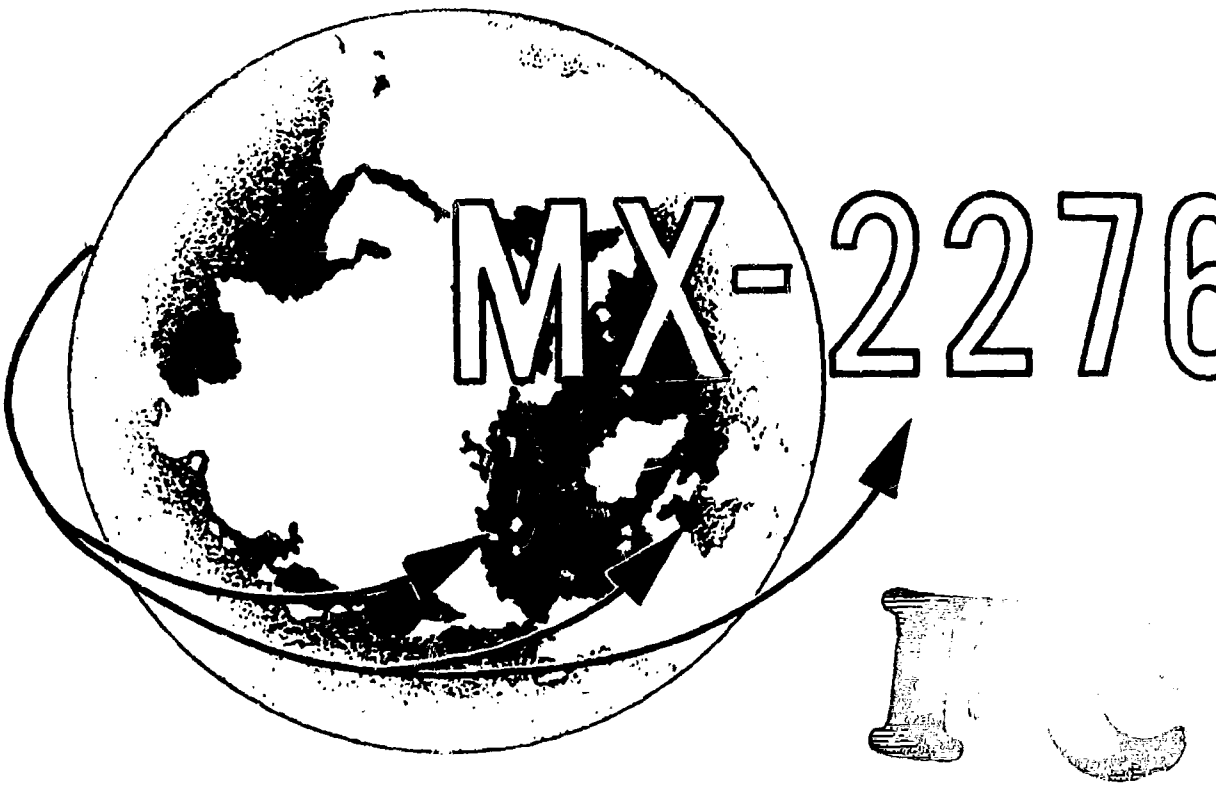

ADVANCED STRATEGIC WEAPON SYSTEM

INTERIM TECHNICAL REPORT

CONTRACT NO. AF33(616)-2419

REPORT NO. D143-945-011

58AA 5179

25 OCTOBER 1954

BELL Aircraft CORPORATION

SECRET

54WCS-12027-3

TABLE OF CONTENTS

TABLE OF CONTENTS (CONTD)

ILLUSTRATIONS

ILLUSTRATIONS (CONTD)

ILLUSTRATIONS (CONTD)

ILLUSTRATIONS (CONTD)

TABLES

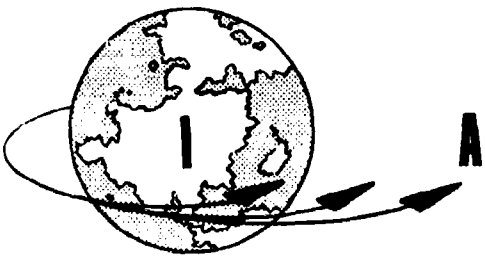

ABSTRACT

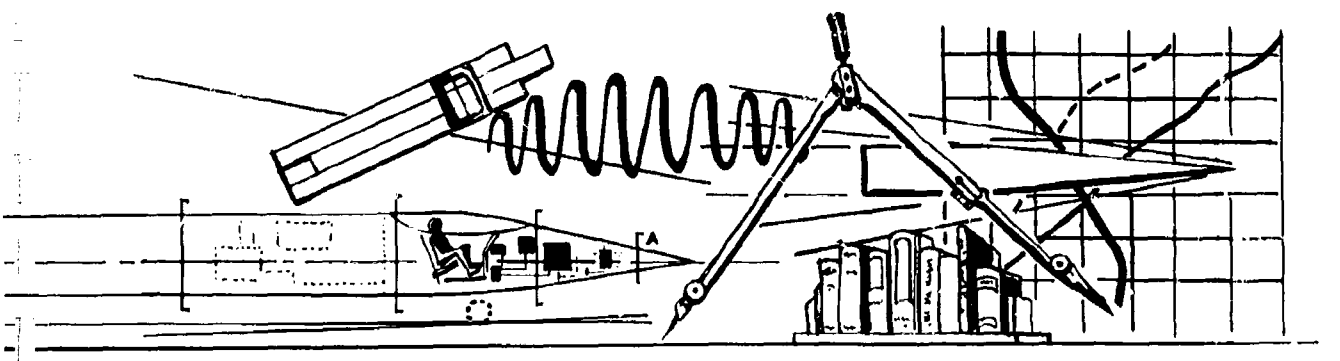

The first six months of a study contract to investigate the design and development problems of the MX-2276 weapon system have been completed. The necessary environment for the pilot has been determined and methods for providing the proper environment are suggested. A method for determining the size of cooling system required using intrawall cooling is presented.

The equations of linear motion of a vehicle such as Stage III have been derived. Various methods of simplifying these equations will be investigated. Tables of the flow parameters for shock flow and isentropic flow which incorporate van der Waal's forces and variable specific heat have been prepared for the range of altitude and Mach numbers under consideration. A series of parameters defining the limits to which present theory and test data are applicable with respect to the MX-2276 flight regime have been selected and, where necessary, modified.

Methods for the computation of skin friction and heat transfer coefficient for both laminar and turbulent boundary layers up to $M \approx 10$, have been selected. Using these heat transfer coefficients, methods for calculation of outside skin temperatures and heat flux densities have also been selected up to $M \approx 10$.

Test data for the characteristics of wings, bodies, and wing body combinations have been compared with applicable theory.

Methods for determining gust criteria and loads have been determined. Flight loads due to centrifugal effects have been calculated for both boost and cruise phases of flight. Various materials have been examined for use as structure, insulation, and cooling media and representative samples selected for use in preliminary calculations. Parameters have been selected for comparing these materials for applications involving tensile strength, compressive strength of stable and elastically unstable elements, stiffness, heat

capacity of cooling fluids, and insulating value of conduction barriers. A limitation of 0.2% permanent set due to creep was arbitrarily established for comparison of structures for this characteristic. The problem of thermal shock has been investigated using sample structural elements and several tentative solutions are suggested. Radiation and conduction insulating barriers have been compared and the radiation type shown to be superior from a weight standpoint.

A multiaxis inertial navigation system supplemented by radar correction, has been recommended for both bomber and missile. A transverse polar coordinate system has been selected. The accuracy requirements and quality of components have been generally ascertained.

The field of liquid rocket propellant combinations has been reviewed and four combinations have been selected for further study. These are selected primarily on the basis of performance and development time, those requiring least development time having poorest performance and vice versa.

A preliminary investigation of the advantages to be obtained through the use of a propellant consisting of 50% oxygen-50% fluorine with JP-4 has been completed. In conjunction with this, the total weight decrease made possible through the use of an expendable first stage as well as second stage is also shown.

The initial results of an analysis to determine the size and complexity of a weapon capable of one circumnavigation of the globe have been obtained. Four possible flight paths were utilized and their effect upon the weight and energy required, as well as the resultant velocity and altitude over the target, have also been ascertained.

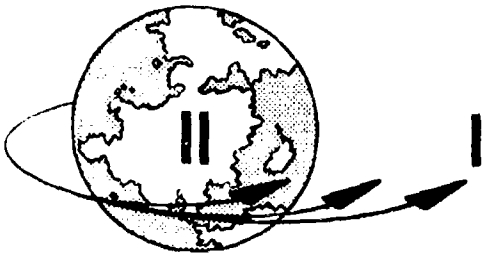

II INTRODUCTION

In July 1953 the Bell Aircraft Corporation completed an introductory study of a manned, rocket-boosted, glide aircraft which could satisfy the requirements of an Advanced Strategic Weapon System and is capable of both long range bombing and reconnaissance missions. This weapon system (presented in Reference 1) consists of a multistage carrier, a guided glide missile, and the navigational guidance, control, command and other equipment necessary to integrate the human and missile into the weapon system. The initial concept consisted of a three-stage carrier including a first stage manned, recoverable booster airplane, a second stage expendable booster, and a third stage manned, rocket-boosted glide airplane. During take-off and powered climb the aircraft has primarily the characteristics of a guided rocket, while aircraft characteristics predominate after separation of the stages. The pilot can monitor the flight of the aircraft, evaluate defense weapon concentrations, operate or monitor mapping and photographic equipment, assist in missile guidance and target identification, evaluate damage, and land the aircraft after the mission.

On 1 April 1954 a one-year program was initiated at Bell Aircraft Corporation, for the New Development Office, Bombardment Aircraft Branch, WADC in accordance with USAF Contract No. AF33(616)2419 and RDO No. R441-47 for further study of this weapon system (now designated MX-2276). The objective of this study is to determine the technical problems involved in the design of a rocket-propelled, manned strategic weapon system. Specifically this study is to investigate the problem areas in the light of existing data and current research programs.

The major effort was to be devoted to items such as:

1. Requirements for crew, showing not only the functions, workload, effectiveness, and environment but also comparing relative development problems of manned and unmanned systems.

2. Evaluation of relative size and complexity of reconnaissance and reconnaissance/bombardment systems. A preliminary analysis of a weapon capable of one complete global circumnavigation is to be included.

3. Aerodynamic investigations, especially lift and drag at hypersonic speeds, heat transfer and weapon system performance. Stability, control, launching, and stage separation problems were also to be considered.

4. Guidance, navigation, bombing, and other equipment studies showing suitable systems and radar operation at high altitudes.

5. Evaluation of propellant combinations with respect to system complexity, chamber cooling, and effect on over-all vehicle size.

6. Investigation of structural problems showing material properties, cooling or insulation effects, and designs for optimum strength to weight ratio. A preliminary structural design is to be shown supported by design criteria and weight estimates.

Additional optimization of the weapon system was not included in this work. The results of this study will provide the firm technical basis necessary for future planning on programs, funds, and facilities.

This report is submitted in compliance with the contractual requirement that an Interim Technical Report be issued at the discretion of the contractor but not later than 1 February 1955.

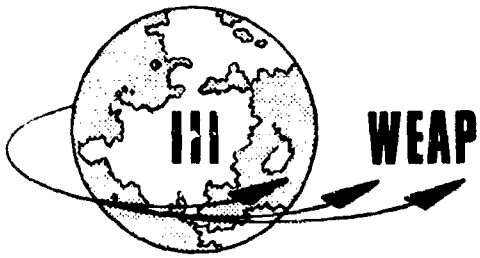

III WEAPON SYSTEM DESCRIPTION

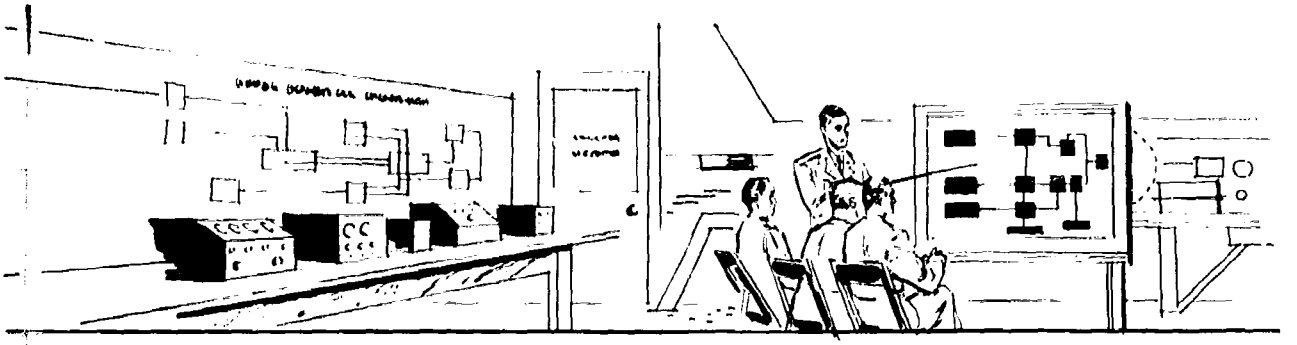

A. ORIGINAL CONCEPT

1. CONFIGURATION

The configuration proposed in Reference 1 has not been changed during this study phase, although the results of these studies indicate the desirability of some changes. This original configuration consists of (1) Stage I, a manned, liquid rocket powered booster airplane: (2) Stage II, an expendable liquid rocket-powered booster; (3) Stage III, a manned, liquid rocket-boosted glide aircraft; and (4), a guided, unpowered missile containing a 2800-pound special warhead.

Stage I is a canard configuration which has conventional tricycle landing gear and flaps. During ascent it is controlled by means of gimbal-mounted thrust chambers, and after burnout aerodynamic surfaces are used for control and recovery employing conventional airplane landing techniques.

Stage II is an expendable booster which is destroyed after separation. Gimbal-mounted thrust chambers are used for control of this stage also.

Stage III is a modified delta configuration which performs the strategic mission. Control is provided by conventional aerodynamic surfaces. A retractable, tandem, two-skid, landing gear is provided for recovery.

2. NAVIGATION

A multiaxis inertial navigation system in conjunction with a three-axis autopilot system will automatically navigate the weapon system to the target and on to the landing point. Corrections for map or system inaccuracies can be made by the pilot using optical or radar information.

A second multiaxis system, which is erected using the carrier inertial information as a reference, will be used to navigate the unpowered missile to the target. After missile launch, a final correction for target location can be made by the pilot. Since Stage III will pass over the target prior to the missile's arrival, the pilot can observe the actual target location by radar or optical means. This information can then be used to compute a correction which is transmitted to the missile via a radio command link.

3. MISSION

The primary functions of this weapon system are long-range strategic bombing and high-altitude reconnaissance. The high speeds and altitudes at which this system operates make the vehicle extremely invulnerable to any defenses presently conceived. The range of the system is great enough so that it can be used on shuttle missions from bases located in the northern United States, across enemy territory, to bases located in friendly territory. With the present range (10,600 nautical miles), two bases outside the U. S. would suffice for complete coverage of enemy territory.

On a typical mission, the vehicle containing all stages is launched vertically from a suitable platform, utilizing the thrust from Stages I and II, and enters a curvilinear flight path which ultimately becomes horizontal. When Stage I burns out it is separated and glides back to a landing. Stage II continues to boost the remaining vehicles along the curvilinear path and is destroyed after its propellant is exhausted. The Stage III power plant is then started, and peak altitude and velocity are reached at burnout. This stage then glides along a maximum L/D path to its destination. The missile is launched at the proper time for destruction of the target. At the completion of the flight, Stage III is landed by the pilot.

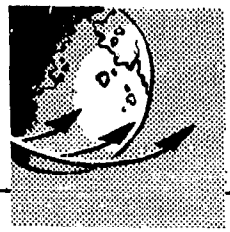

B. SYSTEM TRENDS

On the basis of current studies, certain interesting system trends can be shown. These include the effect of increased propellant performances on take-off gross weight, the effect of expendable boost stages, and the circumnavigation possibilities.

I. PROPELLANT PERFORMANCE

To show the effect of increased propellant performance on take-off gross weight required to attain the speed and altitude performance shown in Reference 1, a propellant combination consisting of an oxidizer mixture of 50% oxygen with 50% Fluorine with JP-4 as fuel was assumed. A summary of the results consisting of the weight of individual stages and the take-off weights is presented in Table I. In these calculations a motor chamber pressure of 1000 psi was assumed. The specific impulse values were extrapolated from experimental values achieved with a 300-psi chamber pressure motor. Use of this propellant reduces the take-off gross weight from 851,000 to 548,000 pounds. Further studies using this propellant are being made.

TABLE I. EFFECTS OF PROPELLANT AND STAGING COMBINATIONS

	Staging	I & III - Winged II - Ex.	III - Winged I & II Ex.	I & III - Winged II - Ex.	III - Winged I & II Ex.
Stage I	Propellant	O_2 - NH_3 - N_2H_4	O_2 - NH_3 - N_2H_4	O_2 - F_2, JP-4	O_2 - F_2, JP-4
	I_{sp}	285	285	316	316
	Dry Weight*	165,000	88,000	107,400	46,400
	Prop. Wt.	486,000	382,000	302,000	227,000
	Total Wt.	651,000	470,000	409,400	273,400
	% Struct. Wt.	15.3	7.6	15.3	7.6
Stage II	Propellant	O_2 - NH_3 - N_2H_4	O_2 - NH_3 - N_2H_4	O_2 - F_2, JP-4	O_2 - F_2, JP-4
	I_{sp}	315	315	349	349
	Dry Weight	30,000	30,000	21,100	21,100
	Prop. Wt.	125,000	125,000	81,500	81,500
	Total Wt.	155,000	155,000	102,600	102,600
	% Struct. Wt.	8.5	8.5	8.5	8.5
Stage III	Propellant	N_2H_4 - WFNA	N_2H_4 - WFNA	O_2 - F_2, JP-4	O_2 - F_2, JP-4
	I_{sp}	310	310	349	349
	Dry Weight**	18,800	18,800	16,600	16,600
	Prop. Wt.	26,200	26,200	19,400	19,400
	Total Wt.	45,000	45,000	36,000	36,000
	% Struct. Wt.	20.0	20.0	20.0	20.0
	Gross Weight	851,000	670,000	548,000	412,000

* - All weights are in pounds

** - Includes 4200 lb payload weight

2. EXPENDABLE STAGES

In order to determine the effects of staging methods other than those used in the original concept, the effects upon gross weight of making both first and second stages expendable were calculated. Removing the wings of the first stage reduced the structural weight from 15.3% to 7.6% of the gross weight. This weight decrease results in an improved propellant-to-gross weight ratio, thus requiring less propellant to achieve the same performance. Table I lists the take-off gross weight values for both staging combinations and for both the original propellant and the oxygen-fluorine and JP-4 combination. With the improved propellants, and both first and second stages expendable, a reduction in take-off gross weight from 851,000 lb. to 412,000 lb. was calculated.

3. CIRCUMNAVIGATION POSSIBILITIES

a. General

A preliminary study of a manned global weapon system capable of one or more circumnavigations of the globe has been initiated. Since this study has not been completed, no conclusions can be shown; however, the initial results exhibit some interesting trends which are summarized below.

Before presenting these results, the advantages of a weapon system capable of circumnavigation should be reviewed. It is recognized that the increase in performance of a rocket-driven airplane by increasing the speed from high hypersonic to circular velocity is a logical step toward improved over-all economy and, in some respects, toward less stringent operational conditions. Some of the advantages of such a weapon system are:

1. Reduction in Aerodynamic Heating and Structural Weight

Since such a weapon could be supported inertially for a major portion of its total range, flight at maximum lift over drag attitude for maximum aerodynamic range may no longer be required. Hence, the vehicle may descend at $(C_L)_{max}$ rather than $(C_L/C_D)_{max}$ so that higher glide altitudes are maintained at a given speed and less intense friction and heating is encountered.

2. Independence of Foreign Bases

All operations (both launch and landing) can be conducted from permanent bases within the continental United States. This greatly facilitates the handling of high energy rocket propellants and large booster stages.

3. Rapid Assessment of Mission

The results of a mission are immediately available for evaluation and efficient execution of subsequent strikes.

4. Temporary Satellite

The number of circumnavigations can be more than one for extended reconnaissance activity.

b. Preliminary Results

Four types of flight paths have been considered in this initial study. A general description of each of these paths will be given along with some factors which must be considered when evaluating their relative merits. A preliminary weight estimate was made using the Oxygen/Fluorine-JP-4 propellant combination discussed in Section IV-E. All results are based on an arbitrary payload of 3000 pounds (including pilot and reconnaissance equipment) and three stages of which the first and third are winged.

PATH I

The final stage is delivered horizontally at high altitude and descends along a spiral which contacts the launching site after one circumnavigation (Figure 1). This path was discussed briefly in Reference 1.

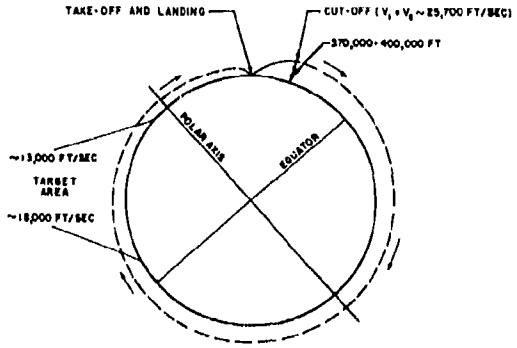

Figure 1. Path Type I: Delivery at Circular Velocity; One Circumnavigation; Spiral of Descent, Not Necessarily at L/D_{max}

The altitude at the end of boost is 370,000 to 400,000 ft at a local circular velocity of roughly 25,700 ft/sec. The range at $(L/D)_{max}$ flight below a velocity 23,000 ft/sec is approximately 26,000 n.mi. (nonrotating earth, or pole-to-pole circumnavigation assumed). Since the earth's circumference is 21,500 n.mi. this path contains a sizeable reserve available for maneuvering or for descent at a higher lift coefficient than permissible for $(L/D)_{max}$. The flight time is approximately 1.75 hours. This time period, as well as the range given, does not include the powered path which amounts to approximately 800 n.mi. range and eight minutes duration. Although the cutoff velocity is only 25,700 ft/sec, the ideal velocity, which represents the total energy requirement for which the vehicle must be laid out, corresponds approximately to 30,000 ft/sec. Ideal velocity is defined as the speed attained by a vehicle in loss-free powered flight.

PATH II

The final stage is delivered into an elliptic path of near-circular (very small eccentricity) shape (Figure 2). The vehicle then passes through an apogee at comparatively high altitude. At this apogee a small impulse (burst of power) is needed such that the vehicle enters a new ellipse whose perigee lies at an altitude of 300,000 ft and is located over the target area. This type of path offers the possibility for more than one pass over the target area (i.e., more than one circumnavigation). This can be accomplished at an energy cost which is not appreciably higher than that for Path I. In the case of Path I, several circumnavigations would require the vehicle to be above 300,000 feet (viz. 500,000 to 600,000 feet) during the first passes.

The final stage is delivered at an altitude of 300,000 ft and a trajectory angle of 5 degrees at about 24,300 ft/sec. The corresponding ideal velocity is about 28,500 ft/sec. Within 14.4 minutes after cutoff the vehicle has reached its summit (apogee) at 154 n.mi. altitude. At that point it has a speed of 23,570 ft/sec and has covered a surface range of about 3000 n.mi. from the launching point. The vehicle now spends its residual propellant to produce a velocity increment of 1,600 ft/sec, boosting its apogee speed to 25,180 ft/sec. The vehicle then heads back toward the earth and, after another 44 minutes, reaches the perigee point at 250,000 to 300,000 ft altitude at a speed of 26,000 ft/sec (i.e., nearly circular speed). The horizontal range from the launching site is now 14,000 n.mi. The dynamic pressure near the perigee at that speed is approximately 27 lb per sq ft (250,000 ft altitude), so that aerodynamic control appears possible. The vehicle has ample energy reserve to deviate,

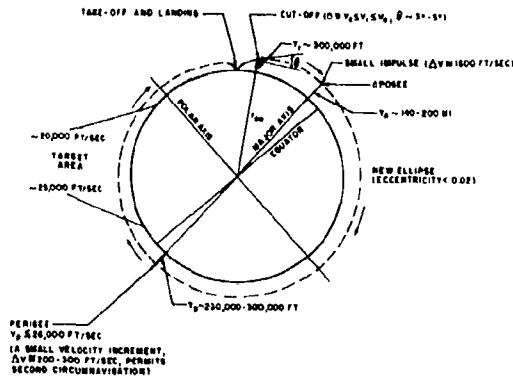

Figure 2. Path Type II: Low Eccentricity Ellipse with Perigee Near Target Area

during the subsequent subcircular glide, from its initial great circle path, or to descend through the denser atmosphere (below 200,000 ft) with $(C_L)_{max}$ rather than $(L/D)_{max}$. It was found that only a very small additional velocity increment near the perigee would permit another circumnavigation. In the present example, the over-all ideal velocity is 28,500 + 1,600 = 30,100, that is, approximately the same level as Path I.

PATH III

The vehicle is delivered horizontally at a suitable altitude but at a speed which is in excess of the local circular velocity. This excess (designated elliptic excess) would send the vehicle into an elliptic orbit, if it were not forced to stay in the circular path by a negative lift produced by aerodynamic forces which are sufficiently strong at this altitude and speed (constrained circular path Figure 3). The vehicle then begins its flight at a negative angle of attack, which decreases as the vehicle is slowed down. When reaching circular speed the vehicle has zero-lift attitude and thereafter passes into a positive angle of attack position until maximum lift (or lowest speed) is attained. This terminates the constant altitude flight and subsequently the vehicle begins to lose altitude.

A representative path consists of a horizontal altitude of 290,000 ft at a velocity

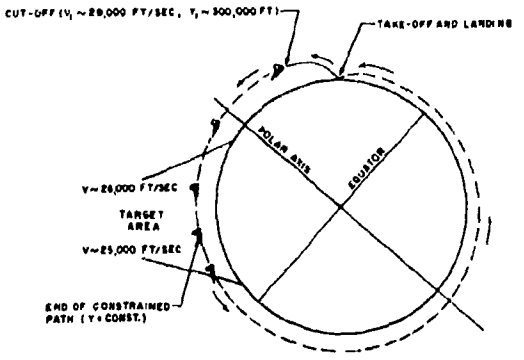

Figure 3. Path Type III: Constrained Path

of 29,000 ft/sec. The dynamic pressure at this speed is about 14.5 lb per sq. ft, and the pilot's initial negative weight is 26% of his surface weight. The vehicle can remain at this altitude down to a lower velocity limit of approximately 24,500 ft/sec. The range covered during the deceleration from 29,000 to 24,500 ft/sec is approximately 5000 n.mi. and requires about 19 minutes flying time. During this period the "negative" apparent weight of the pilot is reduced from 26% of his true weight through zero to a "positive" apparent weight of 8%. The powered path range in this case is longer, at least 1,000 n.mi., so that, when the velocity is down to 24,500 ft/sec, the vehicle is approximately 6,000 n.mi. away from the launching site, that is, right over the center of the Russian target area, assuming the vehicle follows the direct route rather than flying in the opposite direction like the preceding paths. With 24,500 ft/sec, the vehicle has then another 15,500 n.mi. to go. This appears feasible, if an $(L/D)_{max}$ descent is taken. The ideal velocity required in this case is about 32,000 ft/sec.

PATH IV

This type consists of a circular path at high altitude with sustainer motor for maintaining constant circular velocity. In order to restrict the propellant requirements for cruise, the drag must be very small; hence, the altitude must be high. It will be seen below that, for moderate propellant consumption of not more than 200 lb per revolution, the vehicle must maintain altitudes of 450,000 ft and above. Figure 4 shows this consumption per revolution as function of the cruise altitude, operating at a specific thrust of 350 lb thrust per lb propellant per second, for a mean vehicle weight of 10,000 lb. The altitude range considered lies in the free molecule flow regime and the drag coefficient, based on the lifting area, is found to lie between 0.35 and 0.7, depending on body shape and gas composition. A lifting area load of 20 lb per sq ft has been assumed. It can be seen that cruising within the altitude limit of 300,000 ft is prohibitively expensive, in spite of the high specific thrust. Cruising altitudes of the order of 450,000 ft or above evidently are required.

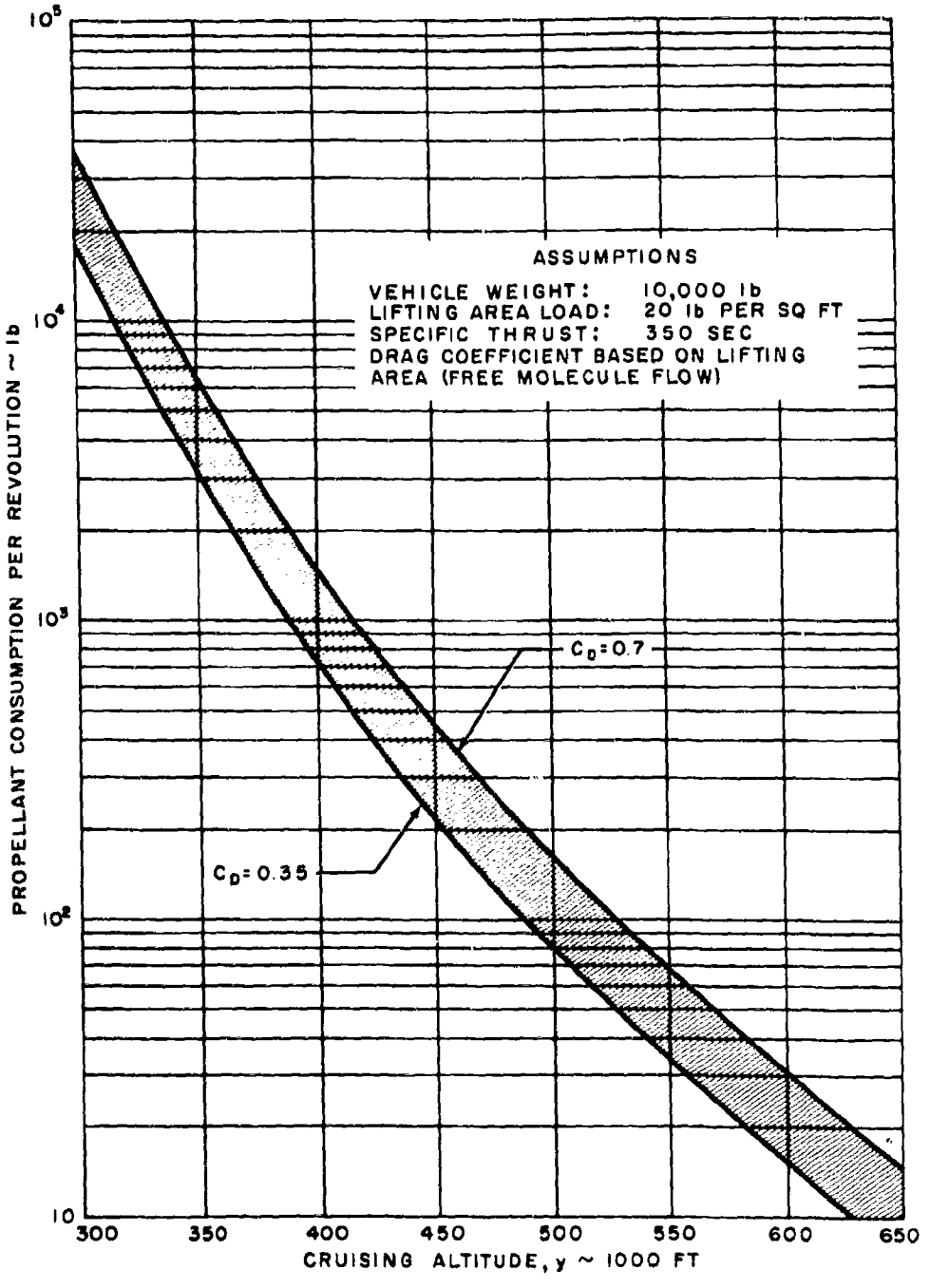

Figure 4. Path Type IV: Sustained Path. Approximate Propellant Consumption per Revolution vs Cruising Altitude

The above typical flight paths illustrate the requirements associated with circumnavigation. A comparison between these flight path prototypes indicates the following general results which should only be interpreted qualitatively at the present time.

1. Energy Requirement

Most energy is needed for the constrained path (III). For the sustained path (IV) the requirement depends upon altitude and duration of flight (number of revolutions). For paths I and II the energy requirement is lowest, if one revolution is considered.

The effect of over-all energy requirement (in terms of ideal velocity) on the take-off weight of a three-stage vehicle carrying a payload (pilot reconnaissance equipment) of 3000 lb is indicated in Figure 5. The band covers a number of variations of energy distribution among the stages. It does not, however, include the effect of altitude variation for Path IV. Stages 3 and 1 are assumed to be winged; Stage 2 is expendable.

From the operational point of view, the global weapon system places even more emphasis than the intercontinental weapon system on payload weight reduction, in order to keep the take-off weight increase at a minimum. Thus, since it appears that reconnaissance missions require less payload weight than bombing missions, the global weapon system seems to lend itself primarily to a reconnaissance type of operation. However, this excludes bombing missions only if the payload weights involved are considerably larger.

2. Number of Revolutions

With comparatively little additional energy (corresponding to a velocity increment of not more than 1000 ft/sec) it is possible to increase substantially the number of revolutions with paths I and II. For path III, more than one revolution appears to require an excessively high energy increment. For path IV conditions depend upon flight altitude.

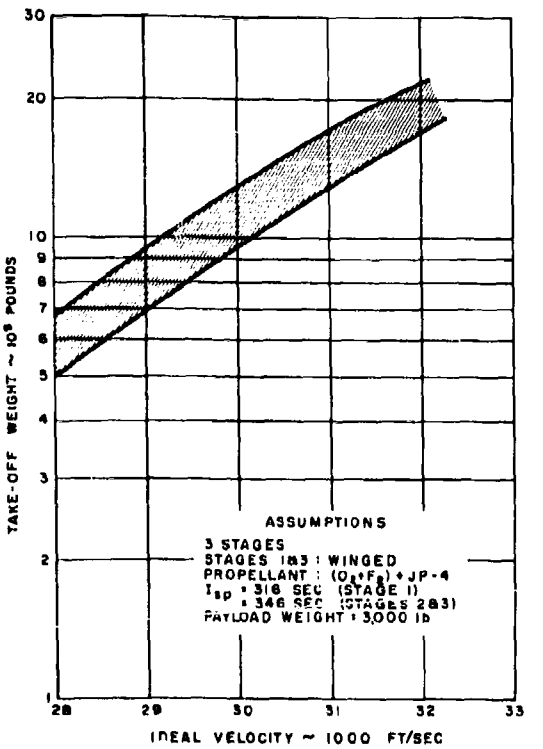

Figure 5. Range of Take-Off Weights of Global Weapon System as Function of Ideal Velocity

3. Altitude over Target Area

To insure maximum possible radar reconnaissance, a tentative maximum altitude of 300,000 feet over the target area was assumed. The condition is fulfilled in the case of Path I for 1 revolution only, for Path II for more than one revolution, but very probably not more than 3 within the energy range under consideration. The condition is also fulfilled in the case of Path III, but very likely not for Path IV, because of excessively large propellant consumption at the lower altitudes.

4. Maximum Altitude in Path

Path I probably will not exceed an altitude of 400,000 ft (except for more than one

revolution), Path III will stay within the 300,000 ft limit. However, Path II, being an ellipse, will yield maximum altitudes beyond 100 miles, probably as much as 150 to 200 miles. Altitudes for Path IV will probably not have to exceed 100-110 miles.

5. Stability and Control

Dual control systems for atmospheric and vacuum operation will be required for all paths, with the exception of Path III. For operation in a vacuum a jet control system is required. Aerodynamic control can be used as soon as the dynamic pressure has reached an adequate value (at least about 10 lb per sq ft). Thus, the global vehicle will normally use two control systems. This naturally increases the weight and complexity of vehicle stability and control equipment.

6. Weight Conditions

More or less extended periods of weightlessness will be experienced in all cases (particularly Path II), except in Path III, where the weight is "negative" (upwardly directed) during the initial portion of the unpowered flight. In Path IV the weight is never zero, because of the sustainer thrust. However, for reasons of economy the sustainer thrust must be so small that the conditions of weightlessness are approached closely, and are maintained for the duration of the cruise flight. So far, no indications could be found to make the condition of negative weight appear prohibitively unattractive. Orientation is furnished by instruments. Physiologically, negative weight increases the blood circulation through the brain and provides at least some feeling of weight and direction, thereby making it possibly more attractive even than a condition of complete weightlessness. The negative weight variation with speed is shown in Figure 6.

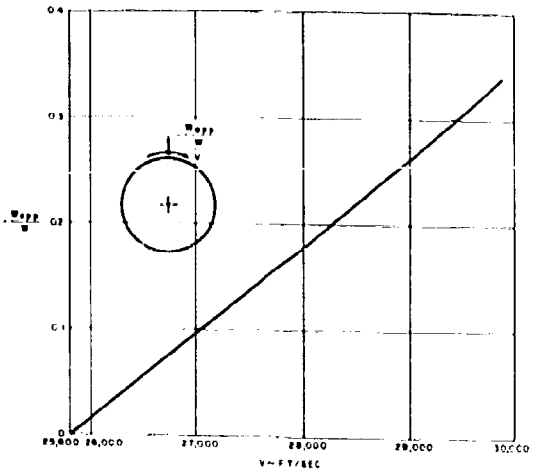

Figure 6. Negative Apparent Weight in Constrained Path as a Function of Flight Velocity

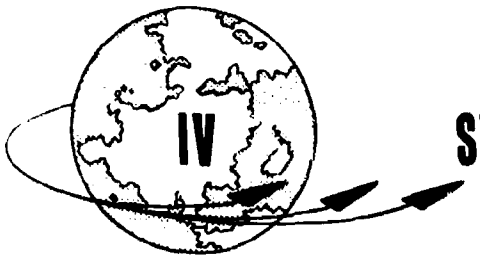

IV STATUS OF STUDY

A. PILOT ENVIRONMENT

1. GENERAL

The material in this section will be concerned with the operator in Stage III unless it is specifically stated otherwise. The proper environment for the pilot of Stage I can be provided and maintained much more readily than the proper environment in Stage III. For this reason, the investigation has been limited chiefly to a study of the problems of Stage III.

The extreme temperatures resulting from the high speeds, and the lack of air resulting from the high altitude, make it necessary that the entire environment for the Stage III pilot be artificially supplied and controlled. This environment must consist of conditions in which the pilot can exist with sufficient comfort to accomplish the necessary functions. In this weapon system these functions must combine to give the manned system better performance and reliability than are attainable with an automatic system. The provision of this environment increases weight both directly, such as the pilot's weight, and indirectly such as the increased structural weight required for the loads introduced by the cabin pressurization. The entire weight of pressurization, refrigeration, etc., cannot be charged to the man, since an automatic system would also require these provisions. However, any increased capacity of these systems must be charged directly.

The design of all systems used in connection with the environment must be coordinated with other systems performing similar functions in other portions of the airplane. The systems providing the greatest possibilities in this respect are the cooling systems. Cooling will be required for pilot, equipment, power plant, and possibly structure. As many of these systems should be combined as possible in order to eliminate duplication of equipment.

2. ENVIRONMENTAL REQUIREMENTS

a. Thermal

The thermal environment of the human includes consideration of the following parameters as a function of time: cabin wall temperature, solar radiation, pilot's clothing, and cabin air (velocity, temperature, pressure, and humidity). The effects of these parameters have been studied and correlated in Reference 2; however, the clothing used did not include a ventilating suit.

A typical calculation using these data indicates that a man wearing a light summer flying suit would be capable of maximum performance for a period of one hour under the following conditions: cabin pressure 5 psia, vapor pressure 0.6 inches of mercury, cabin air velocity 200 ft/min, cabin air temperature 70° F. These conditions were selected as typical of those which can be achieved for Stage III and still can be tolerated for one hour (approximate flight time of MX-2276.) These typical conditions were used for sample calculations of systems requirements as will be discussed later. Through the use of a ventilating suit, it is possible that conditions more extreme than these can be tolerated, with the same human performance capabilities, for a one-hour period. The ventilating suit is still in the process of development and testing; however, it will be incorporated in the study as soon as data become available.

b. Pressure and Composition

The pilot's environment will be satisfactory from a physiological standpoint if a pressure of 5 psia is supplied, 3 psi partial pressure of oxygen and 2 psi partial pressure of nitrogen. The pressure will be controlled to a 5 psi differential. However, inasmuch as the ambient pressure is of the order of 0.07 psf at the beginning of cruise, increasing to 13.9 psf at the end of cruise, for all practical purposes the 5 psi is the absolute cabin pressure. Although this value is appreciably lower than normal sea level pressure (14.7 psi) or the minimum presently allowed in bombers (7.5 psi, Reference 3), it is satisfactory from the standpoint of physiological functions. From the standpoint of explosive decompression, the lower pressure is much more satisfactory than the higher pressures mentioned above. Tests have shown that normal humans can withstand explosive decompression through 5 psi without major injury. In contrast, dogs have lived through 7.5 psi decompression only with expert medical care, and have sustained permanent, major injuries.

In order to prevent aeroembolism at these low pressures, the human would be required to prebreath 100% oxygen for about two hours prior to launch. By this means, enough of the nitrogen dissolved in the blood stream will be eliminated to prevent any dissolution at the reduced pressures. Another method for eliminating the dissolved nitrogen consists of prebreathing a helium-oxygen atmosphere since helium is not soluble in the blood. However, this system remains to be investigated.

It is presently planned to bleed the cabin atmosphere at a steady rate. By this means, it is possible to eliminate products of respiration, and prevent the accumulation of any toxic gases either from equipment or from impurities in the gas supply.

3. METHODS OF MAINTAINING ENVIRONMENTAL REQUIREMENTS

a. Thermal

The two major factors to be controlled

in the thermal environment are the cabin entrance air temperature and the cabin wall temperature. If a stored gas atmosphere is used (see next section), the cockpit air temperature can easily be kept to low values. Such an atmosphere would be stored either under pressure or possibly as a liquid. In either event, the temperature after expansion to 5 psi would be very low. In fact, it would probably be necessary to provide some type of heat exchanger to warm the expanded gas to the desired inlet temperature (since these temperatures must be above freezing). This process could be utilized in one of the several cooling systems required.

The cabin wall temperature is a more complicated problem. The extremely high boundary layer temperatures, together with the high potential heat fluxes make it very difficult to maintain the wall temperatures at tolerable values (180-190°F). Two methods of maintaining these temperatures appear feasible:

(1) Insulation of the cabin walls.

(2) Circulation of the coolant through the cabin walls. This is the intrawall cooling of Reference 4.

The method which will be used will be a combination of both systems.

In order to illustrate these methods, the necessary equations will be shown and the results of a sample problem will be presented. In this problem, the cabin wall is considered to be made up of two layers of insulation separated by a duct through which coolant is passed. The insulation may also have skins on either side for structural purposes. The small thicknesses and high conductivity of these skins, if of metal, combine to produce a very small temperature gradient through the skins. As a consequence these skins have very little effect on the heat transfer characteristics of the over-all wall, and are not considered in the following calculations. Figure 7 illustrates the wall as it appears from a thermal standpoint, and Table II contains the nomenclature used.

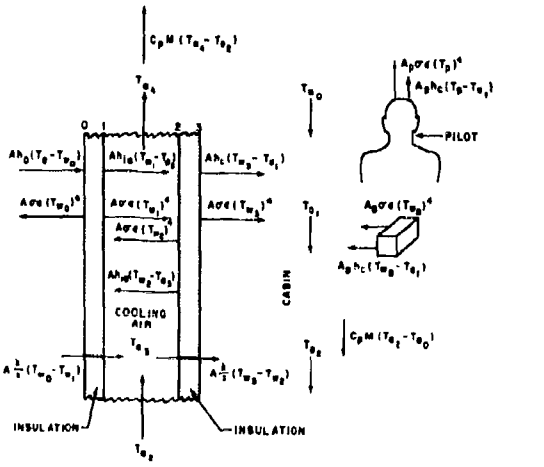

Figure 7. Heat Balance Through a Cooled Cabin Wall

The equations used in the analysis are as follows:

$$Ah_0(T_c - T_{s_0}) = A\sigma\epsilon(T_{s_0}^4) + A\tfrac{k}{L}(T_{s_0} - T_{s_1}) \quad (1)$$

$$A\tfrac{k}{L}(T_{s_0} - T_{s_1}) + Ah_{1_0}(T_{w_1} - T_{s_1}) + A\sigma\epsilon\left[(T_{s_1})^4 - (T_{w_2})^4\right] \quad (2)$$

$$Ah_{1_0}(T_{w_1} - T_{s_0}) + A\sigma\epsilon\left[(T_{w_1})^4 - (T_{s_2})^4\right] + A\tfrac{k}{L}(T_{s_2} - T_{s_0}) + C_pM(T_{s_0} - T_{s_2}) \quad (3)$$

$$Ah_{1_0}(T_{w_1} - T_{s_2}) + Ah_{1_0}(T_{w_2} - T_{s_1}) + C_pM(T_{s_0} - T_{s_2}) \quad (4)$$

$$A\tfrac{k}{L}(T_{s_2} - T_{s_0}) + Ah_0(T_{w_2} - T_{s_1}) + A_p\sigma\epsilon\left[(T_{w_2})^4 - (T_{s_2})^4\right] + A_p\sigma\epsilon\left[(T_{s_2})^4 - (T_p)^4\right] \quad (5)$$

$$C_pM(T_{s_2} - T_{s_0}) + Ah_c(T_{w_2} - T_{s_1}) + A_ph_c(T_{w_2} - T_{s_1}) + A_ph_c(T_p - T_{s_1}) + \text{Pilot's metabolistic heat} + \text{Equipment heat} \quad (6)$$

$$\tfrac{1}{2}(T_{s_0} + T_{s_1}) = T_{s_1} \quad (7)$$

$$\tfrac{1}{2}(T_{s_2} + T_{s_c}) = T_{s_2} \quad (8)$$

Inasmuch as the problem is concerned chiefly with heat flow into the cabin, the external heating conditions are not included in detail. In equation (1), which contains these conditions, only the terms for heat transfer from the boundary layer to the skin and radiation from the skin to the atmosphere are included. Other terms representing secondary effects such as atmospheric and solar radiation have not been included.

TABLE II. NOMENCLATURE

A	=	Cabin Wall Area ~ sq ft
h_o	=	External Heat Transfer Coefficient ~ BTU/hr-sq ft - °F
Te	=	Effective Boundary Layer Temperature ~ °R
T_{w_o}	=	External Wall Temperature ~ °R
σ	=	Stefan - Boltzmann Constant
ϵ	=	Emissivity
k	=	Thermal Conductivity of Insulation ~ $\frac{\text{BTU In.}}{\text{hr-sq ft - °F}}$
X	=	Insulation Thickness ~ in.
T_{a_0}	=	Cabin Inlet Air Temp. ~ °R
T_{a_1}	=	Average Cabin Air Temp. ~ °R
T_{a_2}	=	Cabin Exit AirTemp. = Duct Inlet Air Temp. ~ °R
T_{a_3}	=	Average Duct Air Temp. ~ °R
T_{a_4}	=	Duct Exit Air Temp. ~ °R
T_{w_1}	=	Duct Wall Temp. Outside Wall ~ °R
T_{w_2}	=	Duct Wall Temp. Inside Wall ~ °R
T_{w_3}	=	Cabin Wall Temp. ~ °R
h_{l_a}	=	Heat Transfer Coefficient of Duct Air ~ BTU/hr-sq ft - °F
h_c	=	Heat Transfer Coefficient of Cabin Air ~ BTU/hr-sq ft - °F
A_p	=	Surface Area of Pilot ~ sq ft
T_p	=	Pilot Surface Temp. ~ °R
Tw_B	=	Temp. of Surface of Equipment ~ °R
A_B	=	Surface Area of Equipment ~ sq ft

With the terms used it is possible to determine the magnitude of the heat flow into the wall, and the reduction in outside wall temperature is of particular interest from structural considerations.

The equations shown may be interpreted as follows:

(1) The heat convected from the boundary layer to the wall, minus the heat radiated to the atmosphere, is equal to the heat conducted through the outside wall.

(2) The heat transferred through the outside wall is equal to the heat convected to the coolant plus the heat radiated across the coolant duct to the opposite wall.

(3) The heat convected and radiated from the outside wall of the duct is equal to that conducted through the inside wall plus that used in heating the coolant.

(4) The heat convected from the inside duct wall plus the heat convected from the outside duct wall is equal to the heat added to the coolant.

(5) The heat conducted through the inside wall is equal to that convected to the cabin air, plus that radiated to (or from) the pilot's body and the equipment.

(6) The heat added to the cabin air is equal to that convected from the wall, plus the heat convected from the pilot's body, plus the heat convected from the equipment, plus the pilot's metabolic heat, plus the instrument heat load.

(7) The average cabin air temperature used in the calculations is the arithmetic average between the inlet and outlet cabin air temperature.

(8) The average duct temperature used in the calculations is the arithmetic average between the inlet and outlet duct air temperatures.

In these equations the heat radiated to and from the coolant in the duct is considered to be negligible.

These equations do not lend themselves to a closed solution because of the 4th powers in the radiation terms. Therefore, the equations were solved on a trial and error basis, by assuming various coolant temperatures. For the sample problem, the following values were assumed: equivalent boundary layer temperature 23,620°R (corresponding to M = 16.4 at 200,000 ft, one of the worst heating conditions), coolant air flows of 500 and 1000 lb/hr, cabin wall area of 138 sq ft, cabin inlet air temperature 35°F, and cabin wall temperature 190°F.

Figure 8 shows the results of these calculations as a function of the final coolant air temperature. Several interesting results may be seen from the figure. First, the required thicknesses of insulation inside and outside the coolant duct vary with the coolant air temperature. The combined thickness becomes a minimum at a specific coolant temperature, which provides the minimum installation weight.

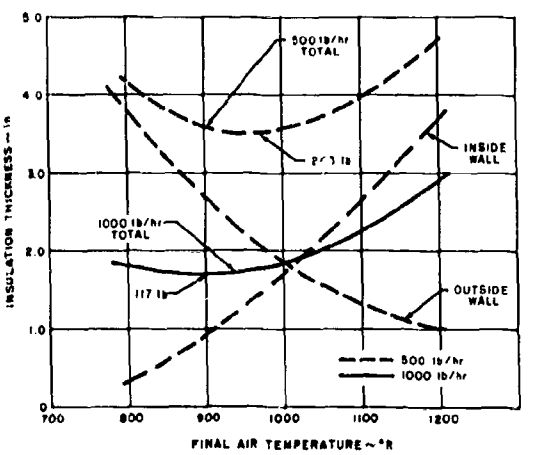

Figure 8. Insulation Thickness as a Function of Final Temperature of Coolant Air Using Intra-wall Cooling

Second, considering the flight is of one hour duration, the total weight of insulation plus coolant decreases (at the minimum) from 1117 lb with 1000 lb/hr flow to 743 lb with 500 lb/hr flow. For comparison with these numbers the amount of insulation required, if insulation only were used, was computed. This showed a total of 12.2 inches or 841 lb was required. Thus, the use of a stored coolant would result in the lightest over-all system for keeping the wall temperature down to the desired values. The ducted wall also requires less vehicle frontal area, inasmuch as twelve inches insulation mean a diameter increase of two feet as compared with a diameter increase of six or seven inches with the wall ducts.

The foregoing material is presented chiefly to show the method of analysis and at the same time give some idea of the magnitudes of the parameters involved. It appears that the greatest weight savings may be accomplished by the use of better coolants. One of the most promising coolants is water. The higher specific heat, greater density, and high heat of vaporization of water make it appear more desirable than air as a coolant. The use of water would entail several additional problems, however. It will require a separate pumping arrangement and system, whereas the air system could be combined with the air system used for cabin ventilation and cooling. The change of state of the water will also introduce problems of volume and heat transfer within the system. Further calculations will be carried out when the external heating conditions are more firmly established.

b. Pressurization and Composition

It is presently planned to provide the cabin atmosphere from a stored gas, either pressurized or liquified. The gas will consist of a mixture of oxygen and nitrogen such that when expanded to 5 psi the gas will be composed of 3 psi oxygen and 2 psi nitrogen. The liquified gases have the advantage of smaller stored volume, and the heat required for the change of state could be provided advantageously by some of the portions of the vehicle which require cooling. In either case the stored atmosphere would be under extreme pressures thus making it relatively easy to provide the desired environmental pressure of 5 psi.

One system which has many advantages, provided the required amount of gas is not too large, consists of circulating the gas through the cabin, thence through the cooling ducts. After passage through the ducts the gases are exhausted overboard. This system would provide breathing oxygen, circulation about the pilot for cooling him, a bleed for noxious or toxic gases, and a coolant for the intrawall system. However, inasmuch as the coolant is air, the system would not be very satisfactory for adaptation to use for any skin cooling which may be necessary.

Previous experience with pressurized cabins indicates that a 5 psi cabin pressure differential can be maintained with a small amount of leakage. Techniques and seals for accomplishing this have already been developed. Any leakage which does occur will be advantageous since a certain amount of atmosphere bleeding is required anyway.

The amount of oxygen required for breathing during a one-hour flight is of the order of 10 to 15 pounds. This amount is relatively small compared to the amounts required for circulation and bleeding. If the cabin air is circulated through the walls, the amount used for breathing will be a very small percentage of the whole.

The pressurization system should be regulated to reduce the cabin pressure at a slower rate than the ambient pressure during boost. This feature is desirable to prevent aeroembolism. However, it will result in cabin pressure differentials of more than 5 psi over a short period, hence higher cabin structural weight.

c. Accelerations

The launching acceleration program presently contemplated is not critical as far as human tolerance is concerned. This program (Reference 1) consists of a sawtooth program

with a maximum of 4g axial loading. It is not contemplated that the pilot will be rotated; hence the axial accelerations will be transverse on the human (i.e., normal to the chest). In this direction these loads are not critical. Sawtooth acceleration patterns of similar magnitude and duration have been run with human subjects without any adverse results. If desired, when the acceleration program is definitely known, the exact pattern can be tested using human subjects and existing facilities. Although none of the proposed accelerations will be of sufficient magnitude to require the use of a g-suit, it is proposed that this feature will be included in the operator's clothing.

d. Vision

The chief reasons for providing the pilot with the capability of vision outside the aircraft is for secondary guidance and landing the aircraft after completion of the mission. It is doubtful that a protruding windshield or canopy could be constructed which could withstand the structural loads under the heating conditions encountered. In addition, the installation of either of these would place a drag penalty and/or an additional cockpit heating load (due to solar radiation) on the vehicle.

The use of a periscope, on the other hand, almost eliminates these problems, and with the proper installation, provides equal or better visibility. The present concept utilizes an ocular periscope with protruding hemispherical domes on either side of the nose of the vehicle. This would provide the required lateral and downward vision. An ocular type is preferred since it makes possible a greater field of view than is attainable with a projection type. However, the use of an ocular type requires that the helmet visor remain open in order that the eye can be placed near the ocular. If the field of view is not needed, a projection type would overcome this disadvantage, although if the visor is closed it will reduce the vision to some extent also. Additional advantages of the projection type are the possibility of looking at both the radar scope and the visual presentation with less eye adaptation time, and a similar possibility for scanning other instruments in the cockpit.

If the visual system is to be used for guidance, even secondary guidance, it must have the capability of accurately locating a checkpoint with respect to the location computed by the inertial system. If the projection type is used, this feature may be included by means of cursors which can be moved over the face of the projection. If an ocular is used it may be necessary to use a system which can be scanned manually, with cross-hairs which can be placed on the checkpoint. The location of these cross-hairs can be fed into computers for calculation of the checkpoint location. In either case such a system must be integrated with the radar and the inertial system.

e. Emergency Provisions

The emergency provisions are a major factor in the over-all weapon system design because of the extremes of speed, altitude, and range of the flight. Each of the major factors will be treated separately.

(1) Explosive Decompression

In order to reduce the dangers from explosive decompression, the pressure in the cabin atmosphere has been limited to a differential of 5 psi. As previously stated, normal humans can and have withstood explosive decompression through this differential without permanent injury. As additional protection, in order to keep such decompression to a minimum, a partial pressure suit will be worn by the pilot at all times. This suit will normally remain uninflated, but at the time of decompression it will inflate automatically. This suit will incorporate a helmet and supply of gas for breathing after decompression. If the helmet visor is to remain open, it must have an automatic closure device which will be actuated when the suit is pressurized. Although a total pressure suit would be much better from a physiological standpoint, it restricts the human operation much more than the partial pressure suit, even when uninflated.

(2) Emergency Escape

There are two phases of the emergency escape problem which must be considered: escape during the boost period, and escape during cruise at high speeds and high altitudes. The use of an escape capsule is not contemplated because of the limited advantages to be obtained at the expense of large weight increases.

During the boost period, the vehicle will achieve relatively high speeds at lower altitudes with the result that an ejected pilot will be subjected to large aerodynamic forces. However, the boost period is of the order of 400 seconds but only during approximately 100 seconds of this time does the dynamic pressure exceed the maximum at which ejections have been safely accomplished. Since the upper limit of safe ejection has not yet been established, this time period during which ejection is not safe may be even shorter. If an emergency should occur during this period, the pilot should stay with the aircraft until the speed is reduced to a value where ejection may be carried out in safety.

During the cruise period, the vehicle will be flying at extreme speeds, but also extreme altitudes, with the result that the dynamic pressure is low enough that ejection can be accomplished safely. However, ejection at these speeds and altitudes will result in extremely long trajectories of the pilot and seat, and consequently long periods of fall. Although the pilot's clothing will include a partial pressure suit and a supply of breathing gas, the proper procedure would be to remain with the vehicle until more satisfactory speeds and altitudes are attained. In order to make the vehicle more suitable for this purpose it will be equipped with dive flaps or similar device, the fuel tanks will be purged with an inert gas, and provision will be made for inerting the cockpit also.

As a result of the foregoing considerations it has tentatively been decided to use an ejection seat in the airplane and to utilize the entire Stage III as an escape vehicle. In the event ejection is required at extreme speeds and altitudes, the pilot will be provided with adequate equipment for his protection.

f. Pilot Clothing

The pilot's clothing must provide four special functions, three of which have been mentioned:

(1) Partial pressure suit - for emergencies entailing explosive decompression.

(2) Ventilating suit - for cooling the pilot under extreme conditions. This suit is presently under development.

(3) Anti-g suit -for emergencies involving high g maneuvers.

(4) Exposure suit - for protection of the pilot on land or sea, subsequent to emergency exit.

The latter suit must be capable of protecting the pilot in tropic or arctic regions and if he should descend into water. Since the flights involved will be of extremely long range, a single flight may traverse all of the above regions, and an emergency could occur over any one.

Clothing containing all of the above features has been developed or is under development. Programs are presently under study for the combination of all of the features into a single garment or into two garments which can be worn concurrently.

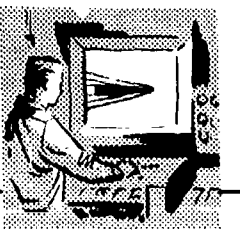

B. AERODYNAMICS

I. GENERAL

During the first half of the present study the greater portion of the aerodynamic effort has been concerned with investigations of a basic nature - determining the apparent aerodynamic problems of the MX-2276 system, finding what is known, either theoretically or experimentally, and what is unknown or not well understood. Some effort was also expended towards developing or refining methods of analysis to be used in the study of MX-2276 performance, heat transfer, stability, etc.

The general approach to the aerodynamic study is discussed here, and following this introduction the findings thus far from the specific subject studies are discussed. Finally, plans for the next portion of the study are outlined briefly.

a. The Flight Plan

In order to plan a program for the investigation of the basic problems and to hold the present investigation to applicable cases, it was first necessary to define the flight conditions under which it is expected that the MX-2276 system will operate. For this purpose it was felt that the original flight path (Reference 1) would be sufficient even though it might be modified by future optimization studies. Figure 9 shows the flight path altitude and velocity and the flight times for the various portions of the flight. The dynamic pressure, q, a measure of the aerodynamic forces involved during the flight, is plotted on Figure 10. It will be noted that the q at the high Mach number, high altitude portion of flight is very small - not enough to support the aircraft if it were not for the reduction of effective gravity due to centrifugal force.

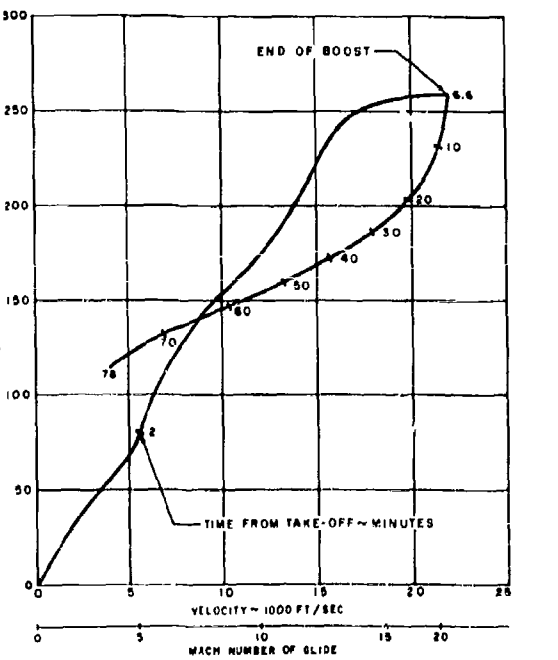

Figure 9. Flight Path: Altitude vs Velocity

To provide further perspective, several flight limits of interest have been plotted with the flight path on Figure 11. It is reasoned that the very low static wing loading of $(W/S)_O = 10$ psf at the high hypersonic lift coefficient of $C_L = 0.20$ defines an upper altitude limit for level flight (and for maximum L/D glide). The effective reduction of gravity g/g_O, due to the centrifugal forces involved in flying a circular path about the earth's center and due to the decrease in gravity with altitude, is included in this limit curve. The satellite limit is that where the effective gravity is zero and no lift is required.

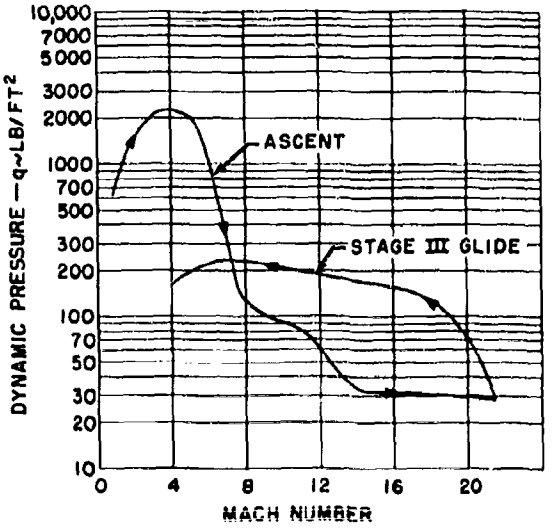

Figure 10. Dynamic Pressure vs Mach Number

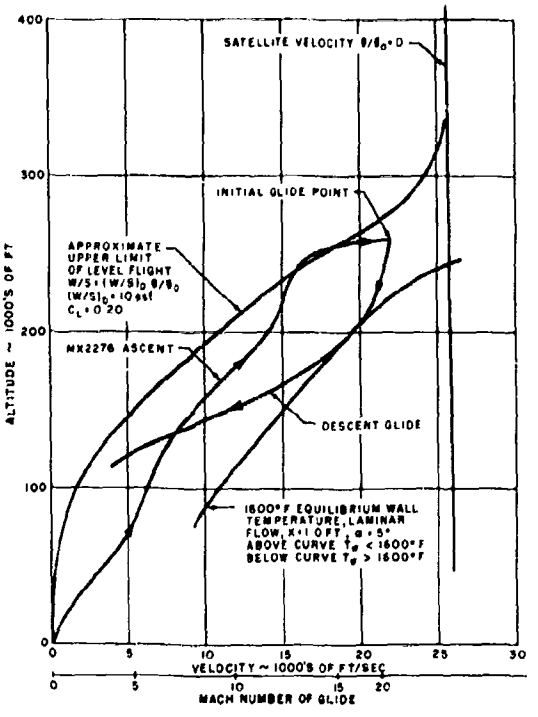

Figure 11. Flight Limits

It is seen that the ascent of the MX-2276, which is more of a nonlifting ballistic trajectory, crosses over the level flight limit while the glide, as would be expected, is under it. The curve of 1600°F wall temperature illustrates a thermal limit with respect to the flight path. If 1600°F were the upper limit allowed for the configuration noted, flight would have to be above the curve (as it is for the present flight path) or cooling would be necessary. For the glide phase this thermal limit also implies restrictions on wing loading and lift coefficient.

b. Literature Survey and Visits

From the flight path discussed in the above paragraphs, it is apparent that the MX-2276 vehicle will be operating in regions of flight for which there is little or no past experience to rely upon, and for which theoretical and experimental investigations are only just beginning to produce useful results. For this reason, the first step in the program was to set up as complete as possible a bibliography of all information pertaining to hypersonic and high-altitude flight, and to insure the maintenance of such a file. Accordingly, a systematic search of the publications of government, military and university research and development facilities, of military contractors, and of all pertinent scientific periodicals was made to obtain references to all literature applicable to our work.

The fields of interest in this search necessarily encompassed many areas of fundamental physics and chemistry, such as those concerned with dissociation and ionization at high temperatures, real gas effects in the equation of state for air, emissivities of gases, etc., as well as the more obvious subjects of supersonic and hypersonic flow, boundary layer theory and experiment, flight mechanics, etc. Experience gained during the previous study of hypersonic aircraft leading to the proposal of Reference I as well as continued interest in the field since then, served as a guide in this search. It may be of interest to note that more than 2000 pertinent references have been recorded to date.

A listing of all research facilities and of leading workers in various aspects of the field

was also started, in order to obtain cognizance of sources of information bearing on hypersonic, high altitude flight.

A series of trips to various research and industrial facilities has been made to discuss the pertinent problems within the fields of interest previously mentioned, and to examine facilities available.

c. Flight Mechanics

The study of the aerodynamic aspects of the MX-2276 was organized essentially in two parts which have been carried out concurrently.

One line of investigation concerns the problems of flight mechanics proper. In order to provide an accurate basis for the determination of the performance and stability of a long range hypersonic aircraft, it is necessary to start from equations of motion which include all the forces acting on a body moving in space. These equations have been derived and are presented and discussed in a later section of this report. They are given in a convenient and useful form; namely, one which expresses motion relative to an observer fixed on the surface of the earth as caused by forces acting along the standard aircraft axes.

The next step, which is under way, is to simplify these equations for practical application by considering the relative weight of all terms for the range of variation of the pertinent aerodynamic parameters. In this way, the accuracy involved in any approximation of the complete equations can be controlled and evaluated. When a sufficiently accurate reduced version of the complete equations is obtained, the accuracy of the original preliminary performance calculations (Reference 1) which were based on the standard, simplified flight equations, will be evaluated.

d. Aerodynamic Parameters

The second group of investigations, on which the larger effort has been expended, is directed at providing methods of known accuracy for the computation of aerodynamic performance, stability, and heating parameters, and at indicating qualitatively and quantitatively possible ways of controlling these parameters. The investigations in this group are of two types.

The first class of investigations encompasses those of a more fundamental nature and is concerned essentially with the basic concepts of flow phenomena which form the foundation for aerodynamic methods for analyzing hypersonic aircraft. Included in this category are the following studies where work has progressed sufficiently far to be reported herein.

(1) A primary study, prerequisite for any accurate analysis of flow at hypersonic speeds, is one of the behavior and properties (viscosity, heat conductivity, specific heat, etc.) of air in the whole range of temperature, pressure, and density of interest. Even at low supersonic speeds the actual variation of these properties is significant in boundary layer analyses, while at high Mach numbers, the effect of variable specific heat, dissociation, and ionization must also be taken into account in developing the tables of shock flow and isentropic flow which are basic to the calculation of pressure and temperature distributions.

(2) An analysis of the flow pattern about a flat plate flying in the range of speeds and altitudes associated with MX-2276 was made to delineate the various flow regions, and to indicate what flow patterns can be assumed and what fundamental equations will adequately and consistently represent the physical problem in each region. This is the necessary basic step in evaluating the limit of applicability of various aerodynamic theories and methods. This analysis also indicates specifically where new theory and experiments are required.

(3) Some basic investigations of aerodynamic phenomena which will be encountered at Mach numbers above about 10 are under way. These are concerned with the possibility of erosion of the solid surface by the air in high speed flow, the effect of dissociation in the mechanism and the magnitude of aerodynamic heating, and the possibility of heat radiation from a hot boundary layer into a solid surface.

The second class of investigations is concerned with obtaining and evaluating methods of analysis for immediate use in the flight regimes where an adequate theoretical and experimental basis for such methods exist, i.e., where the flow phenomena and all influencing factors are reasonably well known and understood. At present, this is restricted to continuum flow under conditions where the flow pattern is essentially separable into inviscid and viscous regions with no slip conditions in the viscous regions and negligible interaction between the two regions, and for maximum temperatures below that for significant dissociation of the air. The work to date in this category includes methods for determining skin friction; methods for determining heat transfer coefficients; studies of boundary layer transition and transpiration cooling; a compilation and review of currently available test data for the L/D of body and wing section shapes; and a study and comparison of methods for obtaining the aerodynamic characteristics of wing sections at hypersonic speeds.

2. FLIGHT MECHANICS

In order to conduct a detailed study of the problems involved in hypersonic flight, it is essential to both performance and stability analyses that the equations which are employed accurately describe the motion of the vehicle.

Previously, the equations of linear motion for an aircraft had been simplified to a great extent by neglecting terms which were small in magnitude mostly due to relatively small flight velocities. The effects of centrifugal and Coriolis accelerations, gravity variations with altitude and earth orientation, and the earth's rotation were neglected compared with those of lift, drag, thrust, and weight of the aircraft. Therefore, the apparent, i.e., relative, motions of the aircraft seen by an earth fixed observer could be calculated using the following familiar equations:

$$T \cos \upsilon - D - W \sin \gamma = m \frac{d^2x}{dt^2} \qquad (1a)$$

$$T \sin \upsilon + L - W \cos \gamma = m \left(\frac{dx}{dt}\right) \left(\frac{d\gamma}{dt}\right) \qquad (1b)$$

where: m is the mass of the aircraft

W is the weight of the aircraft

T is the thrust

L is the aerodynamic lift

D is the aerodynamic drag

x is the linear displacement of the aircraft in the flight direction

γ is the angle between the flight direction and the horizontal

υ is the angle between the thrust line and the flight direction

Herein, the complete equations of linear motion are derived so as to include most all the effects not found in Equation (1). Since the inclusion of all the forces acting on a body moving in space obviously results in highly complex expressions, the effects of making certain simplifying assumptions has been investigated (Reference 5). It was found that the gravitational attraction of both the sun and the moon, and hence more distant heavenly bodies, could be neglected. It was further found that the inertial axis system (i.e., that axis system which is usually considered fixed in space at the center of the sun and to which absolute accelerations and velocities are referred by Newton's law, $\sum F = \frac{d}{dt}(mV)$ could be assumed fixed in space and located at the center of the earth. In the derivation of the "complete" equations of motion of this report the above simplifying assumptions are made along with the additional assumption that the rotation of the earth about its axis is constant.

As the equations of motion can be derived so that the motions are relative to any arbitrary axis system, special consideration must be

given to the choice of an axis system which proves most convenient and useful. Since, in this case, it is of primary interest to determine aircraft range relative to the earth, the equations of motion are derived to yield displacements relative to an observer fixed on the earth's surface as caused by forces acting along well-known aircraft axes.

The detailed derivation and the results are presented in the Appendix. The equations of linear motion are now available in their most complete form, and it is possible, by using one of several methods, to calculate the flight path relative to the earth of an aircraft flying in any direction at any latitude. However, as shown, the equations of linear motion are extremely complex for the general case. The possibility of neglecting terms and making simplifying assumptions will have to be investigated so that the amount of labor and time to calculate fairly accurate flight paths may be reduced.

Similar equations are presently being developed to express the angular motions of the aircraft relative to the earth. The complete set of equations, expressing linear and angular motion, will then form the basis from which the stability and control characteristics of a hypersonic vehicle may be investigated.

3. AERODYNAMIC PARAMETERS

a. Properties of Air: Flow Tables

An accurate knowledge of the physical properties of air at high temperatures (up to about 10,000°R) is a prerequisite for accurate analyses of high speed boundary layer or shock flows. Because of the complexity and experimentally unverified assumptions involved in computing these data, the field is still in a state of development and hence no authoritative source for such data exists. The aerodynamicist interested in flow problems involving high temperatures is thus forced to search the literature for information on the thermodynamic properties of air and also to evaluate this information to some extent and even to compute basic tables.

The usual gasdynamic tables for air which give the relations between state parameters before and behind normal or oblique shocks and which relate the state parameters in isentropic flow (cf e.g., Reference 29) are based on the assumptions that air is an ideal gas with constant specific heat. While the specific heat of air is nearly constant below 600°R, it increases rapidly for higher temperatures; furthermore, as shock strength increases with Mach number, the densities produced by shocks at hypersonic speeds are sufficiently high so that the behavior of the air deviates appreciably from that of an ideal gas. A program to compute tables of flow parameters for shock flow and isentropic flow, incorporating the effects of van der Waal's forces and variable specific heat for the range of temperatures at which dissociation is considered to be negligible, was under way at Bell Aircraft before the start of the MX-2276 study contract; these calculations have been completed and tables are being issued (Reference 92). A similar set of tables is contained in the Handbook of Supersonic Aerodynamics, Vol. 5 (Reference 59). However, the Bell Aircraft tables are more complete, i.e., they cover the whole range of altitude and Mach numbers corresponding to practical hypersonic flight conditions and, furthermore, they are presented in a form convenient for rapid practical use.

The above-mentioned shock flow tables were used for some sample calculations, assuming 100,000 ft altitude, to compare shock flow in an ideal air with shock flow in "Real" air taking into account variable specific heats and real gas effects. The results are shown in Figures 12 to 14, where the subscripts 1 and 2 denote qualities before and behind a shock, respectively. It is seen that at this altitude ideal gas flow predicts the pressure ratios behind shock quite closely even at a Mach number of 25, but that it overestimates the temperature ratio at this Mach number by 10%.

The effect of dissociation on the composition of air and on the values of the thermodynamic parameters is required for some boundary layer studies and as a prerequisite for extension of the flow tables to the dissociation

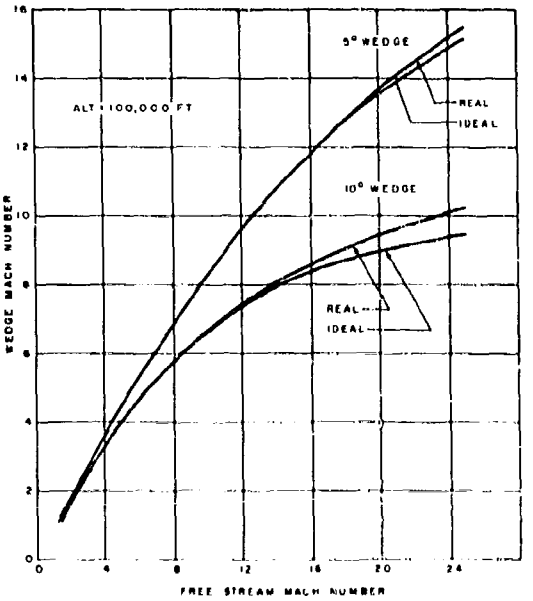

Figure 12. Wedge Mach Number vs Free Stream Mach Number

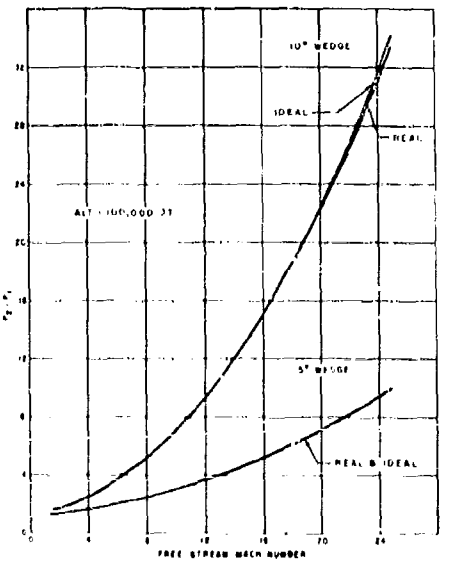

Figure 13. Static Pressure Ratio vs Mach Number

range of temperature. Previous tables of Hirschfelder and Curtiss, Reference 91, were based on a value of 7.54 electron-volts for the dissociation energy of nitroge , which is now generally regarded as incorrect. At the present time there exist no accurate tables of the composition of air at temperatures above 5400°R. Sources which may be calculating such tables are being checked.

An analysis was made of the theory underlying shock flow and isentropic flow in the dissociation range of temperature, and a procedure for calculating flow tables (using IBM equipment) was developed. Actual programming and carrying out of these extensive calculations await accurate tables for the composition of air considering dissociation effects.

b. Study of the Realms and Boundaries of Fluid Flow

In 1946, Tsien (Reference 9) suggested a set of criteria which roughly divided fluid

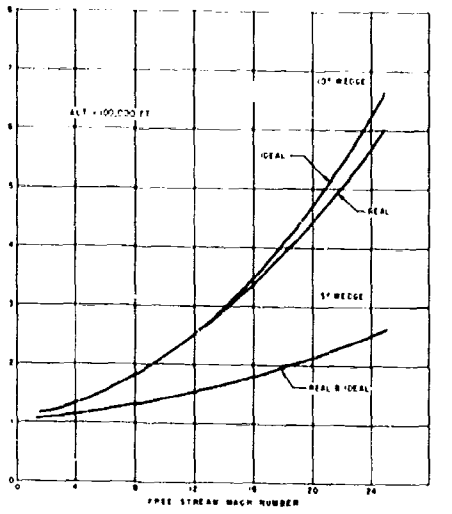

Figure 14. Static Temperature Ratio vs Mach Number

mechanics into several now familiar "realms" determined by the Mach number and Reynolds number of the flow. Essentially he defined the gasdynamic region, the slip flow region, and the molecular flow region. The nature of the flow phenomena and the form of the appropriate equations and boundary condition governing the flow is the same within a given region but is considerably different between the regions. The aim of the present study was to delineate more completely the various flow patterns and flow regions which would be encountered in hypersonic flight and to indicate in each region the fundamental equations and boundary conditions which must be considered in order to consistently and adequately represent the physical situation.

Nomenclature

a	velocity of sound
c	mean molecular speed
M	Mach number
p	pressure
Pr	Prandtl number
R	Universal gas constant
Re	Reynolds number
x,y	coordinates along and perpendicular to surface, respectively
γ	Ratio of specific heats
δ	boundary layer thickness
λ	mean free path
μ	viscosity
ν	kinematic viscosity
ρ	density

Subscripts

c	compressible
i	incompressible
w	wall
∞	free stream

In the following, our interest is restricted to the Reynolds numbers encountered in flight, namely $Re >> 1$, and to the continuum and slip flow regions.

Tsien defined the boundary between continuum and slip flow by the condition.

$$\frac{\lambda}{\delta} = 0.01 \qquad (1.1)$$

That is, he arbitrarily assumed that slip effects would start to be significant at a point in the boundary layer when the ratio of mean free path to local boundary layer thickness was 1/100. To translate this criterion into terms of M and Re, he took $\delta \approx x/\sqrt{Re}$, and then $\lambda \approx \nu/a$ from simple kinetic theory. Hence

$$\frac{\lambda}{\delta} = \frac{\nu}{a}\frac{\sqrt{Re}}{x}\frac{V}{V} = \frac{M}{\sqrt{Re}}$$

so that condition (1.1) becomes

$$\frac{M}{\sqrt{Re}} = 0.01 \qquad (1.2)$$

This boundary is shown in Figure 15.

Tsien, then, essentially estimated his boundary layer thickness from incompressible theory (Blasius' solution for incompressible flow is $\delta = \frac{5.2x}{\sqrt{Re}}$), and in application took λ as the free stream value. He neglected the numerical constants in the expression for δ and λ ($\lambda = 1.485\frac{\nu}{a}$) probably because of the arbitrary definition of the slip boundary as $\frac{\lambda}{\delta} = 0.01$. If these numerical constants are

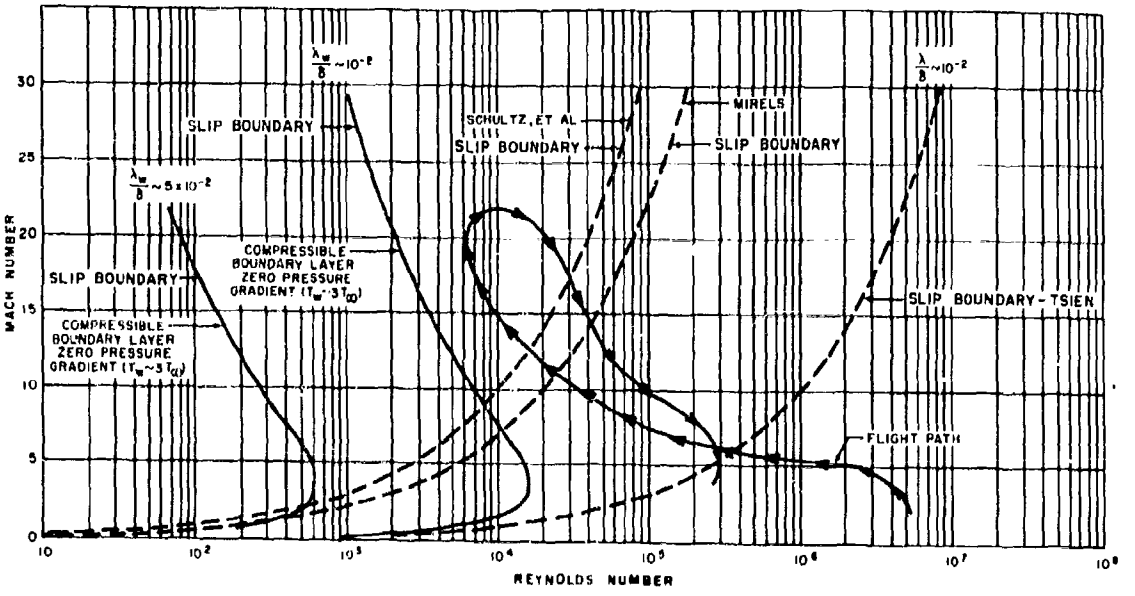

Figure 15. Realms and Boundaries of Fluid Flow

taken into account, the criterion (1.1) becomes

$$\frac{M}{\sqrt{Re}} = 0.035$$

A number of other investigators, Schultz, et al (Reference 10), Donaldson (Reference 11), Roberts (Reference 12), have also suggested criteria to define the realms of fluid mechanics; these have been compared by Siegel in Reference 13. Essentially these criteria differ from Tsien's in the value chosen for the physical ratios $\frac{\lambda}{\delta}$ assumed to define the slip region, but are similar in that the boundary layer thickness is estimated from incompressible theory. The criteria of Reference 10 and 11 are essentially equivalent and reduce to the assumption that

$$\frac{\lambda}{\delta} = 0.05$$

for the slip boundary, i.e., that

$$\frac{M}{\sqrt{Re}} = 0.1, \qquad (1.3)$$

when numerical constants in the expressions for δ and λ are employed. The difference between the criteria of Equations (1.1) and (1.3) is essentially due to the arbitrary definition of the value of λ/δ where slip effects would be expected to be significant. Which definition is more approximate is a question to be determined by experiment. It must be remembered, furthermore, that both criteria in the form of $\frac{M}{\sqrt{Re}}$ are dependent on the assumptions made for the boundary layer thickness.

Mirels' approach (Reference 14) to the definition of a boundary between slip and continuum flow was different from that outlined above. He first solved the Rayleigh problem for a compressible viscous gas, subject to slip at the wall. He then used this solution to obtain an estimate of skin friction on a semi-infinite flat plate under slip conditions, by relating time in the Rayleigh problem to distance downstream of the plate leading edge. The transformation from time to distance was chosen to yield an expression for skin friction which is in agreement in the continuum no-slip region with the known Chapman-Rubesin solution for compressible boundary layer on a flat plate. This transformation is thus proven valid only for low supersonic Mach numbers. Assuming slip to be significant in the region where the skin friction computed by the above-mentioned slip analysis differs from that obtained by a continuum analysis by 5% or more, a criterion for this boundary can be expressed in the form

$$\frac{M}{\sqrt{Re}} = 0.065 \qquad (1.4)$$

This boundary is also plotted in Figure 15. While Mirels' analysis does take into account the compressible nature of the boundary layer flow, it is probably not consistent at the high Mach numbers, say for M > 5.

As a first step in deriving a more complete and realistic delineation of the realms of fluid mechanics, an analysis following Tsien's was carried out, taking into account the compressible nature of the boundary layer which is manifested by a thickening of the boundary layer with Mach number (for constant Re) and variation of the mean free path λ through the boundary layer because of the temperature variation.

An approximate expression given by Howarth for the boundary layer thickness on an insulated plate, assuming Pr = 1, namely

$$\delta_c \simeq \delta_i \ (1 + 0.08M^2) \qquad (1.5)$$

is used in the following analysis for simplicity. The expression (1.5) for δ is compared with the results of the more exact theory of Crocco and an approximate theory of Young in Figure 16, and is seen to give the correct trend of boundary layer thickening with Mach number.

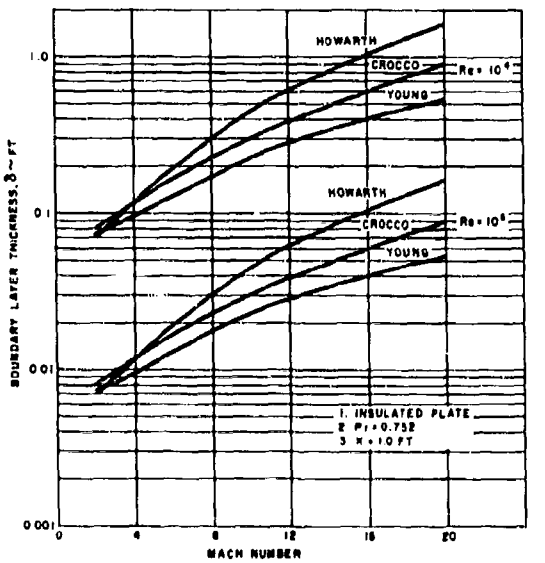

Figure 16. Boundary Layer Thickness vs Mach Number for a Flat Plate

With this δ, and taking the significant value of λ for slip as that at the wall, the ratio of λ/δ can be expressed as

$$\frac{\lambda_w}{\delta_c} = \lambda_\infty \left(\frac{T_w}{T_\infty}\right) \frac{1}{\delta_i (1 + 0.08M^2)} \qquad (1.6)$$

In the above, λ_w is obtained from elementary kinetic theory as follows:

$$\lambda = 1.485 \frac{\nu}{a} = 1.485 \frac{\mu}{\rho a}$$

$$= \frac{1.485}{\sqrt{\gamma R}} \frac{\mu}{\sqrt{T}} \frac{1}{\rho}$$

and $\mu = \text{const.} \sqrt{T}$;

thus $\lambda = \text{const.} \frac{1}{\rho}$.

With the usual assumptions of ideal gas and pressure constant across the boundary layer,

$$\frac{\rho_w}{\rho_\infty} = \frac{T_\infty}{T_w}$$

and thus, $\lambda_w = (\frac{T_w}{T_\infty})\lambda_\infty$.

As has been shown above

$$\frac{\lambda_c}{\delta_1} = 0.285 \frac{M}{\sqrt{Re}}$$

and assuming a practical value of $T_w = 3T_\infty$, then Eq. (1.6) becomes

$$\frac{\lambda_w}{\delta_c} = 0.8 \frac{M}{\sqrt{Re}} \frac{1}{(1 + 0.08M^2)} \qquad (1.7)$$

Now, using the same basic definition as Tsien for the slip boundary, namely $\frac{\lambda_w}{\delta_c} = 0.01$, we obtain the slip boundary as

$$\frac{M}{(1+ 0.08M^2)} \frac{1}{\sqrt{Re}} \approx 0.012;$$

this boundary is plotted in Figure 15. Also shown is the slip boundary defined by $\frac{\lambda_w}{\delta_c} = 0.05$, to compare with the criteria of Shultz, et al.

The results of elementary considerations of the boundary between continuum and slip flow are summarized in Figure 15. Previous analyses, Mirels' excepted, which set the condition for the slip boundary variously as $\frac{\lambda}{\delta} = 0.01$ and $\frac{\lambda}{\delta} = 0.05$, did not take into account the compressible nature of the boundary layer in translating this physical condition for the boundary into the more useful condition in terms of M and Re. The validity of Mirels' analysis for the higher M is doubtful. The present analysis accounts in an approximate way for the thickening of the boundary layer with increasing Mach number, and the practical effect of aerodynamic heating in raising the temperature of a plate in hypersonic flow and hence increasing the mean free path in the flow adjacent to the plate. It is seen that for an assumed physical condition, for the magnitude of $\frac{\lambda}{\delta}$ where slip effects might be considered as significant, the previous analyses give a much more conservative boundary in the M - Re plane than the more practical analysis considered herein. As an indication of the regions of interest to MX-2276, the path of a point 1 ft. back from the leading edge of a flat plate following the flight path of Figure 9 is plotted in Figure 15.

The next step in building up a precise delineation of the realms of fluid mechanics was to consider the effect of bow shock wave-boundary layer interaction. The usual picture of the flow pattern over a flat plate at zero angle of attack is shown in Figure 17. It consists of a narrow boundary layer region adjacent to the plate where the viscosity of the fluid is manifested, and a larger region outside of this layer where the flow can be considered as essentially inviscid. The shock wave is formed because of streamlines of the inviscid outside flow are deflected by this boundary layer, i.e., the inviscid flow actually "sees" a nearly parabolic section corresponding to the boundary layer displacement thickness rather than the flat plate. This "induced" shock and the flow behind it cause a pressure gradient along the plate. For the usual supersonic flow condition of low Mach number and high Re, the boundary layer is sufficiently thin so that the "induced" shock is weak and its effect on pressure over the plate negligible. In this case the flow is analyzed in two parts; the inviscid flow over the flat plate (or, in general, a body shape) ignoring the boundary layer, and the boundary layer on the plate (or general body) in uniform

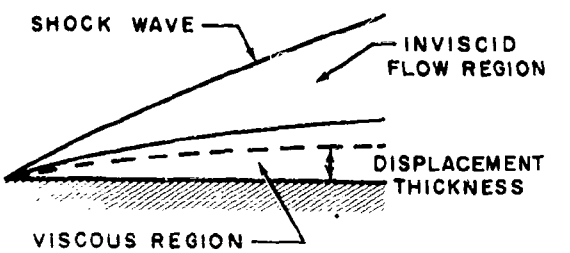

Figure 17. Flow Pattern over a Flat Plate at Zero Angle of Attack

flow (or in the derived flow field for the general body shape). For higher M and lower Re the boundary layer thickens sufficiently to cause an appreciable interaction between the inviscid and viscous flow regions in this type of analysis. Physically, a weak interaction is defined by the ratio of the induced pressure gradient to the inertial term in the equations governing the boundary layer flow. When the order of magnitude of this ratio is less than 1/100, the interaction can effectively be ignored; when the ratio is of the order of 1/100, the interaction is called weak; and when the ratio is of the order one or more, the interaction is called strong. In the latter case the flow pattern as assumed in Figure 17 is not obtained, but rather the whole region between plate and induced shock must be considered as viscous.

The analysis of Shen, Reference 17, for the problem of weak interaction shows that the ratio of induced pressure gradient/inertia terms at a distance, L, from the plate leading edge can be expressed in terms of the parameter $1/(M\frac{\delta}{L})^2$; thus, this ratio is 1/100 when $\frac{M\delta}{L} = \frac{1}{10}$. To delineate the region of weak interaction in the M-Re plane, it is necessary first to obtain an expression for $\frac{\delta}{L}$ in terms of M and Re. The value of δ, uncorrected for interaction, may be applied in order to obtain an estimated lower bound of the region of weak interaction. Consequently, the Howarth formula (1.5) could have been used. However, it was convenient to follow Shen (loc. cit.) and use the relation

$$\frac{\delta}{L} \approx M^{1+\omega}\, Re^{-1/2}$$

which accounts somewhat more accurately for the boundary layer behavior at the higher Mach numbers. The weak interaction boundary can then be expressed as

$$M\frac{\delta}{L} \approx \frac{M^{2+\omega}}{Re^{1/2}} = \frac{1}{10}. \qquad (1.8)$$

where $\omega = 0.78$ was used in computing the boundary shown in Figure 18. Lees and Probstein, Reference 18, arrived at the same boundary given by Equation (1.8), but used the less general assumption that $\omega = 1$ throughout their analysis.

In the case of strong interaction the ratio (induced pressure gradient/inertia terms) is still $1/(M\frac{\delta}{L})^2$. In this case, however, the value of $\frac{\delta}{L}$ must be obtained by considering the induced pressure gradient which appreciably influences the boundary layer growth. Shen, Reference 20, Li and Nagamatsu, Reference 21, and Lees, Reference 19, obtained essentially the same result,

$$\frac{\delta}{L} = \text{const.}\,\frac{M^{\omega/2}}{Re^{1/4}}\,. \qquad (1.9)$$

Hence, the strong interaction boundary defined by the ratio (induced pressure gradient/inertial terms) equal to one can be expressed as

$$\frac{M^{2+\omega}}{Re^{1/2}} = 1 \qquad (1.10)$$

This boundary is also shown in Figure 18. It is interesting to note that the parameters defining the weak and strong interaction boundaries in the M-Re plane turn out to be identical.

The boundary between continuum and slip flow regions was rederived for the region where strong interaction would be expected. The analysis follows along the same lines as explained above, where now the expression of Equation 1.9 for the growth of δ as influenced by the self-induced pressure gradient is used, with the values of 0.6 for the constant in this expression given by Li and Nagamatsu (loc. cit.) and Shen (loc. cit.). For the criteria that slip occurs when $\frac{\lambda_w}{\delta_c} = 0.01$ (assumed by Tsien), the boundary in the M-Re plane, taking into account compressibility effects including strong bow shock-boundary layer interaction, is

$$\frac{6\,M^{3/5}}{Re^{3/4}} = \frac{1}{100}\,. \qquad (1.11)$$

This boundary is shown in Figure 18 and can be compared there with the criterion of Tsien

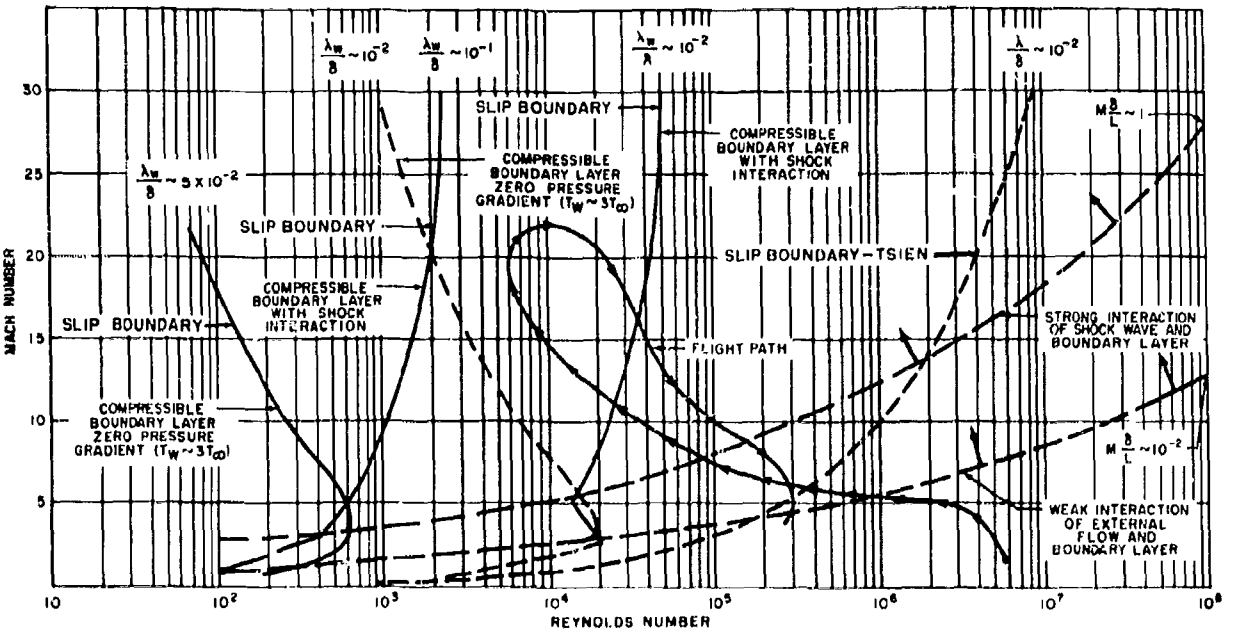

Figure 18. Realms and Boundaries of Fluid Flow

from Figure 15 (who assumed essentially an incompressible boundary layer) and the boundary obtained previously by taking into account compressibility effects without a self-induced pressure gradient. The Tsien criterion is seen to predict slip at lower Mach numbers and Reynolds numbers in comparison with the more realistic boundary derived herein, while the latter does the reverse. A boundary in the M-Re plane defined by the more optimistic physical criteria that slip effects will not become significant until

$$\frac{\lambda_w}{\delta_c} = \frac{1}{10}$$ is also shown.

In Figure 18, each boundary calculated for the strong shock region is joined to the corresponding boundary previously obtained without shock interaction by a straight line through the region of weak interaction; the boundaries could not be obtained any more accurately in the latter region since the actual form of the growth of δ there is not known.

The above delineation of the various regions in the M-Re plane where continuum flow can be assumed, where slip flow probably occurs, and where significant shock wave-boundary layer interaction occurs is of practical importance in evaluating the limits of applicability of the various aerodynamic theories and methods. It indicates the fundamental equations and boundary conditions which govern the flow (and hence, by deduction, the aerodynamic parameters) at each flight condition. Some further considerations on the appropriate fundamental equations to describe hypersonic flow are given briefly below.

One consideration is whether or not the Navier-Stokes equations adequately describe the physical flow throughout the whole field of interest. So far the adequacy of the Navier-Stokes equations has been tacitly assumed in the use of expressions for the boundary layer thickness, δ, derived from these equations and in the analysis of shock boundary layer interaction. It is known, however, that the Navier-Stokes equations are

only a first approximation to the complete equations governing viscous flow, as derived from the kinetic theory of nonuniform gases by Maxwell, Boltzmann, Chapman, Enskog, and others. The kinetic theory gives two correction terms to the Navier-Stokes equations which, while negligible for gases under ordinary pressure, become important for rarified gases and very high speed gas flow.

In order to obtain a clear indication of where the Burnett (Reference 22) correction terms to the Navier-Stokes equations may be expected to be significant, a careful analysis of the order of magnitude of all the Burnett terms relative to the Navier-Stokes term in the complete boundary layer equations was made. The approach followed was similar to that given by Tsien (Reference 9, pp. 655-656) who, however, only checked the relative magnitude of typical terms, rather than every term. The very lengthy and detailed analysis required for a careful comparison will not be reproduced here, but the essential results can be roughly interpreted as follows:

(a) In the x-momentum equation the ratio of Burnett to ordinary viscous term is $M\frac{\lambda}{\mathscr{L}}$, where $\mathscr{L}$ is a characteristic length of the plate.

(b) In the y-momentum equation, the ratio of Burnett to ordinary viscous term is

$$M\,\frac{\lambda}{\delta}\,\frac{\mathscr{L}}{\delta}$$

Thus in the region where $M\frac{\lambda}{\delta} \ll 1$, but $M\frac{\lambda}{\mathscr{L}}$ is between 0.1 and 1, the ordinary (Navier-Stokes) x-momentum equation may be used. Now from (b), $\frac{\partial p}{\partial y}$ due to the Burnett terms is $M\frac{\lambda}{\delta}\frac{\mathscr{L}}{\delta}$ times the y-inertia terms (Navier-Stokes), and the y-inertia term in $\frac{\delta}{\mathscr{L}}$ times the x-inertia term, hence $\frac{\partial p}{\partial y}$ is $M\frac{\lambda}{\delta}$ times the x-inertia term.

When the value of $M\frac{\lambda}{\delta}$ is not negligible compared with one, the Navier-Stokes equations must be supplemented by Burnett terms in order to provide an adequate and consistent approximation to the physical flow. The additional terms first appear in the y-momentum equation and imply that there is a pressure gradient across the boundary layer, the magnitude of which, in any particular case, must come from a solution of the appropriate equations. It is stressed at this point that the purpose of the foregoing analysis was to determine the fundamental set of equations and boundary conditions which govern the flow in the range of hypersonic flight conditions of interest and, in particular, to indicate where the Navier-Stokes equations are no longer adequate. The Navier-Stokes equations are the basis of practically all present boundary layer theories from which, in turn, methods for prediction of skin friction and heat transfer parameters are derived. The present analysis serves as a guide in evaluating the accuracy of their use and as a basis in which more exact theories and then methods can be developed.

In Figure 19, a curve of $M\frac{\lambda}{\delta} = \frac{1}{10}$ is shown; above this curve the order of magnitude of some Burnett terms is at least 1/10 that of the Navier-Stokes terms and should therefore be included in fundamental equations, while below the curve the order of magnitude of the Burnett terms are less than 1/10 that of the Navier-Stokes equations, and may or may not be significant.

For comparison, a curve of $M\frac{\lambda}{\delta} = \frac{1}{100}$ is also presented. The above analysis suggests a pressure gradient across the boundary layer in high Mach number flow which should be possible to verify by experiment. Previous boundary layer experiments in hypersonic flow have been at Reynolds numbers much higher than that at which this effect is predicted.

The expression for δ as a function of M and Re used in obtaining this curve varies as the regions of strong interaction, weak interaction or no interaction are encountered. This accounts for the appearance of discontinuities in the $M\frac{\lambda}{\delta}$ curve at the interaction boundaries. Because of the approximate nature of these considerations, the boundary curves obtained are

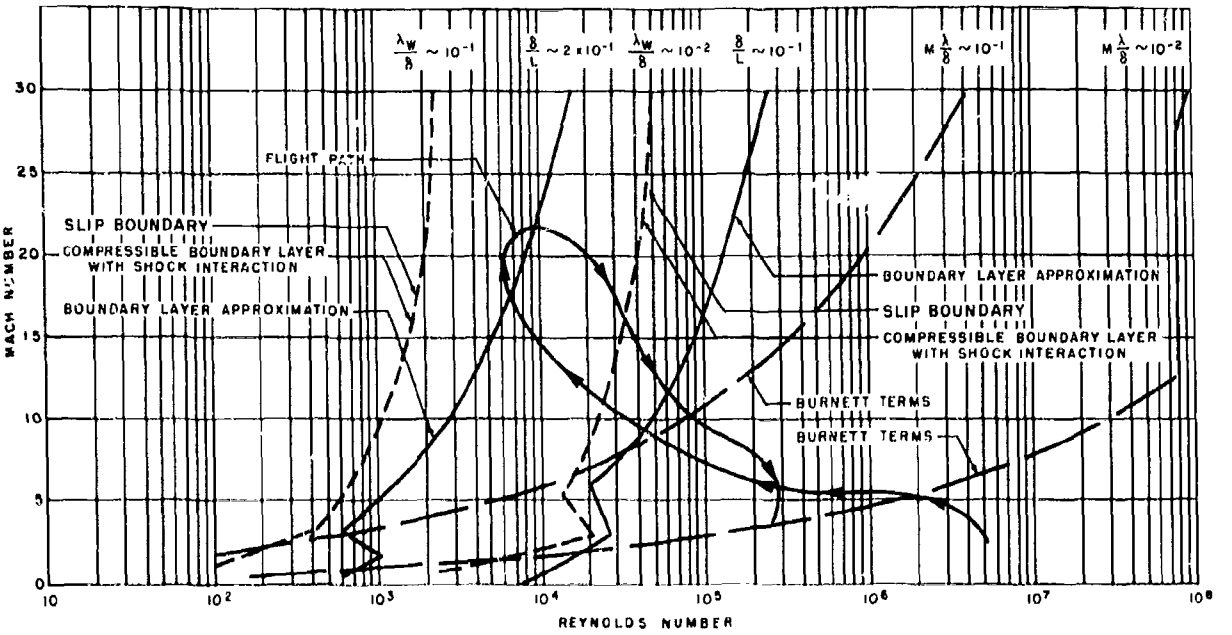

Figure 19. Realms and Boundaries of Fluid Flow

only indicative of where the effect considered may occur and should not be construed as being exact.

The foregoing considerations were concerned with determining the appropriate fundamental equations to describe a given flight condition. In considering boundary layer flow, however, the complete fundamental equations are not amenable to solution. Employing the usual boundary layer approximations (i.e., following the assumption that owing to the extreme thinness of the boundary layers, derivatives of a quantity normal to the boundary layer are of an order of magnitude larger than derivatives of the same quantity along the layer), an order of magnitude analysis leads to a reduced approximate set of equations - the usual boundary layer equations (starting from the Navier-Stokes equations). Because of the thickening of the boundary layer with increasing Mach number and decreasing Reynolds number of flight, it is of interest to note where the validity of this approach will be expected to break down. The indicative quantity for this purpose is $\frac{\delta}{L}$, the ratio of boundary layer thickness to distance from the plate leading edge. Curves of $\frac{\delta}{L} = \frac{1}{10}$, and $\frac{\delta}{L} = \frac{1}{5}$ are shown in Figure 19; above the curve $\frac{\delta}{L} = \frac{1}{5}$ the ratio of $\frac{\delta}{L}$ is greater than $\frac{1}{5}$, and below it less than $\frac{1}{5}$; the $\frac{\delta}{L} = \frac{1}{10}$ curve is interpreted in the same fashion. Certainly when $\frac{\delta}{L} = \frac{1}{5}$ and probably even when $\frac{\delta}{L} = \frac{1}{10}$, the validity of the usual boundary layer approximation must be carefully considered.

Figure 20 shows a superposition of the various "boundaries" shown separately for clarity in Figures 15, 18, and 19. These boundaries were obtained from a consideration primarily of the mechanics of fluid flow. It is of interest also to indicate where thermodynamic effects may become important and should be taken into

account in analyses of boundary layer flow. For this purpose, an estimate was made of the flight conditions - Mach number and altitude - at which the maximum temperature attained in the boundary layer would cause a preassigned amount of equibilrium dissociation of the air. The results are shown in Figure 21; the exemplary amounts of dissociation considered were 0.5% and 5%, and the degree of dissociation as a function of temperature and pressure was obtained from the tables of Krieger and White, Reference 23*. The temperature distribution in the boundary layer was interpolated from Crocco's work (Reference 16) for the cases of an insulated flat plate and for the more practical case of a plate with $T_W = 3T_\infty$

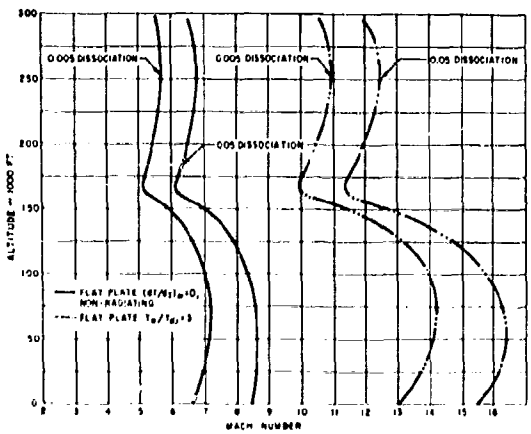

Figure 21. Flight Regions of Dissociation in Boundary Layer

* It is known that these tables are somewhat incorrect, cf. sect. IV-B3a, but they are sufficiently accurate for the present analysis.

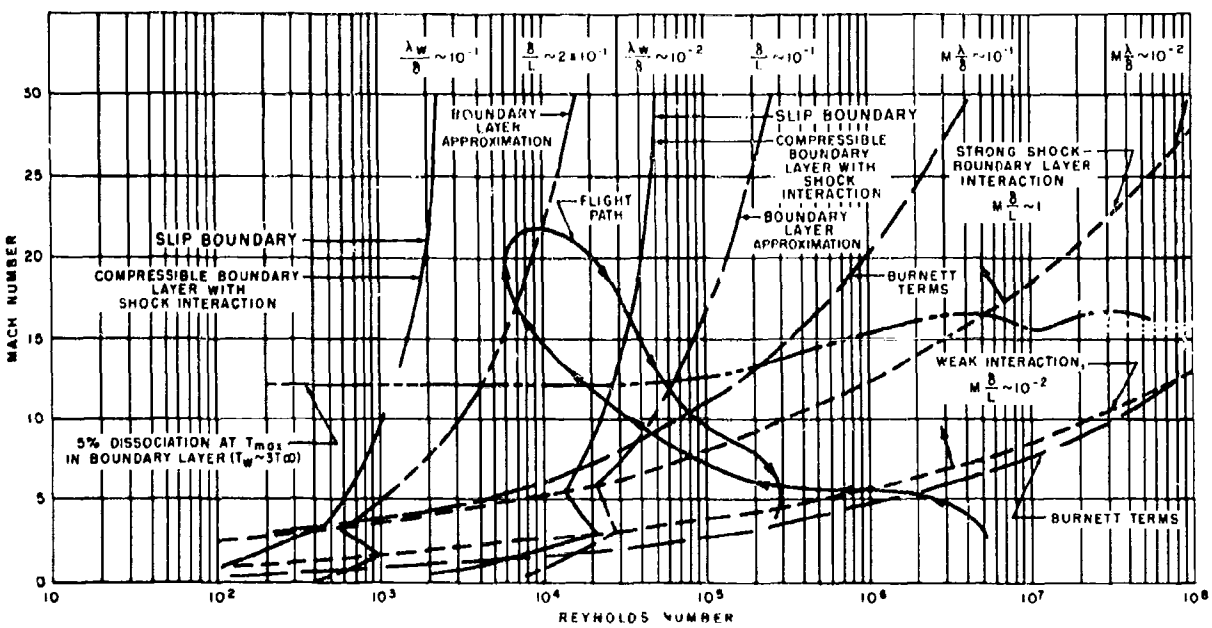

Figure 20. Realms and Boundaries of Fluid Flow

The curve for 5% dissociation with $T_W = 3T_\infty$ was then replotted in Figure 20. In the region above this curve, there will be approximately 5% or more dissociation of the air at some point in the boundary layer. This rough consideration only indicates where dissociation might have an effect in the boundary layer and therefore should be considered in the fundamental equation governing flow in this region. The exact nature and magnitude of the effect of dissociation on skin friction and heat parameters can then be determined only by a solution of the appropriate equations. The latter has been attempted for some special cases by Moore and Crown (References 24 and 25).

The various "boundaries" and "indicator" curves arising out of the whole of the foregoing analysis have been replotted in Figure 22 (located in the pocket in the back cover) in a Mach number-altitude plane, as they apply to a point one foot back from the leading edge of a flat plate. The wing chord of a possible design configuration for an MX-2276 (of Reference 1) type aircraft ranges from 40 to 8 feet, with a weighted mean of about 18 feet. Thus conditions at a point one foot from the leading edge are significant in determining over-all as well as local values of the aerodynamic parameters.

c. Thermodynamic Phenomena in Hypersonic Flow

The fundamental nature of the thermodynamic problems encountered in the Mach number range from zero to twenty-five can be clearly demonstrated by a diagram of the energy spectrum of the gas on the atomic scale. The average translational kinetic energy of each molecule of air relative to the aircraft can be expressed in the form $\frac{m}{2}\frac{3a^2}{\gamma}\left(1+\frac{\gamma}{3}M^2\right)$, where a is the velocity of sound, γ is the ratio of specific heats, and m is the mass of a molecule of the air. This relationship between kinetic energy and Mach number is represented by the parabolic curve in Figure 23. The characteristic energy values for the vibrational energy levels, and the dissociation energies of the air molecules are indicated as well as the sublimation energies of typical solids.

From this energy diagram it can be seen that the relative kinetic energy of the typical gas molecule at high Mach number is greater than the energy of its chemical bond, i.e., it has sufficient energy to produce dissociation. Furthermore, at sufficiently high speeds, the relative kinetic energy is greater than the energy required to remove a single atom from a common metal, i.e., the sublimation energy. These facts suggest that thermodynamic and chemical phenomena not apparent at ordinary supersonic speeds will be observed at high Mach numbers because there is now enough energy available to produce them. For example, the accommodation and slip coefficients, which depend on the nature of the interaction between the gas particles and the surface, would not be expected to retain their low speed values.

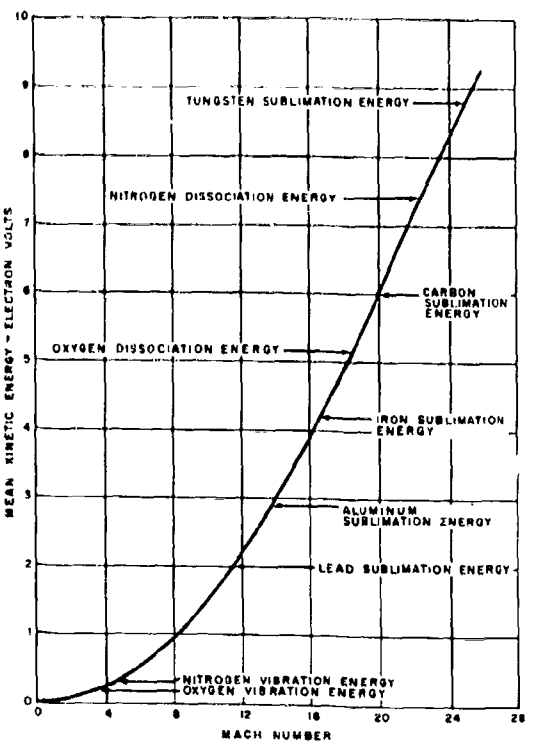

Figure 23. Kinetic Energy of Air Molecules as a Function of Mach Number

The possibility of erosion of the solid surface by the air at high Mach numbers is sufficiently large to warrant a brief investigation of this problem. Consideration is being given to devising simple experiments which could demonstrate this effect.

The problem of aerodynamic heating in hypersonic flow at Mach numbers greater than 10 where dissociation must be taken into account was first considered in some detail by Moore (Reference 24) and subsequently in brief by Hanson (Reference 26) and Crown (Reference 25). However, none of these investigators considered the role played by diffusion in the mechanism of heat transfer whereby the dissociation energy is transported from the hotter to the cooler part of the gas, although it is known both theoretically and experimentally from the works of Langmuir (Reference 27), Nernst (Reference 28), and other investigators, that diffusion will appreciably affect the values of the transport properties of the gas. An investigation and an evaluation of this effect is now under way.

The study (cf. Reference 93) to estimate the effect of heat radiation into a surface from an adjacent hot boundary layer (where $T_{max} \cong$ 10,000° R) will be completed as soon as the basic physical data on the emissitivity of air are obtained.

d. Aerodynamic Heating

(1) General

In the hypersonic flight regime contemplated, the heat transfer from the viscous boundary layer to the aircraft skin produces skin temperatures of the same order as the limiting temperatures for the integrity of the structural materials (e.g., see the skin temperatures given in Reference 1). Thus, temperature becomes a paramount consideration of the structural designer. Also, the structural temperatures place definite restrictions on the flight plan and the aerodynamic configuration and so must be included in the preliminary design of a vehicle as well as in later more detailed studies. A review of the extensive literature on aerodynamic heat transfer and discussions with other research agencies has disclosed a number of methods for estimating high speed heat transfer characteristics which are not in complete agreement. For this reason, the greatest part of the heating study made to date has consisted of an analysis of methods of estimation of heat transfer. This led to the selection of the method described herein for the preliminary engineering estimations of heat transfer which are to be made under the study contract. The nature of the heat transfer calculation is such that any small gain in accuracy is accomplished only through a considerable increase in time and complexity of calculation. A comparison between the temperatures obtained using this approximate method and those obtained when additional refinements are included will be presented in the future.

In the strictest sense, the method described applies only to two-dimensional, flat plate flow with no pressure or temperature gradients. However, it should be remembered that it is proposed to use the method only as a first approximation. It will not be used where it is known to give misleading results. The method is also subject to the general gas dynamics limitations discussed earlier (See Section IV-B, 3b) and does not include the effects of dissociation or of shock-boundary layer interaction. The use and limitations of the method will be discussed in more detail later in this section.

(2) Skin Friction and Heat Transfer Coefficients

The first step to be considered in the calculation of viscous heating is the estimation of the heat transfer coefficient. Implicit in this estimation is the consideration of the closely related skin friction coefficient. The method proposed for the estimation of these coefficients is the use of the well-known constant property incompressible relations extended to supersonic and hypersonic conditions by evaluating the air properties in these relations at a reference temperature - a weighted mean temperature which occurs within the compressible boundary layer. The reference temperature is expressed as a function of the wall, stream, and recovery temperatures (and thus Mach number).

This semi-empirical theory was derived for laminar flow but, from its agreement with test results, also appears to be applicable to turbulent flow. It is well adapted to engineering calculation and has been used in other hypersonic studies (References 30 and 31).

Eckert (Reference 32) in a recent survey of heat transfer also recommends this approach and shows that excellent agreement can be obtained with the more exact theories in the laminar flow case and with the available experimental data in the turbulent flow case. Eckert presents and discusses the method in considerable detail. Therefore, it is presented only in brief form here for the sake of completeness and to indicate the interpretation proposed for the current study.

The following relations are stated for incompressible flow. In their use and extension, two-dimensional plate flow with no pressure or temperature gradients is implied. The symbols used are given in Table III. The wall shearing stress is expressed as

$$\tau_W = c_f \frac{\rho}{2} V_\delta^2 .$$

For laminar flow, the skin friction coefficient and Stanton numbers are

$$\frac{c_f}{2} = 0.332/\sqrt{Re} = 0.332/\sqrt{\frac{V_\delta \rho x}{\mu}}$$

$$St = \frac{h}{c_p \rho V} = \frac{c_f}{2} (Pr)^{-2/3} .$$

For turbulent flow, the skin friction coefficient and Stanton number are

$$\frac{c_f}{2} = 0.0296\ Re^{0.2} = 0.0296 \left(\frac{V_\delta \rho x}{\mu}\right)^{-0.2}$$

$$St = \frac{h}{c_p \rho V} = \frac{c_f}{2} S ,$$

where S is approximately 1.2 (Reference 32).

TABLE III

AERODYNAMIC HEATING SYMBOLS

c_f	Skin friction coefficient	dimensionless
c_p	Specific heat, constant pressure	Btu/lb-°F
c_v	Specific heat, constant volume	Btu/lb-°F
g	Gravitational constant	ft/sec^2
G	Solar radiation	Btu/ft^2-hr
h	Convective heat transfer coefficient	Btu/ft^2-°F-hr
J	Mechanical equivalent of heat	ft-lb/Btu
M	Mach number	dimensionless
P	Pressure	lb/ft^2
Pr	Prandtl number	dimensionless
q	Rate of heat flow	Btu/ft^2
r	Recovery factor	dimensionless
R_o	Gas constant	lb/°F
Re	Reynolds number	dimensionless
St	Stanton number	dimensionless
T	Temperature	°R
V	Velocity	ft/sec
w	Specific weight	lb/ft^3
x	Distance from leading edge	feet
y	Thickness of skin	feet
α	Absorptivity	dimensionless
γ	Ratio c_p/c_r	dimensionless
ϵ	Emissivity	dimensionless
θ	Time	seconds
μ	Viscosity	lb-sec/ft^2
ρ	Density	slugs/ft^3

TABLE III

AERODYNAMIC HEATING SYMBOLS (CONT)

σ	Stefan-Boltzmann constant	1.73×10^{-9} x BTU / sq ft x $°R^4$ x hr
ω	Power law exponent	dimensionless

Subscripts

c	Compressible flow
i	Incompressible flow
L	Laminar flow
r	Recovery - boundary layer - adiabatic wall
t	Total stagnation
T	Turbulent flow
W	Wall condition
δ	Local free stream

Superscript

'	Indicates reference temperature conditions

If the pressure across the boundary layer is assumed constant, the following expressions for heat transfer coefficients can be written:

Laminar flow:

$$h = 928.0 \left(\frac{P_\delta V_\delta}{x}\right)^{1/2} \left[\left(\frac{\mu}{T}\right)^{1/2} - \frac{c_p}{Pr^{2/3}}\right]$$

Turbulent flow:

$$h = 10.66 \left(\frac{P_\delta V_\delta}{x^{0.2}}\right)^{0.8} \frac{\mu^{0.2}}{T^{0.8}} c_p .$$

The question then arises, at what temperature should the temperature variant properties, ρ, μ, cp, and Pr be evaluated. The boundary layer temperature profile varies considerably as a function of velocity and wall temperature. Rubesin and Johnson (Reference 33) have advanced a constant property solution for laminar flow based upon the reference temperature

$$T'/T_\delta = 1 + 0.58 \left(T_w/T_\delta - 1\right) + 0.032 M_\delta^2 .$$

This relation also has been used in turbulent analysis, e.g., References 30 and 31.

In discussions with personnel at the NACA Ames Laboratory the following reference temperature was proposed.

$$T'/T_\delta = 1 + 0.45 \left(T_w/T_\delta - 1\right) + 0.040 M_\delta^2 .$$

Use of this reference temperature had given good correlation with the turbulent skin friction data obtained from wind tunnel tests by Chapman and Kester (Reference 34) and with turbulent data from the free flight wind tunnel, at least partially presented in Reference 37. They had also compared the friction coefficients from tests of low speed flow in heated pipes with those predicted using the T' method and had found verification.

Eckert recently has modified the coefficients in the T' relation to

$$T' = 0.5 \left(T_w + T_\delta\right) + 0.22 \left(T_r - T_w\right) ,$$

or for comparison with the previous relations to

$$T'T_\delta = 1 + 0.5 \left(\frac{T_w}{T_\delta} - 1\right) + 0.22 r \cdot \frac{\gamma - 1}{\gamma} M_\delta .$$

This relation appears to have been derived from the more exact laminar theory for a greater range of temperatures than the equation of Johnson and Rubesin.

The preceding T' relations have been used with the incompressible relations stated to give the curves shown in Figure 24 which are compared with available turbulent data. In calculating the curves it was assumed that $r = 0.9$, $\gamma = 1.4$, and $\frac{\mu'}{\mu_\delta} = \left(\frac{T'}{T}\right)^{0.72}$. It is seen that for the case of $T_W = T_r$ they are very similar and are in good agreement with the test data. For the two conditions where T_W is close to T_δ, the NACA and the Eckert relations give the closest agreement with the data. In view of this the Eckert T' relation will be used; it appears to have been carefully considered and to have a greater range of applicability with respect to laminar flow, and compares favorably for turbulent conditions.

The following equations give the relationship of actual compressible skin friction for both laminar and turbulent flow.

Laminar Flow:

$$\frac{c_{f_c}}{c_{f_i}} = \left(\frac{\mu'}{\mu_\delta}\right)^{1/2} \quad \left(\frac{\rho'}{\rho_\delta}\right)^{1/2},$$

Turbulent flow:

$$\frac{c_{f_c}}{c_{f_i}} = \left(\frac{\mu'}{\mu_\delta}\right)^{0.2} \quad \left(\frac{\rho'}{\rho_\delta}\right)^{0.8},$$

where the c_f's are both defined by the relation $c_f = \frac{\tau_W}{1/2 \rho_\delta V_\delta^2}$ and the primed quantities are evaluated at the reference temperature. The above equations have been evaluated and are plotted versus T' in Figure 25 using 400°R as a base. The solid lines represent the functions that are obtained by using the NACA-NBS tables (Reference 35).

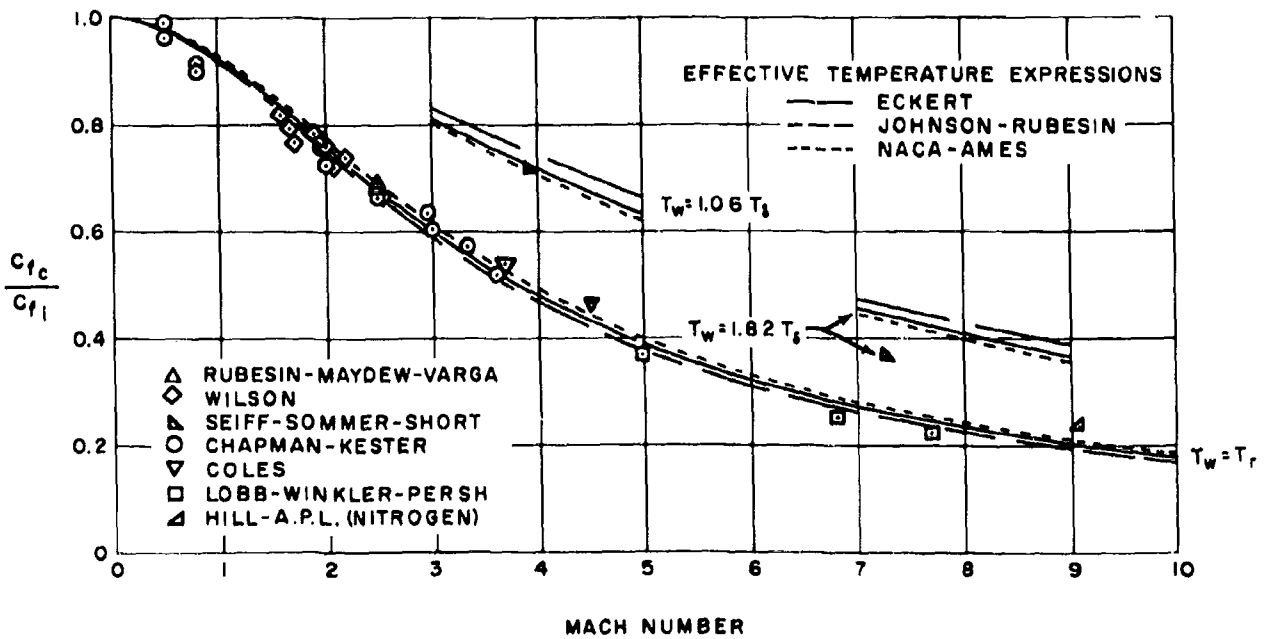

Figure 24. Variation of Compressible Skin Friction Coefficient for Turbulent Flow (Comparison of Experiment with the Effective Temperature Method)

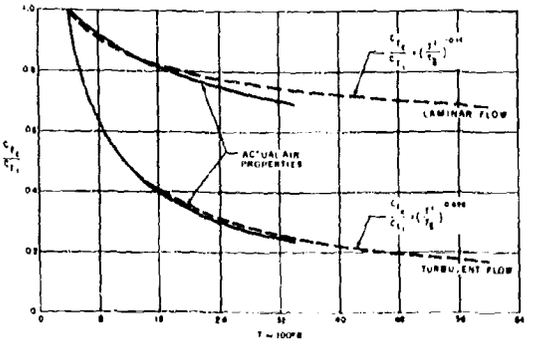

Figure 25. Skin Friction Coefficient Correction Factor

Similarly, from the heat transfer coefficient equations, the following relations give the ratio of the compressible heat transfer coefficients to the incompressible coefficients.

Laminar flow:

$$\frac{h_c}{h_i} = \left(\frac{\mu'}{\mu_\delta} \cdot \frac{T_\delta}{T'}\right)^{1/2} \cdot \frac{c_p'}{c_{p_\delta}} \left(\frac{Pr_\delta}{Pr'}\right)^{2/3},$$

Turbulent Flow:

$$\frac{h_c}{h_i} = \left(\frac{\mu'}{\mu_\delta}\right)^{0.2} \left(\frac{T_\delta}{T'}\right)^{0.8} \cdot \left(\frac{c_p'}{c_{p_\delta}}\right).$$

These equations are evaluated and plotted in Figure 26 as a function of T' with 400°R as the base. Again the solid lines give the results using the NACA-NBS tables. However, the Prandtl number is given only to 1800°R in these tables; after this point it is assumed the Prandtl number has a constant value of 0.715, after Chapman and Cowling. It is felt that other property values at the higher temperatures are less certain and it must be stated that at the higher values of T', particularly above 1800°R, the validity of the curves becomes less certain.

The effective temperatures encountered in the proposed MX-2276 flight plan will be greater than those for which there are established values for the air properties, as shown by the solid lines in Figures 25 and 26. One then wonders how to extend the curves reasonably. Power law variations of the air properties with temperature suggest themselves because of their convenience and because they have commonly been used as approximations in this situation in heat transfer work. A fair over-all fit to the actual data curves is attained through use of the following air property variations.

$$\frac{\mu'}{\mu_\delta} = \left(\frac{T'}{T_\delta}\right)^{0.72}$$

$$\frac{k'}{k_\delta} = \left(\frac{T'}{T_\delta}\right)^{0.83}$$

$$\frac{c_p'}{c_{p_\delta}} = \left(\frac{T'}{T_\delta}\right)^{0.08}$$

$$\frac{\rho'}{\rho_\delta} = \left(\frac{T'}{T_\delta}\right)^{-1.0}.$$

These relations give the dashed curves on Figures 25 and 26. It is seen that the power law representations are best for the turbulent case where they match the tabulated value curves

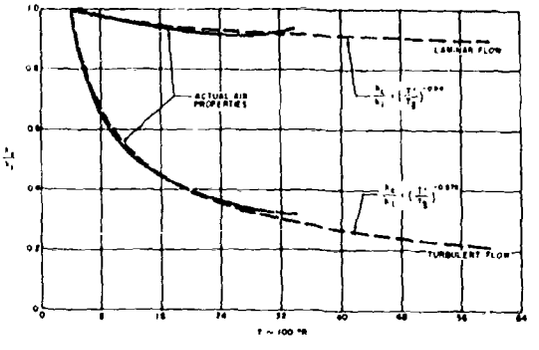

Figure 26. Heat Transfer Coefficient Correction Factor

fairly well, particularly in the temperature range below 1800°R where the tabulated values are most certain. The power law variations appear to less advantage in the laminar case but may be adequate for the laminar heat transfer where the total h_c/h_i variation is small.

If for the present the power variations of compressible heat transfer coefficient with temperature are adopted, then:

Laminar flow:

$$\frac{h_c}{h_i} = \left(\frac{T'}{T_\delta}\right)^{-0.040} ,$$

Turbulent flow:

$$\frac{h_c}{h_i} = \left(\frac{T'}{T_\delta}\right)^{-0.576} ,$$

and then through substitution of the equation for effective temperature the carpets shown on Figures 27 and 28 are obtained. These give, perhaps, a better picture of the effects of Mach number and wall-to-stream temperature ratio on heat transfer coefficient.

It will be noted that the effects of wall-to-stream temperature ratios T_W/T_δ on the heat transfer coefficient in turbulent flow are quite large. Other boundary layer theories advanced (e.g., Van Driest, Reference 36) also show this. Data from the NACA Ames free flight wind tunnel, presented on Figure 24 (from Reference 37), also indicate the increase in skin friction and heat transfer with decreasing T_W/T_δ for turbulent flow. This has also been confirmed in discussions with the NACA-Langley PARD division concerning their free flight tests at $M \leq 5$. However, recent turbulent flow tests at the Naval Ordnance Laboratory hypersonic wind tunnel reported by Lobb (Reference 38) at $M = 5$, 6.8, and 7.7, and unpublished data from both the NOL and the Johns Hopkins University Applied Physics Laboratory hypersonic tunnels at $M = 9$ do not show this trend. They show no appreciable effect of T_W/T_δ or, if anything,

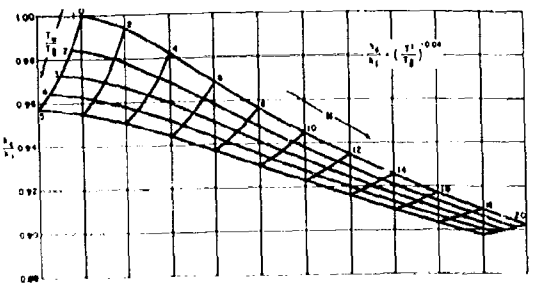

Figure 27. Heat Transfer Coefficient Correction Factor for Laminar Flow

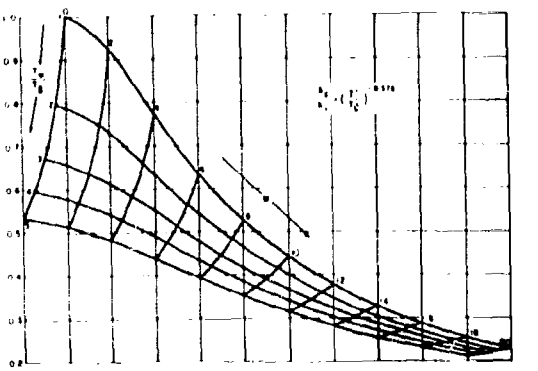

Figure 28. Heat Transfer Coefficient Correction Factor for Turbulent Flow

a slight decrease in friction coefficient as wall temperature decreases from recovery temperature. There is some question as to the validity of these latter tests because they were made on the tunnel walls where the boundary layer development has not been exactly typical of flat plate flow; but in the area of measurement the streamwise pressure gradients were small and the boundary layer measurement techniques appear to have been excellent. More experimental information is needed to resolve these differences. If the effects of T_W/T_δ are as indicated by NOL and APL, the present method is conservative in this respect, as their points agree well with the curve of c_{f_c}/c_{f_i} for the condition $T_W = T_r$ predicted by the present method.

Finally, if the power law representations are chosen, the heat transfer coefficients for laminar and turbulent flow are given by the following:

Laminar flow:

$$h_c = \frac{0.00963}{T_\delta^{0.04}} \left(\frac{V_\delta P_\delta}{x}\right)^{0.5} \left(\frac{h_c}{h_i}\right)_L ,$$

Turbulent flow:

$$h_c = \frac{0.0334}{(T_\delta)^{0.676}} \left(\frac{V_\delta P_\delta}{x^{0.2}}\right)^{0.8} \left(\frac{h_c}{h_i}\right)_T ,$$

where the values of h_c/h_i correspond to the proper values $\frac{T'}{T_\delta}$

Heat Transfer Equations

The convective heat transfer per unit area is

$$q = h_c (T_r - T_w)$$

where the recovery temperature, T_r, is given in the relation

$$r = \frac{T_r - T_\delta}{T_t - T_\delta} = \frac{T_r - T_\delta}{V^2/2J_g c_p} .$$

The recovery factor, r, for laminar flow is closely approximated by $r = \sqrt{Pr'}$ and for turbulent flow by $r = \sqrt[3]{Pr'}$, and is evaluated at the reference temperature. The adiabatic temperature rise at hypersonic speeds, $T_t - T_\delta$, is very large; thus c_p can be expected to vary significantly. The variation of c_p with temperature is approximated from Reference 39 as

$$c_p = c_{p_\delta}\left[1 + \frac{\gamma-1}{\gamma}\left(\frac{5500}{T}\right)^2 \cdot \frac{e^{5500/T}}{\left(1-e^{5500/T}\right)^2}\right]$$

Equating the change in kinetic energy to the change in the total heat or enthalpy when the air is brought to rest, and integrating from T_δ to T_t, gives

$$V^2 = 12{,}003 \left[T_t - T_\delta + \frac{1572}{e^{5500/T_{t-1}}}\right].$$

The values of $T_t - T_\delta$ obtained from this function when $T_\delta = 400°R$ are shown in Figure 29. Also plotted on this figure are 0.85 and 0.9 (approximately the laminar and turbulent recovery factors) times these values to indicate the recovery temperature rises. The adiabatic temperature rise for a constant c_p is included for comparison.

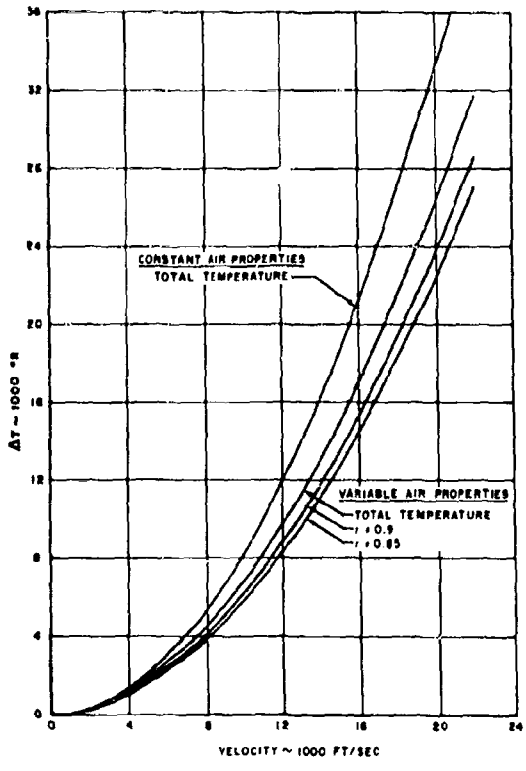

Figure 29. Stagnation Temperature Rise (No Dissociation)

The general equation of heat balance per unit area of aircraft surface is written as

$$h_e (T_r - T_w) + \alpha G - \epsilon \sigma T_w^4 = 3600 \, wcy \frac{dT_w}{d\theta}$$

where α G is a weighted average of the amount of radiation, both solar and nocturnal absorbed by the surface, $\epsilon \sigma T_W^4$ is the heat radiated from the surface, and $wcy \frac{dT_W}{d\theta}$ is the resultant heat absorbed by the surface. For the transient state the equation may be solved by successive difference equation solutions, substituting $\frac{\Delta T_W}{\Delta \theta}$ for the derivative. In the equilibrium case the latter term is zero and the convective heating by the boundary layer is exactly balanced by the radiation. In calculating hypersonic heat transfer for the MX-2276, the α G term has been found to be relatively small and may be neglected.

The emissivity of the surface, ϵ, is seen to be a powerful factor in establishing the surface temperature. A value of $\epsilon = 0.9$ was used in the MX-2276 proposal calculations (Reference 1) and is admittedly quite high, but it appears to be obtainable for particular surfaces as indicated in References 40 and 42. More research on this problem is definitely necessary as it may materially affect the vehicle design. During the course of the present study the effects of emissivity on the surface temperatures of the MX-2276 will be demonstrated.

(3) Use and Limitations of the Method

The preceding discussion was concerned primarily with two-dimensional flow having no streamwise pressure or temperature variations. This is realized on a flat plate parallel to the stream direction as long as the boundary layers are thin and the leading edge effects are not large. Constant pressure is also encountered in supersonic wedge flow and in the supersonic flow immediately adjacent to conical surfaces. For the wedge flow, the method applies directly if the local stream conditions are used. The cone flow is not two-dimensional and some correction must be made. It has been found that local laminar skin friction and heat transfer is similar to that of flat plates when the cone Reynolds number is three times that of the flat plate. This gives a correction of $\sqrt{3}$ times the plate coefficients when applied to the cone. A similar correction factor has been derived for turbulent cone flow to be 1.15 times the plate coefficients. Flow on the surface of a cylinder can also be considered plate flow if the radius of the cylinder is large with respect to the boundary layer thickness.

The effects of pressure gradients on slender bodies have been found to be small with respect to skin friction and heat transfer. Since the shapes contemplated for the MX-2276 are very thin or slender and are generally made up of the surfaces discussed above, it appears that the effect of pressure gradients is not an important consideration for the greater portions of the aircraft. An exception is in the immediate vicinity of the wing leading edges and body nose which must have finite radii. Heat transfer to these surfaces requires another approach which will be taken up later in the study.

As has been discussed earlier, the flight of the third stage takes it into flow regimes where the boundary layers become very thick, and induce pressure gradients and/or interact with the bow shock waves. The present method obviously cannot be applied where these effects are strong. These phenomena have their own theories and will be treated as special problems later in the study.

The streamwise temperature gradients on the third stage (as shown in Reference 1) are large, particularly near the leading edge. Chapman and Rubesin (Reference 41) indicate the effect of these gradients may be significant. This problem is now under study. The heat transfer values obtained will be compared with the values estimated with the method given herein. It is not expected that they will alter the flat plate results sufficiently over the majority of the surface to negate the value of the flat plate method for preliminary estimations.

As discussed earlier, the boundary layer air may dissociate when the temperature within it become sufficiently high, which may change the skin friction and heat transfer. Several studies, (References 24 and 25) have included the effects of dissociation and have shown the over-all effects are small. It is not felt at this time, from the insight gained in the present study, that these results can be considered conclusive. In view of this, beyond M ≃ 10, where appreciable dissociation may occur in the boundary layer, the results of the present methods for heat transfer and skin friction can be considered only speculatively.

e. Transition

In Section IV-B3, methods have been given for the determination of the local skin friction and heat transfer parameters for the cases when the boundary layer is laminar or turbulent. In any practical computation of friction drag or aerodynamic heating, the state of the boundary layer must first be assumed, i.e., a knowledge of the transition point is required. The effect and the importance of the many variables which could affect transition and the mechanism of transition itself is not yet understood, hence, the assumptions of theory are incomplete and experiments are not fully controlled. The best that can be done at the present time is to assume a transition Reynolds number based on the trends exhibited by available wind tunnel and flight test data. In the original proposal report (Reference 1) a transition Reynolds number of $Re = 2.8 \times 10^6$ at all Mach numbers was assumed. This appears to have been conservatively low judging from the trends exhibited by the test data (Figures 30 and 31), from theoretical predictions, and by discussions with several experimenters during visits to other research agencies. However, it is interesting to note that even on the basis of the assumed transition Reynolds number of 2.8×10^6, the boundary layer over the wing of the MX-2276 (chords varying from 10 to 40 ft) is practically all laminar for the major portion of a typical flight path where M > 10 and Re/ft is less than 1×10^5.

A theory for the prediction of transition Reynolds number actually does not exist, although the results of theoretical investigations of the stability of the laminar boundary layer in a compressible fluid (e.g., References 57 and 58) are often used as a basis for such predictions. This theory, which is also limited to the lower supersonic Mach numbers, cannot be expected to yield more than qualitative results and trends, as it is based on a linearized method of small disturbances, while transition is a nonlinear problem of a different order. Besides, the model of boundary layer stability is only an approximation to the actual mechanism of transition which is still unknown.

A survey of experimental data on determination of the transition point has been made and the results are summarized in Figures 30 and 31. As can be seen from Figure 30 no sharply definitive results can be found because of the varied tunnel characteristics; however, trends can be established. In the wind tunnel, the transition point is located through examination of the plots of recovery factor or skin friction coefficient versus Reynolds number, or through Schlieren photographs or other visual methods such as china clay, etc. For firing range flight tests such as those in Reference 43, shadowgraph methods can be used to find the transition point or, if telemetered data is available, graphical analyses as mentioned above are used.

The effects of various parameters on the location of the transition point has been investigated experimentally. These parameters include: addition and removal of heat, surface roughness, angle of attack, wind tunnel turbulence, free-stream stagnation pressures, and leading edge thickness. References 44 to 51 found that heating of the surface results in earlier transition while cooling has the reverse effect, as predicted by the small disturbance theory of boundary layer stability (cf. Reference 57). However, the stabilizing effect of heat removal is greatly reduced if flow disturbances are present such as those caused by roughness, tunnel turbulence, or transition-inducing devices (References 44 and 45). Reference 44 shows that if the insulated plate friction coefficient is large, the transition Reynolds number is greatly influenced by heat flow; if small, heat flow effects are greatly reduced. Increased surface

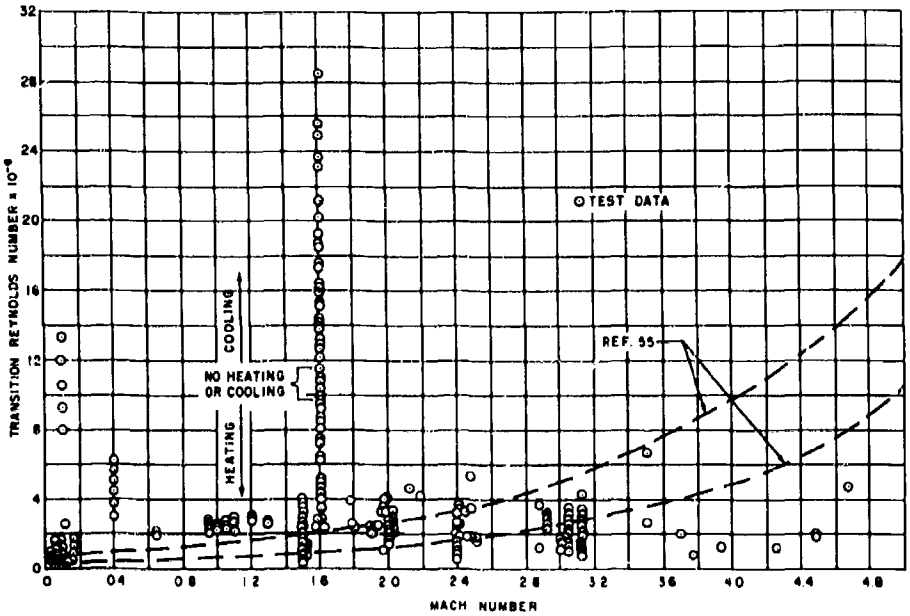

Figure 30. Transition Reynolds Number from Wind Tunnel Tests

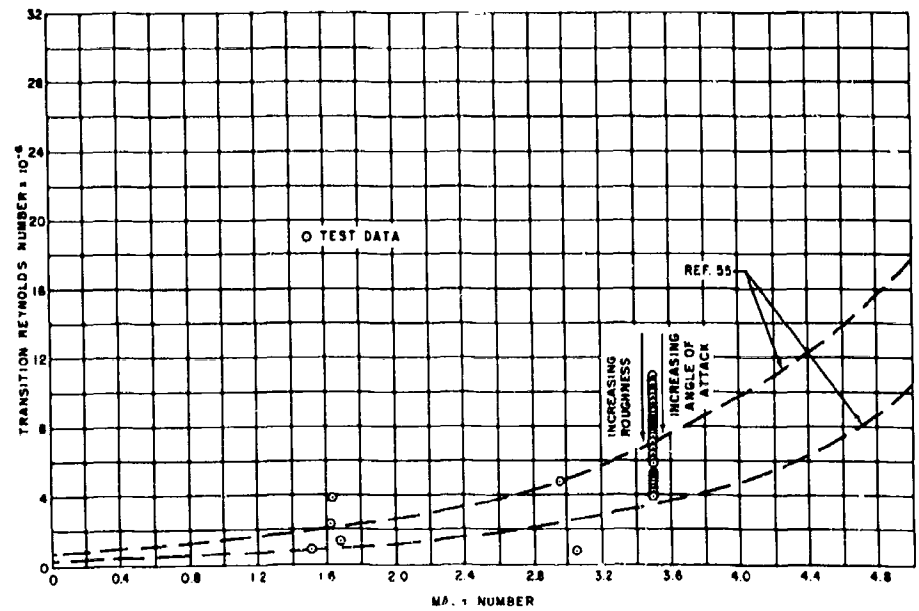

Figure 31. Transition Reynolds Number from Flight Tests

roughness results in earlier transition; as does an increased angle of attack upon the transition on the upper surface of the model (as illustrated in References 43, 52 and 53). Transition Reynolds number increases with the free-stream stagnation pressure and also with the leading edge thickness of the model, according to Reference 54. Wind tunnel turbulence may have a great effect upon the location of transition areas, tending to decrease the transition Reynolds number, as the degree of turbulence increases. Therefore, wind tunnel results are often characteristic of the tunnel used, since stream-turbulence is a function of the tunnel design. In Reference 56, a conical model was tested in various NACA supersonic wind tunnels. Tunnel flow characteristics were so varied that no conclusive results could be found. However, in most cases at least, trends can be established through wind tunnel experimentation even though specific data may be questionable.

It seems apparent, therefore, that any reliable information on transition point must come from carefully instrumented and analyzed flight tests, where all possible controlling factors are considered. These are needed, particularly at Mach numbers greater than three. There seems to be some hope that with research missiles now reaching towards Mach ten, that flight test transition data in this neighborhood will be available in the near future.

f. Transpiration Cooling

In order to evaluate the merits of transpiration cooling as a method of alleviating the high temperatures expected on some local areas of hypersonic aircraft, it is necessary first to survey and summarize the theoretical and experimental literature on the subject and to reduce this information to a convenient form for use in design study calculations. This has been done with the pertinent information available, and a tentative procedure was developed for estimating the effects of transpiration cooling. This method will be presented at a later date when it is augmented by more information, particularly experimental, which it is expected will be gained by the forthcoming visits to research facilities working in the field of transpiration cooling.

The practical application of transpiration cooling involves the use of porous materials and coolants. Investigations of the characteristics of these materials, both theoretical and experimental, are reported in References 60 through 73. While the result of most of these investigations are concerned with hot-gas flow through tubes, the evaluation of the characteristics of porous materials and coolants are useful.

In general, if such a cooling method is used, it is felt that a compromise will have to be made between the desired porosity and the structural strength of porous materials. For example, two common methods of fabricating porous materials are generally used. These are: (a) the sintering of metal powder, with an added volatile agent, such as ammonium bicarbonate, under high pressures; and (b) the sintering of metal powder with no agent under low pressures. In order to make large surfaces, high pressures, which result in higher tensile strengths and moduli, will have to be used. However, high pressures result in reduced porosity and permeability, and, hence, force the compromise. Porosities of from 40% to 70% will probably be of the most use.

The choice of a suitable material becomes important since an increase in porosity from 25% to 40% may result in a drop of approximately 80% in yield strength, and a drop of 90% to 95% in modulus of elasticity. In several of the referenced articles, porous specimens of copper, iron, nickel, stainless steel, and a ceramic material were investigated. Stainless steel or nickel specimens retain a fair amount of their strength while providing a fair amount of porosity. A combination of medium-coarse metal powder and a fine-grained volatile agent seems to provide good permeability and yet would have fair tensile properties. Reference 67 suggests that wire cloth might be a solution.

The permeability of a porous specimen was found to vary with the 1/5 or 1/6 power of the porosity, depending upon the metal used, for a given coolant. For gaseous coolants flowing through a porous wall of given porosity, the flow rate was found to vary almost linearly

with the difference between the squares of the pressures on either side of the wall. For liquid coolants, it is theorized that the flow rate would vary with the pressure drop across the wall. Coolants investigated included hydrogen, nitrogen, air, and water. Although liquid coolants are more effective owing to their latent heat of vaporization, an additional problem is inherent in their use, namely the fact that a liquid flow through a porous wall may show a marked decrease with time due to the clogging of the pores by contained solids or trapped filtered gases. This effect increases with a decrease in pore size. For a liquid coolant to be effective, it should have as high a heat capacity as possible, with a low vapor temperature. Reference 73 suggests that, on this basis, liquid hydrogen would be a good choice. Of the gaseous coolants tested, hydrogen again proves best, requiring only about 1/5 of the weight flow of that of nitrogen to maintain a given characteristic temperature ratio. In theory and experiment, it has been exemplified that for a given system this characteristic temperature ratio $\left(\frac{T_{gas} - T_{wall}}{T_{wall} - T_{coolant}}\right)$ is a function only of the ratio of the flow rate of coolant per unit area to the stream flow rate per unit area. This latter ratio is dependent upon the coolant, wall material, and geometric configuration of the surfaces, although Reference 66 states that the material influence is secondary in nature.

Difficulties in practical application of transpiration cooling arise from the difficulties in maintaining a desired coolant flow distribution. Variable coolant flow is obtained by varying either or both porosity and thickness. Reference 61 states that thickness effects may be approximated by existing theory. However the obtaining of a desired porosity in a surface is very difficult, even under laboratory conditions.

g. Wing Aerodynamic Characteristics at Hypersonic Speeds

For a limited region of the hypersonic flight regime encountered by the MX-2276 vehicle, the aerodynamic characteristics of wings may be treated theoretically within the concepts of continuum flow of an ideal, inviscid gas (Section IV-B3b). Within this region, the shock expansion theory, and approximations to it, may be expected to give reasonably accurate predictions, for airfoils at hypersonic speeds, of the two-dimensional lift, drag, and moment due to aerodynamic pressure forces. At present, the shock expansion theory, and the theories of Linnell and Dorrance (References 74 and 75), which are basically small-disturbance approximations to the shock expansion theory, appear most favorable. The shock expansion theory, while giving the most accurate results is, however, limited in its application to generalized studies because of the labor involved in determining the aerodynamic characteristics of arbitrary airfoil shapes. The small-disturbance theories are more useful in this respect, in that they may be employed to give the generalized characteristics of families of airfoil shapes, provided that a sufficient degree of accuracy is maintained in the predictions. As an example, the section lift coefficient of a 4%-thick half-diamond airfoil has been calculated over a Mach number range of 4 to 20. These results appear in Figure 32. As is seen, the method of Linnell agrees very well with the more exact shock-expansion theory, while the results given by the method of Dorrance are less accurate, even in the lower Mach number range for which it was intended (Reference 75).

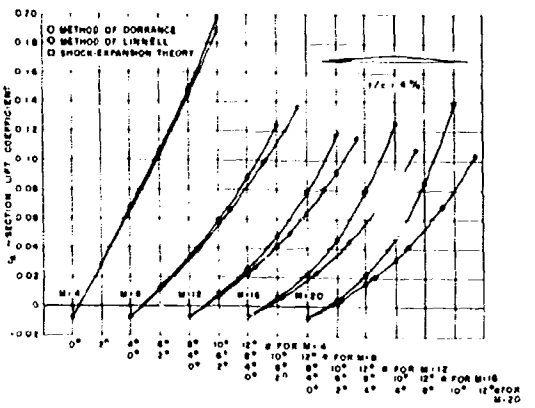

Figure 32. Comparison of Various Methods for Predicting Wing Lift

As an example of the nondimensionalized form in which the small-disturbance theory may be presented, the section lift coefficients for half-diamond airfoils of arbitrary thickness are presented in Figure 33.

As explained in Section IV-B3b of this report, the region of utility of the aerodynamic theory based on the concept of continuum flow of an ideal, inviscid gas may be extended somewhat into those flight regimes where the effects of fluid viscosity become important, by considering an effective change in the aerodynamic contour due to thickening of the viscous boundary layer. The presently available data on the characteristics of airfoils at hypersonic velocities have been obtained from tests conducted at a Mach number and Reynolds number at which the effect of a thickened boundary layer should be considered, and hence do not allow the direct evaluation of the inviscid theory itself. At the present time, the computation of the effects of a thickened boundary layer has not been completed.

However, in order to present a quasi evaluation of the two-dimensional inviscid theory without boundary layer correction, a comparison is made in Figure 34 of the inviscid two dimensional method of Linnell with the experimental data of Reference 76 for an aspect ratio 1.0 wing with a half-diamond airfoil section. The experimental wing lift coefficients, which are given from three-dimensional force data and also from integrated two-dimensional pressure distributions, give reasonable agreement with Linnell's inviscid method. Furthermore, the comparison of the two-dimensional pressure data and the three-dimensional force data indicate, as do other available tests of various wings, that at hypersonic speeds the effects of wing planform on the aerodynamic characteristics of the wing are small, and that the major considerations are the effects of wing section profile and thickness. This gives a general validation to the presently accepted practice of predicting the hypersonic characteristics of three-dimensional wing from two-dimensional theory. Until a better method becomes available, the two-dimensional method of Linnell, which allows the rapid evaluation

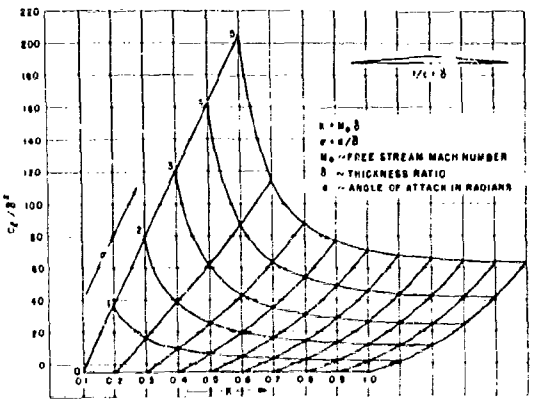

Figure 33. Two-Dimensional Lift Coefficients of Half Diamond Airfoils at Hypersonic Speeds

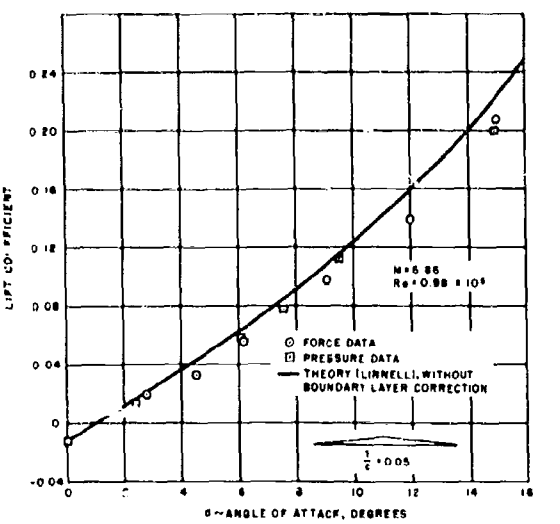

Figure 34. Comparison of Theorectical and Experimental Lift of a Half Diamond Airfoil with a 5% Thickness Ratio

of wing section characteristics, appears adequate for determining the characteristics of wings in continuum flow.

h. Body Aerodynamic Characteristics at Hypersonic Speeds

Methods are available by which the body characteristics may be determined in the field of continuum flow of an ideal inviscid gas. However, with the exception of cone flow, the labor and complexity involved has prevented the application of such approaches to the determination of the aerodynamic parameters in hypersonic flow. In order to circumvent this difficulty, the Newtonian impact theory has been widely applied by many authors (despite the questionable nature of the foundation of this theory), with the justification that relatively good agreement is obtained with the available experimental data. It should be noted that this justification is valid only in the region of Mach number and Reynolds number in which ideal inviscid continuum flow also applies, since it is in this area that the available experimental data have been obtained.

In order to establish a background of what is known, a review of the currently available test data pertaining to L/D has been carried out. Lift and drag data (and thus L/D) are available to a Mach number of 7; a few test points of zero lift body data extend to a Mach number of 10.

Some systematic configuration testing has been done between Mach numbers 3 and 7 in References 79 through 86. Typical body shapes of these tests are shown in Figure 35.

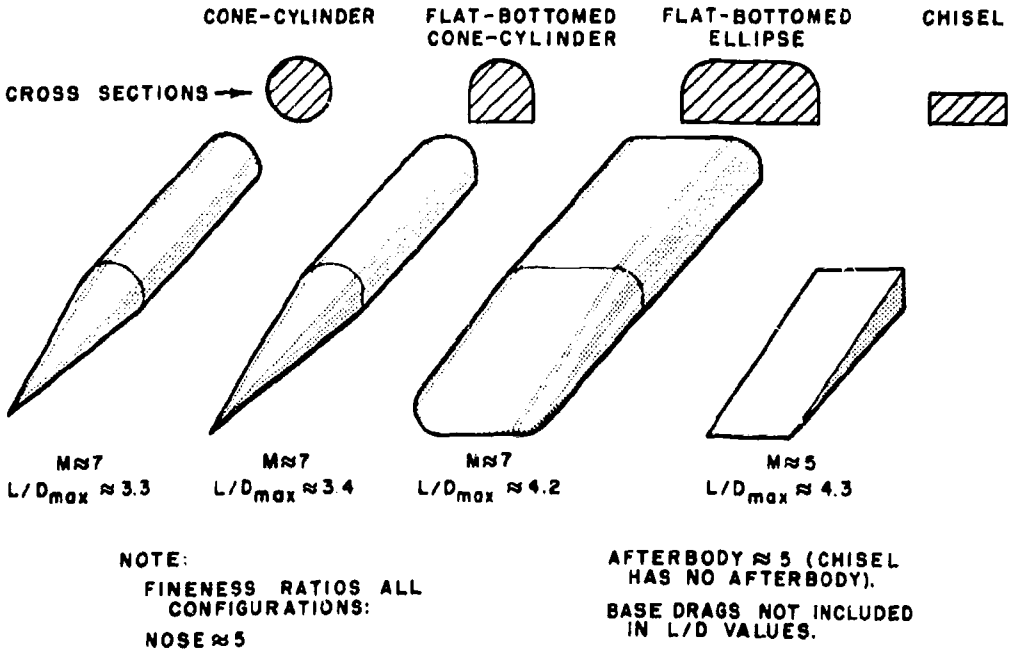

Figure 35. Hypersonic Body Shapes Tested

Maximum L/D ratios are plotted in Figures 36 and 37 for bodies of various nose and afterbody fineness ratios, cross sections and Mach numbers. Indications from these data are that the maximum L/D is greatly influenced by the nose fineness ratio while the afterbody fineness ratio is less important. Mach number is shown to have little or no effect. This figure also shows that flat bottomed bodies with cone-cylinder upper surfaces have somewhat lower maximum L/D ratios at supersonic speeds. This trend seems to be reversing at the low hypersonic speeds. In both cases the body lift at maximum L/D is generally higher for the flat-bottomed body than the body of revolution. Flattening of the flat-bottomed body cross section to make approximately semi-elliptical cross sectioned bodies or wedge-shaped bodies (tending to approach very low aspect wings) increases the maximum L/D ratio over that of a body of revolution. It should be noted that the base drag is not included in the L/D values shown.

Maximum L/D ratios for various cross sectioned bodies with a fineness ratio of approximately 10 and at several Mach numbers are plotted in Figure 38. Also shown in this figure are maximum L/D ratios for wings with various section profiles and a constant thickness ratio of 5 percent (References 86 and 76). The one known wing-body combination test at a low hypersonic Mach number is also included (Reference 90). This figure shows the same trends as

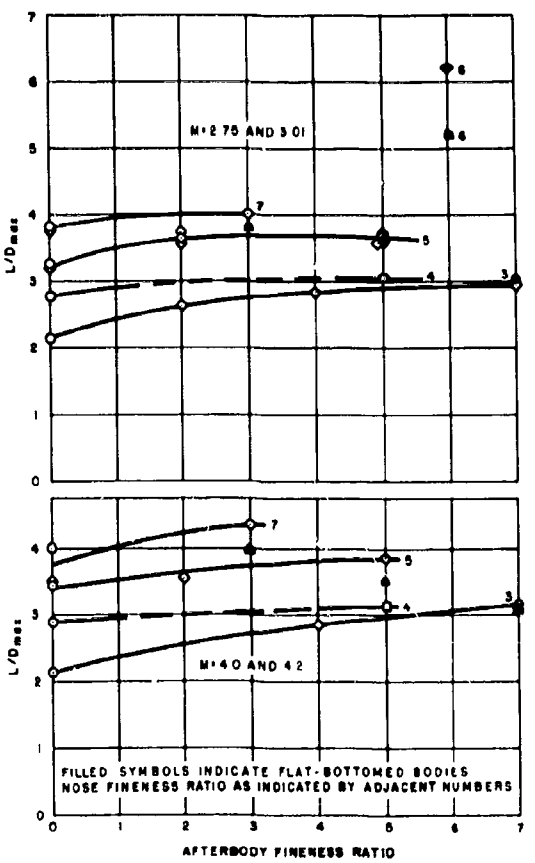

Figure 36. Variation of Body L/D_{max} with Afterbody Fineness Ratio, Nose Fineness Ratio, and Mach Number

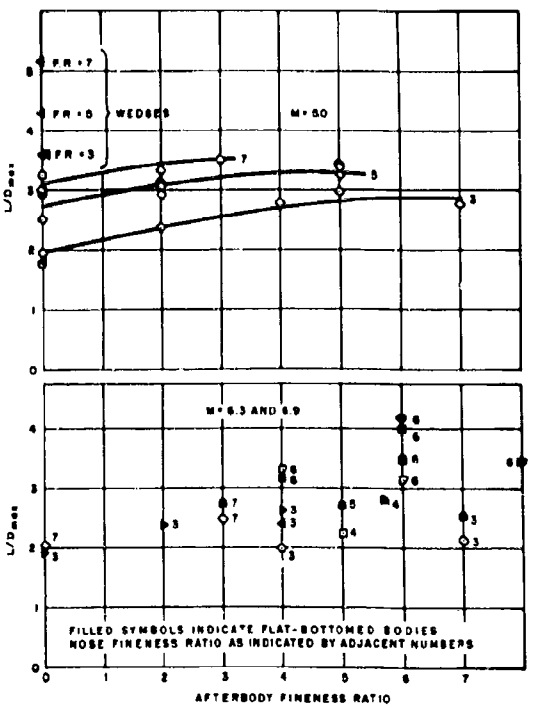

Figure 37. Variation of Body L/D_{max} with Afterbody Fineness Ratio, Nose Fineness Ratio, and Mach Number

mentioned above and in addition points out the relative aerodynamic efficiencies of bodies and wings.

Comparisons of theoretical and experimental body aerodynamic coefficients for several bodies and Mach numbers (presented in References 81, 85 and 86) are plotted in Figures 39, 40, and 41.

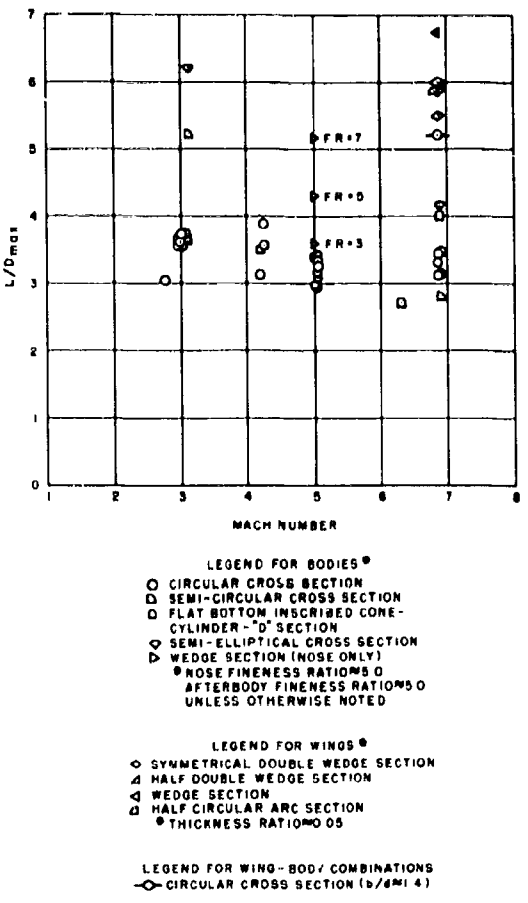

Figure 38. Variation of Body and Wing L/D_{max} with Mach Number and Cross Section

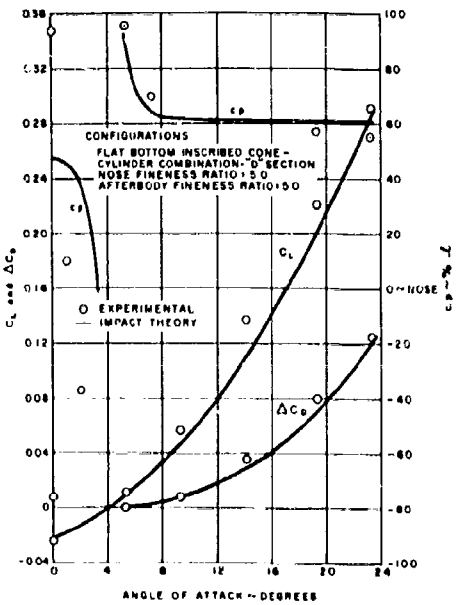

Figure 39. Comparison of Theoretical and Experimental Body Aerodynamic Coefficients at M = 6.3

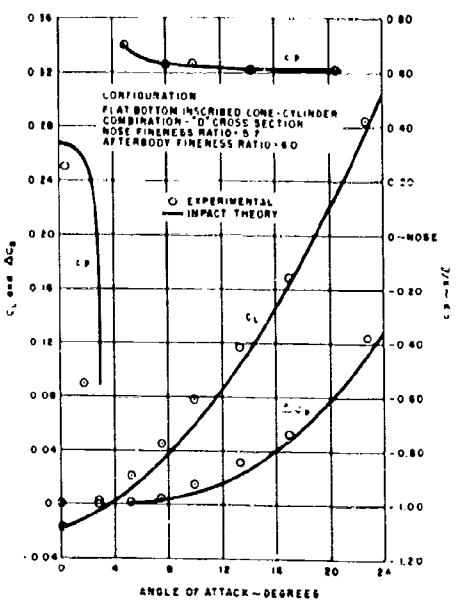

Figure 40. Comparison of Theoretical and Experimental Body Aerodynamic Coefficients at M = 6.9

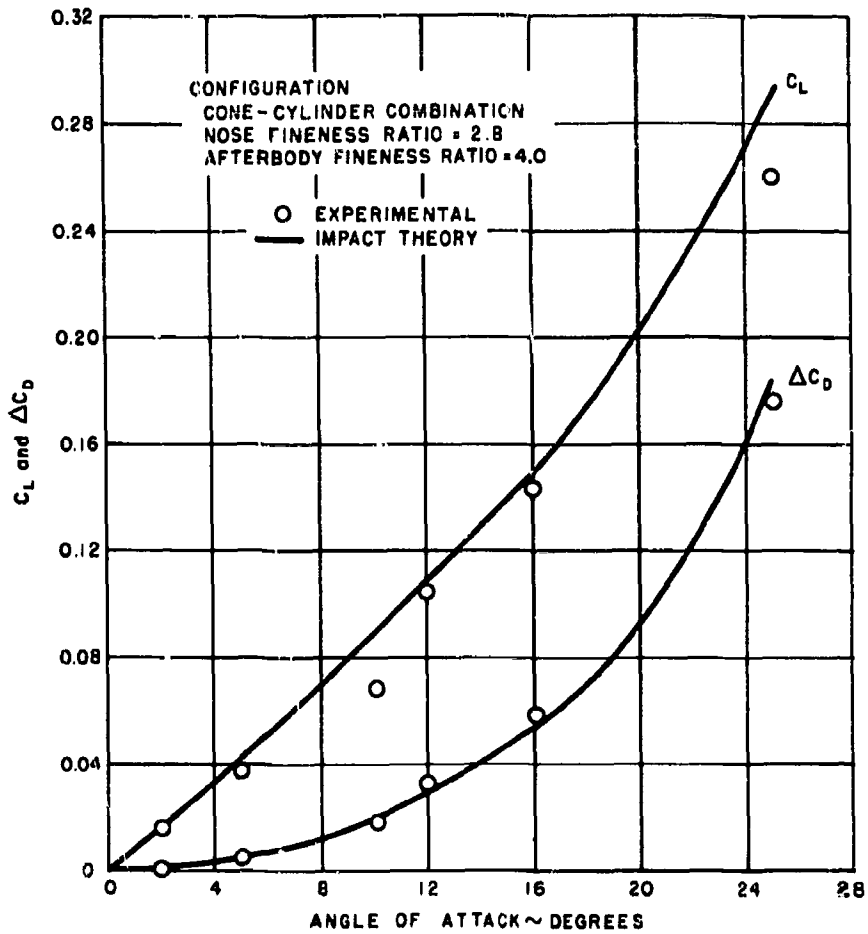

Figure 41. Comparison of Theoretical and Experimental Body Aerodynamic Coefficients at M = 6.9

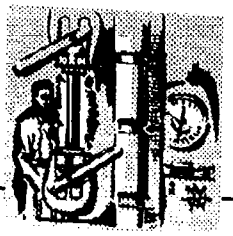

C. STRUCTURES

1. GENERAL

The primary objectives of the MX-2276 Structures study are as follows: (1) establish the basic criteria which will govern the structural design of the vehicle; (2) assemble typical loads analysis methods which will be used, and preliminary loads, where possible; (3) collect mechanical and physical property data on materials considered applicable to the vehicle; (4) study methods of insulating and cooling which may be used to obtain the required heat protection; and (5) apply the foregoing methods of analysis, and data, in sample preliminary structural analyses to verify the internal structural configurations and weights of the original proposal (Reference 1). Under each of the above objectives a number of study items are investigated. These are broadly summarized in the following paragraphs.

New environmental conditions, as well as unique performance characteristics, demand a close scrutiny of basic criteria assumptions. For conventional aircraft, for example, gust-environment conditions as well as performance levels and maneuver-condition combinations are stipulated in experience-proven specifications. Since the MX-2276 vehicle probes into regions beyond those covered by present aircraft design specifications, a logical set of gust design conditions and environment must be established. The required maneuvers differ considerably from those of conventional piloted aircraft, requiring evaluation and selection of reasonable condition combinations. Likewise, stage-separation conditions must be selected to suit the vehicle configuration.

Loads analysis methods of an "unconventional" nature are involved with: centrifugal forces in flight-loads equations, Coriolis-force effects, separation loads, unique handling-condition loads, and hypersonic flight-load magnitudes and distributions. These are studied either in general terms, or relative to the original vehicle configuration defined in Reference 1.

A survey was made of technical literature, catalogs, and brochures to collect data necessary for an evaluation of materials for use in the MX-2276 airframe. The materials considered include both the well-established materials — aluminum, magnesium, and the alloy steels — and also the more recent developments such as temperature-resistant plastics, titanium, high-temperature alloys, and ceramics. Properties are also presented for fluids suitable for use in structural cooling systems, and for low-conductivity materials which may serve as insulators. The structural material properties are presented on curves of structural parameters vs temperature to be used in airframe weight comparisons.

Theoretical material is provided to develop means for rapidly comparing various types of insulation. Both radiation and conduction barriers are considered and curves developed to expedite the numerical work. With the aid of these curves, the insulation necessary to achieve a specified structural temperature in a given time, and with a given structural configuration, may be quickly determined. With the aid of these curves preliminary designs of insulation have been developed suitable for the protection of an MX-2276 Structure in a variety of materials.

In the subsections which follow, these study items which have been completed in the first half of the study phase are presented under the appropriate primary-objective heading.

Naturally, a number of voids are evident, but no attempt has been made to summarize the status of study items which have been only partially explored. However, in Section VI there is included a listing (by subject heading) of the study items still to be completed. Since the last primary objective (structural analysis of vehicle configurations) is to be accomplished virtually at the end of the study, no stress analysis material is included in this report.

2. CRITERIA AND LOADS

a. Atmospheric Data

The initial MX-2276 flight path as proposed in Reference 1 reaches altitudes up to 259,000 feet. Future proposals including orbital flight may cover altitudes as high as 100 miles or more. Research, showing typical upper atmosphere properties, is summarized in References 94 through 101. The typical values of temperature and pressure taken from these references for use in loads analysis are presented in Figure 42 for the altitudes under investigation. Seasonal or geographic variations are not included since they do not materially affect structural design.

b. Design Gust Velocities

Gusts at moderate altitudes (0-50,000 feet) are well defined by current government documents and specifications such as References 102 and 103. While some information on high-altitude atmospheric properties has recently become available, knowledge of upper atmosphere disturbances is still limited. Gust intensities and frequencies are known to vary directly as a function of the local thermal disturbances and air density. The lower atmosphere close to the unstable thermal surface of the earth is the region most likely to contain severe gusts. By contrast, the upper atmosphere (100,000 feet and up) is subject only to the steady thermal variations of day and night with little or no cloud effects. Additional disturbances are caused by meteor flights, but these have an aggregate effect which is insignificant compared to the mass of air involved.

Wind phenomena are closely allied to gusts when there are wind velocity and direction differences in strata through which the vehicle passes at high velocities. A compilation of wind velocities at various altitudes is shown in Figure 43. These values when reduced to comparable equivalent velocities show high equivalent wind velocities at low altitudes and considerably smaller equivalent velocities at high altitudes. A direct relation between low altitude winds and gusts is evident and at present

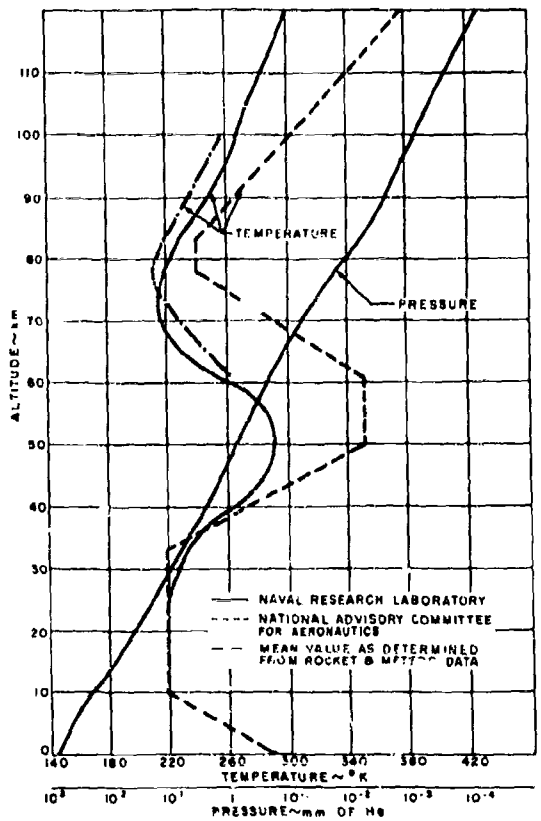

Figure 42. Typical Upper Atmosphere Characteristics

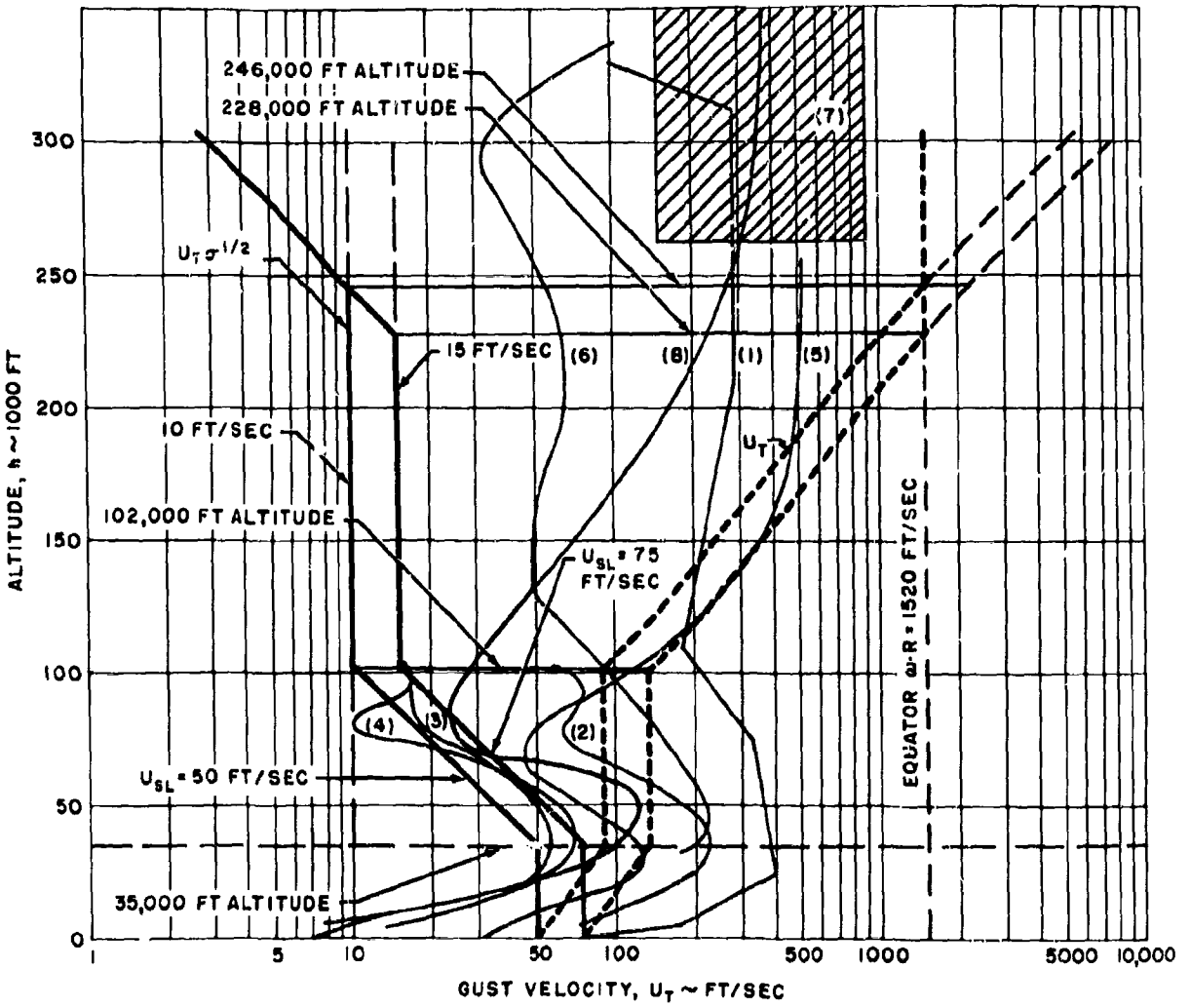

CURVE	PROBABLE MEASURED WIND VELOCITY	CURVE	PROBABLE MEASURED WIND VELOCITY
1	100%	5	50%
2	99.6%	6	100%
3	50%	7	100%
4	50%	8	AVERAGE

Figure 43. Typical Design Gust Velocities vs Altitude

there is no reason to believe that this relationship does not also exist at high altitude. Accordingly, in the absence of detailed knowledge of the wind "fringe gradient" at high altitudes, the wind velocity is treated as equivalent to a sharp-edged gust velocity.

From the foregoing reasoning, the well established gust criteria of Reference 103 for conventional aircraft design altitudes is extended to include high-altitude gusts (winds). Figure 4 of Reference 103 specifies that the gust velocities at higher altitudes are reduced by the ratio of $\sigma^{1/2}$ at altitude to $\sigma^{1/2}$ at 35,000 feet. At 102,000 feet altitude such a procedure results in a 10 ft/sec equivalent gust at 35,000 feet. The 10 ft/sec gust velocity represents a conservative gust condition derived from recent NACA data. Current investigations have not shown gusts, or winds, of greater magnitude at altitudes over 100,000 feet, and therefore in this criterion the 10 ft/sec equivalent gust is retained until an altitude of 246,000 feet is reached. At this point, the true gust velocity is equal to the rotational speed of the earth's surface at the equator. This high velocity is considered to be a sufficient upper limit for gust velocities at 246,000 feet and above, since jet stream and other high altitude wind velocity data do not indicate greater true velocities than those obtained from the foregoing. These design gust velocities, as well as the proportionate velocities for a 75 ft/sec equivalent gust at 35,000 feet, are shown in Figure 43.

c. Gust Load Calculations

The nomenclature for this section is presented in Table IV. The lift curve slope variation with Mach number, which already is well defined by transonic and supersonic research, is presented as a typical relationship in Figures 44 and 45. This curve is used in solving for Δn at transonic and supersonic speeds by the method described below. If the lifting surface in question is swept back, the peak Mach number effect will be shifted in the direction of increasing Mach numbers. This shift must be determined for each swept wing configuration.

TABLE IV. NOMENCLATURE FOR GUST LOAD CALCULATIONS

a	=	$\frac{d_{CL}}{d\alpha}$ Lift coefficient slope
a_R	=	$\frac{a}{a_{\text{Fig. 44}}}$
$\bar{c}$	=	Mean chord of wing
C_L	=	Lift coefficient
g	=	Gravity acceleration
h	=	Altitude
K_1	=	Gust alleviation factor
K_2	=	Gust shape factor
n	=	$\frac{a}{g} = \frac{\text{Acceleration}}{\text{Gravitational acceleration}}$ = Load factor
Δn	=	Gust load factor
Δn^*	=	Specific gust load factor (Figures 46 and 47)
S	=	Area of lift surface
U	=	Gust velocity
U_T	=	True gust velocity
V	=	Flight velocity
V_T	=	True flight velocity
W	=	Weight
α	=	Angle of attack
g	=	$\frac{2W}{\rho g \bar{c} a S}$ = Mass ratio
ρ	=	Density of atmosphere
σ	=	ρ/ρ_o

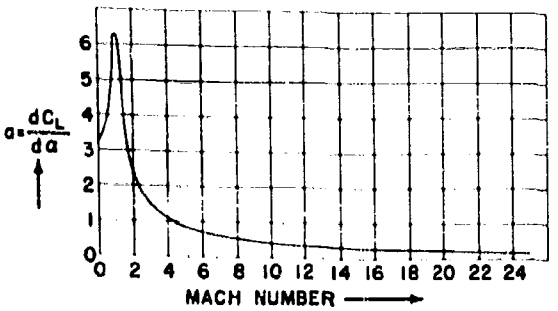

Figure 44. Mach Number Effect on Lift Curve Slope

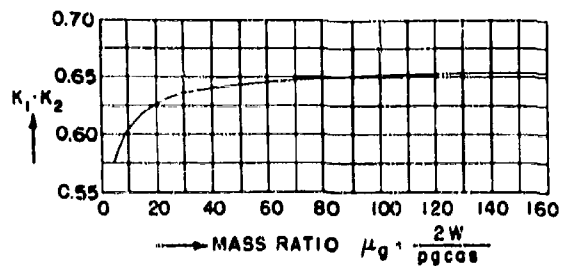

Figure 45. Alleviation Factor (Subsonic)

At subsonic speeds and low altitudes the alleviation factor, K_1, is significant, but at supersonic speeds and high altitudes the mass ratio ($\mu_g = \frac{2W}{\rho g c a s}$) upon which it is based becomes very large so that K_1 approaches 0.88. Therefore, it is not unduly conservative to consider $K_1 = 1$ for supersonic speeds. The second factor, $K_2 = (0.75 + 3.0/\mu_g)$, indicates the gust shape which is usually considered a (1 - cos) function. However, lack of any reliable data on high altitude gust shapes requires that a sharp-edge gust be assumed so that $K_2 = 1.0$.

With these principal variables defined, it is possible to simplify the gust load equations for use at high altitudes and speeds. The evolution of the basic gust load equation follows:

$$n \times W = C_L \times a_{1G} \times \frac{\rho}{2} \times V_T^2 \times S \pm C_L \times \frac{U_T}{V_T} \times \frac{\rho}{2} \times V_T^2 \times S$$

The subscript 1G refers to Steady State load conditions at 1g.

$$n = n_{1G} \pm \frac{U_T \times V_T \times a \times \rho \times S}{2W}$$

Introducing $K_1 \times K_2$ and converting to equivalent velocities

$$n = n_{1G} \pm \frac{(K_1 \times K_2)(U_T \sigma^{1/2})(V_T \sigma^{1/2}) a_R}{498\ W/S} \quad \begin{matrix}\text{(MIL-S-5702)} \\ \text{(Knots)}\end{matrix}$$

By rearranging the above equation, Figures 44, 45, and 46 can be used to obtain a gust load factor.

$$n = \Delta n^* \times a_R \times (K_1 \times K_2)$$

where $\Delta n^* = (U_T \sigma^{1/2} \times V_T \sigma^{1/2} \times \rho \times \frac{S}{W})$ taken from Figure 46 for a given N, h , W/S

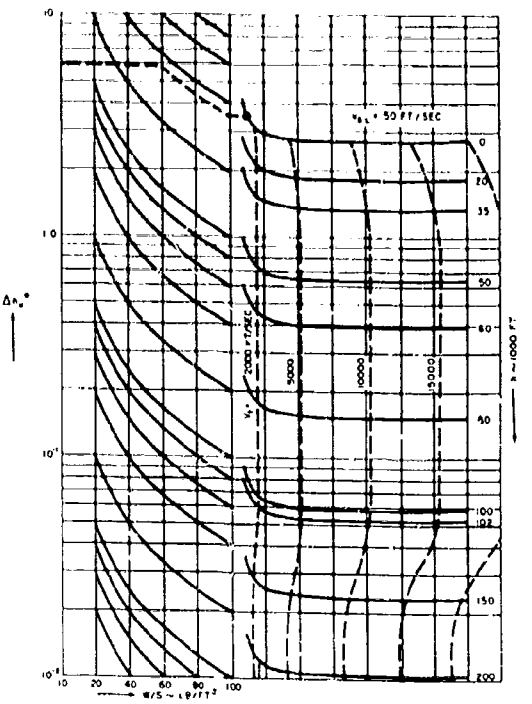

Figure 46. Gust Load Nomogram

α_R is obtained from Figure 44 for a given M or from a similar curve derived for a specific wing

$$\alpha_R = \frac{\alpha}{\alpha_{FIG.44}}$$

$(K_1 \times K_2)$ is taken from Figure 45 for subsonic flight and considered equal to 1.0 for supersonic flight.

Figures 46 and 47 combine the gust velocity variation with altitude shown in Figure 42 with the altitude variation of air density. Only a wing loading, W/S, value is necessary to get a Δn_u* for any Mach number and altitude. Figure 46 also serves to illustrate the very low magnitude of gust load factor at altitudes above 100,000 feet. Depending upon the gust frequencies, the small load factors may have some structural fatigue significance, or possibly result in significant design loads when combined with maneuver loads at large gross weights.

d. Flight Path Loads

A summary of the various factors necessary for deriving programmed flight loads is presented in Figure 48. These values are taken from Reference 1 and are typical for a three-stage configuration as is initially being considered. Neglecting the increase in pressure thrust due to increase in altitude, the n_xW curve of Figure 48 shows that the critical axial accelerations occur at burnout for each stage. As a result of the planned programming, the axial acceleration forces are by far the largest encountered. Therefore, the initial flight load investigation is particularly concerned with axial forces and moments for each stage, combined and separate.

Centrifugal force effects are also investigated in order to provide a foundation for contemplated loads studies of this and other configurations. To the afore-mentioned load effects will be added appropriate magnitude of gust increment loads.

(1) Axial Accelerations

Assuming a free falling flight path, zero angle of attack, and no steering force, permits simplified conservative determination of the axial thrust, mass-inertia, and aerodynamic drag forces. When considering thrust, it is Bell Aircraft's practice (based upon extensive rocket engine design experience) to use a limit thrust load factor of 1.5 for rocket engine start conditions and 1.1 for steady operation conditions. However, with the large number of variable thrust rockets contemplated for the MX-2276 vehicle, it is reasonable to expect that hard starts will occur at low thrust levels so that the 1.1 limit thrust load factor can be applied to all rocket engine operating conditions with full thrust assumed.

The data presented in Table V summarize the axial force factors, stage and interstage loads, as well as the axial force moments about the center of gravity for which the critical flight conditions of take-off, Stage

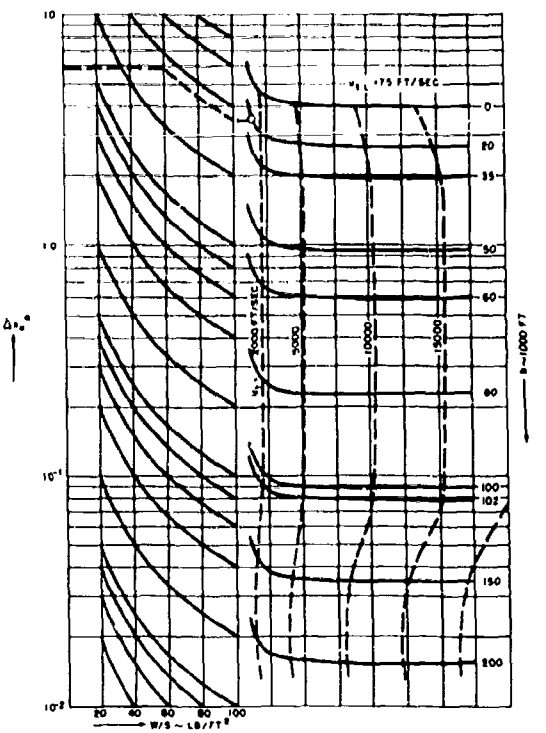

Figure 47. Gust Load Nomogram

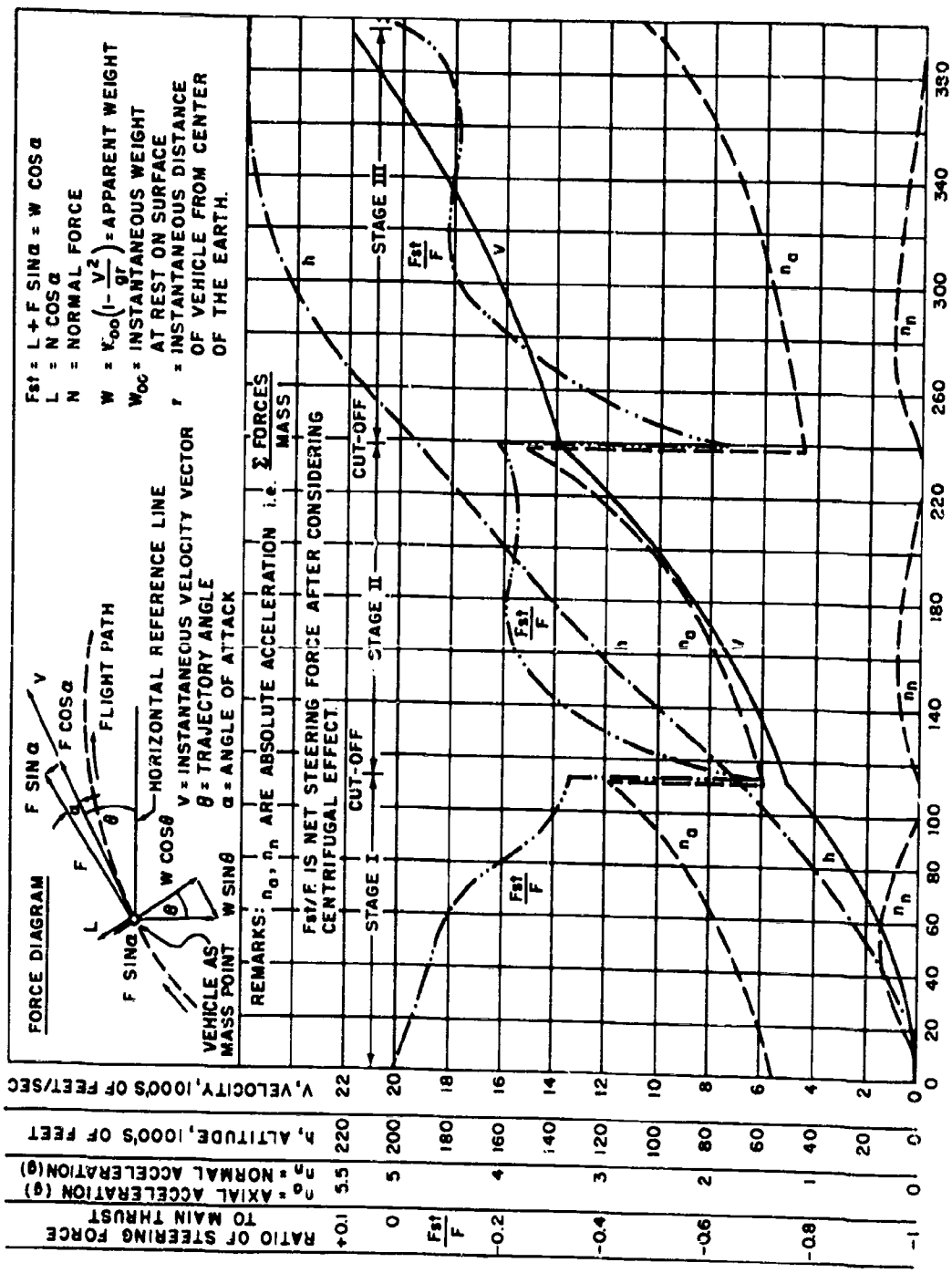

Figure 48. Flight Parameters

I, and Stage II are evaluated. Such axial loads design body sections and may have appreciable effect on design of the lifting surfaces, especially in balancing the axial force moments. These accelerations are not treated in further detail at present in view of future studies of other configurations, flight paths and the possibility of canting the motors to reduce these moments. Condition 2, Stage I cutoff with limit thrust factors of 1.1 applied to both Stage I and II operation, shows some of the largest forces and moments about the cg. By assuming drag, thrust, and mass to be distributed linearly across the depth of each stage, Figure 49 is drawn to provide a first approximation to axial acceleration, force, and moment distributions.

(2) Centrifugal Forces

The vehicle in two-dimensional flight is subject to three acceleration systems: a centrifugal force acting perpendicular to the earth's surface, a second centrifugal force perpendicular to those portions of the flight path not parallel to the earth's surface, and the acceleration along any tangent to the flight path. The two centrifugal force systems are analyzed briefly, and the tangential acceleration is shown as part of the total balance equation.

If atmospheric effects are neglected any mass leaving the earth's surface has an initial tangential velocity equal to the earth's surface velocity. If there were no gravitational

TABLE V.

INTERSTAGE ACCELERATION LOADS

CONDITION	Axial Force Factors			Shear Loads Between Stages		Axial Force Moment About cg (M_y)
	T Thrust	n Accel.	D Drag	I & II	II & III	
	Multiplying Factor	Gravities	Gravities	1000 lb	1000 lb	10^6 ft-lb
1. Take-Off	1.0 I 1.0 II	1.35	0	20	60	+0.62
	1.1 I 1.1 II	1.48	0	30	70	+0.78
2. I Cut-Off	1.0 I 1.0 II	3.0	0.15	375	150	+4.6
	1.1 I 1.1 II	3.25	0.20	415	170	+5.1
	1.1 I 1.0 II	3.20	0.20	425	165	+5.2
3. II Cut-Off	1.1 II	4.0	0.4	-	195.0	+1.4

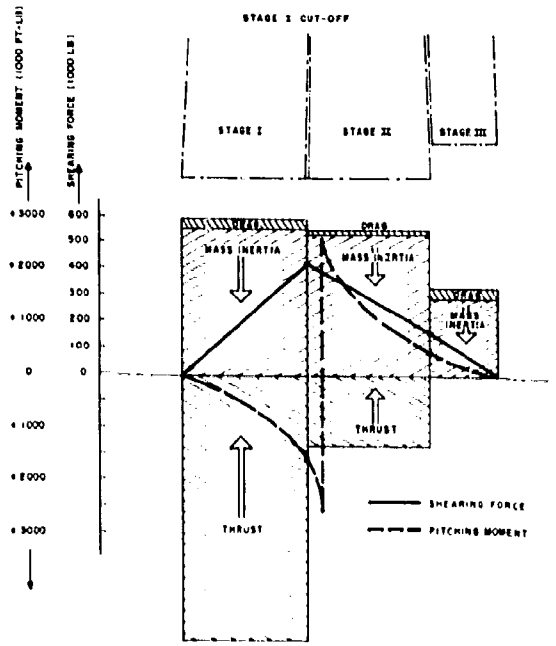

Figure 49. Typical Axial Acceleration Forces

attraction present, the mass would continue on a straight path with its velocity equal to the earth's surface velocity. However, the influence of gravity serves to make the mass part of the earth's rotating system. A centrifugal force which acted at the earth's surface continues to act on the free body according to the following equation:

$$F_c = m\frac{V^2}{R} = m\omega^2 R$$

(The nomenclature for this section is defined in Table VI.)

Those curvilinear portions of the flight path not parallel to the earth's surface are subject to an additional centrifugal force which is dependent upon the curvilinear velocity component resulting from separating the terrestial angular velocity component from the total flight path angular velocities. A graphical illustration of these relations is shown in

TABLE VI. NOMENCLATURE FOR CENTRIFUGAL EFFECT AND FLIGHT PATH BALANCE

C_D	=	Drag coefficient
C_L	=	Lift coefficient
D	=	Drag
F_T	=	Inertial Force tangential to Flight Path
F_N	=	Centrifugal (inertial) force normal to flight path
F_R	=	Centrifugal force due to Curvature of earth surface
F_{RT}	=	Tangential flight path component of F_R
F_{RN}	=	Normal flight path component of F_R
g	=	Gravity acceleration
h	=	Altitude
L	=	Lift
m	=	Mass
n_T	=	Acceleration factors from F_T
n_N	=	Acceleration factors from F_N
n_R	=	Acceleration factors from F_R
n_{RT}	=	Acceleration factors from F_{RT}
n_{RN}	=	Acceleration factors from F_{RN}
q	=	Dynamic pressure
r	=	Radius of flight path
R	=	Radius of earth surface
S	=	Lift surface
T	=	Thrust
V_T	=	Velocity tangential to flight path
V_H	=	Horizontal velocity
W	=	Weight
ΔW	=	Decreasing of weight during burning time

TABLE VI. NOMENCLATURE FOR CENTRIFUGAL EFFECT AND FLIGHT PATH BALANCE (CONT)

- α = Angle of attack
- θ = Angle of longitude
- ρ = General radius
- ϕ = Angle of flight path tangent vs. earth surface
- ω = Angular velocity

Figure 50. The basic centrifugal force relation is:

$$F_c = m \frac{V^2}{\rho}$$

For the specific flight path conditions the centrifugal effect can be separated in two components F_N and F_R as shown in Figure 50a where centrifugal force normal to flight path (in direction of flight path radius) is:

$$F_N = m V_T \dot{\phi}$$

Centrifugal force due to earth's surface curvature is:

$$F_R = m V_T \dot{\theta}$$

The earth's rotational velocity may be added to $\dot{\theta}$.

The centrifugal effect caused by curvature of earth's surface (F_R) is shown in Figure 51 as percent lift for a given altitude and a horizontal velocity (V_H). The MX-2276 operates up to h = 100 km. In this region the altitude is insignificant for the centrifugal effect caused by earth surface curvature. Figure 52 gives the values for the MX-2276 region.

The diagram for all flight path forces, including centrifugal forces is shown in Figure 50b. The equations for these are provided below:

Flight path balance:

Tangential Forces

$$\bar{T}_T + \bar{W}_T + \bar{D} + \bar{F}_T = 0$$

Normal Forces

$$\bar{T}_N + \bar{W}_N + \bar{L} + \bar{F}_R + \bar{F}_N = 0$$

The tangential and normal load factors from the flight path balance are:

$$n_T = \frac{\bar{T}_T + \bar{W}_T + \bar{D}}{W}$$

$$n_N = \frac{\bar{T}_N + \bar{W}_N + \bar{L} + \bar{F}_{RN}}{W}$$

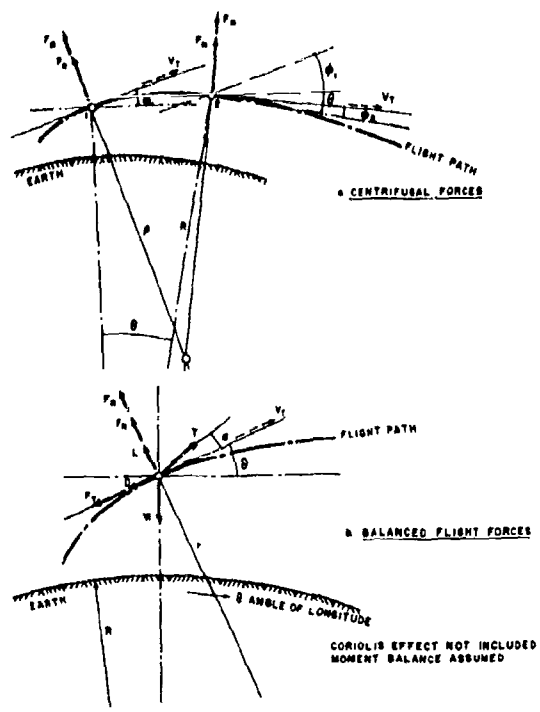

Figure 50. Flight Forces

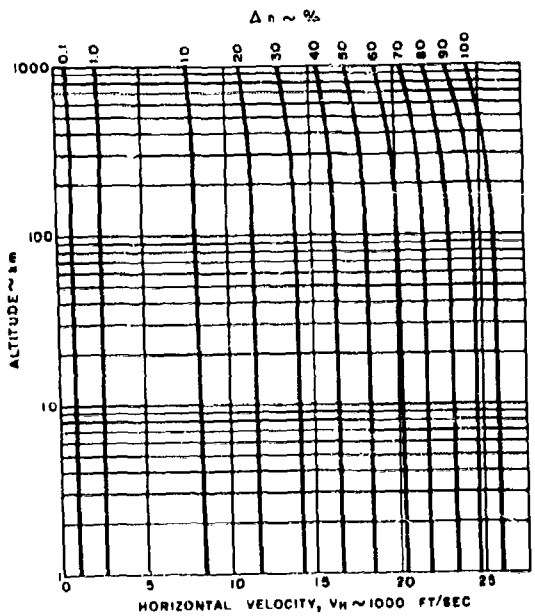

Figure 51. Centrifugal Component Δn for Horizontal Velocity

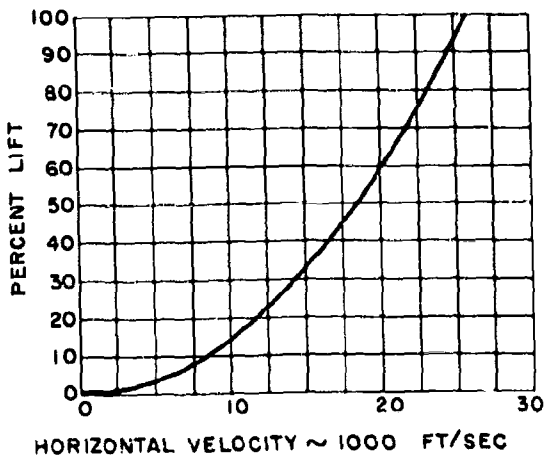

Figure 52. Centrifugal Component for Horizontal Velocity (for Altitudes up to 100 km)

where

$\bar{T}_T = T \cos \alpha$ Tangential to flight path

$\bar{T}_N = T \sin \alpha$ Normal to flight path

$\bar{W}_T = W_h \sin \phi$ Tangential to flight path

$\bar{W}_N = W_h \cos \phi$ Normal to flight path

$W_h = (W_o - \Delta W) \left(\frac{R}{R + h}\right)^2$

$\bar{D} = D = C_D \cdot q \cdot S$

$\bar{L} = L = C_L \cdot q \cdot S$

$\bar{F}_R = n_R \cdot W = m \cdot V_T \cdot \dot{\theta}$ Normal to Flight Path

$\bar{F}_T = n_T \cdot W$ Tangential to flight path

$$n_T = \frac{\dot{V}_T}{g}$$

$\bar{F}_N = n_N \cdot W$ Normal to flight path

$$n_N = \frac{V_T \cdot \dot{\phi}}{g}$$

3. STRUCTURAL MATERIALS

a. Basic Considerations

The choice of a material for a particular engineering application inevitably requires consideration of many factors, and usually evolves into a compromise between desirable and undesirable characteristics. In the particular case of the MX-2276 third stage, two additional features are present which make the problem of material selection much more difficult and at the same time much more important.

The first of these features is the effect on the airframe of the aerodynamic heating produced by the hypersonic speeds. Aerodynamic heating greatly extends the range of materials to be considered since these must now include insulating materials and cooling fluids as well as special alloys developed for high-temperature strength, This heating also increases the number of material characteristics that must be considered since high temperatures produce not only reduced strength and stiffness in most materials but also such other effects as thermal stresses, creep, oxidation, and erosion.

The second feature peculiar to the third stage is the tremendous importance of weight. Weight is, of course, significant in any airframe, but the increased importance of weight in the third stage of MX-2276 is well illustrated by the fact that the saving of one pound of weight in this stage will reduce the total take-off weight of the combined configuration by approximately 40 pounds. This fact not only makes a careful evaluation of material properties necessary but also changes considerably the compromises mentioned in the first paragraph.

As might be expected in the present state of the art, the amount of information available diminishes both as higher temperatures are approached and also as the newer materials are considered. This is particularly true in connection with properties such as fatigue strength, creep resistance, etc., which not only require more extensive test programs than simple tension or compression strengths, but have also, until recently, been only of very secondary consideration to the airframe designer. Many of the data that are available for the newer materials, especially the ceramics, have been obtained for use in some application different from that envisaged in the present study. It is evident that, if any of these materials show promise, considerable test work will be required to obtain design information.

b. Typical Materials Studied

The information assembled so far has been studied in order to pick out a few structural materials which are representative of the various groups and which, at the same time, are good all-round materials from each group. The following list is typical of those which might be applicable for use on the MX-2276.

(1) Aluminum Alloys

24S-T3 bare and 75S-T6 bare have been selected as representative of the aluminum alloys since these materials are in very general use today for airframe construction. Their properties are well known and the effect of these properties on the airframe design is generally understood. Such materials form a good basis for comparison and serve as a reference from which other materials can be judged.

(2) Magnesium Alloys

On the basis of general usage and superior properties FS1-H24 has been chosen as a typical magnesium material.

(3) Steel Alloys

SAE 4130 heat-treated to an ultimate tensile strength of 125,000 psi is considered typical of this group. Higher strengths than this are obtainable but are probably not too practical for general use in the shell of the airframe. Such higher strengths are satisfactory for fittings, attachments, etc., but these items do not constitute a sufficient percentage of the structural weight to warrant consideration at this time. Steel of a lower room temperature strength than 125,000 psi should perhaps be avoided in a structure in which weight is so critical.

(4) Stainless Steels

Type 347 1/2 hard illustrates the general properties of stainless steels which combine high ultimate strength at elevated temperatures, together with high resistance to oxidation and corrosion.

Timkin Alloy 25-20 is also added for a comparison.

(5) Haynes Alloys

Hastaloy C, a nickel-chrome-molybdenum alloy, has the highest strength of the wrought alloys with the exception of Hastaloy B, which is slightly superior. Alloy C was considered of more use for the present work, however, since its oxidation resistance is very much better than that of Alloy B.

(6) Inconel X

Typical of the nickels and nickel alloys, Inconel X has the highest strength and stiffness properties at high temperature together with high resistance to oxidation and relatively good ductility.

(7) Titanium

Representative of the titanium alloys is RC-130A having the highest yield and ultimate strength throughout the temperature range with reasonably good ductility.

(8) Pure Molybdenum

Molybdenum is one of the newer materials of interest for high temperatures. This material is made commercially by both powder-sintering and arc-casting methods. Interest in this material centers in its possible use for leading edges and coverings to retain insulation.

(9) Ceramics

The ceramics have not been studied sufficiently to choose a typical example, if such exists but the properties of Alumina Cermet have been included in the curves presented with this report so that the relative importance of at least this one ceramic can be seen. This material has particularly high strength properties and high stiffness at elevated temperatures while its resistance to both oxidation and thermal shock is considered good. These properties are obtained with a density approximately equal to that of titanium.

It may be noted that no consideration has been given in the above discussion to material and fabrication costs, and the use of strategic material. These items are important, particularly the latter, since so many alloys depend for their high temperature properties on the use of elements in short supply, but it is considered that strength and stiffness properties are of primary importance. At a later date it may be possible to show the penalties involved in the use of cheaper or less strategic material.

c. Material Parameters

The comparison and evaluation of materials are facilitated and placed on a rational basis by the use of parameters which are functions of the material characteristics involved in the application being considered. The optimum material for the particular application being studied is usually the one with a maximum or a minimum value of the appropriate parameter.

A number of simple and well-established parameters have been used in the present work to compare materials for applications involving tensile strength, compressive strength of stable and elastically unstable elements, stiffness, heat capacity of cooling fluids, and the insulating value of conduction barriers. With one exception these parameters assume that the structure is to be optimized with respect to weight and therefore the material density is found in each one. The exception arises in the case of cooling fluids where volume also may be important, and an appropriate parameter has therefore been introduced to show the heat capacity per cubic foot of each coolant. A summary of the parameters used is given in Table VII

In considering the parameters in Table VII, extra precaution must be exercised in the selection of materials for use in the design of compression members. In the preparation of these curves for elements in compression, it

TABLE VII. STRUCTURAL PARAMETERS

Parameter	Material Application
Ftu/d	Tensile Strength
Fcy/d	Compressive Strength - Stable Elements
E/d	Structural Stiffness or Compressive Strength of Columns - Elastic Instability
$\sqrt{E/d}$	Compressive Strength of Cylinders - Elastic Instability
$\sqrt[3]{E/d}$	Compressive Strength of Flat Panel - Elastic Instability
Heat Capacity per pound	Fluids for Cooling
Heat Capacity per cubic foot	Fluids for Cooling
Kd	Insulation for Conduction Barriers

where - Ftu = Ultimate tensile strength
Fcy = Yield strength at 0.002 in./in. permanent set
E = Elastic modulus in compression
d = Material density
K = Thermal conductivity

has been assumed that the geometry of the structure has been established. It might be questioned whether, for a given load condition, a different geometry may not change the relative efficiencies of materials. Obviously, if the geometry is such that the structure is completely stable in compression (a condition which rarely exists) the geometry has no further effect. Fcy in this instance is the only variable that matters. The material efficiencies for the majority of compression structures will depend upon loading, and for any given loading the structural configuration must be optimized for each material and temperature to give the least weight; this weight is to include both load-carrying material and stabilizing structure. Use of these curves for material comparison, therefore, implies that in each case the proportion of stabilizing material to load-carrying material is the same.

The parameters outlined above are adequate for a structural design simply on the basis of static strength. In the past, static strength has been the primary consideration of the airframe designer and, on the basis of this experience, it seems reasonable to continue in this direction. However, stiffness is now assuming significance because of high speeds; the same high speeds together with the use of less ductile materials are introducing fatigue problems, and the high temperatures require considerations of such factors as creep and thermal shock.

Curves representing the material parameters described in this section are shown in Figures 53 through 57 and 63 and 66.

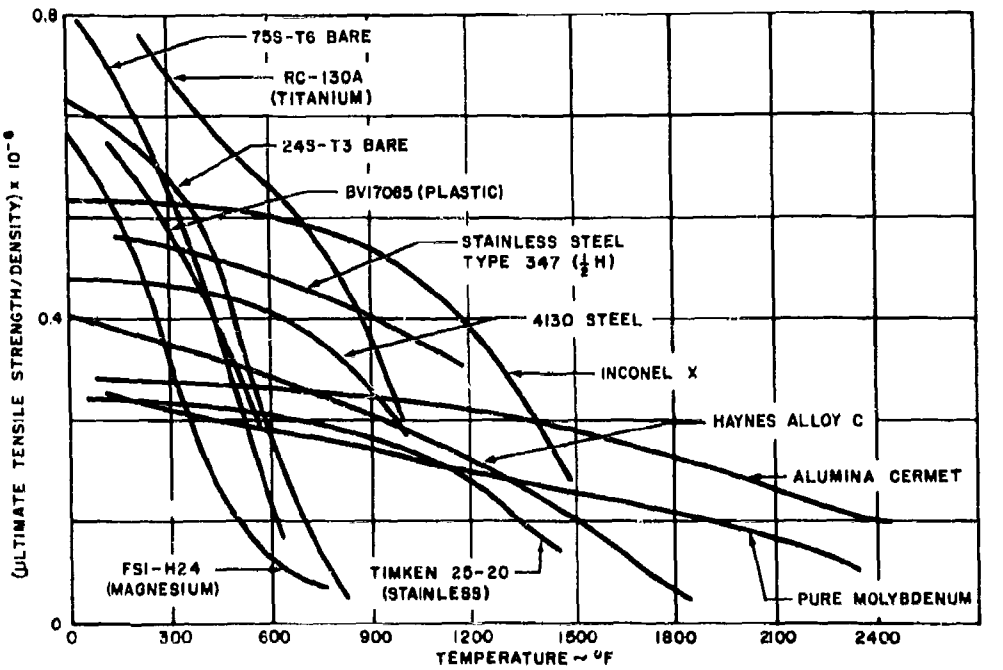

Figure 53. Tensile Parameters of Structural Materials

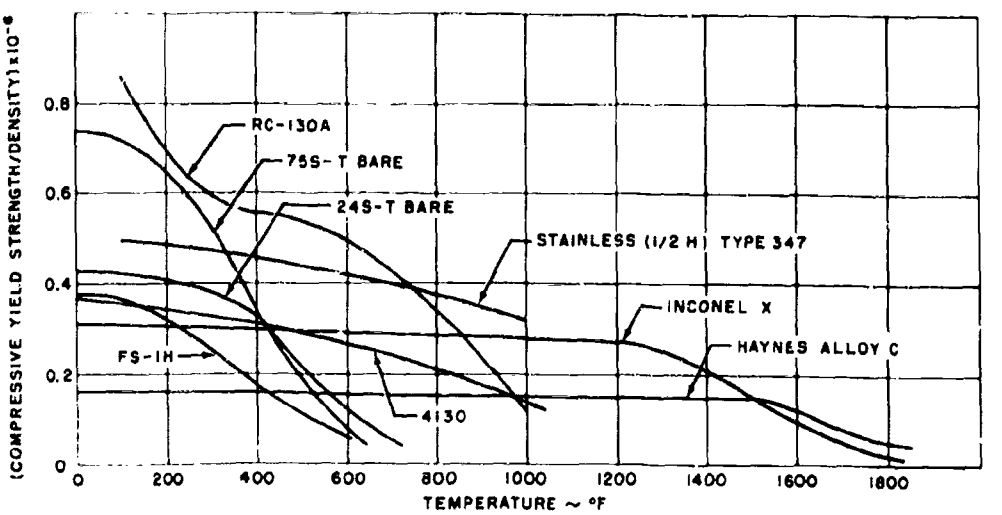

Figure 54. Compressive Parameters of Structural Materials (Stable Sections)

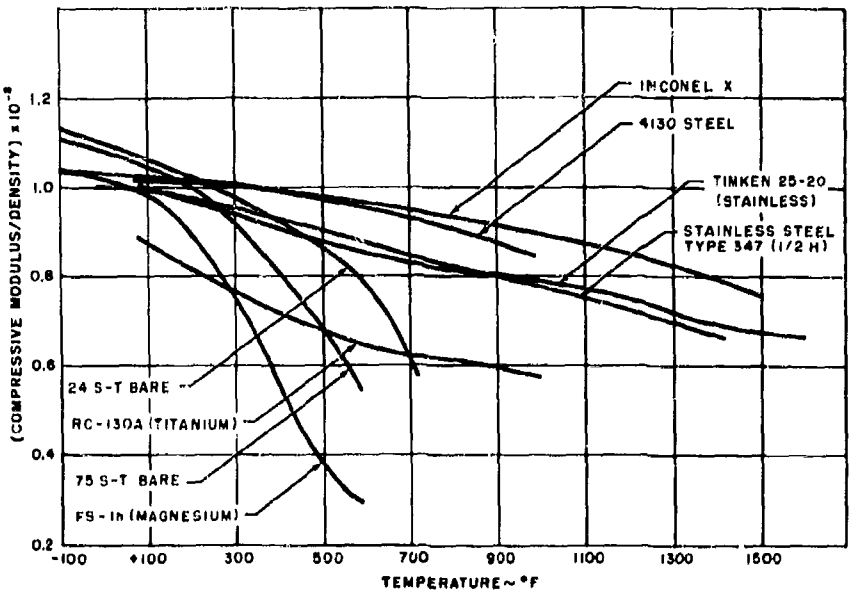

Figure 55. Stiffness Parameters of Structural Materials

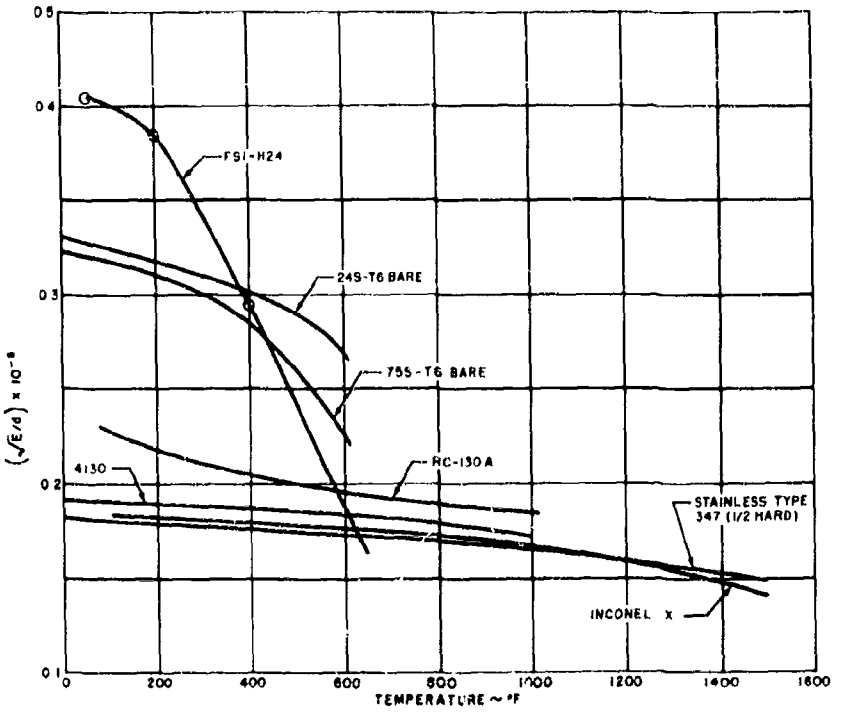

Figure 56. Cylinder Compressive Strength Parameter of Structural Materials (Elastic Instability)

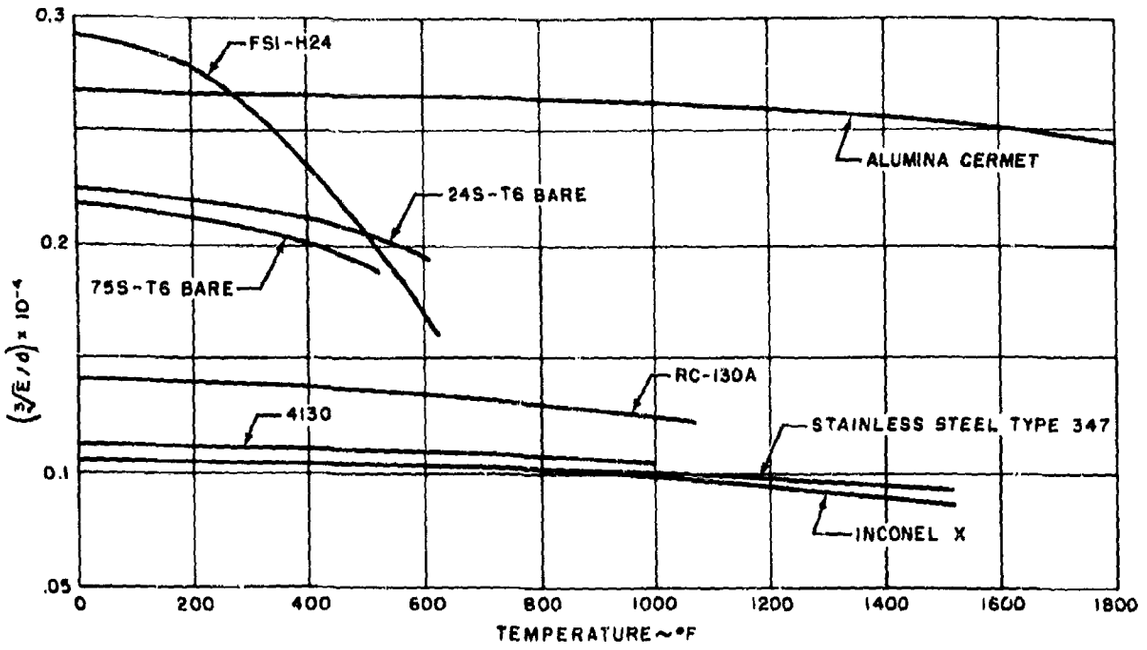

Figure 57. Flat Panel Compressive Parameters of Structural Materials (Elastic Instability)

d. Creep Considerations

The general approach to the creep problem has been to set up conservative, arbitrary limits of permanent set and then to show that, for the MX-2276 application, these limits impose very little restriction on the use of any of the materials considered. The study of creep has been extended to include not only the increased structural deformation resulting from the application of stress for an extended time, but also the phenomena of stress rupture and creep buckling.

In order to set up creep limits for a practical structure, it would be necessary, after establishing the point in the structure at which the limiting value of permanent set had been reached, to calculate from the stress distribution, the creep strains at all other points in the structure. To these strains, it would be necessary to add the creep of joints, connections, etc., and an integration would then give the permanent structural deformations. After repeating this process for a number of loading conditions, it would still be necessary to decide to what degree the deformations were interfering with the satisfactory performance of the airframe.

To avoid this complication, while retaining a basis for comparing the creep resistance of materials, it has been decided to adopt a procedure analogous to the existing yield criteria wherein the stress at which 0.2% permanent set is achieved in a simple tension or compression test specimen is indicative of the gross working stress at yield or limit load. The permissible permanent set due to creep has also been arbitrarily selected as 0.2% when measured on a simple tension test specimen subjected to the same temperature and time conditions as the actual structure. This value of permanent set is considered very conservative. Not only is 0.2% a very small value, but it will occur, in the practical structure, only in very local areas of the airframe. Further conservatism is added to the study by assuming that all creep strain is permanent since there

is some evidence that a part of the creep strain is recoverable after removal of the load.

In order to apply creep limitations, it is also necessary to assume a required life for the airframe. Ten to fifteen flights, each of approximately 80 minutes, is presently considered to be an economical life for the third stage MX-2276. To allow a reasonable margin on this value, a life of 100 hours has been chosen for design. This lifetime of 100 hours will be spent mostly at stress levels corresponding to 1g loading, with fluctuations of short duration to higher and lower stresses. To allow for the cumulative creep effect of these alternating stresses, the creep limitation has been defined as no more than 0.2% permanent set after 100 hours at a stress corresponding to 1.2g loadings in the airframe. The 1.2 factor is taken from Reference 103.

Inspection of creep curves shows that at high stress levels and high temperatures, considerable creep may take place in a few minutes. It has been decided, therefore, to use a second creep limitation in which two-thirds of the stress at limit loads must be sustained for one hour with no more than 0.2% permanent creep. In lieu of better information, the limit load factor for the MX-2276 third stage will be assumed, during the present part of the study, as 3.0.

With these considerations, diagrams have been drawn of allowable stresses against temperature for several materials, and a typical diagram for Inconel X is shown in Figure 58. This diagram shows the design limit stress that may be used without exceeding a permanent set of 0.2% due to yielding, and also the stress levels at which 0.2% permanent set due to creep, is reached in one hour and 100 hours, respectively. These latter curves will be associated with loading levels of 2.0g and 1.2g, respectively. Therefore, for comparison they have been plotted on the diagram after being ratioed by 3.0/2.0 and 3.0/1.2, respectively. By this means they are directly comparable with the 0.2% yield curve which is produced by the 3.0g limit load. The inside envelope of the three curves drawn for each material gives an equivalent limit stress to be used for design. This equivalent stress will insure that at no time during the life of the airframe will the permanent set at any point in the structural material exceed a total of 0.4%, of which 0.2% is due to creep and 0.2% due to yield.

In order to compare the creep and yield characteristics of various materials, the equivalent limit stresses, determined as described above, have been divided by the material densities and plotted against temperature. The results are shown in Figure 59. Before conclusions can be drawn from these curves, it will be necessary to give some thought to the choice of safety factors since, depending on safety factor, either strength or deformation may govern the design stress. It is apparent, however, that the creep limitations imposed do not seriously limit the use of any of the materials presented, except perhaps 75S-T aluminum alloy above 400°F. Satisfactory creep figures for a titanium alloy have not yet been found, but a curve will be added for this material when available.

All stress rupture data that have so far become available have been obtained by loading the test specimen to a certain stress level and maintaining this stress for an extended time until failure. For the MX-2276 application, however, it is of more interest to know the ultimate stress available after a stress equivalent to 1.2g (for example) has been sustained for 100 hours. All the available evidence shows that, at least for metallic materials, the strain at stress rupture is never less than 2.0% and is generally much more. This is at least ten times the creep that will be present after one hundred hours. Therefore, it may be assumed that at the end of its design life the airframe is so far from rupture at the 1.2g stress level that it is still capable of being loaded up to its short time ultimate stress. On this basis, stress rupture no longer becomes a consideration in material comparison. Of course for any particular material that is chosen for structural use it will be necessary to check for stress rupture in more detail.

The discussion above, together with the associated curves, is applicable only to the

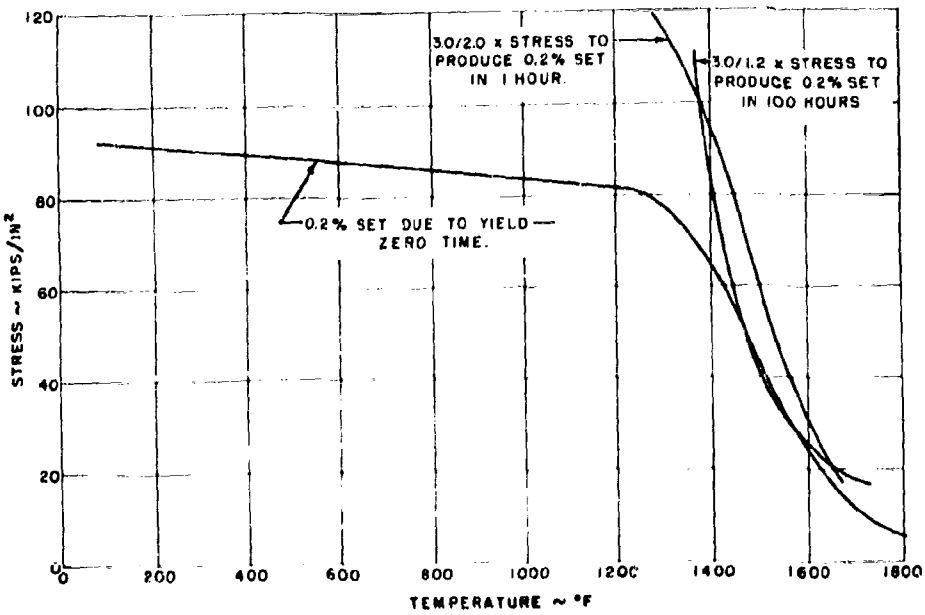

Figure 58. Inconel-X: Effect of Permanent Set Limits on Design Limit Stress

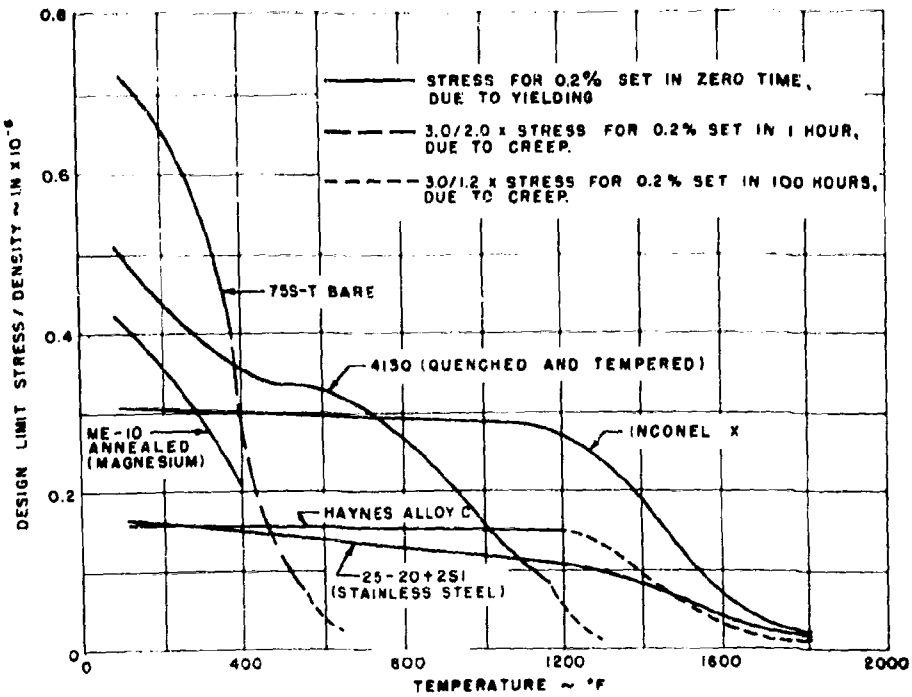

Figure 59. Comparison of Design Limit Stresses

MX-2276 third stage airframe. Propellant tanks may be designed as pressure vessels to different permanent set conditions and probably to different factors of safety. Some of the propellant tanks will also serve as part of the primary structure and will, therefore, be subject to both airframe and tank design conditions. The effect of these additional considerations on the relative creep resistance of various materials has not been evaluated.

Buckling, as a result of creep, has been briefly studied, but as yet no conclusions which will indicate the relative susceptability of materials to this phenomenon, have been formulated.

c. Thermal Shock Stresses

In an effort to consider the problem of thermal shock and its effects on a structure for the MX-2276, attempts were made to calculate the temperature gradients in an uninsulated skin material subjected to a temperature rise in the outside fibers of 600°F per minute, using the Schmidt plot method. It was soon apparent that this method was quite impractical for the solution of this problem because of the fixed relationship, in the Schmidt plot method, between the time interval and the number of points through the material thickness at which the temperature is given. Selecting a sufficient number of points through the material thickness to insure reasonably accurate temperature gradients, results in a very small time increment and consequently, a time-consuming graphical process. Accordingly, analytical solutions were developed to give the temperature gradients through the skin due to a temperature at the outer surface that varied linearly with time. In conjunction with these equations, the same temperature rise of 600°F per minute was used. This value is achieved during the initial acceleration and climb, and preliminary work suggests that it is the maximum reached throughout the flight. More detailed calculations of maneuvers, landing, and post landing when the aircraft may be stationary on the ground, but still hot, are necessary, however, before all temperature gradients will be known.

Results of this work showed that insignificant stresses occur owing to temperature gradients through the skin or covering, provided that the material is metallic. With a ceramic covering, tensile stresses of the same order as the ultimate strength are reached in a 1/4-inch thickness, with higher values as the thickness increases. Considerable alleviation will be achieved, however, if the ceramic is used in small panels, comparatively free around the edges.

The same thermal considerations have also been applied between various elements of the structure, such as between the skin and shear webs or between the skin and ribs of a wing. This investigation shows that thermal stress within the structure is indeed a significant problem, and will be of primary importance in establishing the structural configuration. Allowing the skin temperature to rise at 600°F per minute, and assuming a large mass of skin relative to the internal structure produces tensile stresses at the center of a 10-inch deep shear web which vary from 140,000 psi in an aluminum structure to 250,000 psi in a structure of stainless steel or Inconel X. Similar effects occur, of course, between fuselage skin and frames, and also between stringers and skin where the tendency would be to bend and ultimately to buckle the stringers. Depending also on the relative masses of covering material and internal structure, the reacting compression stresses in the skin may also cause buckling of the skin panels.

It is evident, even from these very preliminary numbers, that thermal stress is a serious problem in the MX-2276 structure, despite the moderate rates of skin temperature rise that are expected to occur. Various solutions to this problem, which will continue to make use of conventional shell construction, are of course apparent. The addition of insulation, for instance, would have the effect of materially reducing the rate of temperature rise in the skin. It seems probable that a small amount of insulation, which may be quite insufficient to prevent equilibrium temperature being reached in the structure, may considerably reduce the thermal stresses. More consideration will be given to this possibility following the study of insulation.

Careful use of dissimilar materials will also reduce thermal stresses, and calculations show that an alloy steel skin with an aluminum web reduces the web tensile stress to 39,600 psi, while if a copper web with a steel skin were practical, this stress would be only 18,700 psi. This method of alleviating stress due to temperature changes would unfortunately introduce another system of thermal stresses when equilibrium of the whole structure is reached, owing to the different coefficients of expansion of the materials. The use of INVAR, a very low expansion stainless steel, is presently being investigated.

The remaining method of avoiding thermal stresses is to depart from conventional shell structures and devise arrangements in which structural redundancies are absent, so that thermal expansions are unrestrained. These structures would include simple trusses, beams and ribs with corrugated webs, etc. Such thoughts were the basis for the unconventional structural arrangement presented originally in Reference 1. So far, the present work has justified these ideas.

f. Weight Comparisons

For purposes of obtaining an indication of and illustrating the effect of some of the parameters mentioned in previous paragraphs upon the weight of structures, Figure 60 has been prepared. This plot shows the ratio of the weight of an uninsulated and uncooled structure operating at elevated temperature compared with a structure of the same configuration, designed for the same loads but at room temperature. It was constructed considering a wing structure of proportions suitable for the MX-2276, where probably 50% or more of the weight of such a wing will be dependent upon

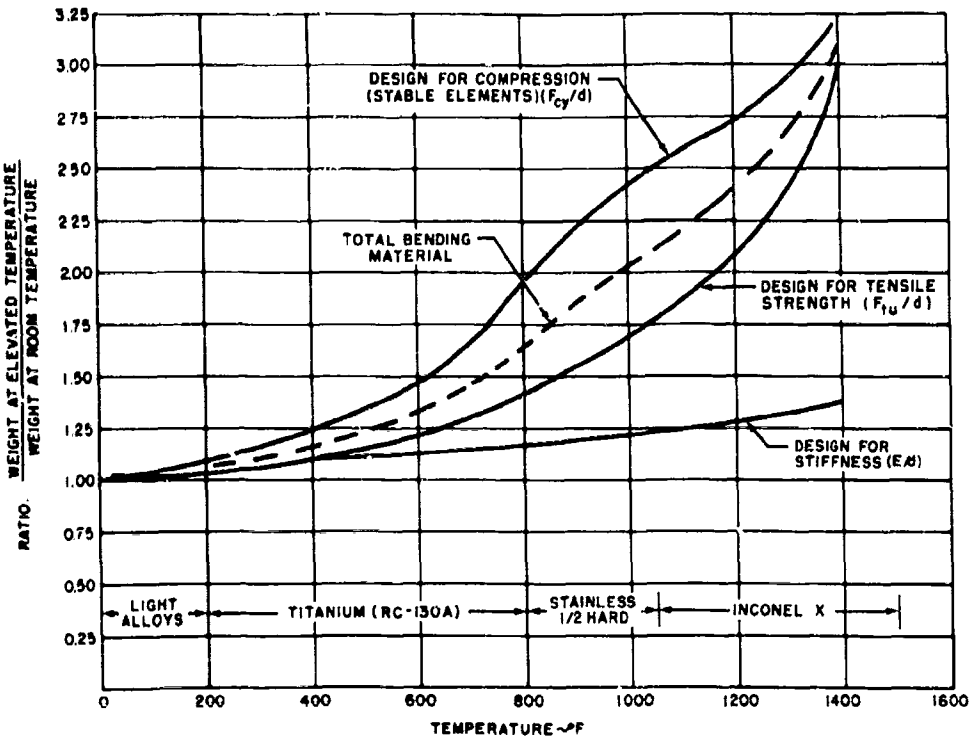

Figure 60. Weight Ratios for Uninsulated, Uncooled Structures

bending material, the material being subjected primarily to tension and compression stresses. The compression material may be well stabilized, such as beam caps, for which case the parameter Fcy/d can be used as a representative value of the compressive strength weight ratio.

It must be remembered however, that other compression strength-weight ratios might be involved in design of the actual structure such as $\sqrt[3]{E/d}$ for elastic instability of skin panels or $\sqrt{E/d}$ for column instability of skin stringer panels, but for this comparison of weights the above parameter is the only one considered. The weight comparison evolved with the use of Fcy/d will be the most optimistic for an uninsulated, uncooled structure.

For the tension parameter only the ultimate tensile strength to density ratio (Ftu/d) is considered.

The best optimum values of ultimate tensile strength to density ratios and compression yield strength to density ratios that are obtainable for any material within any temperature range have been selected, and these in turn have been divided by the corresponding value for 75S-T6 bare material at room temperature – the 75S-T6 material being considered the most representative of present design practice under normal conditions. These have been plotted against temperature along with notations on the plot of optimum materials for that temperature. Since part of the bending material will be in compression and part in tension, the curve of weight ratio for the total bending material will lie somewhere between these solid lines. For the present the dotted line indicates such a curve which in this case is the average of the solid lines.

It may be that because of the high speeds involved, the MX-2276 wing will be designed by stiffness rather than strength, in which case the elastic modulus-to-density ratio will be the important parameter involved. Therefore, a further curve, has been added to show the ratio of the weight of the bending material for such a wing to the weight of an aluminum room-temperature structure. From a comparison of these curves it seems that the recent trend toward designing structures for stiffness rather than strength may well be reversed again in the design of high temperature structures.

g. General Results

From the survey of properties and parameters of materials and the temperature failure phenomena which must be considered for the design of the structure of the MX-2276 for high temperature conditions the following conclusions can be drawn.

(1) For an uninsulated, uncooled structure the principal factors to be considered in a design are the reduction of material physical properties, thermal stress, and possibly creep buckling. As no conclusions have yet been reached at the present time on creep buckling, this is disregarded. The other aspects of creep and stress rupture are no concern for the MX-2276 as Figure 59 shows that the ordinary 0.2% permanent yield criteria as used in present design philosophy remains critical. Stiffness also is of less importance and can be overlooked as a weight consideration as shown in Figure 60.

(2) A number of materials must be considered for applications to high-temperature structures, no one material being adequate (optimum weight wise) to adequately encompass the entire temperature spectrum. Each family of materials (i.e., light alloys, steels – both alloy and stainless, nickels, and ceramics) has a useful temperature range and limit for use. However, even when using the most optimistic material in each temperature range, the trend is for the weight of the structure to get prohibitively higher as the temperature increases. Reference 1 indicates the equilibrium skin temperatures of a large portion of the MX-2276 structural surface may reach a maximum of 1600°F. Reference to Figure 60 indicates that an uninsulated wing at these temperatures might weigh at least three times as much as the same wing designed for the same load conditions, but at room temperatures.

(3) Consideration of the above conclusions lead to the possibilities of using combinations of insulations and structural material to obtain better optimum structure weights. This problem is treated at a later point in this report.

(4) The maximum temperature anticipated for the leading edges and nose of the fuselage structure for the MX-2276 is 3200°F. The present-day absolute temperature limits for reliable structural materials (1400°F to 1600°F) indicates that to provide for temperatures of such magnitude the use of cooling is the only answer.

(5) The majority of the materials selected at the outset of this discussion all seem to be applicable for use, within their temperature limitations, on the MX-2276 at this point. Some materials however, perhaps could be eliminated from further investigation. Plastics, for instance, which might be used as structural material in conjunction with insulation sufficient to keep its temperature within reason, might be considered in lieu of aluminum alloy under the same conditions. Recent preliminary studies of plastic construction indicate that savings in fabrication costs can be realized, while tooling costs are approximately the same as for metal construction. The same studies, however, have also served to emphasize three principal difficulties with plastic construction.

(a) Lower stiffness than comparable metal structure.

(b) Present lack of knowledge and experience in the fabrication of structural components, particularly with respect to allowable stresses.

(c) Questionable structural reliability.

The use of ceramics for structures might also be questioned, because at present they are still unreliable and fairly unknown. Further consideration of ceramics, however, should not be abandoned because, with the present temperature limitations of metals, they may in time become extremely useful for certain parts of the structure, for example, the high-temperature leading edges.

h. Future Work

The major portion of the work on the collection and tabulation of material properties has been completed. However, a low level effort will be put forth in the future to extend the present collection as information becomes available. In particular, creep properties of titanium, and data on ceramics are being sought.

4. HEAT PROTECTION

a. General

The work previously described on structural materials has indicated approximately the weight penalties incurred simply on the basis of strength in designing the MX-2276 third-stage structure without heat protection. At this time it is considered, intuitively, that cooling the major part of the structure will also prove very heavy, though investigations will be necessary later in the study to establish this fact. Insulation however, does show promise of being a practical means of achieving the following conditions:

(1) Reduction of structural temperatures to the point where materials with a useful and reliable load-carrying capacity can be used. (From 1600°F to 1200°F.)

(2) Reduction of structural temperatures still further to allow the use of materials of higher strength-weight ratio.

(3) Elimination of thermal stresses so that the most efficient type of internal structure can be used.

The study of structural insulation for the third-stage has therefore been initiated with two principal objectives:

(1) To provide insulation data for use in the structural configuration studies that will form the latter part of this program.

(2) To investigate the practicability of designing a lightweight, reliable, and easily fabricated structural insulation suitable for the speeds envisioned for MX-2276.

Following these two objectives the insulation work has been divided broadly into two parts:

(1) A brief study of the principles of insulation, the development on the basis of practical assumptions, of simple analytical methods and design charts, and the collection of mechanical and physical properties of insulating materials.

(2) The development of detailed insulation designs.

The first of these two parts required that some time be spent on the study of insulation fundamentals in order to familiarize the structural engineers with the necessary techniques. Insulation, of course, forms an important and well-established part of many other engineering spheres, but to the aircraft structural engineer it is new, previous aircraft experience having been confined almost entirely to jet engine tail pipes. Furthermore the stringent requirements of aircraft applications justifies an understanding of principles, in addition to the use of empirical data, so that any ideas can be fully exploited.

A discussion of the more important of these principles is given below, with an indication of their significance to the MX-2276 vehicle, and these are followed by the necessary mathematical analysis.

In order to devote as much time as possible to practical design, certain simplifying assumptions have been made which are applicable to the present work. These simplifications permit the presentation of two simple charts, so that a number of insulation arrangements can be quickly designed and evaluated.

The other type of information needed for design work is a collection of material properties, and both mechanical and physical properties have been accumulated for materials of very low conductivity, for materials suitable for use as radiation barriers, and for materials to cover or contain the insulation.

Following the second of the two work items noted above, three designs have been developed for insulating structure, and these designs are presented in detail later in this report. Each of the three designs is adaptable to the insulation of structures fabricated from a variety of structural materials. The necessary insulation thicknesses are adjusted in each case to provide structural temperatures appropriate to the structural material being considered, and the total insulation weights for each case are presented in Table X found in Section IV-C4c.

The insulation designs presented are for use with conventional shell construction; future insulation work will be concerned with the development of improved designs. Insulation arrangements will also be devised for use with beam-type wing structures having no structural skin.

b. Insulation Principles

It is well known that the transmission of heat is accomplished by three mechanisms:

(1) Radiation - an electromagnetic form of energy transmission which does not require a medium between the transmitting and receiving agents.

(2) Conduction - the transmission of energy through a medium by molecular agitation.

(3) Convection - the transmission of heat by physical transportation, such as circulation, of liquids or gases.

It is found by experiment that gases, including air, have very low values of conductivity, while liquids are appreciably higher, and solids much higher again. The conductivity of

water is 26 times that of air while the metals range from 350 to 17,000 times that of air. The dense solids such as metals, stone, etc., are completely opaque to radiation and transmit heat by conduction. Fibrous and other loose fill materials, however, will transmit by conduction through the material itself, by conduction through the air trapped within the material, by convection currents in this air, and by radiation across the spaces. From this it follows that as the material density is decreased, the proportion of heat transmitted by radiation and air convection will increase while the proportion transmitted by material conduction will decrease. The sum total of these effects is generally expressed by the conductivity coefficient K.

The heat transmitted between two points by conduction is proportional to the temperature difference between the two reference stations, while the heat transmitted by radiation is proportional to the difference of the fourth powers of the absolute temperatures. If the heat problem of the MX-2276 vehicle is now visualized as a cool structural skin, separated from an outer skin or covering or lamina which may be at an equilibrium temperature of 1600°F or 2060°R, it is apparent that the intervening space should be filled with material very opaque to radiation. Such materials of course are necessarily dense, and therefore heavy, and even if materials of low conductivity are used, such as diatomaceous brick an appreciable amount of conduction is introduced.

A possible solution to this problem is to build up what might be called an artificial insulation, in which very thin layers of dense material of relatively low emissivity are introduced as radiation barriers, and are separated by narrow air gaps to reduce conduction. If these gaps are sufficiently small the heat transmission by convection will also be small, while at the very high altitudes anticipated, the ideal conditions of a vacuum will be approached. In practice it will probably be necessary to use a spacing material between the radiation barriers, and apparently this material should be of very low density to minimize conduction. The fact that such low density material transmits heat by radiation is no longer of consequence, owing to the presence of the radiation barriers.

The chief consideration in the ultimate comparison of insulation arrangements will be weight, and it is evident that the weight of a "radiation barrier" will depend very closely upon such practical considerations as the thickness of material required for fabrication purposes, the condition of the material surface that can be maintained during prolonged use at high temperatures, and the amount of covering or containing structure necessary to maintain a smooth external surface and to carry airloads. Similarly, of course, attachments will form an important weight item with the solid insulation and, depending on its density, this may or may not require external covering, etc.

c. Insulation Design Charts

To evaluate analytically the amount of insulating material required to maintain any given structural temperature, after exposure to the high boundary layer temperatures for a specified time, two simple expressions have been developed based on a number of practical assumptions. These expressions correspond to the two extreme types of heat transmission:

(1) Pure conduction with constant conductivity.

(2) Pure radiation.

The assumptions on which this work is based are as follows:

(1) No heat capacity in the insulation.

(2) Infinite conductivity through the structural skin, applicable to thin shell structures.

(3) Constant external temperature at the outer layers of the insulation.

(4) Constant conductivity with temperature, low conduction materials.

(5) Constant emissivity with temperature, of all surfaces of radiation barriers.

(6) Neglect of conduction paths through the radiation barriers due to spacing material, connections, etc.

Note that assumption (3) permits inclusion of the heat transfer by forced convection from the boundary layer to the outer covering, and also the radiation from the covering back into the boundary layer. This is normally difficult to include in a complete solution because of the fourth power radiation term, but with insulation it can be assumed that heat conducted into the structure is small enough that the outer covering, or the outer layers of insulation, reaches equilibrium temperatures instantaneously. Thus the solutions given below begin with a known constant temperature at the outside.

Each of these assumptions will ultimately require a careful evaluation before accurate insulation sizes can be predicted, but substantial mathematical simplifications are introduced by their use and the results are considered to be a good first approximation.

Beginning with the conduction case, the heat balance equation relating the heat conducted through the insulation to the heat absorbed by the skin is as follows:

$$(T_o - T_s)k/X = \rho\, C_p t\, (dT_s/d\theta)$$

$$\frac{k}{X\rho C_p t}\int_0^{\theta} d\theta = \int_{T_1}^{T_2} \frac{dT_s}{(T_o - T_s)}$$

or $$\frac{k\theta}{X\rho C_p t} = \ln\, (T_o - T_1/T_o - T_s)$$

where T_o = Outside temperature - °F

T_s = Metal sink temperature - °F

T_1 = Initial temperature - °F

k = Thermal conductivity of insulator $\frac{BTU\ in}{ft^2 hr\ °F}$

x = Thickness of insulator - feet

ρ = Density of metal - lb/ft^3

C_p = Specific heat of metal - $\frac{BTU}{lb\ °F}$

t = Thickness of metal - inches

θ = Exposure time - hours

The above equation is plotted in Figure 61, in a form suitable for the rapid estimation of insulation requirements.

The equation for radiation was developed through a method which parallels that for the conduction equation.

The heat transferred from one surface, to another surface at a lower temperature, is given by the relationship

$q_{0-1} = \epsilon_{0-1} (To^4 - T_1^4)$ where ϵ_{0-1} is the effective emissivity of two facing surfaces. If there are many surfaces involved, then:

$$q_{0-1} = \sigma\, \epsilon_{0-1} (To^4 - T_1^4)$$

$$q_{1-2} = \sigma\, \epsilon_{1-2} (T_1^4 - T_2^4)$$

$$q_{2-3} = \sigma\, \epsilon_{2-3} (T_2^4 - T_3^4)$$

$$\vdots \qquad \vdots \qquad \vdots$$

$$q_{n-s} = \sigma\, \epsilon_{n-s} (T_n^4 - T_s^4)$$

Since the heat capacities of the radiation shields are neglected, we can say,

$$q_{0-1} = q_{1-2} = q_{2-3} \cdots\cdots q_{n-s} = q_{o-s}$$

Now, dividing by the effective emissivities, and adding we have:

$$q_{o-s}\left[\frac{1}{\epsilon_{0-1}} + \frac{1}{\epsilon_{1-2}} + \frac{1}{\epsilon_{2-3}} + \cdots\cdots + \frac{1}{\epsilon_{n-s}}\right] = (T_o^4 - T_s^4)$$

The emissivities are assumed equal for all surfaces, then the effective emissivities must likewise be equal, therefore:

$$q_{o-s} = \sigma\, \epsilon_{o-s}/(n+1)\ (T_o^4 - T_s^4)$$

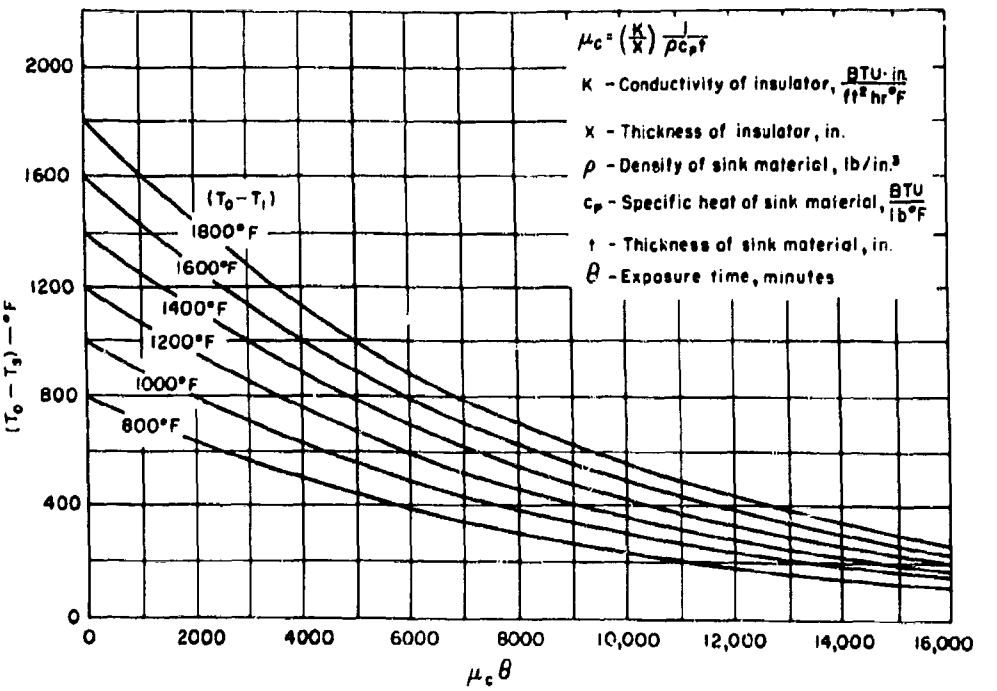

Figure 61. Conduction Barrier Design Chart

If the heat radiated from the outside lamina is absorbed by the metal sink, then, as before, we have a differential equation to evaluate.

$$\frac{\sigma \epsilon_{o-s}}{(n+1)} (T_o^4 - T_s^4) = \rho \, C_p t \, \frac{dT_s}{d\theta}$$

$$\therefore \quad \frac{\sigma \epsilon_{o-s}}{(n+1)(\rho C_p t)} \int_0^{\theta} d\theta = \int_{T_i}^{T_s} \frac{dT_s}{(T_o^4 - T_s^4)}$$

After integrating, the equation becomes:

$$\frac{\sigma \epsilon_{o-s}}{(n+1)(\rho C_p t)} \theta = \frac{1}{4T_o^3}\left[2\left(\arctan \frac{T_s}{T_o} - \arctan \frac{T_i}{T_o}\right) + \ln\left(\frac{T_o + T_s}{T_o - T_s} \cdot \frac{T_o - T_i}{T_o + T_i}\right)\right]$$

where σ = Stefan-Boltzmann constant = 1.73×10^{-9} BTU/hr-sq ft - °R^4

θ = Exposure time - hour

n = Number of intermediate radiation shields - dimensionless

ρ = Density of metal sink - lb/ft^3

C_p = Specific heat of metal sink - BTU/lb - °R

t = Thickness of metal sink - feet

T_o = Outside lamina temperature - °R

T_1 = Initial temperature - °R

T_s = Sink or metal skin temperature - °R

ϵ_{o-s} = Effective emissivity between two adjacent faces =

$$\frac{1}{\frac{1}{\epsilon_o} + \frac{1}{\epsilon_s} - 1}$$

where ϵ_o = Emissivity of one face.

and ϵ_s = Emissivity of the second face.

Evidently, to obtain the minimum value of $\epsilon_{(o-s)}$, the minimum values of both ϵ_o and ϵ_s are required. Generally, $\epsilon_o = \epsilon_s$ so that $\epsilon_{(o-s)} = \frac{\epsilon}{(2 - \epsilon)}$.

The above equation relating temperatures to the structure and insulation characteristics is plotted in convenient form in Figure 62.

d. Insulation Materials

Before proceding with examples of practical insulation designs for MX-2276, it is appropriate to present the mechanical and physical properties that have been collected for the various materials used. These materials may be divided into the following three groups:

(1) Materials of very low total conductivity. Ideally these materials should also possess low weight, mechanical strength, and resistance to high temperatures (1600°F).

(2) Materials for radiation barriers. These should have, and be able to maintain, a surface of very low emissivity, should be light in weight and available in very small thicknesses, and should be resistant to high temperatures.

(3) Materials for the external covering. These should have reasonable mechanical strength at 1600°F.

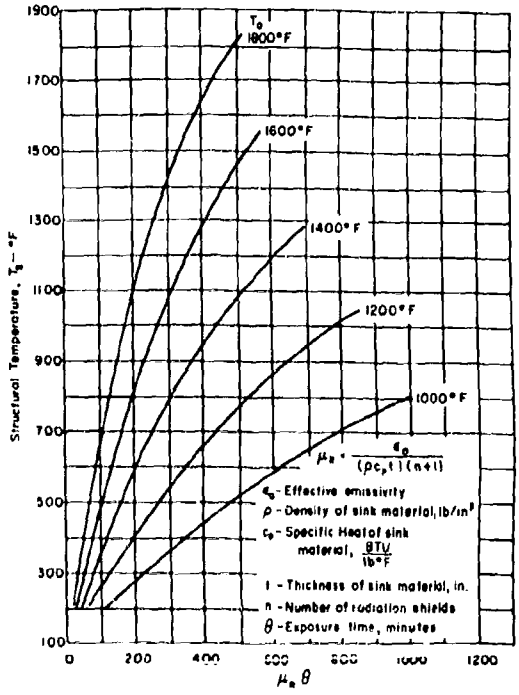

Figure 62. Radiation Barrier Design Chart

(1) Low Conductivity Materials

The densities, conductivities, and useful temperature ranges of a large number of insulating materials have been considered, and values for the more promising of these materials have been incorporated in Figure 63, which is a plot of thermal conductivity x density against mean temperature. This curve, therefore, indicates the materials having the lightest weight for a given value of thermal resistance. In the following notes, only the optimum materials from this curve will be considered.

Of the insulating materials presented in Figure 63, which are not capable of carrying loads, i.e., fibrous or loose fill materials, Fiberfrax is the most efficient. Fiberfrax is a loose material of very fine-blown

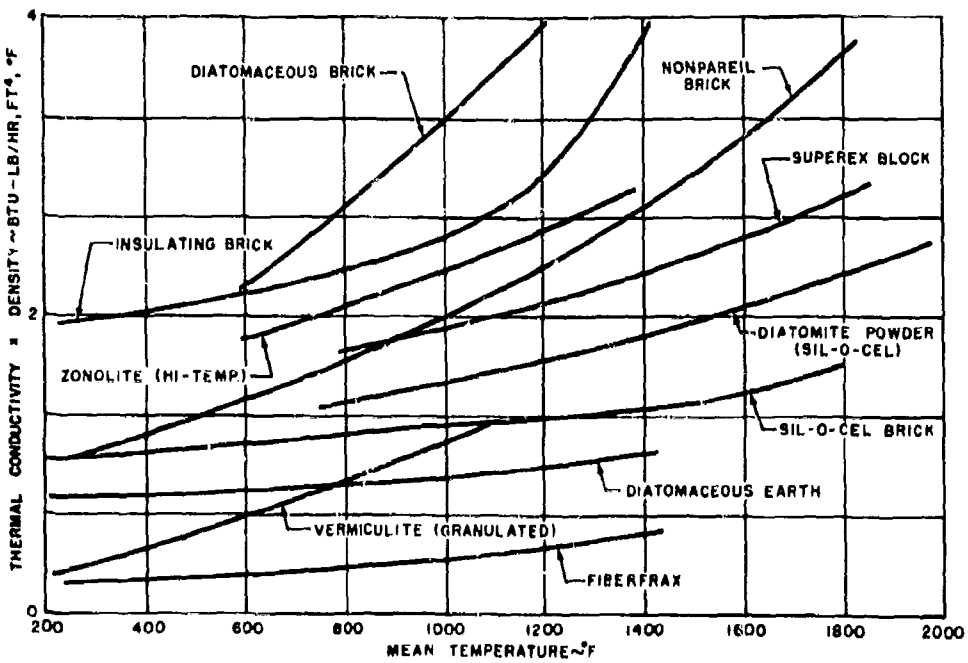

Figure 63. Thermal Conductivity Parameter of Insulating Materials

fibers of aluminum oxide and it can withstand temperatures well in excess of 2000°F. Its optimum density is 6 lb/ft^3, and at this density the thermal conductivity coefficient is as follows:

Temp. (°F)	400	800	1200	1400
K $\frac{\text{(BTU in)}}{\text{(hr-sq ft - °F)}}$	0.36	0.64	1.12	1.48

The optimum of the block-type materials is Sil-O-Cel building block which at a density of 23.5 lb/ft^3 has the following values of conductivity:

Temp. (°F)	200	600	1200
K $\frac{\text{(BTU in)}}{\text{(hr-sq ft-°F)}}$	0.516	0.600	0.708

Further data on this material are lacking at present, but the Babcock and Wilcox Company manufactures an insulating firebrick of similar density and conductivity characteristics, and further properties are related to this material. From the information available on the firebrick, a modulus of rupture of 50 psi can be expected and the working temperature may be 1600°F.

(2) Materials for Radiation Barriers

From this point of view of strength and temperature resistance, Inconel is the choice for the radiation barrier material but unfortunately this, together with most other materials, will oxidize at 1600°F. This oxidation is not likely to be sufficient to be considered as a corrosion, but the presence of only a very thin oxide film will make low emissivity values unobtainable. Preliminary investigation has shown that platinum does not oxidize at any temperature and will therefore retain a polished surface. It is presently proposed, therefore, to plate or clad the Inconel with a very thin layer

of platinum and in this way an emissivity of 0.107 may be expected for the polished surface at 1600°F.

Indications are that the Inconel base material can be obtained as a foil as thin as 0.0005 inch but until inquiries on this point are completed it will be assumed that the minimum thickness is 0.001 inch.

(3) Materials for the External Covering

The material for the external covering of any loose form of insulation will require sufficient mechanical strength at 1600°F, to resist air loads. Possible choices are Inconel, Haynes alloy C, molybdenum, and the ceramics.

The Inconel X has rather low strength values at 1600°F, but considerable information and experience available regarding its fabrication, and since this information is quite favorable, the Inconel X will be used for the present insulation evaluation work.

For Inconel X at 1600°F the following strength and stiffness values, which were obtained from figures 54, and 55 will be used:

$$F_{cy} = 25{,}100 \text{ psi}$$

$$E_c = 21.9 \times 10^6 \text{ psi}$$

Haynes alloy C shows a better strength weight ratio than the Inconel, and accordingly inquiries are presently being made concerning fabrication techniques, welding, heat treatment, etc.

The molybdenum and the ceramics are in a much earlier stage of development than the materials mentioned above and will not be considered for the present application until much more information becomes available.

e. Insulation Designs

Three basic insulation designs have been developed which are suitable for insulating any structure of the MX-2276 third stage that is of conventional shell construction, and which is in areas where outer surface equilibrium temperatures do not exceed 1600°F. This temperature has already been established (Subsection IV-C3g(2)) as the top limit, according to present knowledge, in areas of primary structure.

The three designs may be classified according to the type of insulation used, as follows:

(1) Radiation barrier

(2) Loose fill insulation

(3) Solid block insulation

Each of these designs has its advantages and disadvantages, and these will be discussed below. Each design has been adapted, by adjusting the insulation thickness, to protect primary structures of Inconel X, titanium and aluminum. A complete summary of the corresponding weights is given in Table X.

(1) Radiation barrier

The radiation barrier consists of a number of layers of Inconel foil, 10 x 20 inches and 0.001 inch thick, each layer plated on both sides with a very thin layer of platinum. The platinum will insure that no trace of oxidation occurs so that low values of surface emissivity can be maintained throughout the service life at high temperature. The very thin foil has been selected in the interests of minimum weight, and its use requires that each layer be separated to avoid contact and hence excessive conduction. This is accomplished with spacers consisting of thin sheets (0.005 inch thick) of Fiberfrax. Very low density Fiberfrax is used, approximately 3 lb/ft^3, so that the heat transmitted by conduction along the fibers is very small.

The complete assembly of alternate Inconel and Fiberfrax layers is stapled or wired together at intervals in order to retain the sheets in correct relationship.

This radiation barrier is, of course, quite incapable of carrying aerodynamic loads,

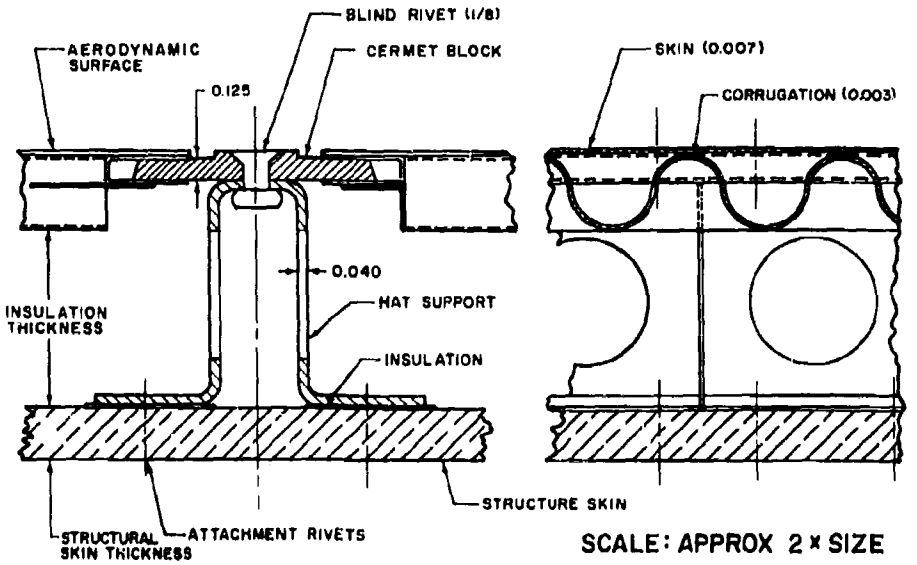

Figure 64. Insulation Retainer Detail

and accordingly it is covered by an outer, air-load-carrying surface of 0.007-inch thick sheet backed with 0.003-inch thick corrugations, 3/8-inch deep and of 3/4-inch pitch. At present, Inconel is proposed as the material for this covering, thus permitting either spot welding or furnace brazing of the skin to the corrugations.

To accommodate thermal expansion of the outer covering relative to the inner structural skin, and also to isolate this covering from primary structural loads, the skin and corrugations are also broken down into panels 10 x 20 inches.

Figure 64 shows a means of attaching these panels to the primary structure while still retaining freedom for thermal expansion, and reducing to a minimum the heat conduction paths through the radiation barrier. The hat section member shown in Figure 64 is riveted permanently to the structural skin. The hat section member may be broken into short lengths to reduce thermal stresses caused by small thermal gradients which may exist through its depth.

To the top of this hat section a cermet strip is attached with blind, Inconel rivets. This strip serves both to carry aerodynamic pressure loads into the hat section member and also to isolate thermally the outer skin-corrugation panel. Thickness of this strip has been kept down to 1/8 inch in the interests of both weight saving and reduction of the effects of thermal shock. The light-gage Inconel channel shown brazed to the skin-corrugation panel forms a clip attaching the panels to the cermet strip. The section shown is typical of all four sides of the panel.

Apart from the question of weight, which is dealt with in Table X, the anticipated difficulties of this arrangement (many of which are presently being studied) include the following:

(a) Possible fabrication and handling difficulties with the 0.003-inch thick corrugations. Contact with the International Nickel

Company has established that such an assembly could be successfully furnace-brazed with Inconel sheet, using the Nicor process, or spot-welded with suitable small welding tools. Still unknown is the technique necessary to form corrugations from very thin sheet.

(b) Preservation of sufficient aerodynamic smoothness, particularly around the edges of the panels.

(c) Possibility of thermal deformations in the skin-corrugation panels due to temperature gradients during transient heating conditions. Owing to the very shallow corrugations, such deflections are expected to be very minor, but this point will require checking.

In establishing the material sizes and thicknesses for the radiation barrier design an external aerodynamic pressure of 200 lb/sq ft, positive or negative, was arbitrarily assumed. A summary of the calculations establishing both the strength under aerodynamic loading, and the insulation requirements, is given below.

Inconel X Corrugated Panel Calculations

Panel size - 10 x 20 = 200 sq in.

Loading = 200 lb/sq ft

$\therefore$ Panel load = $200 \times \frac{200}{144} = 278$ lb

or 13.9 lb/in. of panel width

Considering a one-inch strip of the panel as a simple beam, 10 inches long

$M_{max} = W1/8 = 13.9 \times 10/8 = 17.4$ in.-lb

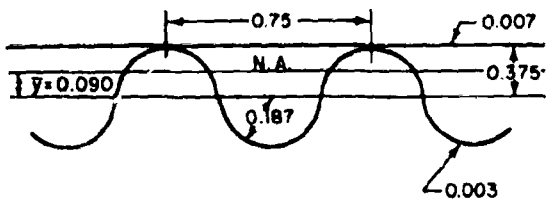

Figure 65. Panel Section

For ease in calculation a 0.75-inch width will be used.

Area of skin = $0.75 \times 0.007 = 0.00525$ sq in.

For a corrugation with a pitch depth ratio = 1

developed width = 2.6 in/in.

$\therefore$ Area = $2.6 \times 0.003 \times 0.75 = 0.0058$ sq in.

$I_o = \pi R^3 t = 3.14 \times 0.187^3 \times 0.003$

$= 0.00628 \times 0.00982 = 0.000060$

$\bar{y}$ of Section = $0.00525 \times 0.190/0.00525 + 0.0058 = 0.00525/0.01105 \times 0.190 = 0.090$ in.

I of Section = $0.0058 \times 0.090^2 + 0.00525 \times 10^2 + 0.000060$

$= 0.000047 + 0.0000525 + 0.000060$

$= 0.000159$ in^4/0.75 inches of panel

I/inch = $0.000159/0.75 = 0.000212$ in^4

I/y (skin) = $0.000212/0.10 = 0.00212$ in^3

I/y (corrugations) = $0.000212/0.277 = 0.000765$ in^3

σ (skin) = $17.4/0.00212 = 8200$ psi

σ (corrugations) = $17.4/0.000765 = 22800$ psi

σ_{cr} of skin (Inconel X at 1600°F) = $3.62E(\frac{t}{b})^2$

$= 3.62 \times 21.9 \times 10^6 (\frac{.007}{.75})^2$

$= 92 \times 10^6 \times 0.000087 = 6900$ psi

σ_{cr} of corrugations (Inconel X at 1600°F)

$= 0.3\frac{Et}{r} = 0.3 \times 21.9 \times 10^6 \times 0.003/0.187$

$= 10{,}600$ psi

$\sigma_{cyp} = 0.81 \times 10^6 \times 0.31 = 25{,}100$ psi

(See Figure 54)

The above calculations show that the proportions of the panel are such as to support the selected airload; slight buckling of the skin might occur between corrugations at ultimate load.

The following conditions apply to all of the calculations for insulations which follow:

(a) Skin thickness assumptions are based upon a loading of approximately 4000 pounds per inch, which is considered typical of the loading which will be encountered in the third stage of the MX-2276. They also correspond to about the average thicknesses required for either a skin-stringer or cylindrical shell-type of construction.

(b) Three typical skin materials are considered working at the following temperatures.

75S-T aluminum alloy	(200°F)	t = 0.125 in.
RC-130A titanium	(600°F)	t = 0.125 in.
Inconel X	(1200°F)	t = 0.100 in.

(c) The time (θ) is taken to be 60 minutes and the temperature of the outside surface 1600°F (T_0). The initial structure temperature is assumed to be 100°F (T_1).

Radiation Barrier Calculations:

θ = 60 min $\quad T_0$ = 1600°F $\quad T_1$ = 100°F

$\mu_R \theta = \frac{\epsilon_0 \theta}{C_p t (n+1)}$ (See Figure 62)

which becomes $n = \frac{\epsilon_0 \theta}{C_p t (\mu_R \theta)} - 1$

where: ϵ_0 = effective emissivity of the reflecting surfaces, assumed the same for each

$\epsilon_0 = \frac{\epsilon}{2 - \epsilon}$

ϵ = emissivity of platinum plated foil

$\epsilon = 0.107$

ρ = structure material density

C_p = structure material specific heat

t = structure material thickness

n = number of radiation shields

$\mu_R \theta$ = constant for particular temperature condition (Figure 63)

$\therefore \epsilon_0 = \frac{\epsilon}{2 - \epsilon} = 0.107/2\text{-}0.107 = 0.107/1.893$

$= 0.0565$

(3) Loose fill insulation

This insulation design is essentially a loose fill of Fiberfrax material having the optimum density of 6 lb/ft^3 and contained within an airload-carrying outer skin exactly as described above for the radiation barriers. The difficulties mentioned above with the radiation barrier system apply here also. The principal differences between the two arrangements are weight and total thickness, this latter an important item with wing insulation since the maximum possible wing depth is required for primary structure. Values for weight and total thicknesses are given in Table X, and calculations for insulation thickness are given in Table IX.

(4) Solid block insulation

This insulation design was developed to eliminate the large amount of delicate sheet metal fabrication inherent in the previous designs, and also to more easily attain the required aerodynamic smoothness. The arrangement is illustrated in Figure 66 which

TABLE VIII

RADIATION BARRIER CALCULATIONS

STRUCTURE MATERIAL	T_s	$\mu_R\theta$	μ_R	ρ	C_p	t	$\rho C_p t$	n
75S-T Bare	200°	40	0.67	0.10	0.21	0.125	0.00262	31
RC-130A	600°	130	2.16	0.17	0.13	0.125	0.00176	14
Inconel X	1200°	360	6.0	0.30	0.105	0.10	0.00315	2

TABLE IX

CONDUCTION BARRIER CALCULATIONS

STRUCTURE MATERIAL	T_s	$T_o - T_s$	$\mu_c\theta$	μ_c	$\rho C_p t$	$\mu_c \rho C_p t$	K		X (Inches)	
							Fiber-frax	Sil-O-Cel	Fiber-frax	Sil-O-Cel
75S-T Bare	200°	1400	600	10	0.00262	0.0262	0.66	0.61	25.2	23.2
RC-130A	600°	1000	3500	58.4	0.00176	0.102	0.804	0.66	7.9	6.5
Inconel X	1200°	400	11000	183	0.00315	0.576	1.08	0.715	1.87	1.23

TABLE X. INSULATION WEIGHTS

RADIATION BARRIER - WEIGHTS/SQ FT OF SURFACE			
Structural Material / ITEM	Aluminum 75S-T Bare	Titanium RC-130A	Inconel X
Outer Skin	0.320	0.320	0.320
Corrugation	0.320	0.320	0.320
Ceramic Block	0.310	0.310	0.310
Corrugation Edge Member	0.063	0.063	0.063
Hat Section	0.260	0.260	0.260
Radiation Barriers	1.340	0.605	0.086
Fiberfrax Spacers	0.039	0.018	0.002
Total Weight (lb/sq ft)	2.652	1.896	1.361
Total Thickness (in.)	0.56	0.50	0.40
LOOSE FILL INSULATION - WEIGHTS/SQ FT OF SURFACE			
Outer Skin	IMPRACTICAL	IMPRACTICAL	0.320
Corrugation			0.320
Ceramic Block			0.310
Corrugation Edge Member			0.063
Hat Section			0.500
Fiberfrax Fill			0.940
Total Weight (lb/sq ft)			2.453
Total Thickness (in.)			2.25
BLOCK INSULATION - WEIGHTS/SQ FT OF SURFACE			
Sil-O-Cel Block	IMPRACTICAL	IMPRACTICAL	2.43
Ceramic Bolt			0.14
Ceramic Coating			0.30
Total Weight (lb/sq ft)			2.87
Total Thickness (in.)			1.24

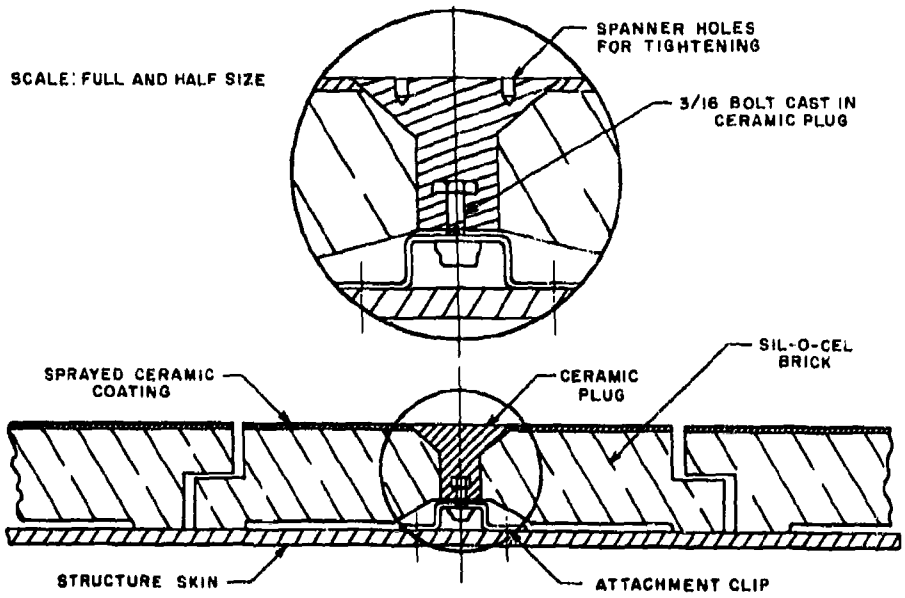

Figure 66. Solid Insulation Design Detail

shows a covering for the structural shell of 10 in.-square blocks of insulating fire brick material. Thickness of the blocks is arranged to give the required structural temperature-time conditions.

Each block is held in position by a single center attachment consisting of a large countersunk pin of ceramic material, in which is embedded a standard bolt of heat-resisting steel or Inconel. The combined ceramic-metal bolt is screwed into a captive nut carried by a small bracket attached permanently to the structural skin.

Each block is spaced from its neighbors with a gap sufficient to accommodate thermal expansion and structural strains, and the edges of the blocks overlap to seal the structure from direct contact with the hot boundary layer.

The outer surface of the blocks is protected from abrasion, and the porosity is rendered aerodynamically smooth by a sprayed ceramic coating. It is anticipated that this coating could be thick enough that the whole surface, including the attachment bolts, could be ground smooth after assembly on the airframe. Contact between the blocks and the structural skin is restricted to a small area around the edge of the block, so that additional insulation is provided by the gap between the blocks and the skin.

With the arrangement described above any block is readily removable for replacement or for access to the skin beneath.

This design depends upon the mechanical strength of the insulation material to resist aerodynamic loads, and available information suggests that this strength, although small, is adequate due to the comparatively large thicknesses required. In view of the nature of the material, however, this point is considered worthy of much more consideration, and accordingly samples of the material have been requested for inspection and evaluation. At the present time these samples have not been received.

Two other problems with this type of insulation require further investigation. These problems are the possibility of thermal shock failures in the insulating block, and the question of adhesion between the block and its ceramic coating. More consideration can be given to these questions when samples are received.

Calculations pertaining to the solid insulation design are summarized below.

Conduction Barrier Calculations:

θ = 60 min T_0 = 1600°F T_1 = 100°F

(T_0-T_1) = 1500°F

$$\mu_c = (k/x)1/\rho\ C_p t$$

or $$x = (k/\mu_c)1/\rho\ C_p t$$

where: x = thickness of insulator, in.

k = conductivity of insulator

ρ = structure material density

C_p = structure material specific heat

t = structure material thickness

μ_c = constant (from Figure 64).

f. Cooling

The subject of cooling has not been pursued to any great extent to date. Some data have been collected for the cooling or heat capacities of some cooling fluids which might find application in the design of the MX-2276 airframe. Figure 67 is a plot of heating capacity per pound of coolant weight vs final coolant temperature, resulting from this preliminary study.

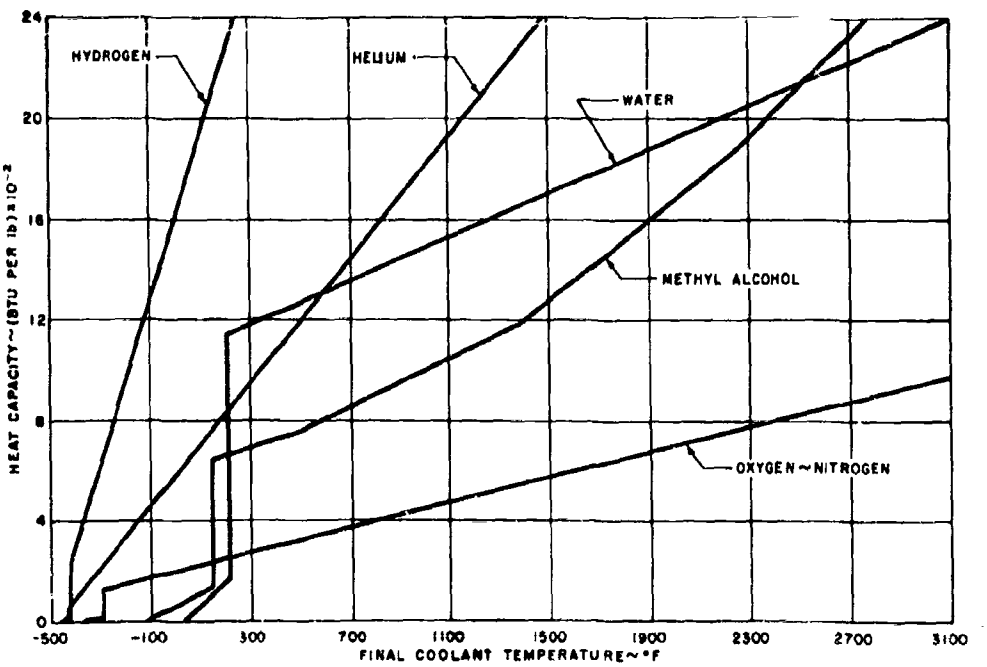

Figure 67. Heat Capacity of Cooling Fluids.

Cooling arrangements that will be considered in future studies will include systems using circulating liquids, with or without vaporization; sweat cooling with liquids; cooling by the ejection of gas; and cooling by ablation. As with the insulation studies, the studies of cooling will concentrate on methods which, after an initial consideration, show the most promise. Factors to be considered will include the following:

(1) Choice of cooling liquids or gases, including precooled coolants.

(2) Selection of materials for cooling pipes, or the surface, etc., of the cooled regions.

(3) Methods of pumping and circulating coolants.

(4) Comparison of weights of various cooling methods including fluid or gas weights, associated structure, piping, etc; and weight of pumping machinery. Weights will be compared on the basis of total heat input with a consideration also of the external skin temperatures.

(5) Methods of attaching the cooling elements and the associated structure to the primary airframe structure with allowance for thermal expansions, and structural deflections. Typical splices and joints, connections for coolant lines; etc.

g. Discussion and Results

Before considering the results presented above, it should be noted that one of the original assumptions made in the calculation of insulation thicknesses was that the heat capacity of the insulation could be neglected. In the case of the extreme thicknesses of the solid insulation shown above, this assumption is obviously not valid, but it is also clear that even when appropriate corrections are made, the radiation barriers are much superior on a weight basis, to either the solid block insulation or the Fiberfrax. It should be emphasized that this conclusion is not general, but applies only to the MX-2276 third stage. It is, in fact, a direct result of the long flight time. The solid insulation weight is proportional to time of flight, while only the smaller part of the radiation barrier weight depends on time.

This conclusion also applies only to insulation designed to protect shell-type structures. Reference 1 originally proposed that certain portions of the third-stage wing be constructed of a grid of Haynes Stellite alloy with the spaces filled with blocks of diatomaceous earth, each block being the full depth of the wing section. This proposal is not invalidated by the above conclusion; its evaluation will come later in the program, under "Structural Configurations."

Considering now the unit weights of radiation barrier type insulation, as presented in Table X, the weights shown for the titanium and Inconel structures are of the same order (approximately 2 lb/sq ft) as the insulation weights contemplated in the original proposal, Reference 1. It is inappropriate, in this section, to consider structural configurations, but a very preliminary calculation of weights of structure plus insulation, based on Figure 64 and Table X, suggests that the insulated aluminum structure will give the lightest weight.

If this present conclusion is upheld by more refined calculations it will still be necessary to optimize the maximum structural temperature for minimum weight of combined insulation and structure.

The wetted area of the MX-2276 third stage is approximately 2200 square feet. If it is assumed that 75% of this area will require insulation, then the total weight of insulation, for a shell-type aluminum structure, will be of the order of 4400 lb.

The need for refining the design of Figure 64 to obtain minimum weight, is immediately apparent, and this can be accomplished by some or all of the following methods:

(1) Variation of outer panel length and width until the optimum combination of skin-corrugation weight and edge attachment weight is obtained.

(2) Refinement of the detail design of the edge attachments.

(3) Venting between inner and outer surfaces of the skin-corrugation combination so that pressures are more nearly equalized and more airload is carried directly on the structural skin. This will permit thinner skin and corrugation material.

(4) Further development of the laminated Inconel foil and Fiberfrax barriers to achieve lower values of emissivity, and thinner foils and spacers.

(5) Development of alternate designs for the outer covering and its attachment.

(6) Using layers of radiation foil of lesser density material, such as aluminum, adjacent to the structural member, especially in the case where aluminum structure is used and lower structure temperatures are maintained.

h. Future Work

As in the case of structural materials, the major portion of the work of collecting and tabulating insulating materials is complete; the information however will be expanded as information becomes available. Most of the future work anticipated will be to improve and optimize insulation combinations as suggested in the previous paragraph of conclusions.

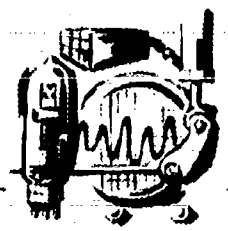

D. NAVIGATION AND CONTROL

I. GENERAL

a. Requirements

The selection of the navigation system for the MX-2276 bomber and missile is a function of the mission requirements. The requirements which have been assumed as a basis of system comparison are as follows:

(1) Bombing mission: the missile should have an accuracy such that the missile warhead can be detonated with a one-mile CEP, at a target whose local map coordinates are previously specified, at any range between 2000 and 8000 nautical miles from the take-off site.

(2) Reconnaissance mission: The bomber should be capable of flying over a specified map-line with a lateral tolerance of 5 miles over a distance from 2000 to 8000 nautical miles from the take-off site. Information must be available to permit orientation and correlation of optical and radar information with an rms error of 1/2 nautical mile using map geodetic controls at take-off and landing sites.

(3) Bomber landing mission: The bomber should be capable of navigating automatically to a specified landing site at a distance of 6000 to 10,000 nautical miles from the take-off site, with an error of less than 10 nautical miles.

b. Types of Systems

Four classes of navigation systems

were considered which might be applicable to the MX-2276 weapon.

(1) All-inertial guidance.

(2) Doppler-aided inertial guidance

(3) Position-aided inertial guidance

(a) Loran type

(b) Radar beacon

(c) Navarho

(d) ATRAN map-matching

(e) Star tracker

(4) All-positional electronic guidance (Same position-fix possibilities above)

c. Criteria

These classes of navigation were evaluated considering the following aspects in addition to the basic accuracy requirements:

(1) Weight of airborne equipment (plus cost and power consumption)

(2) Number of ground stations and their complexity (plus operating personnel, maintenance cost, etc.)

(3) Present state of the art (and estimate of development in 10 years)

(4) Flexibility of use and capability of independent action by pilot.

(The factors shown in parentheses were secondary considerations only.)

d. System Selected

As a result of these studies, the primary navigation system chosen is all-inertial; the radar and optical systems are used primarily for reconnaissance but can serve the pilot as standby sources of navigation information for use at his discretion in diverting to an alternate target or landing site, correction of mapping errors, or other action requiring judgment and decision.

2. INERTIAL GUIDANCE SYSTEM

a. General

The tremendous speed, short time of flight, and long range of Stage III create many navigational problems which are peculiar to this particular weapon system. Therefore, it might be expected that the solutions will be somewhat unconventional compared with present navigation and guidance schemes. However, the methods under consideration are of the type which should evolve from the present trend of development, rather than revolutionary systems which require completely new fields of research.

The short time of flight involved in the MX-2276 missions is advantageous to the inertial instrumentation. On the other hand, the long range makes the task of accurate navigation rather difficult. This becomes obvious when the various effects which have to be accurately accounted for in the navigation system are considered. These effects range from the complexities connected with three-coordinate navigation, and the difficulties encountered in avoiding polar ambiguities of the coordinate system, to the accurate simulation of earth curvature, earth rotation, and Coriolis, centrifugal, and gravitational accelerations. Nevertheless, it appears that with new or improved methods and components, the gradual progress in all fields pertaining to inertial guidance promises satisfactory solutions within the necessary time period. Such expectations appear particularly justified considering the rapid progress in the field of guidance over the past 10 to 15 years.

However, considering the present state-of-the-art, the question arises as to whether or not it is possible to improve the

performance of an inertial navigation system in this particular case, by means of Doppler or search radar. Owing to the relatively high accelerations, the ascending portion of the flight is the most difficult phase as far as gyro drift, accelerometer characteristics, etc., are concerned. During the cruise phase the accelerations are much lower, hence, the errors are much smaller. Therefore, if it is possible to achieve precise initial conditions in the inertial system at the beginning of the cruise phase, the navigation system can perform much better over the whole flight path. For this reason, the over-all gain from correcting the inertial system over the ascending portion of the flight path can be very significant. The combination of the inertial system with a Doppler radar or a similar system which can provide accurate velocity information during the boost period, will provide such a gain.

For example, it is conceivable that a ground-based installation like the Azusa system (a phase-comparison system) could determine bomber velocity information during the boost phase with the necessary accuracy. This velocity could be measured in three coordinates, resolved into the present coordinates of the navigation system, and compared with the velocity outputs of the inertial system. These velocity error signals in three coordinates may be determined, and used to keep the stabilized platform aligned, and to correct for any deviations in the velocity stages of the inertial system. Combinations of Doppler and inertial systems have already been instrumented sucessfully, so that no major problems should be presented from this standpoint.

A suitable practical method for comparison of Doppler and inertial velocity data can be designed along the following lines. Doppler computations and resolutions into inertial system coordinates are performed on the ground. Inertial velocity data are transmitted to the ground. Error signals determined from the comparison of Doppler and inertial data are transmitted back to the bomber where they can be used for correction of the navigation system. This would keep the additional equipment in the bomber at a minimum.

The disadvantages in the use of a ground-based Doppler radar are increased complexity of the over-all instrumentation, a decreased reliability resulting from the increased complexity, the vulnerability of a large ground installation to enemy attack, and the difficulties and time required to build or replace these installations. The Doppler ground installation can be replaced by a Doppler radar in the bomber, thus overcoming some of these disadvantages; however, the increase in bomber equipment weight would be a very serious problem. Moreover, the required Doppler accuracy of better than 0.01% of the velocity (which reaches a maximum of 22,000 ft/sec) appears to be far in the future if the radar weight and complexity are limited.

The use of position-monitoring of the inertial system utilizing a search radar in the bomber has provided improved inertial system operation in some applications, and was therefore investigated for this application. The monitoring can be performed through the use of checkpoints consisting of radar reflectors along the initial flight path of the bomber. This means intermittent correction of the inertial instrumentation by radar position measurements. This preliminary study considered that the boost flight time is in the order of 6 to 10 minutes, and that the range error of the inertial system at the beginning is very small. The results indicate that present day radar accuracies (in the order of 1500 ft CEP) would have to be improved more than ten times to appear promising in this connection. This is partially due to the fact that both altitude and speed of the MX-2276 are very high. On this basis, the possibility of improving the accuracy by position monitoring during boost appears very poor.

In summary, the basic inertial system with improved components and techniques appears capable of satisfactory accuracy. Considerable improvement in the capability of present day inertial systems might be gained if the conditions at the beginning of cruise are known very accurately. The use of a ground-based Doppler radar system during boost will provide a better knowledge of these conditions at that time. However, the use of an airborne search radar does not appear to offer any improvement.

The following study presents the investigations of the inertial instrumentation alone. Through a complete investigation of the problems and the design of this system, a more definite conception of the navigation system can be obtained. After this concept is determined, the combination of such an inertial system with available ground-based Doppler systems can be studied more completely.

b. Bomber Navigation System

In order to produce instantaneously accurate position information during the flight it is necessary to install a navigation system in the bomber. This will enable the pilot to coordinate all observations along the flight route as to their positions on the globe. The requirements for such a navigation system are that it can operate over the total conceivable area for any MX-2276 mission and avoid any ambiguities or coordinates which are difficult to instrument.

(1) Suitable Navigational Coordinate Systems

One of the simplest systems to instrument is the conventional latitude and longitude coordinate system where the measurements are performed along the horizontal north and east directions. However, this system has definite disadvantages. Since the operational area of MX-2276 extends across the northern polar region an ambiguity at the north pole appears unavoidable with this conventional system. In order to overcome this difficulty, a transverse polar system has to be chosen, where the total conceivable operational area does not coincide with one of the system poles. This offsets to a considerable extent the simplicity of the conventional polar coordinate system, but permits navigation over vast areas of the globe.

Such a transverse system is based on its orientation on a great circle between take-off and landing point. Since it is desirable for reasons of simplicity to measure horizontal accelerations in two mutually perpendicular coordinates, a system based on transverse longitude and latitude appears to be suitable. Two possibilities exist as to the identification of the great circle between take-off and landing point; with a meridian, or with the equator of such a system.

The choice between these two possibilities is determined by the range of the system. If the system is chosen where the great circle between take-off and landing site represents a meridian, a range of 10,000 n. miles seems practically impossible. The reason for this is that at both the take-off and the landing site the bomber approaches too closely the poles of this transverse system which are about 10,800 n. miles apart. The equator system has no such limitations. Therefore, it is the system considered in the following description.

(2) The Transverse Polar Coordinate System.

As mentioned above, this coordinate system is defined so that its equator represents a great circle between take-off and landing site. However, the target which is to be crossed by the bomber during one mission can conceivably be off this great circle by an appreciable distance.

Let Λ denote the angle between the earth's equatorial plane and the plane of the great circle defined above (Figure 68). Define the principal meridian as the meridian passing through the northernmost point of the great circle. Let L' be the range coordinate measured in an eastern direction along the great circle from the principle meridian, and λ' the cross-range coordinate measured perpendicular to the great circle, positive in the northern direction. Any point on the earth can then be defined by the coordinates (L', λ'). Moreover, L' and λ' form a conventional longitude-latitude system with the previously defined great circle as its equator (Figure 69). This system will be referred to as the transverse longitude and latitude coordinate system.

(3) The Stabilized Platform of the Navigation System

The navigation system working on the basis of this coordinate system contains a

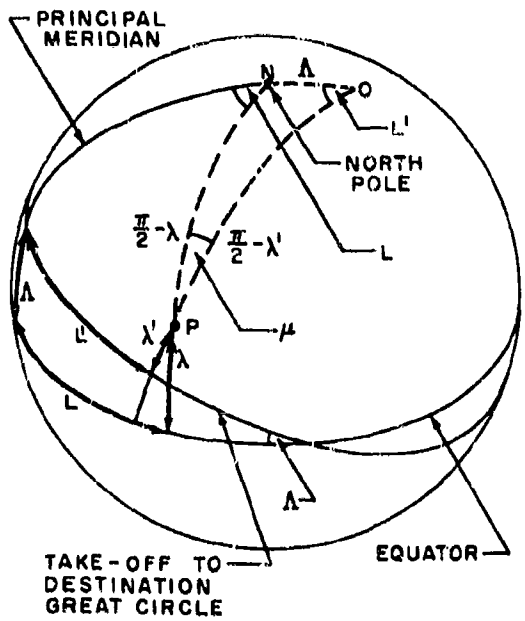

Figure 68. Location of Transverse Coordinate System with Respect to Conventional Latitude and Longtitude

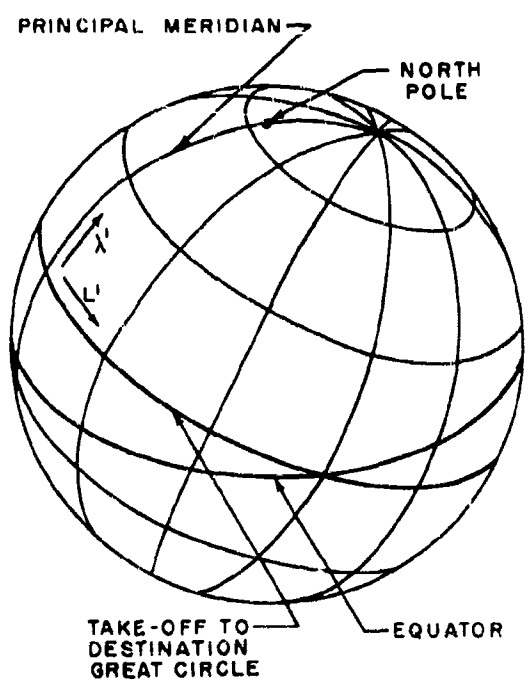

Figure 69. Transverse Coordinate System

gyro-stabilized platform. This makes it possible to maintain the three accelerometers with their measuring axes along the coordinates of transverse longitude and latitude and the vertical direction on the earth.

The platform is gimballed in 3 axes, coincident with yaw, pitch, and roll in horizontal flight (Figure 70). The inner element of the platform is separated into the accelerometer section and the gyro section which are rotatable relative to each other about an axis parallel to λ'. It so represents a four-gimbal system which appears to be favorable in connection with the special geometry selected and the expected flight paths of the bomber.

As the general direction of all bomber flight paths is along the equator of the transverse system, the horizontal velocity components normal to it remain rather small. Hence, whereas it appears imperative, because of the high speed, to introduce the platform rotation about the λ' -axis by other than torquing means, it is entirely feasible and practical to handle the small angular velocities about the L'-axis by gyro torquing. This permits the construction of this four-gimbal arrangement, which is far superior to any five-gimbal platform from the standpoint of weight and size. The platform shown in Figure 70 combines the advantages of the gyro torquing techniques with those of a multiple gimbal arrangement.

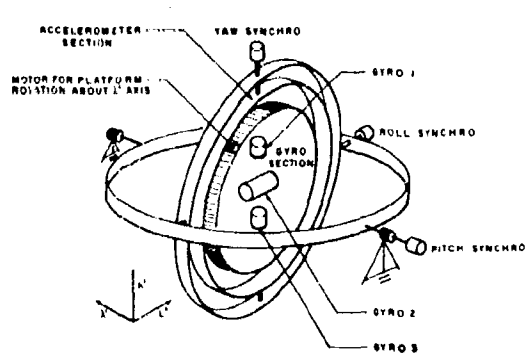

Figure 70. Possible Platform Design for MX-2276 Navigation System

The platform is rotated for earth rotation both about the vertical and about an axis parallel to L' by torquing of the gyros. The rate of angular motion due to earth curvature about the λ' -direction is introduced by a mechanical rotation between the gyro and the accelerometer section. This is performed by a motor turning the accelerometer portion relative to the gyro carrier according to the distance measured in the L'-direction, (see Figure 70). This appears advantageous from the standpoint that the high velocity components of the bomber developing along the L' -direction would require a very great torquer accuracy with respect to its range, if the rotation of the platform had to be performed by torquing. Since the velocity components in the λ' -axis are comparatively small and the deviations from the great circle are assumed not to exceed about 1000 n. miles, the corresponding rotations of the accelerometer system about the vertical and the L'-direction are performed by torquing of the gyros.

(4) Position Computer of the Navigation System

The second important portion of the navigation system is the position computer. This uses the output of the three accelerometers and computes, mainly by double integration, the instantaneous position of the bomber in the transverse longitude and latitude coordinate system. Moreover, it supplies the various signals for torquing the gyros and rotating the accelerometer platform section relative to the gyro section. This instrumentation is represented by the block diagram of Figure 71. The nomenclature for the block diagrams is presented in Table XI.

It will be noted that in each of the two horizontal position channels, a Schuler loop is used to keep the accelerometers level. It is anticipated that at the long range of the MX-2276, corrections will have to be made for the change in radius of curvature of the geoid as a function of latitude, direction, and altitude. If a direction angle, μ , is defined as the angle between north and the positive λ' -direction, and λ represents geographic latitude, a solution of the triangle PNO on Figure 68 results in the following expressions:

$$(1)\ \sin\lambda = \cos\Lambda \sin\lambda' + \sin\Lambda \cos L' \cos\lambda'$$

$$(2)\ \sin\mu = \sin\Lambda \frac{\sin L'}{\cos\lambda}$$

Approximating the geoid by an ellipsoid with equatorial radius, a, and eccentricity, e, the desired curvatures at altitudes, h , above sea level can be shown to be the following:

$$(3)\ \frac{1}{R_{\lambda'}} = \frac{1}{a}\sqrt{1-e^2\sin^2\lambda}\left[1+\frac{e^2}{1-e^2}\cos^2\lambda\sin^2\mu\right]\frac{1}{1+\frac{h}{R_{\lambda'}}}$$

$$\approx \frac{1}{a}\left[1+e^2\left(\sin^2\Lambda\sin^2 L' - \frac{1}{2}\sin^2\lambda\right) - \frac{h}{a}\right]$$

$$(4)\ \frac{1}{R_{\lambda'}} = \frac{1}{a}\sqrt{1-e^2\sin^2\lambda}\left[1+\frac{e^2}{1-e^2}\cos^2\lambda\cos^2\mu\right]\frac{1}{1+\frac{h}{R_{\lambda'}}}$$

$$\approx \frac{1}{a}\left[1+e^2\left(1-\sin^2\Lambda\sin^2 L' - \frac{3}{2}\sin^2\lambda\right) - \frac{h}{a}\right]$$

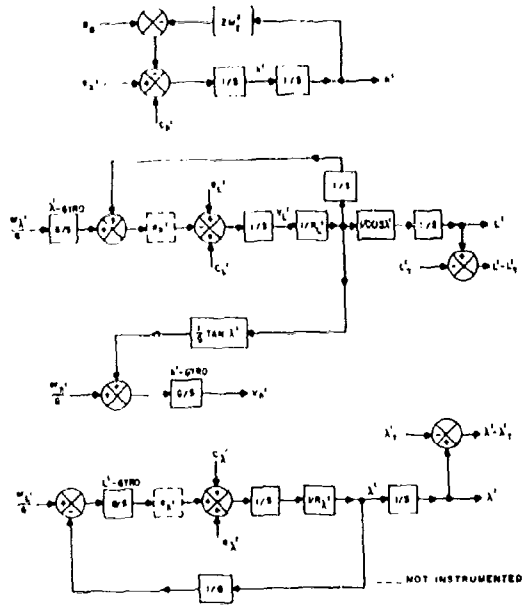

Figure 71. Schematic Diagram of Navigation System

TABLE XI. BLOCK DIAGRAM NOMENCLATURE

a	=	Acceleration
c	=	Acceleration Correction
g_o	=	Gravitational Acceleration at Sea Level
h	=	Altitude above Sea Level
R	=	Earth Radius
V	=	Velocity on the Earth
λ'	=	Transverse Latitude
ν	=	Platform Angle
L'	=	Transverse Longitude
ω	=	Component of Earth Rotation
ω_E	=	g_o/R
ψ	=	Yaw Angle
θ	=	Pitch Angle
ϕ	=	Roll Angle
$\Delta\psi$	=	Angular Deviation between Horizontal Projection of Line of Sight and Attitude Axis of Missile
ρ	=	Range to go
——	=	Electrical Information
– –	=	Mechanical Information

SUBSCRIPTS:

H	=	Horizontal
D	=	Dive
S	=	Slant
P	=	Platform
h'	=	Vertical Direction
λ'	=	Cross Range Direction*
L'	=	Range Direction

*Range being defined as great circle between take-off and landing site

Using equation (2), and neglecting fourth and higher powers of e and second and higher powers of h/R in the approximations ($e^2 = 0.006723$).

The rates of rotation to be introduced to the gyro torquers for the earth's rotation, Ω, are:

(5) $$\omega_r = \Omega \sin\lambda$$

about the vertical axis,

(6) $$\omega_{L'} = -\Omega \cos\lambda \sin\mu = -\Omega \sin\Lambda \sin L'$$

about the L'-axis, and

(7) $$\omega_{\lambda'} = \Omega\cos\lambda\cos\mu = \Omega(\cos\Lambda\cos\lambda' - \sin\Lambda\cos L'\sin\lambda')$$

about the λ'-axis. Equation (2) was used in deriving equations (6) and (7).

A separate channel is used to compute vertical velocity and altitude, since these are needed in the computation of horizontal position. A vertical accelerometer indicates vertical acceleration plus gravity. Variation of gravitational acceleration with altitude must be taken into account in subtracting the gravity component. The acceleration of gravity g varies with altitude as follows:

(8) $$g = g_0\frac{R^2}{(R+h)^2} \approx g_0\left(1-\frac{2h}{R}\right) = g_0 - 2\omega_E^2 \cdot h$$

where $\omega_E^2 = g_0/R$, and g_0 is the acceleration of gravity at sea level.

In addition, corrections for centripetal and Coriolis accelerations are made at each accelerometer. They are

(9) $$C_h = 2V_{L'}\cdot\omega_{L'} - 2V_{\lambda'}\cdot\omega_{L'}$$

in the altitude channel,

(10) $$C_{L'} = V_{\lambda'}(\dot{L}'\cdot\sin\lambda' + 2\omega_r) - \dot{h}(\dot{L}'\cos\lambda' + 2\omega_{\lambda'})$$

in the L'-channel, and

(11) $$C_{\lambda'} = -V_{\lambda'}\cdot(\dot{L}'\sin\lambda' + 2\omega_r) - \dot{h}(\dot{\lambda}' - 2\omega_{L'})$$

in the λ' -channel. After adding these corrections to the accelerometer outputs, the velocity in each of the three position channels is obtained by integrating, and the angular velocity is the obtained by dividing the horizontal velocity by the proper radius of curvature which is instrumented according to equations (3) and (4). In the λ' -channel, another integration gives a measure of cross-range angle, and can be made to indicate cross-range angle to target by subtracting the cross-range to the target. In the L'-channel, however, the resulting angular velocity is $\dot{L}' \cos \lambda'$, and the longitude is obtained by first dividing by $\cos \lambda'$ and then integrating. Another integrator is needed to rotate the accelerometer gimbal on the platform at the rate $\dot{L}' \cdot \cos \lambda'$.

It only remains to keep the platform properly aligned in azimuth. For this purpose, the vertical gyro is torqued at a rate $\dot{L}' \sin \lambda'$ about the azimuth axis.

(5) Accuracy Considerations

While Figure 71 gives a general idea of the complexity of the bomber navigation system, it is still necessary to determine the general accuracy requirements for the main components. Since they are directly related to the performance characteristics of the bomber, the data that are most significant in this connection are given below.

(a) The very high cruising speed. This reduces the effective vertical acceleration due to the centrifugal effect in some areas down to about 0.25 g_0.

(b) Rather short time of flight for the total mission from take-off point to the landing point.

30 min. flight time to a 5,000 n. miles target

60 min. flight time for about 9,000 n. miles

As the very high speed reduces the effective vertical acceleration to a considerable extent, it proportionally decreases any errors resulting from a horizontal misalignment of the platform. This reduces the gyro performance requirements in terms of drift and torque accuracy by an appreciable amount.

On the other hand, the variable altitude in connection with the high speed necessitates an accurate instrumentation of the vertical coordinate. This means that either a vertical accelerometer with double integrator, or a radio altimeter, has to be used to furnish current altitude and rate of altitude information all along the flight path. If the nonemanating feature of the bomber navigation system is considered to be important, the inertial solution probably will be preferred. Then the vertical accelerometer has to be accurately compensated for gravitational, centrifugal, and Coriolis accelerations. This calls for an elaborate auxiliary computation of these compensation terms.

Since practically all centrifugal and Coriolis effects, as well as those resulting from the ellipsoidal shape of the earth and the variation of g with altitude, are of sufficient importance to be computed and compensated for, the overall complexity of the instrumentation becomes appreciable. Moreover, the high speed introduces the problem of accurately turning the coordinate system for the earth's curvature. As the maximum speed approaches 22,000 ft/sec it requires a rate of platform rotation in the order of 220°/hr. The platform design of Figure 70 tries to avoid those instrumentation difficulties by mechanically rotating the accelerometer portion on the platform relative to the gyro portion, according to the output of the transverse longitude integrator. As it is conceivable that under certain circumstances a lateral velocity component up to 4,000 ft/sec is developed, a rather accurate torquing arrangement for the gyros still remains a necessity. Considering present gyro torquer designs and a maximum permissible torque error of 0.025° / hr, it appears that the accuracy requirement of one part in 2,000 can be considered to be practical.

As far as the gyro accuracy is concerned, the assumption of a drift torque of 0.1°/

hr in an untrimmed condition on the test stand appears to be realistic by the end of the development time of this weapon system. By a slow rotation of the gyro housing about the gyro spin axis, or by reversing its spin direction, a considerable improvement appears possible. Assuming that the performance of such a gyroscopic arrangement is in the order of 0.025°/hr under flight conditions, the resulting error does not exceed 1500 ft over a range of 5000 n. miles. Compatible accuracies in the measurement of acceleration in the order of 3×10^{-5} g are required. Moreover, all the aforementioned correction terms have to be introduced to the accelerometers with corresponding accuracies. Integration by the velocity and range integrators has to be performed with errors not exceeding about 2×10^{-5} if the over-all error is to remain below 1/2 n. mile.

Last but not least, consideration has to be given to the gravitational anomalies, as well as the deviation of the geoid in comparison to the assumed ellipsoid of the earth. Since the gravitational radial anomalies (Bouguer Anomaly) in the United States approach 0.2 cm/sec^2, and deflections up to 30 in. have been observed, these anomalies have to be considered for the proper leveling of the platform. Because of the height of the cruising part of the trajectory it can be expected that at least all local anomalies during the flight of the bomber practically disappear.

(6) Possible Instrumentation

In order to meet these requirements it appears necessary to select an instrumentation which works at least partially on a digital basis. Following is a description of an instrumentation which meets the above-mentioned accuracy requirements and will be available in the near future.

It consists of an accelerometer with digital output and a digital computer for two integrators. The accelerometer is an electrically constrained pendulum working on the basis of a d-c torquer. It is spring suspended and the temperature is closely controlled. The current for constrainment consists of pulses which are accurately defined by the electrical circuit under consideration (Figure 72). They are derived from the discharge of a capacitor connected to a highly stabilized voltage source. The charge and discharge operation is controlled by a relay, which in turn is operated by the pick-off of the accelerometer. The use of this intermittent capacitor feedback for the accelerometer constrainment transforms the acceleration information directly into digital numbers.* This permits a simple electronic counter to compute

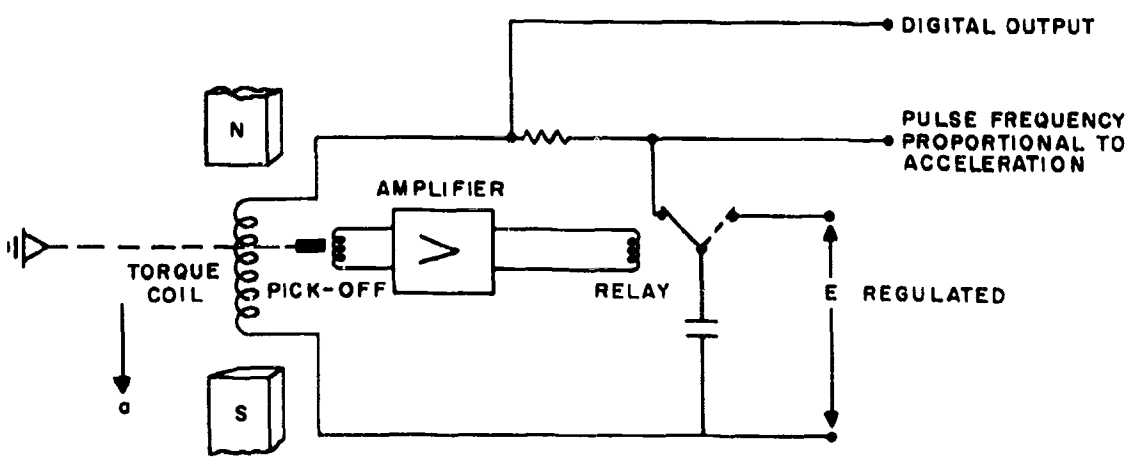

Figure 72. Schematic Diagram of Digital Accelerometer Including Electrical Circuit

the velocity very accurately. Transformation of this digital information into shaft position permits instrumenting the various auxiliary terms like Coriolis accelerations and gyro torques on an analogue basis with sifficient accuracy. Compensation of the accelerometer for Coriolis and centrifugal terms is performed by the use of a second winding on the torquer coil (not shown in Figure 72). The use of a digital integrator furnishes accurate instantaneous position information.

As the computer portions of highest accuracy are instrumented on a digital basis, and all auxiliary terms by analogue computers, it seems possible to achieve the extreme accuracies which are required for such a navigation system with a total error not exceeding about 1/2 n. mile.

c. Bomber Guidance System

Since the high speed of MX-2276 makes it difficult if not impossible for the pilot to control the bomber along a prescribed path to some specific point on the earth, a guidance system for the bomber is proposed. For this purpose the output of the navigation system is modified by subtracting the coordinates L'_T and λ'_T of the desired point to destination (see Figure 71). This means that the position information develops relative to this point in terms of transverse longitude and latitude to go. The guidance computer then resolves these two "range to go" informations, both along the line of sight to the destination point and normal to it, by means of a resolver. Comparison of this resolver angle with the attitude angle of the bomber permits the derivation of a guidance signal which keeps the bomber on the instantaneous line of sight to the desired point of destination. A visual display of the guided bomber on a transparent map will help the pilot to coordinate his actions and will indicate approximately his instantaneous position.

*Experimental work carried out at BAC indicates that the required accuracy can be achieved without great difficulties.

d. Missile Guidance System

It is also necessary to select a system for guiding the missile to the target after it is released from the bomber. The present plan consists of a basic inertial system which can be corrected from the bomber by means of a radio link. The bomber operator can obtain accurate information on the target location, either by radar or optical means, as the bomber approaches the target. These data can be used to compute error signals for transmission to the missile. This correction feature is of extreme value considering the accuracy and lack of map data on target locations.

(1) Choice of Coordinate System

The choice of coordinates for this system is very much dictated by the bomber navigation instrumentation which delivers velocity and position information in a transverse polar coordinate system. As these velocity and position data have to be transferred to the missile guidance system, where they serve as initial conditions, the over-all instrumentation has to be optimized with respect to complexity, weight, and size. Among the various geometrical possibilities for setting up the missile guidance system, the use of a "line of sight" geometry appears to require a minimum of missile equipment. In this case, the stabilized platform is oriented in azimuth so that the measuring direction of one accelerometer points towards the target while that of the second accelerometer is normal to it, in a horizontal plane. The third accelerometer measures in the instantaneous vertical, and is required to furnish computer information for calculating the Coriolis terms in the two horizontal axes.

This geometry requires information about the distance towards the target and the azimuth angle of the line of sight to be set into the guidance system. Since the flight path of the missile extends up to 200 n. miles, the computation of the distance to go has to consider at least the spherical shape of the earth, possibly even the ellipsoidal deviations. This makes such a computation rather involved and so requires extensive computers. Moreover, it is

desirable that a means exist for more accurately determining the target location during missile flight and correcting the missile system by means of a radio link. This means basically a change in the location of the desired detonation point. A detailed instrumentation study reveals that it cannot be done if the advantages of simplicity in connection with a line of sight geometry are to be preserved. The same is true for the computation of the heading angle, which has to be introduced with high precision.

Another possibility is to use the basic velocity and position information in the same coordinates as it develops in the bomber navigation system. This dispenses with any coordinate transformation, but requires a somewhat more complex missile instrumentation. The lack of any change in the coordinate systems between bomber and missile appears to result in a higher over-all accuracy without increasing the complexity of the total arrangement. In this case, any change in target location during the missile flight can be accomplished very easily by varying the target coordinates. It does not require any additional instrumentation in the bomber or the missile.

For these reasons it appears that a geometry of the missile guidance system in the coordinates of the transverse polar system is desirable.

(2) Transfer of Initial Conditions

In order to allow the missile guidance system to perform its proper computations it is necessary to introduce the instantaneously correct initial conditions from the navigation system. They consist of a proper alignment of the stabilized platform in the missile, so that the missile system accelerometers read the same accelerations as those on the bomber platform. Moreover, the velocity, as well as position outputs of the missile system, has to be adjusted to whatever the readings in the navigation system are.

This can be performed by an angular platform alignment about the vertical and a comparison of the position outputs of both systems. Deriving error signals from such a comparison in all three coordinates, and applying those signals as corrections to the missile system, results in a complete platform alignment and the correct setting of the instantaneous velocity and position information. The corresponding block diagram is shown in Figure 73. It indicates the error signals to be fed back to the gyro torques, accelerometers, and velocity stages in the two horizontal axes. In the vertical the error signal from the position comparison is fed only to the accelerometer and the velocity stage. Moreover, an error signal is derived from the h' -gyro misalignment in both systems. This is used to torque the h' -gyro in the missile system so that its horizontal coordinates coincide with those of the bomber system.

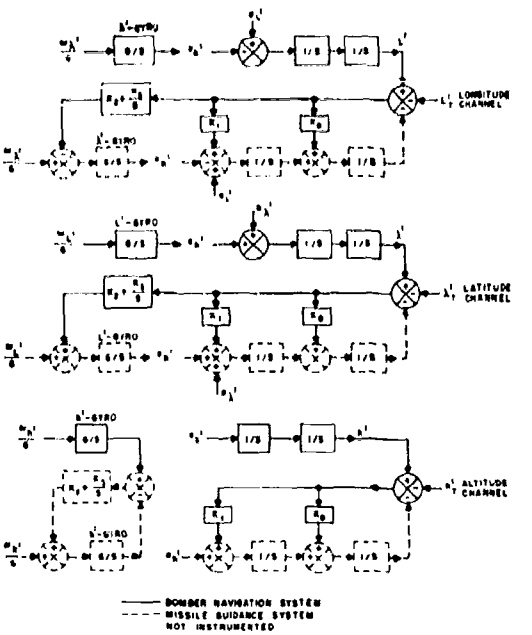

Figure 73. Diagrams of Missile Guidance Systems Alignment Instrumentation (Simplified for Clarity)

In order to compensate for the consistent portion of the missile system gyro drift, the transfer function $K_2 + \frac{K_3}{S}$ is inserted in front of the gyro torquers. This transfer function, producing an integral of the error function, maintains a torque signal at the gyros after the transient response of the alignment loop has died out. This means that the consistent drift torque of each individual gyro remains compensated, even after the position error signal has disappeared. The two horizontal loops of the alignment system are of the fourth order and have to be optimized with respect to the various parameters involved. This means that the noise spectra of all the components as well as the available time for the alignment, have to be considered in the process of determining the natural frequency of the system. Since the speed of the bomber is so high, and the range of the missile position computer is limited by accuracy, the permissible time for the alignment procedure is rather short. It is estimated to be less than one minute. This requires a rather low noise level from the various components of the loops in order to assure sufficiently accurate initial settings, and therefore means an instrumentation of a rather high quality.

(3) Accuracy Requirements

The particular requirements resulting from the alignment of the stabilized platform in the missile determine to a considerable extent the accuracy requirements associated with the various components. In addition, the post-launch operation of the missile system demands some further performance values be met. From preliminary investigations it can be deduced that the random portion of the gyro drift should not exceed about 0.1°/hr, accelerometer errors should stay in the order of 5×10^{-4} g, and the integrator accuracy should amount to at least 1 part in 5,000. The over-all error of such an instrumentation over a 200 n. mile range, including any effects of these errors on the alignment performance, is estimated to be in the order of 1500 ft CEP. These requirements call for very precise instrumentation in the missile.

(4) Position Computer Instrumentation

The inertial instrumentation in the missile can operate on a somewhat similar basis as the instrumentation of the navigation system. This means that accelerometers with digitalized outputs and step motors for the first integration are used. This seems advantageous from the standpoint of simplicity and the high accuracy which is required in the velocity stages. Since the range to be covered is rather small (200 n. miles), conventional analogue integrators probably will be suitable for computing the second integrals. Such a combination of analogue and digital equipment appears to offer many advantages in the course of building a position computer. The block diagram of this position computer and the gyroscopic reference system represented by the stabilized platform is very similar to that of the bomber navigation system. It shows the same basic elements as have already been discussed. Nevertheless, various simplifications in the computation of all auxiliary terms for earth rotation and earth curvature can be introduced because of the lower accuracy requirements for this system. This will reduce the complexity of this system considerably in comparison with the one in the bomber.

The output of the missile system position computer delivers position and velocity in the coordinates of the transverse polar system mentioned above. It should be noted that this position information is relative to the location of the target. This means that the outputs of the three position integrators give the instantaneous missile position in terms of transverse longitude, latitude, and altitude increments from the location of the desired detonation point of the warhead.

For this purpose, the location of the detonation point is fed into the position computer in all three coordinates (see Figure 73). The necessity for detonating the warhead within a well-determined altitude range over the target, again requires an accurately instrumented vertical coordinate of the missile guidance system. Since the time of flight of the missile is rather

short, it seems possible to obtain precise enough altitude information from the inertial instrumentation in the missile.

(5) Flight Path Computer

The "range to go" information in terms of transverse longitude, latitude, and altitude increments in itself is not sufficient to direct the missile to the desired detonation point. It requires a flight path computer which derives from this information the necessary signals for the proper yaw and pitch control.

This computer is based on a resolution of the transverse longitude and latitude increments along the missile attitude and normal to it (Figure 74). This resolution is performed by a resolver on the vertical axis of the missile platform. The output of this resolver delivers practically the "range to go" along a line of sight course and a signal proportional to the angle between the line of sight and the missile attitude axis.

The division of both results in a signal which is suitable for the lateral guidance in a horizontal plane along a line of sight to the target.

A similar arrangement is used in the vertical plane where the horizontal range to go and the altitude increment are resolved by a resolver in the pitch axis of the platform. Here

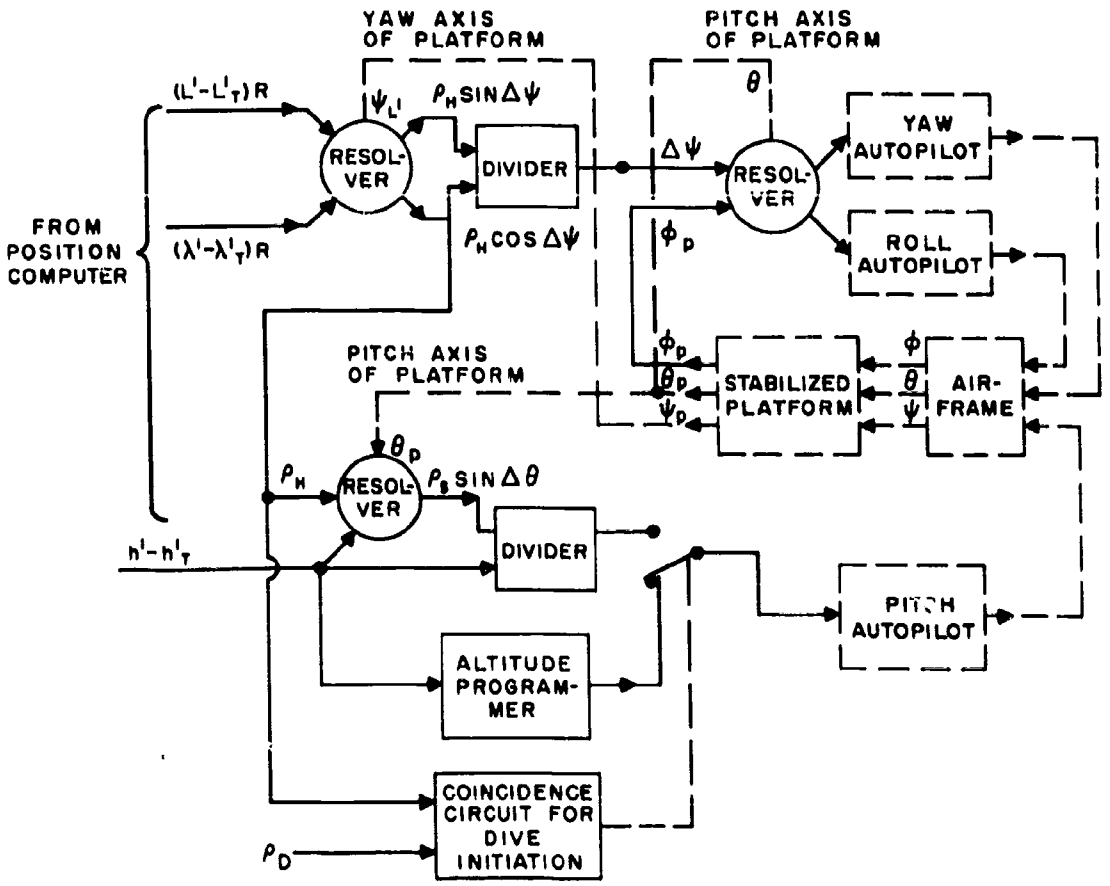

Figure 74. Diagram of Flight Path Computer Including Autopilot System for Missile

too, a command is derived which is proportional to the angular deviation between the missile attitude and the line of sight (in the vertical plane) towards the detonation point (see Figure 74). Accuracy requirements for this flight path computer are low because it represents basically only a nulling device.

(6) In Flight Target Correction

The ability of the pilot to make position fixes by optical or search radar makes possible final corrections for target location as the bomber flies over the target complex, and the missile is on its way. The position of the target area has to be measured within some reference system. Two methods of making this measurement are under consideration. In the first method a position correction may be applied to the reference system supplied by the inertial instrumentation by the observation of a landmark in the target vicinity, the geographic coordinates of which are well known. In the second method, where the exact coordinates of the target or checkpoint are not known exactly, the location of the target can be determined relative to the frame of reference supplied by the inertial instrumentation.

In the first method it is possible to correct the output of the inertial system according to the observed location of the landmark, thus providing an over-all improvement in the navigational information of the remainder of the flight path. The second method does not permit correction of the system output, but allows position correction for the missile flight.

A comparison of the complexity of the instrumentations, the attainable accuracy of the inertial system, and the availability of suitable checkpoints will determine the optimum solution to this particular problem.

In any case, a corrective signal will be computed on board the bomber and transmitted via a radio link to the missile already in flight towards the target. This signal initiates a change in the longitude and latitude increments of the missile position computer which instantly causes the flight path computer to compute different heading and "range to go" signals.

3. RADAR SYSTEMS

The problems of radiation propogation are summarized in Figure 75. These problems will be treated in the following sections.

a. The Beam-Bending Problem

Any radar system for the MX-2276 will suffer from a phenomenon called beam bending which is peculiar to the hypersonic flight realm. The difficulty lies in the effects which ionization and the change in gas density have on the propagation of radar waves. In effect, the air in the vicinity of the bomber forms a weak but nevertheless significant prism which will change the apparent direction of arrival of radar waves and hence could create errors in the radar map. In addition, unless this prism remains constant over a few pulses (and because of turbulence it cannot be completely steady) a blurring of the radar picture will result, much as heat waves blur and distort optical images in a desert.

The present study of this problem has been in two directions: the amount of beam bending to be expected from various assumed shapes and densities of the gas prism, and the effect of ionization of the gas within the prism, i.e., to determine how much ionization can be tolerated.

In the course of this study, the results of similar studies (Reference 105) became available from which, by extrapolation, it could be shown that the effect of density variations on the direction of a radar beam of the proposed type should be completely negligible, but ionization would begin to be a problem at the point where the effective dielectric constant, ϵ, differs from that of free space by about 1%. Calculations were then made of the number of free electrons per cubic centimeter which will result in a 1% decrease in ϵ. A preliminary calculation assuming aerodynamic temperatures, density, etc., resulted in an estimate that the number of free electrons in the vicinity of the leading edge will be close (within an order of magnitude) to this 1% limit for X-band radiation. The extent of which this effect, generated

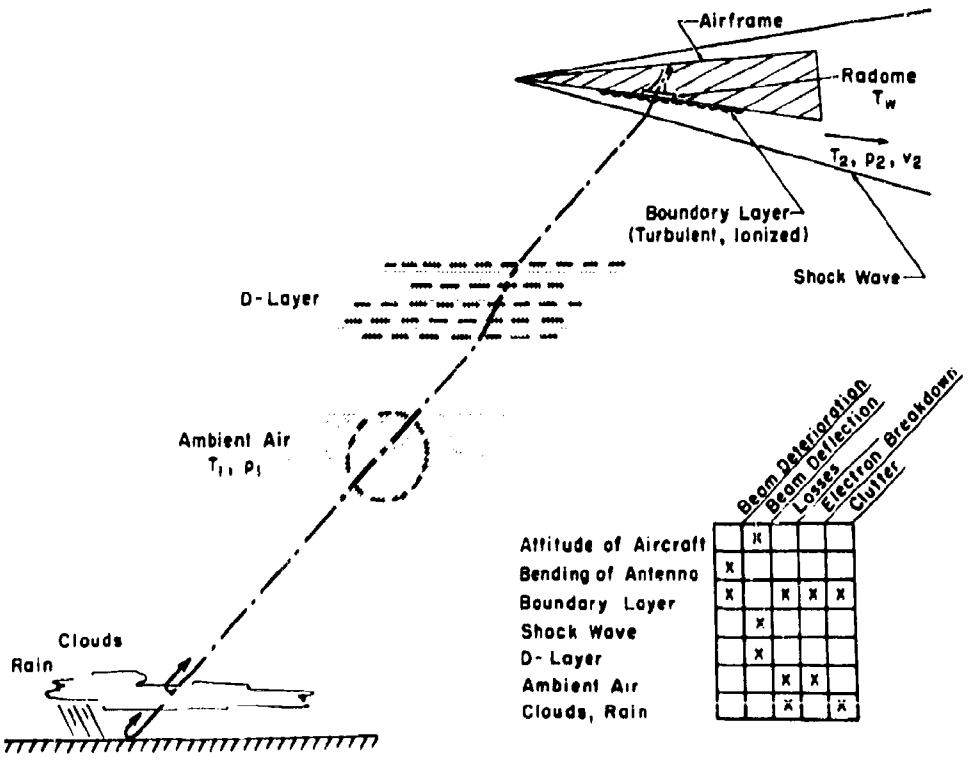

Figure 75. Radiation Propogation Problems

at the leading edge, will be reduced as a function of distance back from the leading edge, is difficult to determine from available information. The electron density at any point will not be far different from the "equilibrium" of thermal ionization corresponding to the local temperature at that point because of the fact that each electron will undergo at least 10^5 collisions during the time it takes the bomber to move 1 foot. Thermal equilibrium should exist after some 10^3 to 10^4 collisions even between an electron and air molecules, so one may assume that thermal ionization equilibrium exists within approximately one foot of the leading edge. Hence, bending by ionization should not significantly affect a radar antenna located a few feet back from the leading edge in the lower surface of the bomber.

A word of explanation is in order here because it has been calculated (Reference 106) that the ionization produced by a long-range ballistic trajectory missile can seriously increase its radar cross-section. There are two reasons why a radar set in MX-2276 should not encounter difficulty: (1) The MX-2276 bomber dynamic pressures during cruise are much less than those encountered by a ballistic vehicle during reentry; hence, peak temperatures are lower and loss of electrons is much more rapid. Consequently, the density of electrons does not have a chance to build up to the critical level where it affects the radar. (2) The critical electron density for radar reflections depends on the square of the radar frequency; radar frequencies considered for MX-2276 are 100 times as great as those considered for detecting the vehicle of Reference 106. Consequently, the minimum significant electron density is 10^4 times as great.

b. The Angular Resolution Problem

(1) General

The primary problem of the radar in MX-2276 is resolution. For reconnaissance or navigation the resolution of present-day radars is barely adequate at altitudes of approximately 10,000 ft. A survey of mapping and charting radar specifications led to the belief that a spot size of 200 ft diameter with 5 half-tone steps is marginally adequate for recognition of city shapes, some major street patterns, and locations of industrial development. While more resolution would doubtless be of great value, it would also require much more bandwidth, power, and development time. The achievement of the stated performance will give MX-2276 radar resolution comparable with that obtained by optical-television methods proposed for reconnaissance satellites (Reference 107).

The desired ground spot size of 200 ft at the maximum slant range of 400,000 feet will subtend an angle of 1/2 milliradian. If an aperture 60 ft long (80% of the over-all bomber length) were possible, the maximum wavelength which would achieve this resolution would be 2 centimeters, and bending of the antenna would have to be kept below 2.5 millimeter (0.1 inch) in at least one direction. This indicates that mechanically scanning antennas having the desired angular resolution would be virtually impossible. The following discussion is therefore limited to generalized side-looking radars, having fixed arrays for antennas, with scanning provided by the forward motion of the bomber. Figure 76 shows the sort of ground coverage which can be achieved by these radars. In a later paragraph, techniques will be discussed by which some of the rigid requirements for the antenna may be alleviated.

c. Range Resolution

(1) Pulse-type Radar

Either pulse-type or continuous-wave (CW) radar can be used to provide resolution in range for a side-looking radar. The use of pulse-type radar in the MX-2276 bomber is

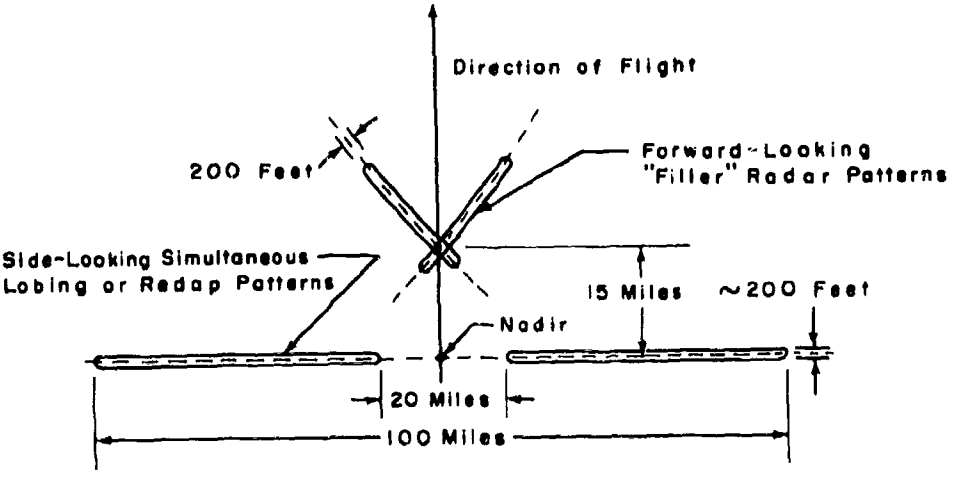

Range Resolution: 10 Miles From Nadir 200 Feet
50 Miles From Nadir 100 Feet

Altitude: 250,000 Feet ≈ 41 Nautical Miles

Figure 76. Ground Resolution Pattern for Proposed Radars

desirable to provide range resolution, because CW systems are inherently somewhat inferior in this respect. In order to get the required radar range with pulse techniques, however, it is essential to use high peak power pulses. With such high peak powers, the problem of electrical breakdown of the air arises, since the atmosphere around the bomber has about the same density that exists in a Neon lamp. Considerable time and effort has been directed toward the theoretical study of this problem, with the results related in detail below.

(2) The Breakdown Problem

The breakdown problem falls into two parts: inside the shock wave and outside it. The problem outside the shock wave (which shall be called the free-stream case) can be approached by laboratory tests of microwave breakdown at reduced air pressures. The problem inside the shock wave (termed the shock wave and boundary layer case) is complicated by lack of knowledge of the aerodynamic conditions such as the temperature and velocity profiles, the composition of the gas, and the extent of dissociation and ionization due to temperature.

The free-stream case has been studied analytically using the microwave breakdown experimental data and theories of Herlin and Brown (Reference 108). The following conclusions have been reached:

(a) The ionization of the gas will come to equilibrium in the very small fraction of a microsecond, so that only equilibrium states need to be examined. This means that no appreciable increase in peak power is made possible by using shorter pulses until the pulse width is shortened to considerably less than one-tenth of a microsecond.

(b) At any frequency of interest, the bomber will pass through a region of critical altitude where the power required to cause breakdown of the free-stream air is a minimum. Therefore only the minima need be considered for design purposes.

(c) This minimum power is inversely proportional to wavelength (in the region of experimental data) and is at least 100 watts per square cm at 4 kilomegacycles for beams of the size and shape considered for this bomber. Since the smallest proposed bomber antenna aperture is about 20,000 sq cm and the lowest proposed frequency is 10 kilomegacycles, a peak power of 4 megawatts would be the minimum which should cause breakdown. It is concluded that the free-stream breakdown problem can be overcome by careful attention to antenna and radome design.

The shock wave and boundary layer case has not been susceptible to such simple analysis. However, this case is not considered to be a limitation in the breakdown problem because:

(a) The pressure and mean free path are such that the minimum of the breakdown curve is not approached.

(b) The shock and boundary layers are relatively thin, so that electrons can diffuse out into the free-space region. Therefore the minimum power required to cause breakdown should be greater than in the free-stream case.

(c) The average thermal energies of molecules and electrons in the boundary layer and behind the shock wave, while much greater than the energies of free-stream molecules, are still not a significant fraction of the energy required for ionization. That is, a much larger number of free electrons will be found in the gas behind the shock wave and in the boundary layer as discussed under "Beam Bending" above, but the average energy which must be supplied to a single electron to enable it to knock another electron out of a neutral atom or molecule is still almost the same as in the room-temperature case.

It must be emphasized in concluding this discussion of the breakdown problem that (a) these are theoretical results, most of which cannot be confirmed by experiment except under actual flight conditions, and (b) the

electrical breakdown of air is greatly influenced by small amounts of impurities and changes in the composition of the air. Until experimental confirmation is available, it is felt that the use of pulsed radar may be permitted for the MX-2276, if care is exercised to keep the peak power within limits.

(3) CW Possibilities

The use of CW radar was suggested as a means of circumventing the breakdown problem discussed above. Although most of the doubts about breakdown have been allayed, some CW schemes were worked out to the point where it became apparent that system complexity would be great and/or antenna systems heavy and very large. The difficulty which arises is the result of the required resolution. If range resolution by pulse timing is not to be used, some other characteristic such as frequency resolution must be combined with antenna beamwidth in order to resolve the desired spot size. Fine frequency resolution usually turns out to require banks of carefully matched filters, while fine antenna beams usually require large, heavy, and complex antennas.

However, the problem of resolution in a pulsed-type radar is not easily solved either. Some combination of the features of pulsed and CW radar systems is possible which will permit the use of some techniques of CW systems to reduce the size and/or weight required for either system alone.

d. Means of Resolution Improvement

It has been stated before that the required angular resolution can be achieved by a 60-foot long linear array operating at 2 centimeters and restricting the bending of the array to 0.1 inch. It is possible that a self-compensating array could be built which would automatically correct for bends by insertion of appropriate phase shifters. The mechanical complexity of such a system would be very great.

The use of simultaneous lobing techniques has been frequently suggested as a means of providing improved resolution. Assuming that the multiple-return problem can be neglected and that a spot deflection scheme is used instead of blanking, it appears that a resolution improvement of 2 or 3 times can be achieved with amplitude or phase-comparison techniques. Taking the more optimistic figure, it is necessary to make the choice of increasing the wavelength to 6 centimeters (C-band), shortening the array to 20 ft, or some intermediate compromise such as 3 centimeters and 30-ft arrays. Two arrays are now required for each side, or a total of 4 arrays. Since the bending tolerance varies inversely as the wavelength, but mechanical problems increase at least as the square of the length, the shortest length and wavelength should be chosen, even at the expense of some increase in atmospheric attenuation and cloud return.

An interesting alternative has recently appeared which theoretically will permit an increase in wavelength to a value less affected by atmospherics, while retaining the resolution and reducing the antenna requirements. The basic system is developed from the Redap system of Philco Corporation (Reference 109) with some simple modifications to adapt it to the MX-2276 problem.

With the Redap system one can use an antenna only 15 ft long and a wavelength of 3 centimeters, while still achieving a resolution of 1/2 milliradian at maximum range. Thus the Redap beam sharpening yields a resolution at least 10 times as good as a conventional radar in this application. The penalty associated with this improvement lies in circuit complexity, to a certain extent in power, and most importantly in antenna stabilization. The Redap antenna must be stabilized to the bomber flight direction with a tolerance of about 0.2 degree. The total movement of the antenna, to take care of variations in angle of attack and crab angle due to winds, is ±1 degree in pitch, and ±2 degrees in yaw. No roll compensation is required. In return for this moderate degree of stabilization, a radar map is obtained which is not distorted or even displaced by lateral maneuvers of the bomber. Relatively simple display mechanisms can be used. A brief description of Redap follows.

The basic idea of Redap is to use the increase in information available from a coherent radar, and the motion of the bomber, to create a virtual aperture much larger than the actual antenna aperture. Thus some increase in electrical complexity can be traded for a large decrease in mechanical difficulty. In essence, a Redap is a sort of zero-frequency Doppler radar, which derives its beamwidth from the fact that only those targets which are at almost exactly right angles to the bomber's flight path will have near-zero doppler shifts.

The wavelength used by a Redap-type radar on MX-2276 can be increased to the point where the near-field effect extends to the maximum range of interest. For 200-foot resolution at 400,000 ft slant range, a 200-foot effective aperture can be used and the wavelength is

$$\lambda_{max} = \frac{A^2}{R_{min}} = \frac{(200)^2}{4 \times 10^6} = 0.1 \text{ ft} = 3.05 \text{ cm (9800 megacycles)}$$

where A is the aperture in feet and R_{min} is the minimum range to the far field. The effective aperture of 200 feet is obtained by adding returns from many successive pulses of the radar. The returns are stored and added coherently in a delay line (made, for example, of quartz). In order to obtain proper phase-addition of returns, the RF phase of the returns must be stored also; this is where the coherent oscillator and its stability requirements enter. According to Reference 109 where the theory of Redap is presented, this heart of the Redap system "has been developed" and a satisfactory memory of up to 100 sweeps is "readily attainable." Since MX-2276 needs to integrate not more than 40 sweeps, this part of the radar seems to impose only packaging difficulties.

For the MX-2276 bomber, an additional measure is necessary to achieve reasonable antenna size and duty factor. Because of the great altitude of the bomber, more than 1/2 of the available time of a conventional radar would be wasted waiting for the first signal to come back from the ground. This time can be utilized by transmitting another pulse as soon as the first part of the ground return comes back. Before any of the second pulse is returned from the ground, all the useful information will have been extracted from the first pulse. The second-time around echoes can be effectively suppressed by control of the vertical antenna pattern, without requiring excessive apertures. This mode of operation is especially useful on MX-2276, because the actual antenna aperture for a Redap system must be at least equal to the distance traveled between pulses, in order that the "diffraction-grating" lobes may be removed by the central beam. For MX-2276 this would be about 25 feet, but by using double-pulse operation, the distance traveled between pulses is halved, so that the length of the antenna may be halved also. If it were not for this feature, there would be little or no benefit in Redap over the simultaneous lobing technique outlined above. The power tube for this application will probably have to be a pulsed high-power klystron or stabilitron, amplifying the signal from a stable local oscillator, in order to achieve the necessary pulse-to-pulse phase stability. Such tubes are now available at S-band and development of an X-band equivalent should be possible by a straightforward development program.

c. Summary of Proposed Side-Looking Radars

In summary, then, it is proposed to study the following two radar systems as the most promising for application to the MX-2276 navigation and reconnaissance problem.

(1) Simultaneous lobing 1.8-cm radar

(2) Redap 3-cm radar

Tentative characteristics of the two radars are listed in the Table XII.

f. Possible Forward-Looking Radar

In addition to the two systems which are discussed in detail above, considerable time has been devoted to the problem of a forward-looking radar. The two reasons for the interest in looking forward are (1) by seeing a target or check-point ahead of the bomber, a longer time will be available for making corrections and commands to the missile. The maximum of 1 minute for making corrections to the missile after its release might be increased by 5 or 10

TABLE XII. TENTATIVE CHARACTERISTICS OF PROPOSED RADAR SYSTEMS

	Simultaneous Lobing	Redap
Wavelength	1.8 cm (K_u-band)	3.0 cm (X-band)
Antenna length	27 ft	15 ft
Pulse width *	0.2 microsecond	0.15 microsecond
Repetition rate	1900 to 3500 per second	1900 to 3500 per second
Illuminated angle	0.125 degree	0.38 degree
Angular resolution after processing	0.05 degree = 0.8 milliradian	0.029 degree = 0.5 milliradian
Means of data stabilization	Fixed antenna, stabilized display	Stabilized antenna, fixed display
Peak power required	500 kilowatts	2.4 megawatts
Average power (max.)	350 watts	1260 watts total
Power tube	Magnetron	Klystron, Master oscillator.power amplifier

*A pulse width of 0.15 microsecond will provide a resolution of 200 ft within 10 miles of the nadir, and a best resolution of about 80 ft at the maximum lateral range of 50 miles.

seconds. (2) neither of the two radars proposed above can see the ground within 10 miles on either side of the ground track. A forward looking radar could provide radar coverage of the ground track, and would also permit correlation and comparison with the optical-camera record which will be useful almost solely within 10 miles of the ground track. (A rearward-looking radar was considered but was dropped because it would not provide the lead-time, and would probably encounter much more severe beam-bending problems because of the unfavorable slant angle through the turbulent trail.)

From this study it was concluded that a single radar to give the required resolution and width of coverage, and to look forward also, is apparently not feasible. A "filler" set, however, which would provide forward and downward coverage only, is possible and could be included if the additional desirable qualities listed above are considered important enough to warrant the use of an additional radar. Forward coverage is achieved by two linear-array antennas whose longitudinal axes are skewed with respect to the bomber's heading. Each antenna is designed to illuminate a cone about its longitudinal axis. The two cones then intersect the ground in a pair of hyperbolas ahead of the bomber as shown in Figure 76. A return in one receiver connected to one of the antennas must then come from a target on the corresponding hyperbola on the ground. The time of the return (measured from the transmitted pulse) measures the slant range and thus locates the target uniquely. The returns could be displayed on the same strip chart used for the main radar,

or displayed on a separate chart for better resolution. Salient characteristics of the radar are listed in Table XIII.

g. Auxiliary Problems

(1) Choice of Radome

The radome material for the MX-2276 bomber has been tentatively chosen as a ceramic material in order to withstand the high temperatures encountered on the bomber's lower surface. Materials of sufficient strength are available since linear arrays will be used, and mechanical support can be provided for relatively small-sized flat panels.

For the K_u-Band system, radome reflection and refraction effects can be virtually eliminated because all dimensions between the array and the antenna are virtually fixed. Therefore, the effect of the radome will be a fixed impedance at the antenna input, and a fixed, calculable deflection of the radar pattern.

For the Redap system the radome problem is slightly more difficult because the antenna must move with respect to the radome. The electrical difficulties, however, are not as severe as those of present supersonic fighters and missiles, because the radome is flat, not curved, and the antenna is an array that is fairly easily calculated. Mechanical difficulties should be less because the radome is relatively narrow and can be supported at frequent intervals.

(2) Missile Command System

The problems of transmitting corrections from the bomber to the missile in accordance with data from the radar have not been examined in detail. However, on a separate contract, Bell Aircraft has been developing a variety of command systems that give a high degree of

TABLE XIII. POSSIBLE "FILLER" FORWARD-LOOKING RADAR

Wavelength	0.85 cm
Frequency	36 kilomegacycles (K_a-band)
Antenna length	12.5 ft
width	6.8 in.
gain	43 db
Illuminated angle	0.11 degree
Angular resolution after processing	0.044 degree = 0.77 milliradian
Pulse width	0.2 microsecond
Pulse repetition frequency	1200 per second (could possibly be doubled)
Peak power	800 kw
Average power	192 watts (or 384 watts if PRF is doubled)
Width of ground pattern	22 miles (11 miles either side)

security, freedom from jamming, and freedom from capture. The state of these developments is such that the MX-2276 problem, while difficult, could use techniques now in existence. Tentative parameters are indicated in the Table XIV.

The figures in Table XIV give an allowable path attenuation of 154 db, which, at this frequency corresponds to a (slant) range of 240 miles. This corresponds to a total delay, between the time that MX-2276 passes over the target and the time that the missile is over the target, of about 1 minute.

(3) Equipment Air Conditioning

The problem of cooling the various electronic equipments in MX-2276 is dependent to a large extent upon the method chosen to cool the cockpit. These two cooling requirements will in all probability be combined in a single system.

Since this problem is intimately connected with the detailed interior design of MX-2276, which has not been the subject of the present study, present efforts have been restricted to a survey of the literature on design of aircraft electronics to improve cooling. It is expected that much of the research and development now in progress in various university and government laboratories will be available for incorporation in MX-2276 when the time comes for detailed layout and design of the equipment compartments.

TABLE XIV. TENTATIVE R-F PARAMETERS OF MX-2276 MISSILE COMMAND SYSTEM

Frequency	3000 mc
Transmit ant. 2-in. helix	+10 db
Receive ant. biconical horn	+ 4 db
Peak power	5 kw (+67 dbm)
Average power (during bursts)	5 watts
Receiver noise power	-100 dbm (superhetrodyne, 2mc b/w)
Minimum signal-to-noise ratio	+20 db
Atmospheric attenuation	- 7 db

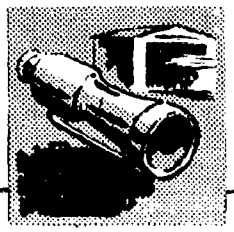

E. PROPULSION

1. GENERAL

The studies in propulsion of the MX-2276 weapon system have thus far consisted of further examination of the propellant combinations described in Reference 1, plus consideration of other propellant combinations. The problems of power plant design and operation, as affected by propellant selection, have been discussed in detail with design engineers and test personnel. This report is not intended as a general review of the propellant field, since such reviews have been made by other agencies for generally similar applications. However, the data and results of these studies have been used extensively in the present investigation.

The procedure being used consists of a consideration of all possible propellants and elimination of the undesirable combinations. This procedure has not been completed. Owing to the fact that a considerable amount of work has been done on various propellant combinations since Reference 1 was prepared and the fact that the problem of regenerative cooling is being considered more closely, it is expected that the final propellant selection will differ somewhat from those of Reference 1.

2. BASIC PROPELLANT SELECTION

Various propellant combinations have been examined on the basis of performance, combustion chamber temperature, regenerative cooling possibilities, potential availability and cost, toxicity, handling experience, and storage stability. These propellant combinations were made up of four oxidizers and five fuels.

The oxidizers considered are liquid fluorine, liquid ozone, liquid oxygen and RFNA. The first three are the highest energy oxidizers available. RFNA is included because of the large amount of operating experience with this oxidizer.

The fuels considered are hydrazine, unsymmetrical dimethylhydrazine, the 60% hydrazine-40% ammonia mixture, JP-4, and the 75% ethyl alcohol-25% water mixture. The first three are relatively high energy fuels. The last two have been used more than any other to date.

These propellant combinations are first compared on the basis of specific impulse.

a. Specific Impulse Values for the MX-2276 Engine Conditions

The theoretical shifting equilibrium values of specific impulse for a chamber pressure of 300 psia and a nozzle exit pressure of 14.7 psia are shown in Table XV for various propellant combinations. Figures 77, 78, and 79 show the theoretical shifting equilibrium values of specific impulse versus chamber pressure with nozzle exit pressures of 14.7, 10.6, and 1.47 psia. Figure 78 corresponds to the first stage of MX-2276, while Figure 79 corresponds to the second and third stages.

The theoretical values of specific impulse shown in Figures 77 through 79 were calculated for various expansion ratios from the data in Table XV. The following conversion factor was used.

$$I_{sp(2)} = I_{sp(1)} \sqrt{\frac{1-\left(\frac{P_{e(2)}}{P_{c(2)}}\right)^{\frac{K-1}{K}}}{1-\left(\frac{P_{e(1)}}{P_{c(1)}}\right)^{\frac{K-1}{K}}}}$$

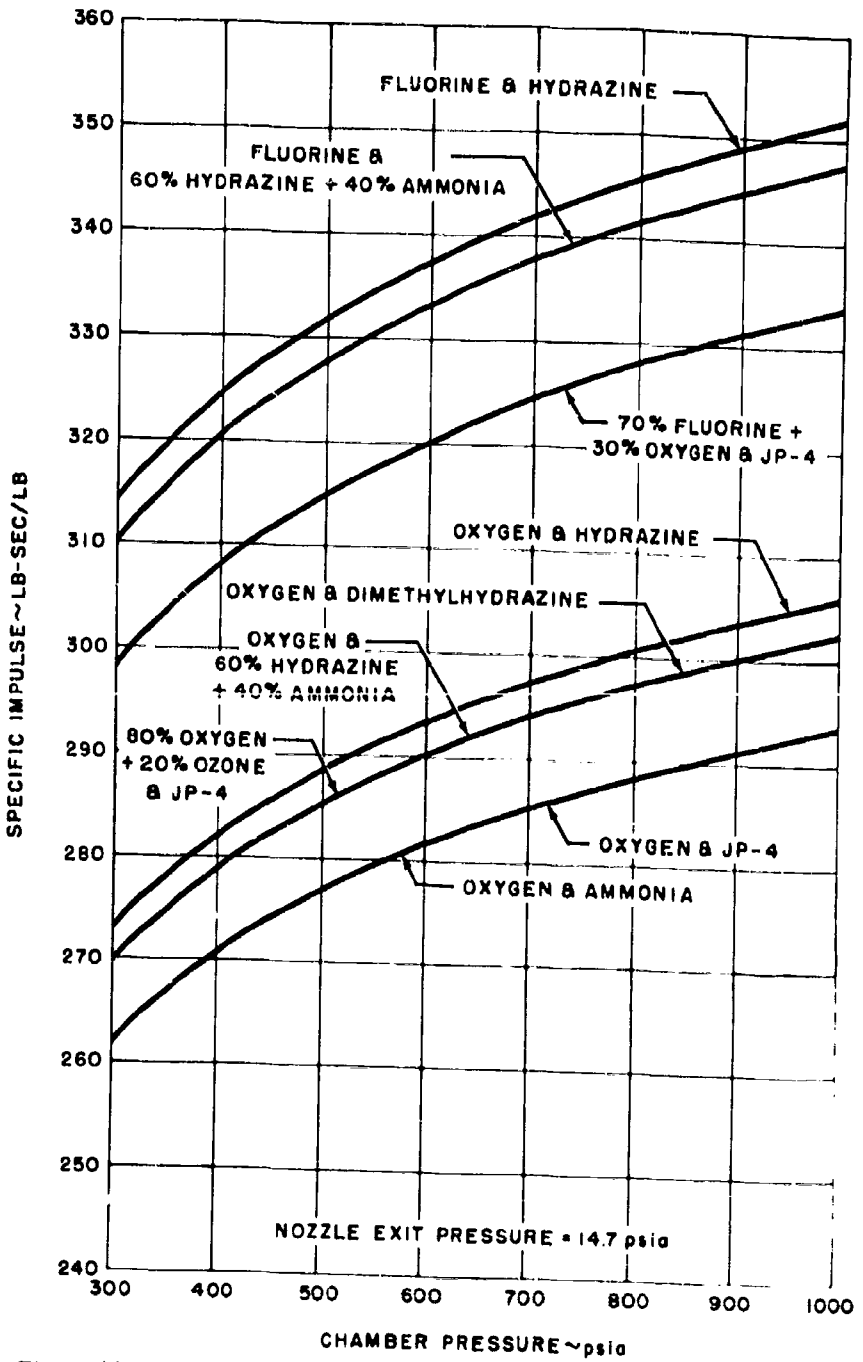

Figure 77. Theoretical Performance of Several Rocket Propellants (Expanded to 14.7 psi)

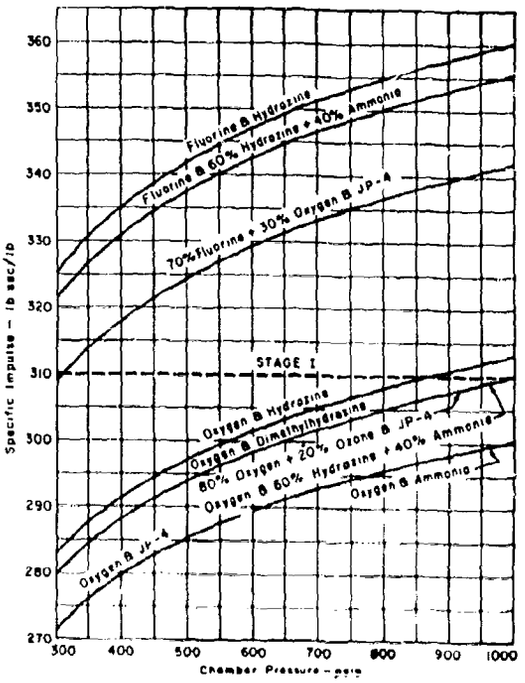

Figure 78. Theoretical Performance of Several Rocket Propellants (Expanded to 10.6 psi)

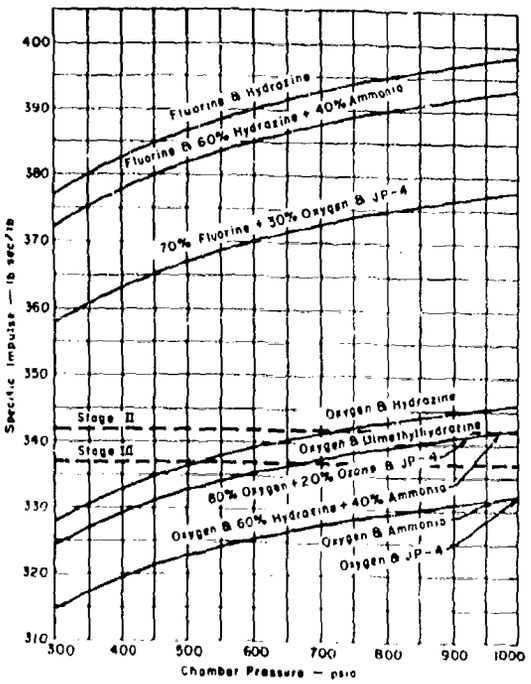

Figure 79. Theoretical Performance of Several Rocket Propellants (Expanded to 1.47 psi)

I_{sp} = specific impulse $\frac{\text{lb-sec}}{\text{lb}}$

P_e = Exit pressure, psi

P_c = Chamber pressure, psi

K = Ratio of specific heats

The additional increase in specific impulse resulting from reduced dissociation effects at the higher chamber pressures was neglected. Calculations show that an increase in specific impulse obtainable with an increase in combustion chamber pressure is almost entirely caused by the increased expansion ratio through the nozzle. However, an increase of approximately one percent may be expected at a chamber pressure of 1000 psia over the value shown in Figures 77 through 79. Various properties of the propellants considered in this evaluation are briefly summarized in Table XVI.

b. Other Factors

Of the possible combinations obtainable from the propellants considered, some can be eliminated immediately. The use of ozone should not be considered at the present time because of the logistics, handling, and toxicological problems of this oxidizer. Concentrations of ozone greater than 25% cannot be handled safely. Use of less than this amount does not provide sufficient increase in performance to warrant its application. RFNA is not satisfactory for MX-2276 since the highest performance of RFNA with any of these fuels is 246 seconds with hydrazine. Other accept-

TABLE XV. THEORETICAL SPECIFIC IMPULSE (SHIFTING EQUILIBRIUM) OF VARIOUS PROPELLANT COMBINATIONS

Propellant Combination	r*	I_{sp}**	P_B	I_d	T_c °K	T_c °F	Ref.
F_2 & N_2H_4	2.2	314	1.32	414	4340	7352	110
F_2 & NH_3	3.0	311	1.17	364	4236	7180	111
F_2 & 60% N_2H_4 + 40% NH_3	3.5	310	1.29	400	4300	7280	110 111
70% F_2 + 30% O_2 & JP-4	3.8	298	1.26	376	4340	7352	112
O_2 & N_2H_4	0.83	272	1.01	275	3248	5386	113
O_2 & $N_2H_2(CH_3)_2$	1.1	268	0.95	256	3100	5120	114
O_2 & 60% N_2H_4 + 40% NH_3	1.06	266	0.97	256	3150	5200	113
80% O_2 + 20% O_3 & JP-4	2.2	270	1.02	275			115
O_2 & JP-4	2.4	262	1.01	265	3410	5678	116
O_2 & NH_3	1.25	262	0.86	225			113
RFNA (Type III)& N_2H_4	1.25	246	1.26	272	2920	4796	117
RFNA (Type III)& $N_2H_2(CH_3)_2$	2.7	242	1.24	263	3100	5120	118
RFNA (Type III) & JP-4	4.6	231	1.26	291	3080	5080	119

* Approximate mixture ratio for maximum specific impulse

** Chamber pressure 300 psia, nozzle exit pressure 14.7 psia, shifting equilibrium

able propellant combinations have performance levels higher than this as shown in Figure 77.

Liquid fluorine, if used with any of these fuels, will give substantially higher performance than other oxidizers. However, it is believed that the use of 100% liquid fluorine as oxidizer should not be considered at the present time. There is relatively little experience with handling, toxicological, and corrosion problems to consider developing a satisfactory rocket engine within the proposed development periods. In addition, the availability and cost of pure liquid fluorine does not encourage the use of this material in the quantities required for this large a program.

This leaves liquid oxygen as the most desirable oxidizer for use in MX-2276 at the present time. Liquid oxygen and JP-4 are already in use for large missile applications and this combination has many advantages to explain its popularity. However, the specific impulse obtainable with this propellant combination cannot be regarded as adequate for the MX-2276 performance level, resulting in an

TABLE XVI. PHYSICAL PROPERTY DATA FOR PROPELLANTS UNDER CONSIDERATION

Propellant	FP °F	BP °F	Sp. Gr.	C_p Btu/lb°F	P_c psia	T_c °F	Cost $/lb Present	Cost $/lb Future
F_2	-360[1]	-306[1]	1.54[6]	0.29[6]	808[11]	-200[11]	20.[13]	1.00
O_2	-362[2]	-297[2]	1.14[2]	0.39[2]	731[2]	-182[2]	0.02[14]	0.02
O_3	-418[2]	-170[2]	1.46[7]		802[12]	10[12]	0.10[14]	0.05
RFNA	-65[3]	140[3]	1.58[3]	0.42[3]			0.10	0.10
N_2H_4	35[2]	236[2]	1.01[2]	0.73[9]	2130[2]	717[2]	2.50	1.00
NH_3	-108[2]	-28[2]	0.66[7]	1.07	1645[2]	270[2]	.03[14]	.03
JP-4	-76[4]		0.78[4]	0.48[4]	310-510[4]	575-710[4]	0.015	0.015
$N_2H_2(CH_3)2$	-71[5]	145[5]	0.79[5]	0.65[10]	882[10]	482[10]	4.50[15]	1.00

FP = Freezing Point

BP = Boiling Point

C_p = Specific Heat

NOTE: Superscript numbers refer to references as follows:

Superscript No.	Reference No.
1	1
2	124
3	127
4	130
5	131
6	120
7	125
8	121
9	129
10	132
11	122
12	126
13	123
14	134
15	133

excessively high take-off weight. It is therefore of interest to investigate the possibility of increasing the performance level of this combination by modifying the fuel or the oxidizer or both in order to improve specific impulse without adversely affecting the other features of this combination.

3. IMPROVEMENT OR SUBSTITUTION OF FUELS

a. Pure Hydrocarbons

Substitution of a pure hydrocarbon for JP-4, or blending JP-4 and a pure hydrocarbon could improve the specific impulse. However, a significant improvement is obtained only by going to the light hydrocarbons which must be kept refrigerated or pressurized. It is doubtful if this complication is justified by the slight increase in performance obtainable. The coolant problem with such a system would be more difficult than with jet fuel.

b. The Hydrazine Fuels

There are three fuels available which can be used with liquid oxygen in MX-2276. These are hydrazine, unsymmetrical dimethyl hydrazine, and the 60% hydrazine-40% ammonia mixture. The performance of these fuels at a chamber pressure of 300 psia expanding to one atmosphere is listed in Table XVII.

The performance of the hydrazine and unsymmetrical dimethyl hydrazine with liquid oxygen is greater than that of the hydrazine-ammonia mixture, the fuel suggested in the MX-2276 proposal. The bulk density and density impulse of the hydrazine-oxygen combination is substantially greater than the remaining two combinations, while that of the unsymmetrical dimethyl hydrazine-oxygen is approximately one percent greater than the proposed MX-2276 propellant. In addition, the performance and mixture ratio of the hydrazine-ammonia mixture and liquid oxygen are slightly different than previously used. The difference in performance of these fuels with liquid oxygen is not sufficient to base a selection on this parameter alone.

Since the MX-2276 thrust chambers must be regeneratively cooled, one of the propellants must be a satisfactory coolant. In the section on oxidizers (Section IV-E4) it is shown that oxygen is not satisfactory. Therefore, the fuel must be usable as a primary regenerative coolant. The coolant properties and related characteristics of the fuels, as well as properties required for handling and logistics must therefore be considered.

c. Hydrazine

The major drawbacks to the use of hydrazine are its relatively high freezing point,

TABLE XVII. PERFORMANCE OF HYDRAZINE FUELS*

Propellant	r	I_{sp}	P_B	Id = $I_{sp} \times P_B$
O_2 & N_2H_4	0.83	272	1.065	290
O_2 & $N_2H_2(CH_3)_2$	1.10	268	0.955	256
O_2 & N_2H_4 - NH_3(60% N_2H_4)	1.06	266	0.951	253

(r = oxidizer/fuel by weight; P_B = bulk specific gravity of propellant)

*at a chamber pressure of 300 psia expanding to one atmosphere.

its toxicity, its poor thermal stability, and its tendency toward accelerated decomposition in the presence of common materials such as mild steel. On the favorable side, hydrazine has a high density, a high specific heat, a low vapor pressure, and good storage stability.

The low thermal stability limit and explosive tendencies of hydrazine vapors presently limit its use as a coolant. North American Aviation, Inc. and the Jet Propulsion Laboratory of the California Institute of Technology have done a limited amount of work on regenerative cooling with hydrazine. JPL regeneratively-cooled 200-pound thrust engines have cooling passages of 347 stainless steel tubes with the bulk temperature of the hydrazine reaching a temperature of 438°F. In tests with engines of other materials, some explosions occurred which were attributed to catalysis by metal oxides or to overheating of hydrazine. In tests in which only a section of the chamber was cooled, bulk temperatures reached as high as 470°F. However, in this case, the hydrazine was only in the section a short time. In any case JPL does not recommend the use of hydrazine as a rocket coolant.

North American Aviation, Inc., has regeneratively cooled 300-pound thrust engines with the bulk temperatures of the hydrazine reaching 230°F. The presence of iron oxides, rust, in the hydrazine was indicated as the cause of some explosions during the early phases of the work.

The results of the above work are too limited in the range of operating conditions to justify the designation of hydrazine as a satisfactory regenerative coolant. This work was done at relatively low chamber pressures and with hydrazine inlet temperatures at normal room temperatures. An inlet temperature of 160°F will raise the bulk temperature at the injector about 100°F above the values obtained. In addition, heat transfer rates will increase almost in proportion to the increase in chamber pressure. Therefore, the use of hydrazine must be avoided until additional development work can be done with cadmium or other metallic stabilizers which tend to reduce the decomposition rates of hydrazine.

Unsymmetrical Dimethyl Hydrazine

Unsymmetrical dimethyl hydrazine has a lower density, a slightly lower specific heat, and a higher vapor pressure than hydrazine. Its toxicity has not been fully determined, but is probably somewhat less than hydrazine. Its storage stability, under conditions of limited contact with air, is very good. It can be stored safely and without fear of deterioration or freezing over a wide range of temperature. Its thermal stability is much better than hydrazine. Its vapors are not explosive. On the basis of its superior physiochemical properties, unsymmetrical dimethyl hydrazine is probably more suitable for regenerative cooling than hydrazine. However, there is no experimental data on regenerative cooling with unsymmetrical dimethyl hydrazine to verify this.

e. Hydrazine-Ammonia Mixture

The addition of ammonia to hydrazine results in a fuel with greater potentialities as a regenerative coolant than hydrazine. Ammonia has three properties which are distinctly advantageous for use as a regenerative coolant. It has good thermal stability, a high specific heat, and a high heat of vaporization. Its major drawbacks are its low density and high vapor pressure at ambient temperatures. The density of the hydrazine-ammonia mixture is higher than that of unsymmetrical dimethyl hydrazine, but the vapor pressure is still high unless the mixture is kept refrigerated.

The vapor pressure and freezing points of hydrazine-ammonia mixtures are shown in Figure 80. The problem of selecting a particular mixture is one of compromising the performance of the resultant propellant combination with the freezing point and vapor pressure of the mixture. In this case, since high performance was considered more important than a low freezing point, a relatively high hydrazine content was selected; namely, 60%. While the high freezing point (-27°F) of this mixture may not be a serious handicap in a weapon of this kind, the high vapor pressure may present some problems. Figure 81 shows the vapor pressure of the mixture as a function of temperature. It can be seen that this pressure is almost as high as ammonia alone.

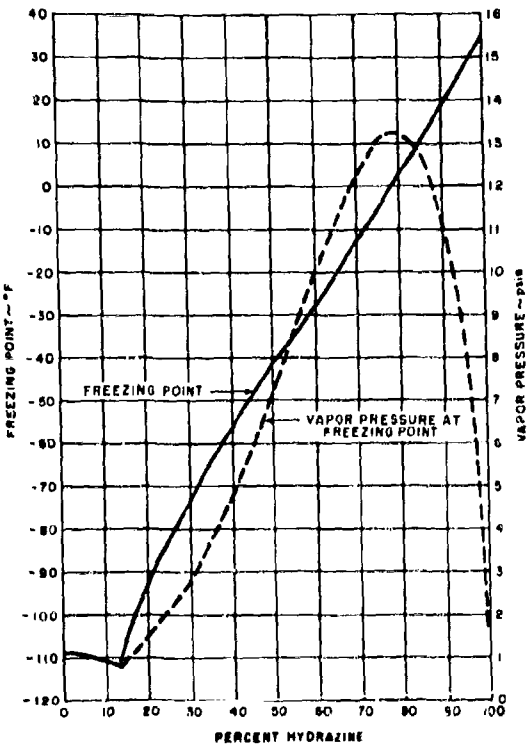

Figure 80. Vapor Pressure and Freezing Points of Hydrazine-Ammonia Mixtures

Practical experience in using mixtures of this kind shows that they must be kept under pressure or the more volatile component will evaporate, changing the composition of the remaining mixture. Pressurization must be maintained even during transfer from one container to another. This presents a complication in the use of this fuel which is not desirable.

Experimental data on regenerative cooling with the hydrazine-ammonia mixture are completely lacking although some tests have been carried out with ammonia. Tests at JPL show that regenerative cooling with ammonia can be accomplished. Since not all the tests were successful, a problem area exists even here with pure ammonia.

On the basis of the above information, no choice as yet can be made between the three hydrazine-type fuels. A program should be initiated to provide the basis for a logical choice between the three fuels. The heat transfer characteristics should be investigated in an apparatus designed for this purpose. Subsequently, thrust chamber firings should be made. Without substantial evidence such as obtainable from actual firings, any choice between the three fuels must be considered conjectural.

4. OXIDIZERS

a. Oxygen as a Coolant

Theoretically, liquid oxygen under pressure greater than its critical pressure can

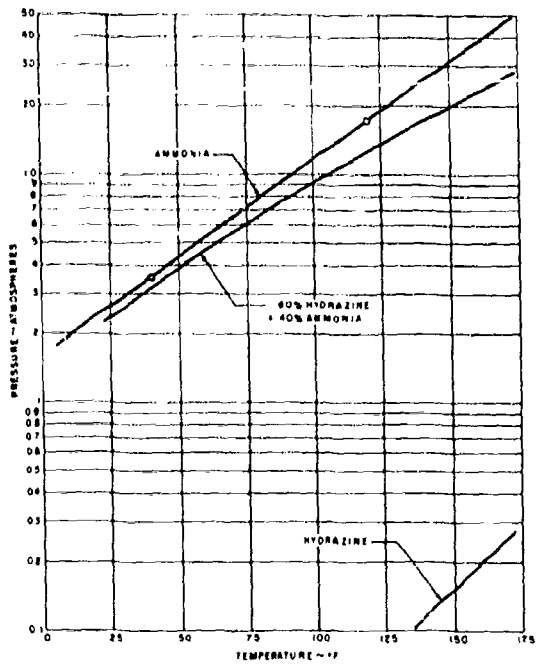

Figure 81. Vapor Pressure vs Temperature for Ammonia, Hydrazine, and Hydrazine-Ammonia Mixture

be used as a regenerative coolant since no phase change will occur in heating it above its critical temperature. The heat transfer process which occurs under these conditions is not very well understood and design data in this field are completely lacking. For this reason some tests were made at Bell Aircraft using liquid nitrogen in a heat transfer apparatus which is used by this company for investigation of cooling characteristics of rocket fuels. Liquid nitrogen was used because the critical point of nitrogen gas was within the pressure limitations of the apparatus and it can be expected to give results similar to those which may be expected for liquid oxygen. These tests show that the wall temperature will increase continuously at pressures (600 psi) above the critical pressure (500 psi) as the heat flux increases. The initially linear curve bends gradually at higher heat fluxes towards higher and higher wall temperatures. The data are presently being reduced and correlated to determine if this is a function of changing physical properties. Burnout heat flux was approximately one-half of corresponding values for JP-4. It is realized, however, that unmodified extrapolation of the results with liquid N_2 to liquid O_2, may not be justified. The corrosive properties of liquid oxygen will undoubtedly limit the use of liquid oxygen as a coolant to those parts of the system where the local temperature and heat rejection rates are relatively low.

b. Addition of Fluorine to Liquid Oxygen

Liquid fluorine is the highest performance oxidizer available for use with fuels containing no carbon. With fuels containing carbon, fluorine alone offers a smaller performance advantage over liquid oxygen, because the fluorine reacts only with the hydrogen, leaving the carbon to burn with oxygen. Therefore, with a hydrocarbon fuel, such as JP-4, the optimum oxidizer appears to be a mixture of liquid oxygen and liquid fluorine (Figure 82).

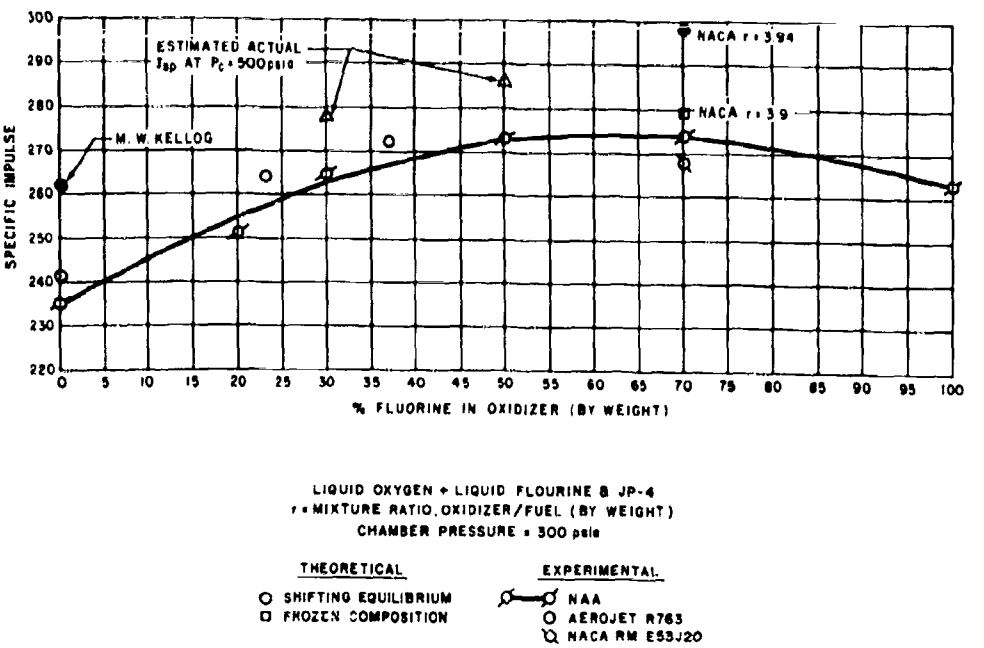

Figure 82. Specific Impulse vs Percentage of Fluorine by Weight in an Oxidizer for a Propellant Consisting of Oxygen Plus Fluorine and JP-4

If it is assumed that oxidation of the fuel occurs selectively, it would seem that maximum performance would occur with an oxidizer mixture that would give exhaust products consisting mainly of carbon monoxide and hydrogen fluoride. The oxidizer mixture for JP-4 would then be a mixture consisting of 70% fluorine and 30% oxygen. Experimental results from North American Aviation appear to bear this out. Tests have shown that performance very near the maximum is attained with an oxidizer consisting of 50% fluorine and 50% oxygen. Smooth hypergolic starts were attained with JP-4 and from 4 to 11 percent fluorine in the oxygen.

It appears, therefore, that some improvement over liquid oxygen and jet engine fuel as a propellant combination is possible, provided that the additional development time necessary for its realization can be included in the schedule of this weapon development. Further study of fluorine as an additive to liquid oxygen is required in order to estimate more carefully the additional development required. Further study of hydrazine fuels, particularly dimethyl hydrazine, is desired also, although this will be a more lengthy investigation.

5. RESULTS

Since this is an interim technical report, no final recommendation of one propellant combination can be made at the present time. Additional work now in progress will facilitate a final selection. The problem of propellant selection has been reduced to a choice of three propellant combinations. The selection of one of these combinations is dependent upon a number of factors which are affected by the over-all program planning and must be considered carefully. These three propellant combinations are:

a. Liquid Oxygen-Jet Fuel

This combination represents the most conservative choice and would permit adaptation to available hardware and the greatest assurance of development within the time period being considered. However, it will result in a larger vehicle than that described in Reference 1.

b. Liquid Oxygen-Dimethyl Hydrazine

This combination permits a higher level of performance and will result in a missile somewhat larger than described in Reference 1. However, the ability to cool a thrust chamber with dimethyl hydrazine has not been established. Some experimental investigation of this fuel must be carried out before this combination can be chosen.

c. Liquid Oxygen + Liquid Fluorine - JP-4

This combination will permit a substantial increase in performance over liquid oxygen-jet fuel. The addition of 20% fluorine will permit a weapon of the same size as that described in Reference 1. The addition of 50% will decrease the size of the vehicle considerably. However, the addition of fluorine, while making the combination hypergolic, will introduce additional handling and material problems. The development time will be extended and the opportunity to use available hardware will be restricted.

Further study and work will be concerned with a more detailed consideration of the over-all missile problems as affected by the selection of one of these propellants. The object will be to select a single propellant combination prior to initiation of any development work.

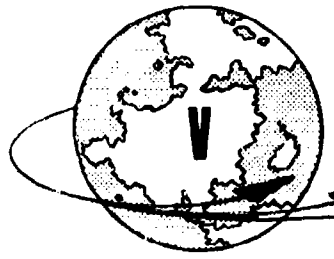

V CONCLUSIONS

The following are tentative conclusions which have been reached at this stage of the investigation. These conclusions may be modified to some degree as the investigation continues.

1. Methods for providing the pilot with a suitable environment for a flight of approximately one hour, have been determined and appear both practical and feasible.

2. In general, present methods for calculating heat transfer and skin temperatures are applicable up to M ≈ 10.

3. Methods are available by which the aerodynamic characteristics of lift and drag may be predicted with engineering accuracy to M ≈ 10.

4. The use of uninsulated or uncooled structures, utilizing even the most heat-resistant materials available, results in structural weights higher than those obtainable using aluminum structure in combination with sufficient insulation.

5. The use of radiation insulating barriers appears superior, on a weight basis, to the use of solid insulations.

6. A multiaxis inertial system appears to provide the necessary guidance accuracy for the weapon system, if the target location is known prior to launch.

7. A side-looking radar seems to provide the most suitable system for the necessary navigation and reconnaissance functions.

8. Thus far, four propellant combinations have been selected for further evaluation.

(a) Liquid oxygen (LOX) and JP-4 constitute the combination requiring least development time and maximum use of available hardware. However, the performance is inadequate for keeping the take-off weight of MX-2276 within the limits obtained in Reference 1.

(b) Liquid oxygen with a hydrazine-ammonia mixture is the propellant combination

assumed in Reference 1 because it has performance superior to that of Lox and JP-4. However, although the fuel mixture probably has better qualities as a regenerative coolant than hydrazine, its actual characteristics in this respect are not yet known. This propellant therefore requires a longer development period than Lox and JP-4.

(c) Liquid oxygen-dimethyl hydrazine is only slightly superior to combination (b) in terms of performance, but dimethyl hydrazine is preferable to hydrazine-ammonia as well as to hydrazine for several other reasons. However, its cooling properties are also not yet known. Therefore for practical application, this combination requires an extended development period.

(d) Liquid oxygen-fluorine and JP-4 provide considerable performance improvement over the previously mentioned combinations, but require appreciably more development efforts. Such development work is presently in progress.

VI PROGRAM FOR REMAINING SIX MONTHS

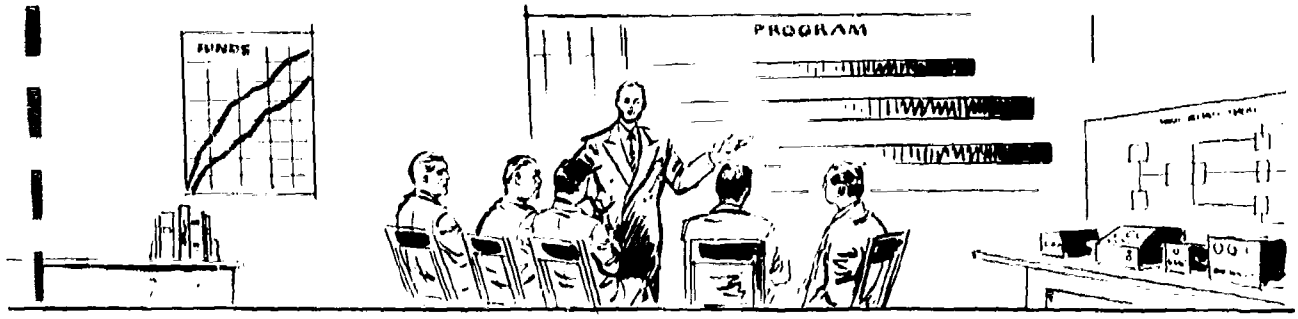

The principal lines of effort during the next six months will be discussed under the particular fields to which they pertain.

A. PILOT ENVIRONMENT

The emphasis will be upon the psychomotor capabilities of the pilot in the environment provided in Stage III. Evaluation of the methods proposed for maintaining this environment and determination of the weight of the various systems will also continue.

B. AERODYNAMICS

1. GENERAL PLAN

During the second half of the present study more emphasis will be placed on obtaining methods of analysis and on making sample calculations to show the magnitudes of the various problems and possible ways of alleviating them. In addition it is planned to re-evaluate the original configuration. Conclusions will then be drawn as to the importance of the various aerodynamic problems, changes indicated in the configuration and courses of future action to be taken. Theoretical and experimental needs will be outlined.

A more specific breakdown of the aerodynamic investigations planned for the second half of the study is outlined here under the headings of the general aerodynamic problem areas.

2. LIFT AND DRAG AT HYPERSONIC SPEEDS

a. Continue the study of theories for the prediction of wing, body and control characteristics - the shock-expansion theory and its modifications, the Newtonian impact theory, the methods for predicting skin friction, etc.

b. Where appropriate consider the effects of the boundary layer - the transition point, self-induced pressure gradients, shock-boundary layer interaction, and slip flow - and the effects of possible dissociation.

c. Apply these methods to the re-evaluation of the lift, drag, and L/D of the original configuration as well as other typical configurations.

d. Outline experimental research needs and recommend test programs for current research facilities or facilities to be completed in the near future.

3. AERODYNAMIC HEATING

a. Continue the investigation of the inclusion of streamwise temperature gradients in heat transfer estimations.

b. Add the effects of self-induced pressure gradient and shock-boundary layer interaction to the analysis of flat plate flow.

c. Study means of analyzing the heat transfer in the vicinity of the wing leading edge and body nose radii and estimate typical skin temperatures in these areas.

d. Evaluate the effect of slip flow dissociation, boundary layer transition, and surface emissivity on the heat transfer and skin temperature.

e. Estimate the transpiration cooling needed to hold parts of the aircraft to given temperatures - the best fluid or gaseous coolants to use and the amount required.

f. Re-estimate typical temperatures for the original flight plan.

g. Make the surface temperature estimations necessary for a study of reducing temperatures by modifying the flight plan.

h. Outline experimental research needs and recommend test programs.

4. PERFORMANCE

a. With the equations of motion presently derived, use the aerodynamic and propulsion parameters estimated for the MX-2276 configuration to find what simplifications in these equations can be tolerated and still retain the desired accuracy.

b. Then having established practical equations for the flight path - the take-off, ascent, and glide - study the effects of flight in different directions about the earth, of configuration changes, and of propulsion system performance on the overall performance.

c. Study the relative trajectories of stage III and the bomb.

d. Investigate the feasibility of reducing stage III temperatures by adjusting the flight path.

5. STABILITY AND CONTROL

a. As part of the investigation of wing, body and control surface characteristics include the estimation of moments and centers of pressure and thus aerodynamic stability parameters.

b. Obtain the equations of angular motion of the stage III relative to the earth. This study will be a continuation from the linear motion study and is presently under way.

c. Indicate the arrangements of body, wings, and control surfaces best suited to hypersonic flight, and in the light of these results examine the original configuration.

6. LAUNCHING AND STAGE SEPARATION

The stability and control problems associated with this subject will be studied.

C. STRUCTURES

1. CRITERIA AND LOADS

Additional investigations into various phases of flight operations are to be made to establish design accelerations in vertical and lateral directions for steady state, dynamic, and gust conditions. Logical combinations of the various accelerations must be deduced to obtain

strength levels consistent with present aircraft design practice.

Calculation methods for arriving at hypersonic and supersonic air-loads determinations for the exposed lift-surfaces and the body, in single and multistage flight, are to be evaluated. Various methods of performing such analyses are to be outlined, and the acceptability of each (for structural loads analysis purposes) determined. Static and dynamic flight conditions are to be covered.

Presently accepted landing load criteria are to be evaluated in the light of the special demands of the MX-2276 configuration and mission. This analysis is expected to result in acceptance, or appropriate modification, of the criteria currently specified by the Air Force, for design of conventional aircraft.

Flight (and other) loading conditions are to be evaluated for critical structural deflections and deformations. Where these are found to be prime considerations, criteria are to be formulated which will provide a deflection basis for design of such structures in lieu of the load criteria basis.

The following miscellaneous criteria will be evaluated to include possible variations in MX-2276 configuration and performance:

a. Factors of Safety

b. Design Weight

c. Fuel Cell Criteria

d. Engine Mount Load Criteria

e. Material Allowable Criteria

2. STRUCTURAL CONFIGURATIONS

Upon completion of the materials, insulation, and cooling studies, the information obtained will be applied to the refinement and development of the MX-2276 structural configuration as outlined in Reference 1. The primary structure will be considered in conjunction with the various arrangements of insulating and cooling that will have been shown to be practical and efficient. Various degrees of heat protection will be considered including, of course, the case of no protection; and various materials will be used in the primary structure. Each combination of structure plus heat protection will be arranged for loading and thermal conditions appropriate to principal structural components of the third stage of MX-2276, and the unit weights of each arrangement will be compared in order to indicate optimums. Similar considerations will be given to secondary structure such as leading edges, control surfaces, etc.

When these studies are completed, it is intended that further proposals, more detailed and with a better background than those of Reference 1, will be made for the structural configuration. On the basis of these proposals, revised estimates of structure weights/gross weight will be made.

3. TEST PROGRAM

At the present time, it is not possible to lay out in detail the test program that will be included in the present study since the types of heat protection and primary and secondary structure that may develop cannot be foreseen. It is intended, however, that the testing will be concentrated on the heat protection problems of insulating and cooling, since it is in these areas that the greatest ignorance exists. Testing will be confined strictly to structural elements which can be recommended theoretically for use in the MX-2276 airframe, of which the one design for a radiation barrier, arrived at in this report, could be a starting point.

D. NAVIGATION AND CONTROL

A more complete investigation of the problems and the design of the inertial system will be made in order to obtain a more definite conception of the navigation system. The combination of the inertial system with various systems for obtaining more accurate conditions at the beginning of cruise will then be studied in more detail.

Simultaneous lobing 1.8-cm radar and Redap 3-cm radar will be studied for use as side-looking radar for stage III. A forward-looking radar will also be examined for use as a "filler" radar.

E. PROPULSION

The work planned for the remainder of the study program will consist of three parts.

1. Continued study of the selected propellant combinations with respect to propulsion system layout, handling, and physical, chemical, as well as thermodynamic properties.

2. Investigation of the possibility of applying nuclear energy for the propulsion of the main power plant or for auxiliary power. While preliminary investigation suggests that this may not be attractive for the generation of auxiliary power, further investigation is desirable.

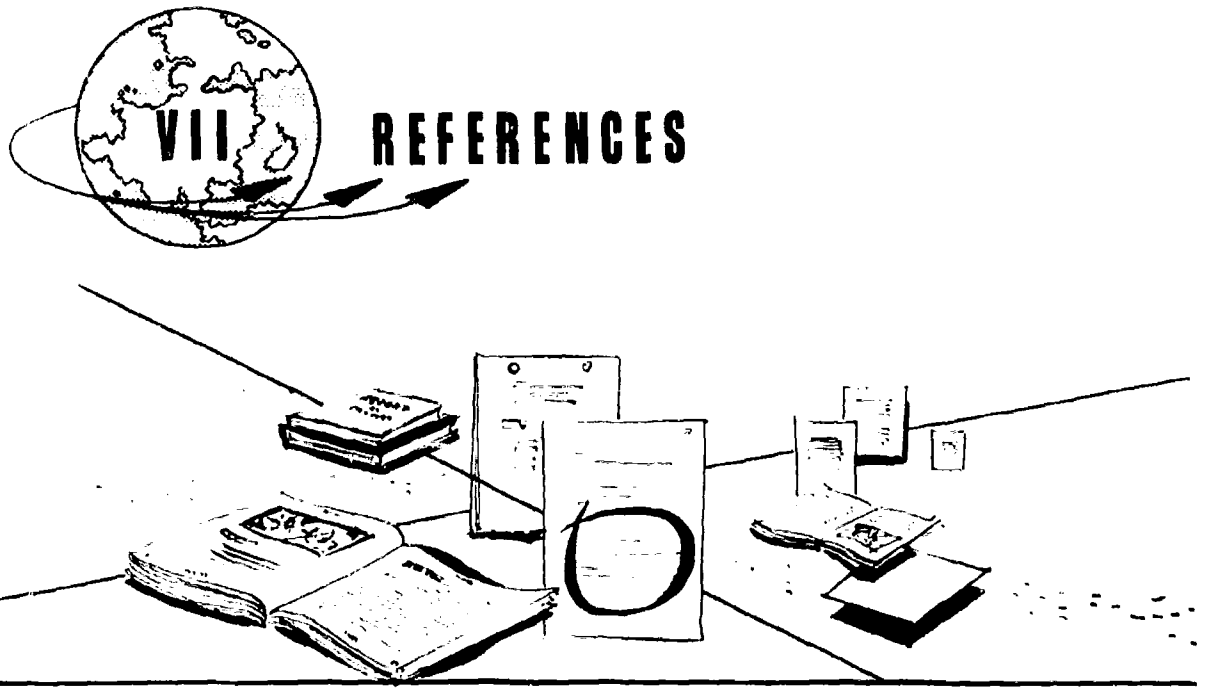

VII. REFERENCES

1. Strategic Weapon System: Bell Aircraft Corporation Preliminary Design Report No. D143-945-010, dated 15 July 1953.

2. Blockley, W. V.; McCutchan, J. W.; and Taylor C. L.: The Prediction of Human Tolerance for Heat in Aircraft: a Design Guide, Department of Engineering, University of California, Los Angeles: WADC Technical Report No. 53-346, dated March 1954.

3. Handbook of Instructions for Aircraft Designers: Air Research and Development Command Report No. ARDCM 80-1, Revised April 1954.

4. Ludwig, L. G.: Intrawall Cooling for Supersonic Aircraft: Cornell Aeronautical Laboratory Report No. BC-531-S-14, dated December 1949.

5. Progress Report No. 3, Bell Aircraft Corporation Report No. D143-981-003, dated 15 July 1954.

6. Rosser, J. B.; Newton, R. R.; and Gross, G. L.: Mathematical Theory of Rocket Flight: McGraw-Hill Book Company Inc., New York (1947).

7. Krueger, R. W.; Grimminger, G.; and Tieman, E.: Flight Mechanics of a Satellite Rocket: Douglas Aircraft Company, Inc., Project Rand Report No. RA-15021, dated 1 February 1947.

8. Handbook of Supersonic Aerodynamics (Vol 1): NAVORD Report No. 1488, dated April 1950.

9. Tsien, H. S.: Superaerodynamics, Mechanics of Rarified Gases: Journal of the Aeronautical Sciences, Vol 13, p. 653, dated December 1946.

10. Shultz, F. V.; Spencer, N. W.; and Reifman, A.: Atmospheric Pressure and Temperature Measurement between the Altitudes of 40 and 110 km.: Upper Air Research

Program Report No. 2, Engineering Research Institute, University of Michigan, dated July 1948.

11. Donaldson, C. D.: An Approximate Method for Estimating the Incompressible Laminar Boundary Layer Characteristics on a Flat Plate in Slipping Flow: NACA RM No. L9C02, dated May 1949.

12. Roberts, H. E.: The Earth's Atmosphere: Aeronautical Engineering Review, Vol 8, p. 19, dated October 1949.

13. Siegel, M. K.: Boundaries of Fluid Mechanics: Journal of the Aeronautical Sciences Vol 17, p. 191, dated March 1950.

14. Mirels, H.: Estimate of Slip Effect on Compressible Laminar Boundary Layer Skin Friction: NACA RN No. 2609, dated January 1952.

15. Howarth, L.: Modern Developments in Fluid Dynamics (High Speed Flow): Vol I, p. 416, Oxford University Press, Oxford (1953).

16. Crocco, L.: Lo Strato Limite Laminare nei Gas: Manografie Scientifiche di Aeronautica, Associazione Culturale Aeronautica, Roma, dated December 1946.

17. Shen, S. F.: On the Boundary Layer Equations in Hypersonic Flow: Readers' Forum, Journal of the Aeronautical Sciences, Vol 19, No. 7, pp. 500-502, dated July 1952.

18. Lees, L. and Probstein, R.: Hypersonic Viscous Flow over a Flat Plate: Aeronautical Engineering Laboratory, Princeton University, Report No. 195, dated April 1952.

19. Lees, L.: On the Boundary Layer Equations in Hypersonic Flow and their Approximate Solutions: Journal of the Aeronautical Sciences, Vol 20, No. 2, pp. 143-145, dated February 1953.

20. Shen, S. F.: An Estimate of Viscosity Effect on the Hypersonic Flow over an Insulated Wedge: Journal of Mathematics and Physics Vol 31, No. 3, pp. 192-205, dated October 1952.

21. Li, T. Y. and Nagamatsu, H. T.: Shock Wave Effects on the Laminar Skin Friction of an Insulated Flat Plate at Hypersonic Speeds: Journal of the Aeronautical Sciences, Vol 20, No. 5, p. 345, dated May 1953.

22. Chapman, S. and Cowling, T.: The Mathematical Theory of Non-Uniform Gases: p. 265, Cambridge University Press, Cambridge (1952).

23. Krieger, F. J. and White, W. B.: The Composition and Thermodynamic Properties of Air at Temperature from 500 to 8000°K and Pressures from 0.00001 to 100 Atmospheres: Project Rand Report No. R-149, dated 1949.

24. Moore, L.: A Solution of the Laminar Boundary Layer Equation for a Compressible Fluid with Variable Properties, Including Dissociation: Journal of the Aeronautical Sciences, Vol 19, No. 8, dated August 1952.

25. Crown, J. C.: The Laminar Boundary Layer at Hypersonic Speeds: NAVORD Report No. 2299, dated 1952.

26. Hanson, C. F.: Note on the Prandtl Number for Dissociated Air: Journal of the Aeronautical Sciences Vol 20, p. 799-800, dated 1953.

27. Langmuir, I.: Phenomena, Atoms and Molecules: Philosophical Library, New York (1950) (Especially Chapter 9).

28. Nernst, Boltzmann Festschrift, 1904, p. 904.

29. Emmons, H. W.: Gas Dynamics Tables for Air: Dover Publications, Inc., New York (1947).

30. Williams, E. P.; Dhanes, L. W.; Huntzicker, J. H.; Lew, R. J.; Lieski, H. A.; Moore, L. L.; and Young, G. B. W.: Long Range Surface-to-Surface Rocket and Ramjet Missiles - Aerodynamics: Project Rand, The Rand Corporation, Report No. R-181, dated 1 May 1950.

31. Kumm, E. L.: Engineering Considerations in Supersonic Heat Transfer: (Talk), Redstone Arsenal, Aerophysics Development Corporation, dated 7 April 1954.

32. Eckert, W. R. G.: Survey of Heat Transfer at High Speeds: WADC Technical Report No. 54-70, dated April 1954.

33. Rubesin, M. W. and Johnson, H. A.: A Critical Review of Skin Friction and Heat Transfer Solutions of the Laminar Boundary Layer of a Flat Plate: Transactions of the American Society of Mechanical Engineers, Vol 71, No. 4, pp. 385-388 1949.

34. Chapman, D. R., Kester, R. H.: Turbulent Boundary Layer and Skin Friction Measurements in Axial Flow Along Cylinder at Mach Numbers Between .5 and 3.0, NACA TN 3097, March 1954.

35. The NBS - NACA Tables of Thermal Properties of Gases; U. S. Department of Commerce, National Bureau of Standards.

36. Van Driest, E. R.: Turbulent Boundary Layer in Compressible Fluids: Journal of the Aeronautical Sciences, Vol 18, No. 3, pp. 145, 160, 216, dated 1951.

37. Sieff, A.; Sommer, S. C.; and Short, B. J.: Some Free Flight Measurements of Turbulent Skin Friction and Heat Transfer at High Supersonic Speeds: NACA Conference on Aerodynamics of High Speed Aircraft - July 1953.

38. Lobb, R. K.; Winkler, E. M.; and Persh, J.: Experimental Investigation of Turbulent Boundary Layers in Hypersonic Flow: I.A.S. Preprint No. 452.

39. Eggers, A. J., Jr.: One Dimensional Flow of an Imperfect Diatomic Gas: NACA TN 1861, dated 1949.

40. Johnson, H. A., et al.: A Design Manual for Determining the Thermal Characteristics of High Speed Heat Transfer: University of California, Department of Mechanical Engineering Research Projects, USAAF TR No. 5632, dated 1947.

41. Chapman, R. and Rubesin, M. W.: Temperature and Velocity Profiles in the Compressible Laminar Boundary Layer with Arbitrary Distribution of Surface Temperature: Journal of the Aeronautical Sciences, Vol 16, No. 9, pp. 547, 565, dated 1949.

42. McAdams, W. H.: Heat Transmission (Third Edition), McGraw-Hill Book Company, Inc. (1954).

43. Jedlicka, J. R.; Wilkins, M. E.; and Seiff, A.: Experimental Determination of Boundary Layer Transition on a Body of Revolution at M = 3.5: NACA RM A53L18, dated 15 March 1954.

44. Czarnecki, K. R. and Sinclair, A. R.: Preliminary Investigation of the Effects of Heat Transfer on Boundary Layer Transition on a Parabolic Body of Revolution (NACA RM-10) at a Mach Number of 1.61: NACA RN 3165, dated April 1954.

45. Kline, S. J. and Shapiro, A. H.: Experimental Investigation of the Effects of Cooling on Friction and on Boundary Layer Transition for Low Speed Gas Flow at the Entry of a Tube: NACA TN 3048, dated November 1953.

46. Frick, C. W. Jr., and McCullough, G. B.: Tests of a Heated Low-Drag Airfoil: NACA 12-3-42, dated 3 December 1942.

47. Scherrer, R.: Comparison of Theoretical and Experimental Heat-Transfer Characteristics of Bodies of Revolution at

Supersonic Speeds: NACA Report No. 1055, dated 1951.

48. Scherrer, R.; Wimbrow, W. R.; and Gown, F. E.: Heat Transfer and Boundary Layer Transition on a Heated Cone at a Mach Number of 1.53: NACA RM A8L28, dated 10 January 1949.

49. Scherrer, R.: Boundary Layer Transition on a Cooled 20° Cone at Mach Numbers of 1.5 and 2.0: NACA TN 2131, dated July 1950.

50. Liepmann, H. W. and Fila, G. H.: Investigation of Effects of Surface Temperature and Single Roughness Elements on Boundary Layer Transition.

51. Higgins, R. W. and Pappas, C. C.: An Experimental Investigation of the Effect of Surface Heating on Boundary Layer Transition on a Flat Plate in Supersonic Flow: NACA TN 2351, dated April 1951.

52. Dryden, H. L.: Review of Published Data on the Effect of Roughness on Transition from Laminar to Turbulent Flow: Journal of Aeronautical Sciences, Vol 20, N. and July 1953.

53. Czarnicki, K. R.; Robinson, R. B.; and Hilton, J. R., Jr.: Investigation of Distributed Surface Roughness on a Body of Revolution at a Mach Number of 1.61: NACA RN 3230, dated June 1954.

54. Brinich, P. F. and Diaconis, N. S.: Boundary layer Development and Skin Friction at Mach Number 3.05: NACA TN 2742, dated July 1952.

55. Evvard, V. C.; Tucker, M.; and Burgess, W. C., Jr.: Statistical Study of Transition - Point Fluctuations in Supersonic Flow: NACA TN 3100, dated March 1954.

56. Ross, A. O.: Determination of Boundary Layer Transition Reynolds Numbers by Surface Temperature Measurement of a 10° Cone in Various NACA Supersonic Wind Tunnels: NACA TN 3020, dated October 1953.

57. Lees, L.: The Stability of the Laminar Boundary Layer in a Compressible Fluid: NACA TN 1360, dated July 1947.

58. Lees, L and Lin, C. C.: Investigation of the Stability of the Laminar Boundary Layer in a Compressible Fluid: NACA TN 1115, dated September 1946.

59. Handbook of Supersonic Aerodynamics, Vol 5, NAVORD Report No. 1488, dated August 1953.

60. Hoffman and Gillete, A Study of Porous Metal Cooling: CIT-JPL, Report No. M3-5, dated June 1946.

61. Duwez, P. and Wheeler, L. L.: An Experimental Study of the Flow of Gas Through Porous Metals: CIT-JPL, Progress Report No. 1-66, dated August 1947.

62. Weinbaum and Wheeler, H. L.: Heat Transfer in Sweat-Cooled Porous Metals: CIT-JPL, Progress Report No. 1-62, dated July 1947.

63. Duwez, P.: Experimental Study of Sweat Cooling with Nitrogen and Hydrogen: CIT-JPL, Progress Report No. 4-47, dated September 1947.

64. Duwez, P. and Wheeler, H. L.: Heat Transfer Measurements in a Nitrogen Sweat-Cooled Porous Tube: CIT-JPL, Progress Report No. 4-48, dated November 1947.

65. Wheeler, H. L.; Meyers, Duwez, P.: Preliminary Experiments on a Sweat-Cooled Airfoil in a High Temperature Gas Stream: CIT-JPL, Progress Report No. 4-73, dated May 1948.

66. Wheeler, H. L.: The Influence of Wall Material on the Sweat Cooling Process: CIT-JPL, Progress Report 4-90, May

1949. Conwright and Typaldos, Permeability Distribution in Certain Stainless Steel Cylinders, CIT-JPL, Progress Report 1-76, August 1949.

67. Eckert, Kinsler, Cochran: Wine Cloth as Porous Material for Transpiration Cooled Walls: NACA RM E51H23, dated November 1951.

68. Koffel, W. K.: Preliminary Experimental Investigation of Transpiration Cooling for an Afterburner with a Sintered, Porous Stainless Steel Combustion Chamber Wall: NACA RM E53D08, dated June 1953.

69. Myers and Friedman, J.: Heat Transfer Process for Gas Phase Transpiration Cooling: North American Aviation Report No. AL-274, dated August 1947.

70. Duwez, P., and Wheeler, H. L.: Experimental Study of Cooling by Infection of a Fluid Through a Porous Material: I.A.S. Reprint No. 137, dated March 1948.

71. Friedman, J.: Studies of Gas Phase Transpiration Cooling Using Air as a Coolant: North American Aviation Report No. A1-640, dated August 1948.

72. Jackson, Bearer, and Schwope, Evaluation of Materials for Transpiration Cooling in Supersonic Vehicles: Rand Corporation, Project Rand, Report No. 128, dated January 1949.

73. Klunker, E. B. and Ivey, H. R.: An Analysis of Supersonic Aerodynamic Heating with Continuous Fluid Infection: NACA TN 1987, dated December 1949.

74. Linnell, R. D.: Two Dimensional Airfoils in Hypersonic Flows: Journal of the Aeronautical Sciences, Vol 16, No. 1, dated January 1949.

75. Dorrance, W. H.: Two Dimensional Airfoils at Moderate Hypersonic Velocities: Journal of the Aeronautical Sciences, Vol 19, No. 9, dated September 1952.

76. McLellan, C. H.; Bertram, M. H.; and Moore, J. H.: An Investigation of Four Wings of Square Plan Form at a Mach Number of 6.86 in the Langley 11 Inch Hypersonic Tunnel: NACA RM L51D17.

77. Stone, A. H.: On Supersonic Flow Past a Slightly Yawed Cone; Journal of Mathematics and Physics, Vol 27, No. 1, dated April 1948.

78. Kopal, Z. (Ed.): Supersonic Flow Around Yawed Cones: MIT Center of Analysis Technical Report No. 3, dated 1947.

79. Dennis, D. H. and Cunningham, B. E.: Forces and Moments on Pointed and Blunt Nosed Bodies of Revolution at Mach Numbers from 2.75 to 5.00: NACA RM A52E22, dated 8 August 1952.

80. Neire, S. E.: Experimental Investigation of the Aerodynamic Characteristics of a Ballistic Type Missile: NACA RM A54CO4, dated 23 April 1954.

81. Dennis, D. H. and Cunningham, B. E.: Forces and Moments on Inclined Bodies at Mach Numbers from 3 to 6.3: NACA RM A54E03, dated 25 June 1954.

82. Resnikoff, M. N.: Optimum Lifting Bodies at High Supersonic Airspeeds: NACA RM A54B15, dated 7 May 1954.

83. Jack, J. R. and Moskowitz, B.: Aerodynamic Characteristics of Two Bottomed Bodies at Mach Number of 3.12: NACA RM E53L11b, dated 12 April 1954.

84. Cooper, R. D. and Robinson, R. A.: An Investigation of the Aerodynamic Characteristics of a Series of Cone Cylinder Configurations at a Mach Number of 6.86: NACA RM L51J09, dated 17 December 1951.

85. Ridyard, H. W.: The Aerodynamic Characteristics of Two Series of Lifting Bodies at Mach Number 6.86: NACA RM L54C15, dated May 1954.

86. McLellan, C. H.: Exploratory Wind Tunnel Investigation of Wings and Bodies at M = 6.9: Journal of the Aeronautical Sciences Vol 18, No. 10, pp. 641-648, dated October 1951.

87. Allen, H. J.: Estimation of the Forces and Moments Acting on Inclined Bodies of Revolution of High Fineness Ratio: NACA RM A9126, dated 14 November 1949.

88. Allen, H. J. and Perkins, E. W.: Characteristics of Flow Over Inclined Bodies of Revolution: NACA RM A50L07, dated 5 March 1951.

89. Grimminger, G., Williams, E. P., and Yong, G. B. W.: Lift on Inclined Bodies of Revolution in Hypersonic Flow: Journal of the Aeronautical Sciences, Vol 17, No. 11, pp. 675-690, dated November 1950.

90. Gendtuer, W. J. Jr.: Tests of the Surfboard Glide Configuration and Other Lifting Bodies at Mach Seven in the Langley Field Eleven Inch Hypersonic Wind Tunnel: Consolidated Vultee Aircraft Corporation Report No. A-Atlas-106, dated 30 October 1953.

91. Hirschfelder, J. O. and Curtiss, Charles, F.: Thermodynamic Properties of Air, Vol II: University of Wisconsin, Naval Research Laboratory Report No. CM-518, dated 21 December 1948.

92. McKowen, P.: Flow Parameters for a Real Gas: Bell Aircraft Aerodynamics Research Note No. 56.

93. Advanced Strategic Weapon System, Progress Report No. 4: Bell Aircraft Report No. D143-981-004, dated 15 September 1954.

94. Redstone Arsenal Progress Report Nos. 6, 7, and 9, dated respectively January, March, and September 1953.

95. Mitra, S. K.: General Aspects of Upper Atmospheric Physics: Compendium of Meteorology (1951).

96. Whipple, F. S.: Results of Rocket and Meteor Research: Harvard College Observatory Report, dated 1952.

97. H. B. Tolefson: Preliminary Results from Gust Velocity Measurements at High Altitudes: NACA RM L51L12a, dated 1 April 1952.

98. Allen, H. F.: A Study of Special and Unusual Conditions Affecting High Speed Aircraft and Missiles: University of Michigan Engineering Research Institute Progress Report No. 4, dated February 1951.

99. McDougal, R. L., Coleman, T. L., and Smith, P. L.: The Variation of Atmospheric Turbulence with Altitude and its effect on Airplane Gust Loads: NACA RM L53G15a, dated November 1953.

100. Kallman, H. K.: An Investigation of Atmospheric Properties at Great Altitudes: Rand Corporation Report No. RM-1047, dated 27 February 1953.

101. Handbook of Supersonic Aerodynamics, Vol I: NAVord Report No. 1488, dated 1 April 1950.

102. Pratt, K. G.: A Revised Formula for the Calculation of Gust Loads: NACA Report No. TN 2964, dated June 1953.

103. Structural Criteria, Piloted Airplanes, Basic Flight Criteria: Specification No. MIL-S-5202 (USAF), Proposed Draft released July 1953.

104. Micks, W. R.: A Method for Determining the Effects of Elevated Temperature on Structural Design and Weight: Rand Corporation Report No. R-498, dated March 1954.

105. Sprague, R. S.: Electromagnetic Radiation Bending in the Vicinity of the B-58 and Its Effect on Sensing Elements During

Supersonic Flight: Convair Report No. FZA-4-106, dated 15 January 1954.

106. Siegel, K. M.: Radar Reflection from Shock Fronts: Willow Run Research Center Memo No. 79-25(133)-14, dated 6 May 1953.

107. Lipp, Salter, and Wehner: Utility of a Satellite Vehicle for Reconnaissance: Rand Corporation Report No. RM-217, dated April 1951.

108. Herlin, M. A., and Brown, S. C.: Breakdown of a Gas at Microwave Frequencies: Massachusetts Institute of Technology Research Laboratory of Electronics, Technical Report No. 60, dated 3 May 1948.

109. Sternberg, B. D.: Redap - A New Method for Achieving High Resolution with Airborne Radar: Philco Corporation Research Division (presented at the Fourth Symposium on Mapping and Charting by Radar, St. Louis, Mo.), dated 7 April 1954.

110. Gordon, S. and Huff, V. N.: Theoretical Performance of Liquid Hydrazine and Liquid Fluorine as a Rocket Propellant: NACA RM E53E12, dated 3 July 1953.

111. Gordon, S. and Huff, V. N.: Theoretical Performance of Liquid Ammonia and Liquid Fluorine as a Rocket Propellant, NACA RM E53A26, dated 16 March 1953.

112. Private communication from NACA, Lewis Flight Propulsion Laboratory.

113. Thackery, J. D., et al: An Exploratory Investigation of Mixtures of Hydrazine and Ammonia as Rocket Fuels: CIT-JPL PR 1-69, dated July 1950.

114. Estimated from Frozen Composition Value in Metalectro Corporation Report No. M-52-1-ONR (See Reference 131).

115. Revised Compilation of Computed Specific Impulse Values: Rand Corporation Report No. RM-505, dated April 1950.

116. Combined Bi-Monthly Summary No. 23, CIT-JPL, dated May 1951.

117. Mueller, H.: Bell Aircraft Corporation Memo No. ENG:25:3:0918-1:HM, dated 18 September 1953.

118. Camp, C.: Experimental Performance of the Uns-Dimethyl-Hydrazine - Red Fuming Nitric Acid Rocket Propellant Combination: USAF, Wright-Patterson, WADC, TR 54-81, dated February 1954.

119. Weymouth, F. R.: Thermodynamic Properties of the Products of Combustion of Aviation Gasoline and WFNA, at Rich and Extremely Rich Mixtures: Bell Aircraft Report No. 56-982-011, dated 15 January 1951.

120. Kilner, Scott B., et al: The Density of Liquid Fluorine: Journal of the American Chemical Society, Vol 74, No. 4, p. 1086, 1952.

121. Simons, J. H.: Fluorine Chemistry: Academic Press (1950).

122. Fluorine, Properties and Method of Handling: Manual F-1, Pennsylvania Salt Manufacturing Co., Philadelphia (1946).

123. Fluorine Product Bulletin: Pennsylvania Salt Manufacturing Co., Philadelphia, dated 1 May 1954.

124. Perry, John H.: Chemical Engineer's Handbook, Third Edition: McGraw-Hill Book Company, Inc., New York (1950).

125. Dunnam, M.: Properties of Ozone: Paper given at NACA, November 19-20, 1953.

126. Jenkins, A. C. and Birdsall, C. M.: The Vapor Pressure and Critical Constants of Pure Ozone: The Journal of Chemical Physics, Vol 20, No. 7, pp. 1158-1161, dated July 1952.

127. Liberto, R. R.: Properties of Red Fuming Nitric Acid: Bell Aircraft Report No. D162-982-004, dated 8 March 1954.

128. Private communication from General Chemical Division, Allied Chemical and Dye Corporation.

129. Overstreet, R. and Giauque, W. F.: Ammonia. The Heat Capacity and Vapor Pressure of Solid and Liquid, Heat of Vaporization, The Entropy Values from Thermal and Spectroscopic Data: Journal of the American Chemical Society, Vol 59, pp. 254-259, dated February 1937.

130. Dean, Leo E.: The Physical Properties of JP-4: Bell Aircraft Report No. D162-982-003, dated 21 December 1953.

131. Howitz, D.: Improved Liquid Propellants: Systems with Hydrazine, Hydrazine Derivatives: Metalectro Corporation Report No. M52-1-ONR, dated 1 March 1953.

132. Aston, J. G., et al: The Thermodynamic Properties and Configuration of Unsymmetrical Dimethyl Hydrazine: Journal of the American Chemical Society Vol 75, p. 6202, 1953.

133. Private communication from Westvaco, Chlor Alkali Division, Food Machinery and Chemical Corporation, dated 15 June 1954.

134. Long Range Surface-to-Surface Rocket and Ram-jet Missiles, Propulsion and Fuels: Rand Corporation Report No. R-180, dated May 1950.

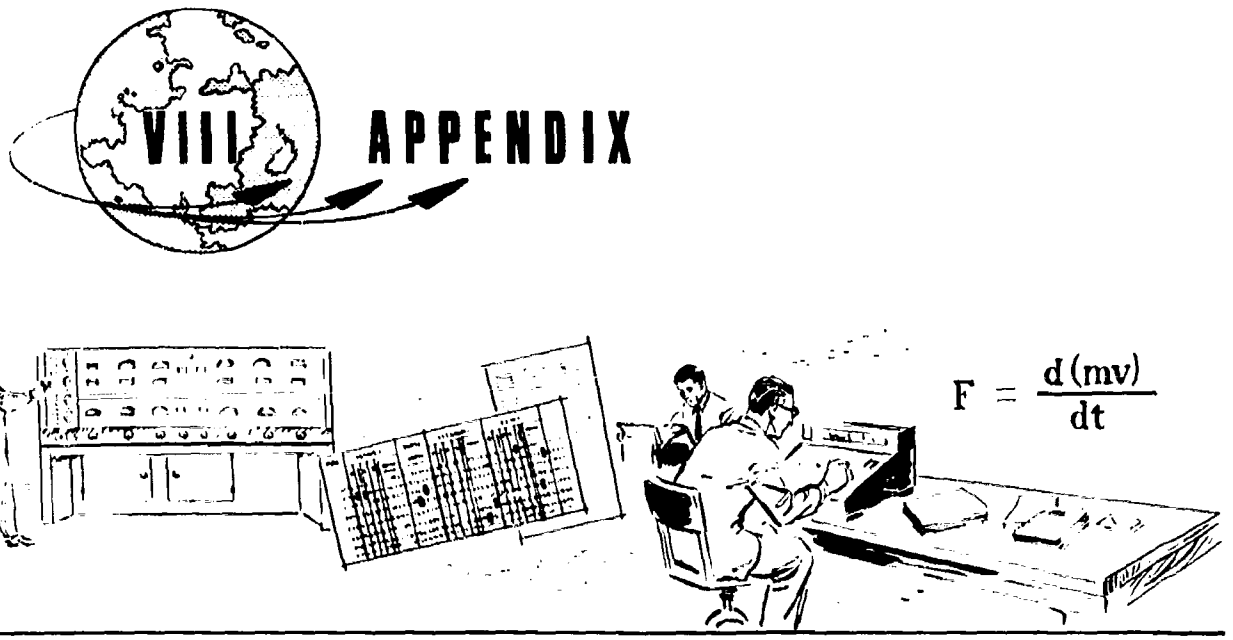

EQUATIONS OF LINEAR MOTION OF AN AIRCRAFT

The forces acting on the aircraft cause "absolute"* accelerations relative to the assumed inertial axis system located at the center of the earth. Thus, the aircraft at an instant of time may be located in space relative to this fixed-axis system X_1, Y_1, Z_1 as shown in Figure 83,

where: point A is the aircraft's center of gravity

r is the radial distance from the origin (O) to the point A

μ is the angle measured in the X_1 Y_1 plane

λ is the angle measured in the AOZ_1 plane

At any instant of time an observer, who is also located in space coincident with point A but stationary with respect to the earth's surface, will see the aircraft moving with a relative velocity, V, in some direction. Hence, a second axis system is established with the observer at the origin. This axis system, herein called X_2 Y_2 Z_2, is illustrated by Figures 84a and 84b, where: The X_2 Y_2 plane is parallel to a plane tangent to the earth's surface at point A'.

* The term "absolute" will be used to indicate the acceleration, velocity, etc. referred to an inertial system.

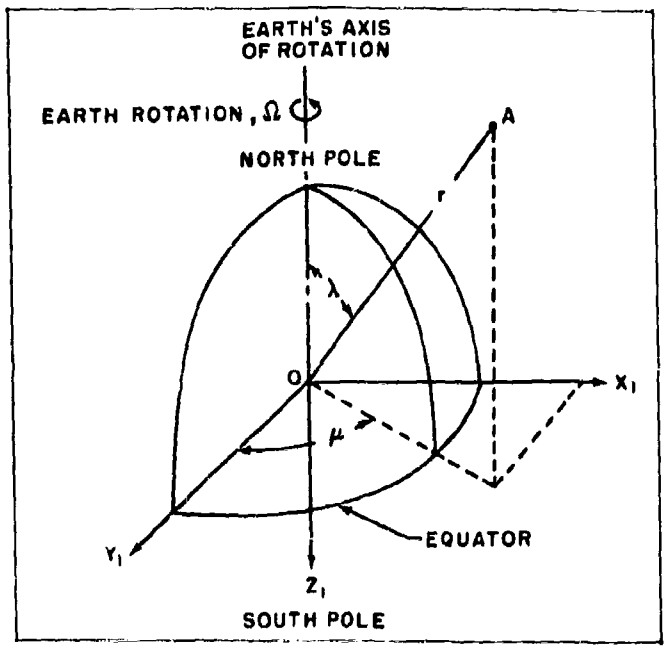

Figure 83. Inertial Axis System

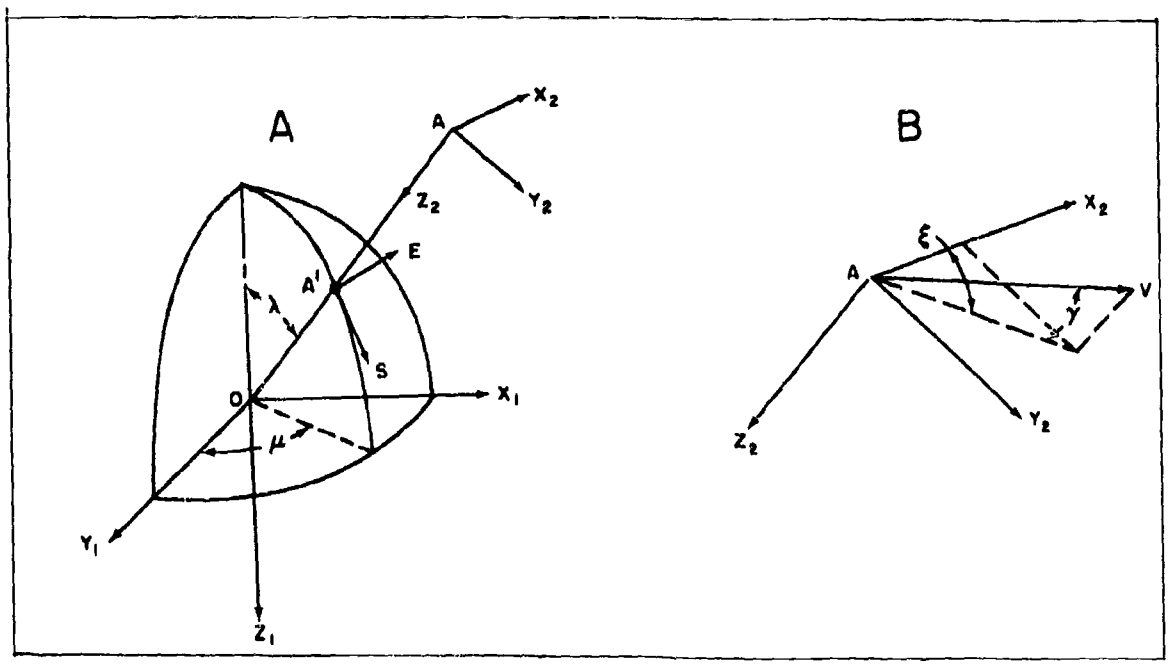

Figure 84. Orientation of Observer

Z_2 is in the direction of r, the instantaneous vertical, and perpendicular to the X_2 Y_2 plane.

X_2 is in the direction of instantaneous east.

Y_2 is in the direction of instantaneous south.

ξ, the azimuth angle, is measured from east in the X_2 Y_2 plane.

γ, the flight path angle, is measured in a vertical plane containing the velocity vector and perpendicular to the X_2 Y_2 plane. It is that angle between the velocity vector and its projection onto the X_2 Y_2 plane.

Likewise, there is a third axis system which is located in the aircraft and rotates with it. This axis system is a right-hand system orientated in the well-known standard manner of aircraft axes (i.e., either body or stability axes) in which the X axis is arbitrarily placed along the thrust line, chord line, flight direction, etc. Herein, this axis system is denoted as the X_3 Y_3 Z_3 system. It is along these axes that the aerodynamic, thrust, and gravity forces are most recognizable. Thus, the linear motions of the aircraft along these axes are derived using the quantities apparent to the observer rotating with the earth; namely, relative velocity, flight path and azimuth angles.

Now that the axis systems to be used in the derivation of the equations of motion have been illustrated, all that remains is the choice of the physical principle upon which the equations of motion are based. The familiar F = ma cannot be used because it refers to a system of constant mass and an aircraft, especially a rocket propelled aircraft with an operating propulsion system, is obviously not such a system. Therefore, the following principle is used in the derivation. "If one has a system S of particles, then the vector sum of all the exterior forces acting on S is equal to the time rate of change of the total momentum of S plus the rate at which momentum is being transferred out of S by the particles that are leaving S." See Reference 6 for further details. This principle can be expressed by the following equations.

$$\begin{pmatrix} F_{X_1} \\ F_{Y_1} \\ F_{Z_1} \end{pmatrix} = \frac{d}{dt} \begin{pmatrix} M\bar{V}_{X_1} \\ M\bar{V}_{Y_1} \\ M\bar{V}_{Z_1} \end{pmatrix} + \dot{m} \begin{pmatrix} \bar{V}_{X_1} - V_{X_{1_e}} \\ \bar{V}_{Y_1} - V_{Y_{1_e}} \\ \bar{V}_{Z_1} - V_{Z_{1_e}} \end{pmatrix} \qquad (2)$$

where: F_{X_1}, F_{Y_1} and F_{Z_1} are the sum of the exterior forces acting on the aircraft in the X_1, Y_1 and Z_1 directions respectively.

M is the mass of the aircraft at any time.

$\dot{m}$ is the rate at which propellants are being consumed.

V_{X_1}, V_{Y_1}, V_{Z_1} are the absolute velocities of the body in the X_1, Y_1, Z_1 directions respectively.

$V_{X_{1_e}}$, $V_{Y_{1_e}}$ and $V_{Z_{1_e}}$ are the velocities relative to the aircraft at which mass is leaving the system in the X_1, Y_1 and Z_1 directions respectively.

By rearranging equation (2) and taking note of the fact that $\frac{dM}{dt} = -\dot{m}$, the following equation results.

$$\frac{1}{M}\begin{pmatrix} F_{X_1} + \dot{m}V_{X_{1_e}} \\ F_{Y_1} + \dot{m}V_{Y_{1_e}} \\ F_{Z_1} + \dot{m}V_{Z_{1_e}} \end{pmatrix} = \frac{d}{dt}\begin{pmatrix} \overline{V}_{X_1} \\ \overline{V}_{Y_1} \\ \overline{V}_{Z_1} \end{pmatrix} \tag{3}$$

or

$$\frac{1}{M}(F_1 + \dot{m}V_{1_e}) = \frac{d}{dt}(V_1) \tag{3a}$$

where:*

$$(F_1 + \dot{m}V_{1_e}) = \begin{pmatrix} F_{X_1} + \dot{m}V_{X_{1_e}} \\ F_{Y_1} + \dot{m}V_{Y_{1_e}} \\ F_{Z_1} + \dot{m}V_{Z_{1_e}} \end{pmatrix}$$

* Such similar notation for matrixes will be used throughout the remainder of the derivation. The subscript denotes the axis system to which the quantity is referred.

$$(\bar{V}_1) = \begin{pmatrix} \bar{V}_{X_1} \\ \bar{V}_{Y_1} \\ \bar{V}_{Z_1} \end{pmatrix}$$

Since the forces along the aircraft's axes are ordinarily used in predicting performance, it is convenient to derive the "apparent"* accelerations along these axes. These accelerations are then integrated to give velocity and displacement increments relative to the earth fixed observer. So that the equations are in terms of quantities recognizable to the observer, the transformation from the axis system X_1 Y_1 Z_1 to the X_3 Y_3 Z_3 system is necessary; this is accomplished in two steps. The first is a transformation from the X_1 Y_1 Z_1 system to the X_2 Y_2 Z_2 system. This is accomplished in the following manner.

$$(\bar{V}_2) = (\bar{\ell})\,(\bar{V}_1) \tag{4}$$

where $(\bar{\ell})$ is a transformation matrix as given by:

$$(\bar{\ell}) = \begin{pmatrix} \cos\mu & , -\sin\mu & , 0 \\ \cos\lambda\,\sin\mu & , \cos\lambda\,\cos\mu & , \sin\lambda \\ -\sin\lambda\,\sin\mu & , -\sin\lambda\,\cos\mu & , \cos\lambda \end{pmatrix} \tag{5}$$

in which the angles μ and λ are those previously illustrated in Figure 83. Likewise, the absolute velocities along the X_3 Y_3 Z_3 axes can be obtained by a second transformation

$$(\bar{V}_3) = (\ell)\,(\bar{V}_2) \tag{6}$$

* The term "apparent" indicates the accelerations, velocities, etc., as seen by the observer on the earth's surface.

where (ℓ) is the transformation matrix given by:

$$(\ell) = \begin{pmatrix} \cos\theta\cos\psi & , \cos\theta\sin\psi & , -\sin\theta \\ -\cos\phi\sin\psi + \sin\phi\sin\theta\cos\psi, & \cos\phi\cos\psi + \sin\phi\sin\theta\sin\psi, & \sin\phi\cos\theta \\ \sin\phi\sin\psi + \cos\phi\sin\theta\cos\psi, & -\sin\phi\cos\psi + \cos\phi\sin\theta\sin\psi, & \cos\phi\cos\theta \end{pmatrix} \quad (7)$$

In which the angles, ψ, θ, and ϕ are angular rotations from the X_2 Y_2 Z_2 axis system to the X_3 Y_3 Z_3 axis system in the yaw, pitch and roll planes respectively. The order of rotation is in the yaw, pitch and roll directions. It should be noted that the angle θ is perfectly arbitrary and need not be the "pitch angle".

Combining equations (4) and (6)

$$(\bar{V}_3) = (\ell)(\bar{\ell})(\bar{V}_1) \quad (8)$$

Differentiating equation (8) with respect to time

$$\frac{d}{dt}(\bar{V}_3) = \left[\frac{d}{dt}(\ell)\right](\bar{\ell})(\bar{V}_1) + (\ell)\left[\frac{d}{dt}(\bar{\ell})\right](\bar{V}_1) + (\ell)(\bar{\ell})\left[\frac{d}{dt}(\bar{V}_1)\right] \quad (9)$$

Differentiating equation (6); substituting the results in equation (9), and making use of equation (4) to substitute for $(\bar{V}_1)$ and $(\bar{\ell})(\bar{V}_1)$

$$(\ell)(\bar{\ell})\left[\frac{d}{dt}(\bar{V}_1)\right] = (\ell)\left[\frac{d}{dt}(\bar{V}_2)\right] - (\ell)\left[\frac{d}{dt}(\bar{\ell})\right](\bar{\ell})^{-1}(\bar{V}_2) \quad (10)$$

By multiplying both sides of equation (3a) by the quantity $(\ell)(\bar{\ell})$ and substituting into equation (10) the following matrix equation is derived

$$(\bar{a}_3) = \frac{1}{M}(\ell)(\bar{\ell})(F_1 + \dot{m}V_{1e}) = (\ell)\left\{\frac{d}{dt}(\bar{V}_2) - \left[\frac{d}{dt}(\bar{\ell})\right](\bar{\ell})^{-1}(\bar{V}_2)\right\} \quad (11)$$

where $(\bar{a}_3)$ are the absolute accelerations along the X_3 Y_3 and Z_3 axes respectively.
The right side of equation (11) is expanded to give

$$(\ell)\begin{pmatrix} \frac{d}{dt}\bar{V}_{X_2} + \bar{V}_{Y_2}\cos\lambda\,\dot{\mu} - \bar{V}_{Z_2}\sin\lambda\,\dot{\mu} \\ \frac{d}{dt}\bar{V}_{Y_2} - \bar{V}_{Z_2}\dot{\lambda} - \bar{V}_{X_2}\cos\lambda\,\dot{\mu} \\ \frac{d}{dt}\bar{V}_{Z_2} + \bar{V}_{X_2}\sin\lambda\,\dot{\mu} + V_{Y_2}\dot{\lambda} \end{pmatrix} \tag{12}$$

As $\bar{V}_{X_2}$, $\bar{V}_{Y_2}$ and $\bar{V}_{Z_2}$ are the absolute velocities of the aircraft's cg in the direction X_2, Y_2 and Z_2 it can easily be seen from Figures 83 and 84 that:

$$\bar{V}_{X_2} = V\cos\gamma\cos\xi + r\Omega\sin\lambda \tag{13a}$$

$$\bar{V}_{Y_2} = V\cos\gamma\sin\xi \tag{13b}$$

$$\bar{V}_{Z_2} = -V\sin\gamma \tag{13c}$$

where Ω is the rotational velocity of the earth.

It is also apparent that

$$\dot{\mu} = \Omega + \frac{V\cos\gamma\cos\xi}{r\sin\lambda} \tag{14a}$$

$$\dot{\lambda} = \frac{V\cos\gamma\sin\xi}{r} \tag{14b}$$

$$\frac{dr}{dt} = V\sin\gamma \tag{14c}$$

Using equations (13) and (14) to substitute for the values of $\frac{d\bar{V}_2}{dt}$, $\bar{V}_2$, $\dot{\mu}$ and $\dot{\lambda}$ the following expressions for a_{X_3}, a_{Y_3} and a_{Z_3} are derived.

$$\begin{aligned}\bar{a}_{X_3} = {} & \dot{V}\left[\cos\gamma\cos\xi(\cos\theta\cos\psi) + \cos\gamma\sin\xi(\cos\theta\sin\psi) + \sin\gamma(\sin\theta)\right] \\ & -V\dot{\gamma}\left[\sin\gamma\cos\xi(\cos\theta\cos\psi) + \sin\gamma\sin\xi(\cos\theta\sin\psi) - \cos\gamma(\sin\theta)\right] \\ & -V\dot{\xi}\left[\cos\gamma\sin\xi(\cos\theta\cos\psi) - \cos\gamma\cos\xi(\cos\theta\sin\psi)\right] \\ & +V\Omega\left[(\sin\gamma\sin\lambda + \cos\gamma\sin\xi\cos\lambda)(\cos\theta\cos\psi)\right] \\ & -\sin\lambda\left(\Omega + \frac{V\cos\gamma\cos\xi}{r\sin\lambda}\right)\left[(V\cos\gamma\cos\xi + r\Omega\sin\lambda)(\sin\theta) - (V\sin\gamma)(\cos\theta\cos\psi)\right] \\ & -\cos\lambda\left(\Omega + \frac{V\cos\gamma\cos\xi}{r\sin\lambda}\right)\left[(V\cos\gamma\cos\xi + r\Omega\sin\lambda)(\cos\theta\sin\psi) - (V\cos\gamma\sin\xi)\right. \\ & \left.(\cos\theta\cos\psi)\right]\end{aligned}$$

$$+\frac{V\cos\gamma\sin\xi}{r}\left[(V\sin\gamma)(\cos\theta\sin\psi)-(V\cos\gamma\sin\xi)(\sin\theta)\right] \qquad (15a)$$

$$\begin{aligned}\bar{a}_{Y_3} = {} & \dot{V}\left[\cos\gamma\cos\xi(-\cos\phi\sin\psi+\sin\phi\sin\theta\cos\psi)+\cos\gamma\sin\xi(\cos\phi\cos\psi\right.\\ & \left.+\sin\phi\sin\theta\sin\psi)-\sin\gamma(\sin\phi\cos\theta)\right]\\ & -V\dot{\gamma}\left[\sin\gamma\cos\xi(-\cos\phi\sin\psi+\sin\phi\sin\theta\cos\psi)\right.\\ & \left.+\sin\gamma\sin\xi(\cos\phi\cos\psi+\sin\phi\sin\theta\sin\psi)+\cos\gamma(\sin\phi\cos\theta)\right]\\ & -V\dot{\xi}\left[\cos\gamma\sin\xi(-\cos\phi\sin\psi+\sin\phi\sin\theta\cos\psi)-\cos\gamma\cos\xi(\cos\phi\cos\psi\right.\\ & \left.+\sin\phi\sin\theta\sin\psi)\right]+V\Omega\left[(\sin\gamma\sin\lambda+\cos\gamma\sin\xi\cos\lambda)(-\cos\phi\sin\psi\right.\\ & \left.+\sin\phi\sin\theta\cos\psi)\right]+\sin\lambda\left(\Omega+\frac{V\cos\gamma\cos\xi}{r\sin\lambda}\right)\left[(V\cos\gamma\cos\xi\right.\\ & \left.+r\Omega\sin\lambda)(\sin\phi\cos\theta)+V\sin\gamma(-\cos\phi\sin\psi+\sin\phi\sin\theta\cos\psi)\right]\\ & -\cos\lambda\left(\Omega+\frac{V\cos\gamma\cos\xi}{r\sin\lambda}\right)\left[(V\cos\gamma\cos\xi+r\Omega\sin\lambda)(\cos\phi\cos\psi\right.\\ & \left.+\sin\phi\sin\theta\sin\psi)-V\cos\gamma\sin\xi(-\cos\phi\sin\psi+\sin\phi\sin\theta\cos\psi)\right]\\ & +\frac{V\cos\gamma\sin\xi}{r}\left[V\sin\gamma(\cos\phi\cos\psi+\sin\phi\sin\theta\sin\psi)\right.\\ & \left.+V\cos\gamma\sin\xi(\sin\phi\cos\theta)\right] \qquad (15b)\end{aligned}$$

$$\begin{aligned}\bar{a}_{Z_3} = {} & \dot{V}\left[\cos\gamma\cos\xi(\sin\phi\sin\psi+\cos\phi\sin\theta\cos\psi)+\cos\gamma\sin\xi(-\sin\phi\cos\psi\right.\\ & \left.+\cos\phi\sin\theta\sin\psi)-\sin\gamma(\cos\phi\cos\theta)\right]-V\dot{\gamma}\left[\sin\gamma\cos\xi(\sin\phi\sin\psi\right.\\ & \left.+\cos\phi\sin\theta\cos\psi)+\sin\gamma\sin\xi(-\sin\phi\cos\psi+\cos\phi\sin\theta\sin\psi)\right.\\ & \left.+\cos\gamma(\cos\phi\cos\theta)\right]-V\dot{\xi}\left[\cos\gamma\sin\xi(\sin\phi\sin\psi+\cos\phi\sin\theta\cos\psi)\right.\\ & \left.-\cos\gamma\cos\xi(-\sin\phi\cos\psi+\cos\phi\sin\theta\sin\psi)\right]+V\Omega\left[(\sin\gamma\sin\lambda\right.\\ & \left.+\cos\gamma\sin\xi\cos\lambda)(\sin\phi\sin\psi+\cos\phi\sin\theta\cos\psi)\right]\\ & +\sin\lambda\left(\Omega+\frac{V\cos\gamma\cos\xi}{r\sin\lambda}\right)\left[V\sin\gamma(\sin\phi\sin\psi+\cos\phi\sin\theta\cos\psi)\right.\\ & \left.+(V\cos\gamma\cos\xi+r\Omega\sin\lambda)(\cos\phi\cos\theta)\right]-\cos\lambda\left(\Omega+\frac{V\cos\gamma\cos\xi}{r\sin\lambda}\right)\left[(V\cos\gamma\cos\xi\right.\\ & \left.+r\Omega\sin\lambda)(-\sin\phi\cos\psi+\cos\phi\sin\theta\sin\psi)-V\cos\gamma\sin\xi(\sin\phi\sin\psi\right.\\ & \left.+\cos\phi\sin\theta\cos\psi)\right]+\left(\frac{V\cos\gamma\sin\xi}{r}\right)\left[V\sin\gamma(-\sin\phi\cos\psi\right.\\ & \left.+\cos\phi\sin\theta\sin\psi)+V\cos\gamma\sin\xi(\cos\phi\cos\theta)\right] \qquad (15c)\end{aligned}$$

The matrix quantity $(\ell)\,(\bar{\ell})\,(F_1 + \dot{m}V_{1_e})$ is the sum of aerodynamic, gravity, and thrust forces acting along the three axes of the aircraft. For rocket-propelled aircraft these are as follows:

$$F_{X_3}' - gM\sin\theta + \dot{m}V_{X_{3_e}} + \left[(P_e - P_A)A_e\right] X_3 \tag{16a}$$

$$(\ell)\,(\bar{\ell})\,(F_1 + mV_{1_e} = F_{Y_3}' + gM\sin\phi\cos\theta + \dot{m}V_{Y_{3_e}} + \left[(P_e - P_A)A_e\right] Y_3 \tag{16b}$$

$$F_{Z_3}' + gM\cos\phi\cos\theta + \dot{m}V_{Z_{3_e}} + \left[(P_e - P_A)A_e\right] Z_3 \tag{16c}$$

where: A_e is the area of the rocket exit

P_e is the pressure of the exhaust at the exit

P_A is the ambient pressure of the atmosphere at the altitude under consideration

F_{X_3}', F_{Y_3}', and F_{Z_3}' are the aerodynamic forces acting along the X_3, Y_3, and Z_3 axes

g is the gravitational acceleration constant at both the altitude under consideration and orientation with respect to the earth.

In the normal rocket aircraft the quantity $\dot{m}V_{Y_{3_e}} + \left[(P_e - P_A)A_e\right] Y_3$, which is a sideward rocket thrust, is zero. Furthermore, if one makes the simplification of measuring θ to the thrust line so that the thrust is acting along the X_3 axis (for such a choice of θ the X_3 Y_3 Z_3 system is a body axis system), it is obvious that the rocket thrust in the Z_3 direction given by $\dot{m}V_{Z_{3_e}} + \left[(P_e - P_A)A_e\right] Z_3$ is zero.

When equations (15) and (16) are combined a very complex expression for the aircraft motion results. However, if the simplifying assumptions are made that $\psi = \xi$ (case of no sideslip) and that $\theta = \gamma$ (the angular rotation in the pitch plane of the X_3 Y_3 Z_3 axis system is through the angle γ from the horizontal to the flight direction making the X_3 Y_3 Z_3 a stability axis system), the following simplified general equations result.

$$\dot{V} = \frac{T}{M}\cos\upsilon - \frac{D}{M} - (g - r\Omega^2\sin^2\lambda)\sin\gamma - r\Omega^2\sin\lambda\cos\lambda\cos\gamma\sin\xi \tag{17a}$$

$$V\dot{\xi}\cos\phi\cos\gamma - V\dot{\gamma}\sin\phi = \frac{Y}{m} + (g - r\Omega^2\sin^2\lambda)\sin\phi\cos\gamma$$
$$+ r\Omega^2\sin\lambda\cos\lambda(\cos\phi\cos\xi + \sin\phi\sin\gamma\sin\xi)$$
$$+ 2V\Omega\left[\cos\lambda(\cos\phi\cos\gamma) - \sin\lambda(\sin\phi\cos\xi\right.$$

$$-\cos\phi \sin\gamma \sin\xi)\Big] - \frac{V^2}{r} (\sin\phi \cos\gamma - \cos\phi \cos^2\gamma \cos\xi \cot\lambda) \quad (17b)$$

$$V\dot{\gamma} \cos\phi + V\dot{\xi} \sin\phi \cos\gamma = \frac{L}{M} + \frac{T}{M} \sin\upsilon - (g - r\Omega^2 \sin^2\lambda) \cos\phi \cos\gamma$$
$$+ r\Omega^2 \sin\lambda \cos\lambda (\sin\phi \cos\xi - \cos\phi \sin\gamma \sin\xi)$$
$$+ 2V\Omega \Big[\cos\lambda (\sin\phi \cos\gamma) + \sin\lambda (\cos\phi \cos\xi$$
$$+ \sin\phi \sin\gamma \sin\xi)\Big] + \frac{V^2}{r} (\cos\phi \cos\gamma + \sin\phi \cos^2\gamma \cos\xi \cot\lambda) \quad (17c)$$

In arriving at equations (17) from equations (15) and (16) it should be remembered that the aerodynamic lift force, L, and drag forces, D, are in the negative Z_3 and X_3 directions respectively, and that the aerodynamic side force (represented by Y) is in the positive Y_3 direction. It is assumed that the thrust line is displaced from the flight path direction by the angle υ, i.e., the inclination at the thrust line from the horizontal is given by the angle $\upsilon + \gamma$.

If additional restrictions are placed upon equation (17), as done in Reference 7, namely: 1) the aircraft is flying in the equatorial plane, 2) the aircraft is flying towards the east, and 3) the angle of bank is maintained zero, then equation (17) is reduced to the form as given in Reference 7. These equations are repeated below.

$$\dot{V} = \frac{T}{M} \cos\upsilon - \frac{D}{M} - (g - r\Omega^2) \sin\gamma \quad (18a)$$

$$V\dot{\xi} \cos\gamma = \frac{Y}{M} \quad (18b)$$

$$V\dot{\gamma} = \frac{L}{M} + \frac{T}{M} \sin\upsilon - (g - r\Omega^2) \cos\gamma + 2V\Omega + \frac{V^2}{r} \cos\gamma \quad (18c)$$

It is seen by comparison of equation (18) with the equations resulting from the combination of equations (15) and (16) that the equations given in Reference 7 are a special case of the general equations of motion. Hence, in using equation (18) to calculate the performance of an aircraft, the limitations placed upon the flight conditions should be realized.

■ ■ ■ ■ ■

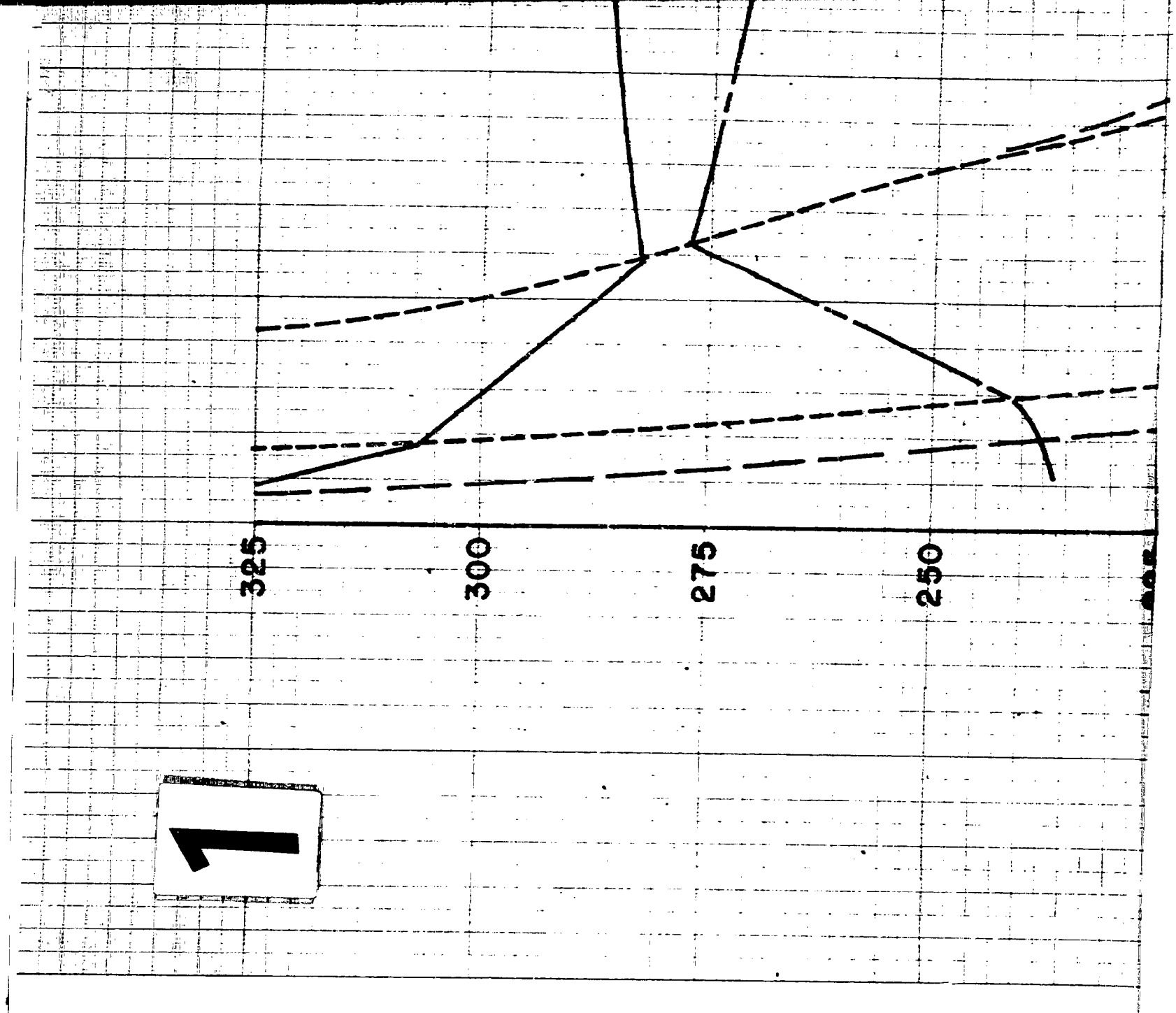

CROSS SECTION MILLIMETER

KEUFFEL
NEW

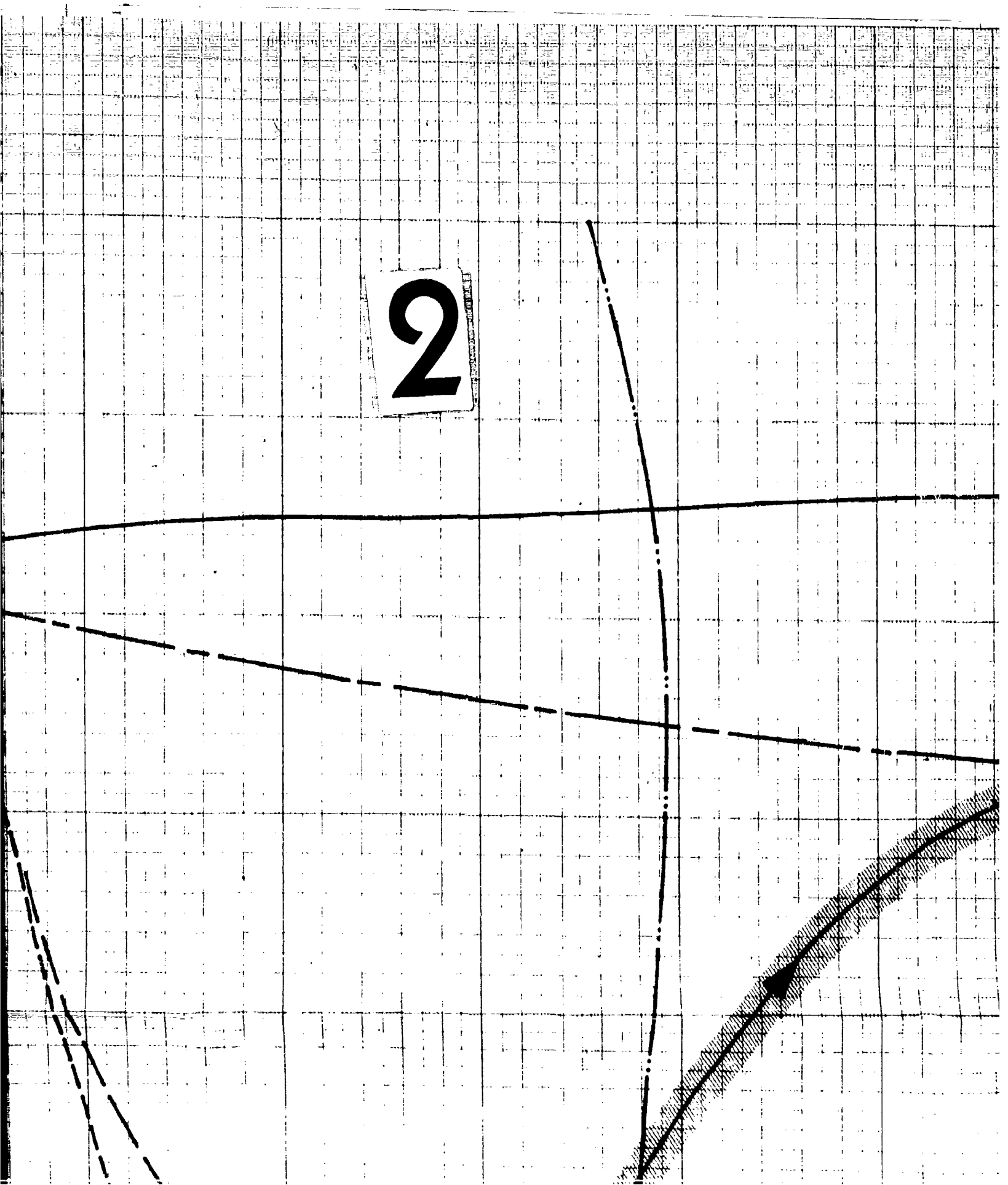
2

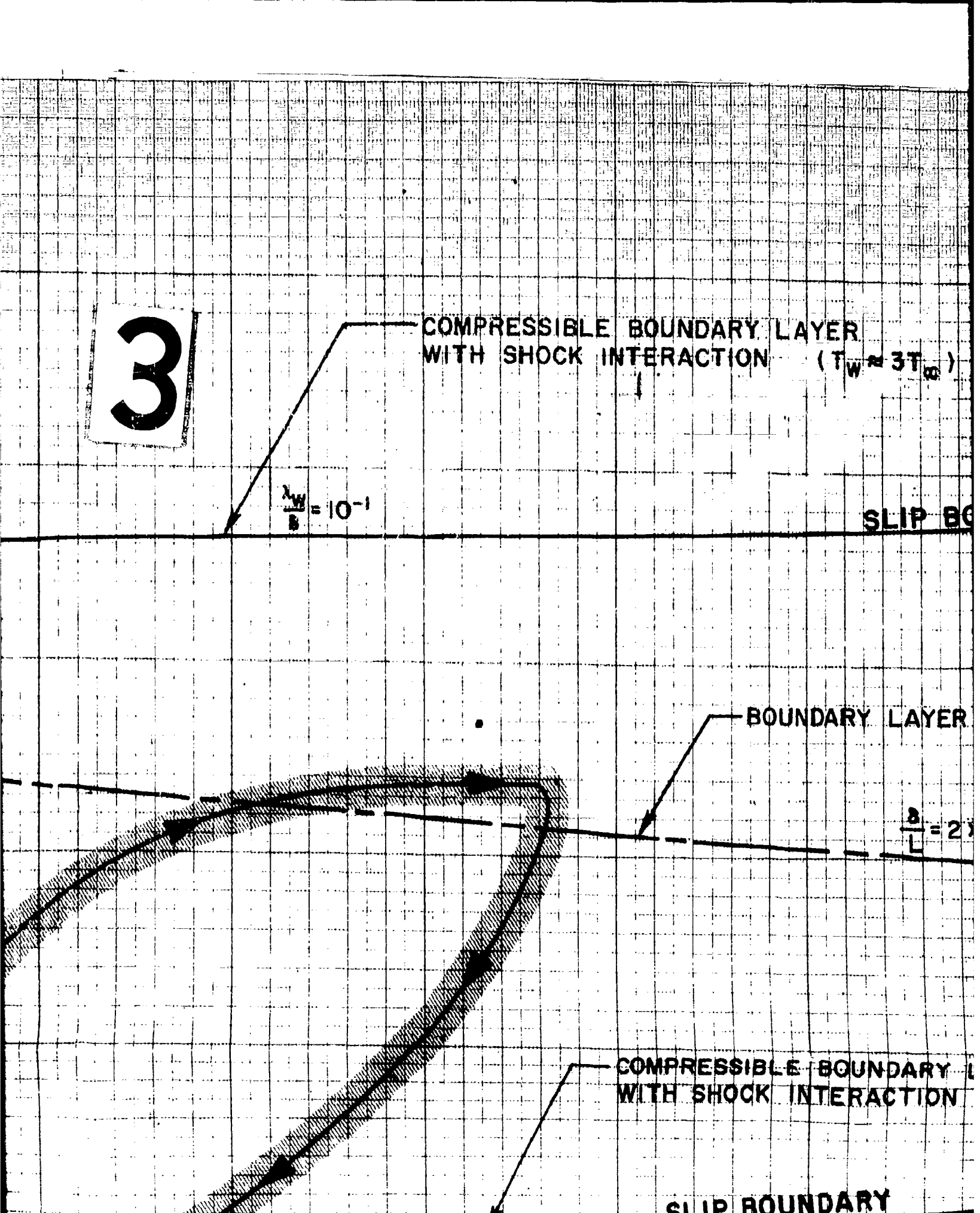
3
COMPRESSIBLE BOUNDARY LAYER
WITH SHOCK INTERACTION ($T_w \approx 3T_\infty$)
$\frac{\lambda_w}{\delta} = 10^{-1}$
SLIP BO
BOUNDARY LAYER
$\frac{\delta}{L} = 2$
COMPRESSIBLE BOUNDARY L
WITH SHOCK INTERACTION
SLIP BOUNDARY

SECRET

MPRESSIBLE BOUNDARY LAYER
TH SHOCK INTERACTION ($T_w \approx 3T_\infty$)

4

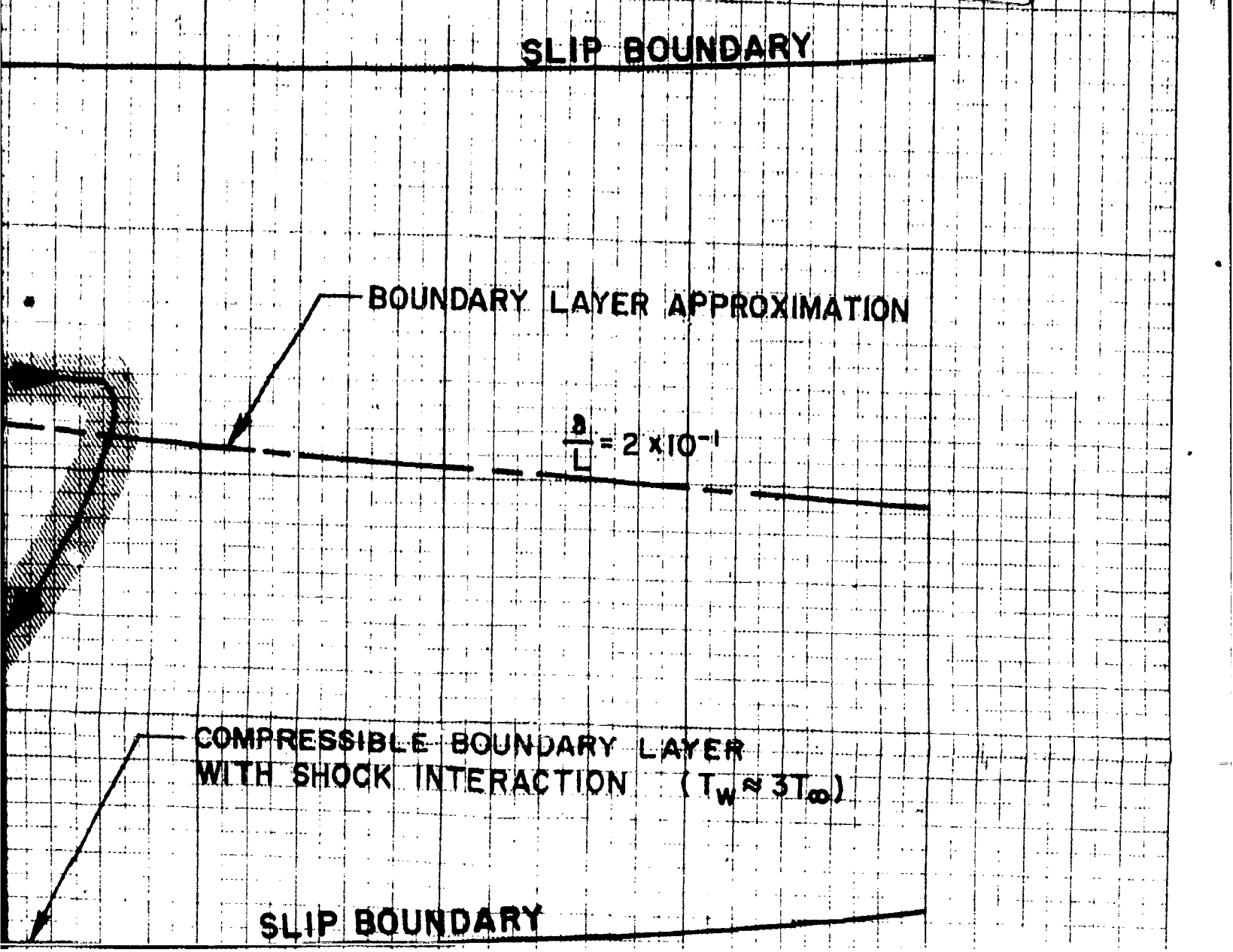

5

ALTITUDE ~ THOUSANDS OF FT

225
200
175
150
125
100
75

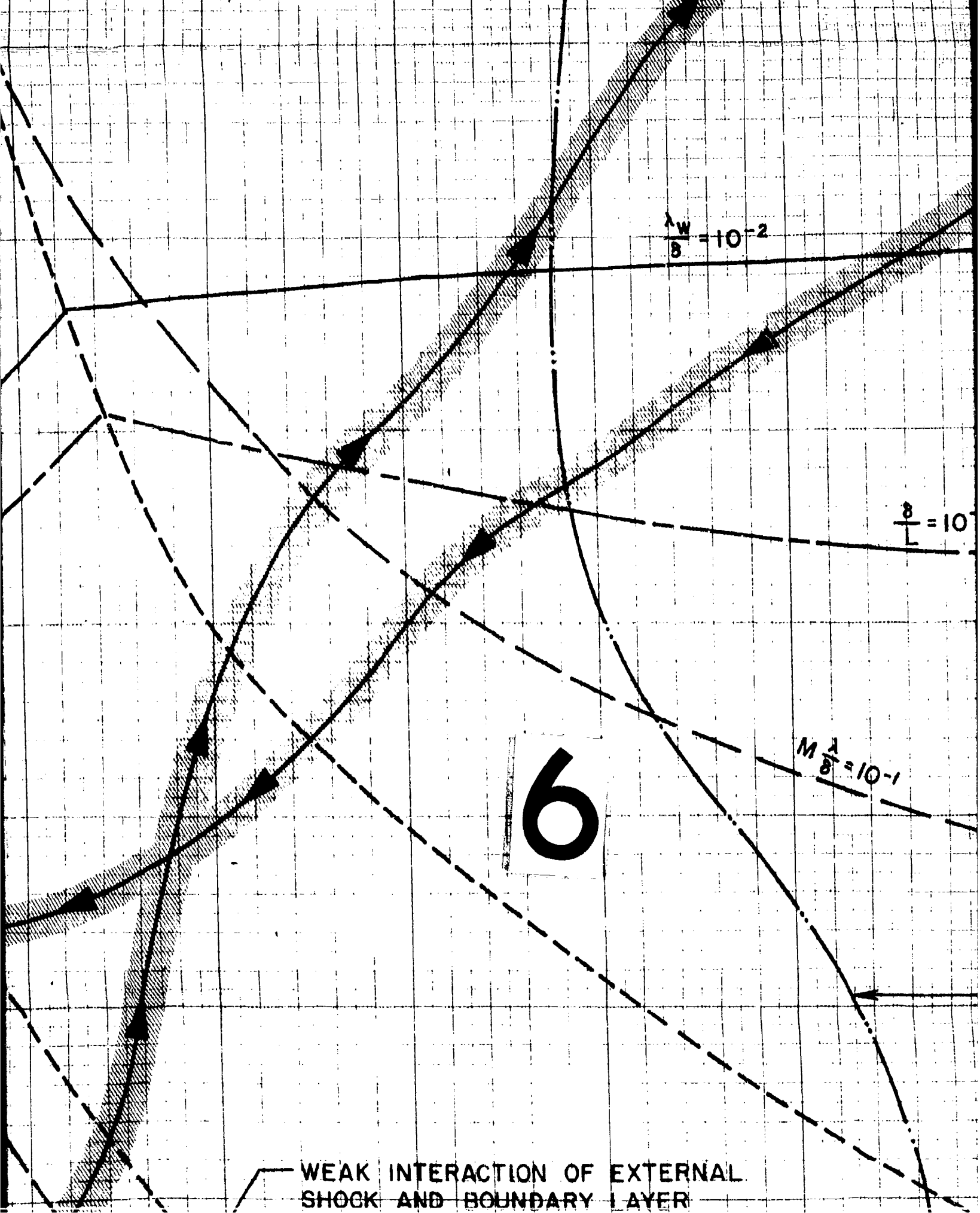
$\frac{\lambda_W}{\delta} = 10^{-2}$
$\frac{\delta}{L} = 10$
$M\frac{\lambda}{\delta} = 10^{-1}$
6
WEAK INTERACTION OF EXTERNAL SHOCK AND BOUNDARY LAYER

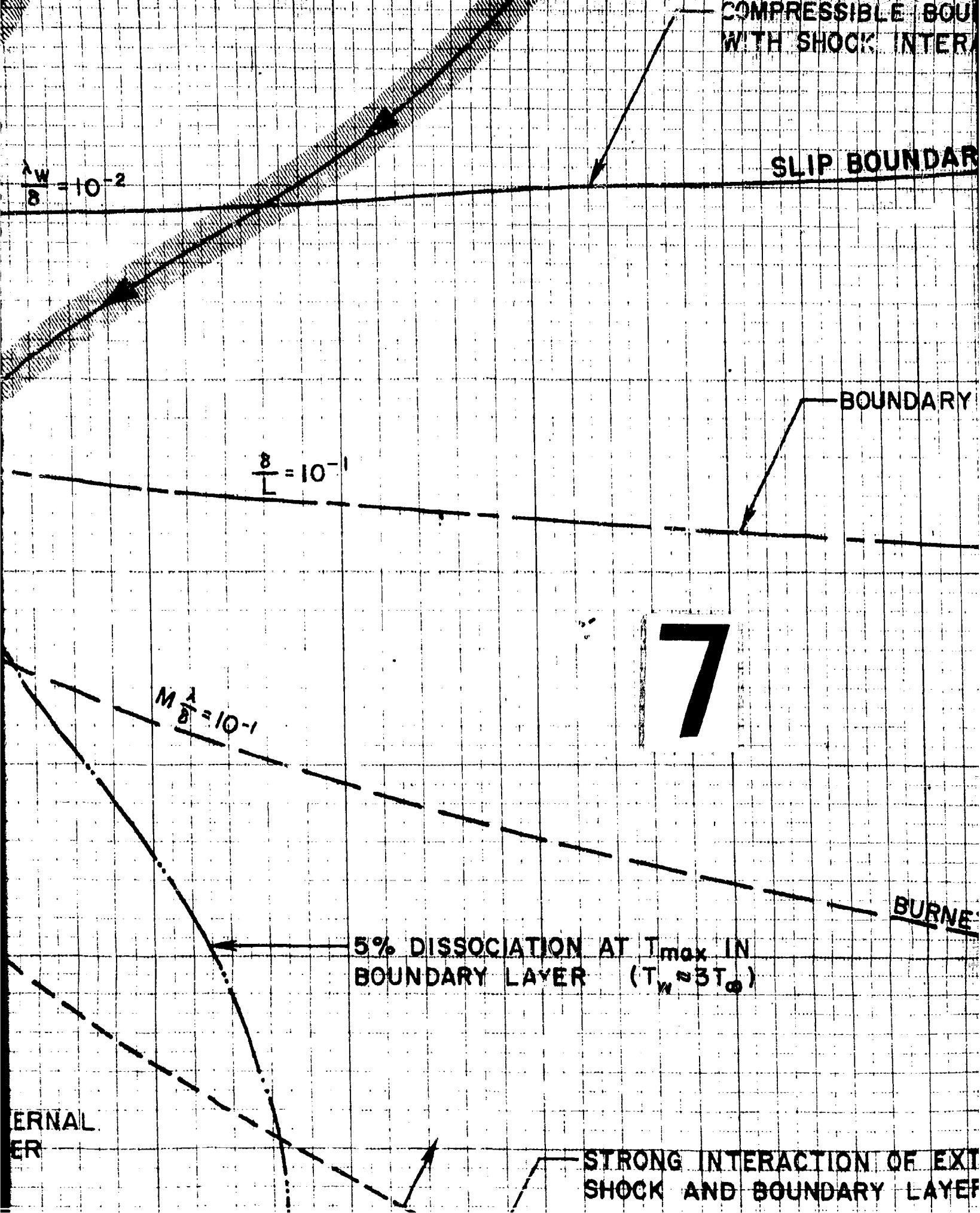
COMPRESSIBLE BOU
WITH SHOCK INTER
SLIP BOUNDAR
$\frac{\lambda_w}{\delta} = 10^{-2}$
BOUNDARY
$\frac{\delta}{L} = 10^{-1}$
7
$M\frac{\lambda}{\delta} = 10^{-1}$
BURNE
5% DISSOCIATION AT T_{max} IN
BOUNDARY LAYER ($T_w \approx 3T_\infty$)
ERNAL
ER
STRONG INTERACTION OF EXT
SHOCK AND BOUNDARY LAYE

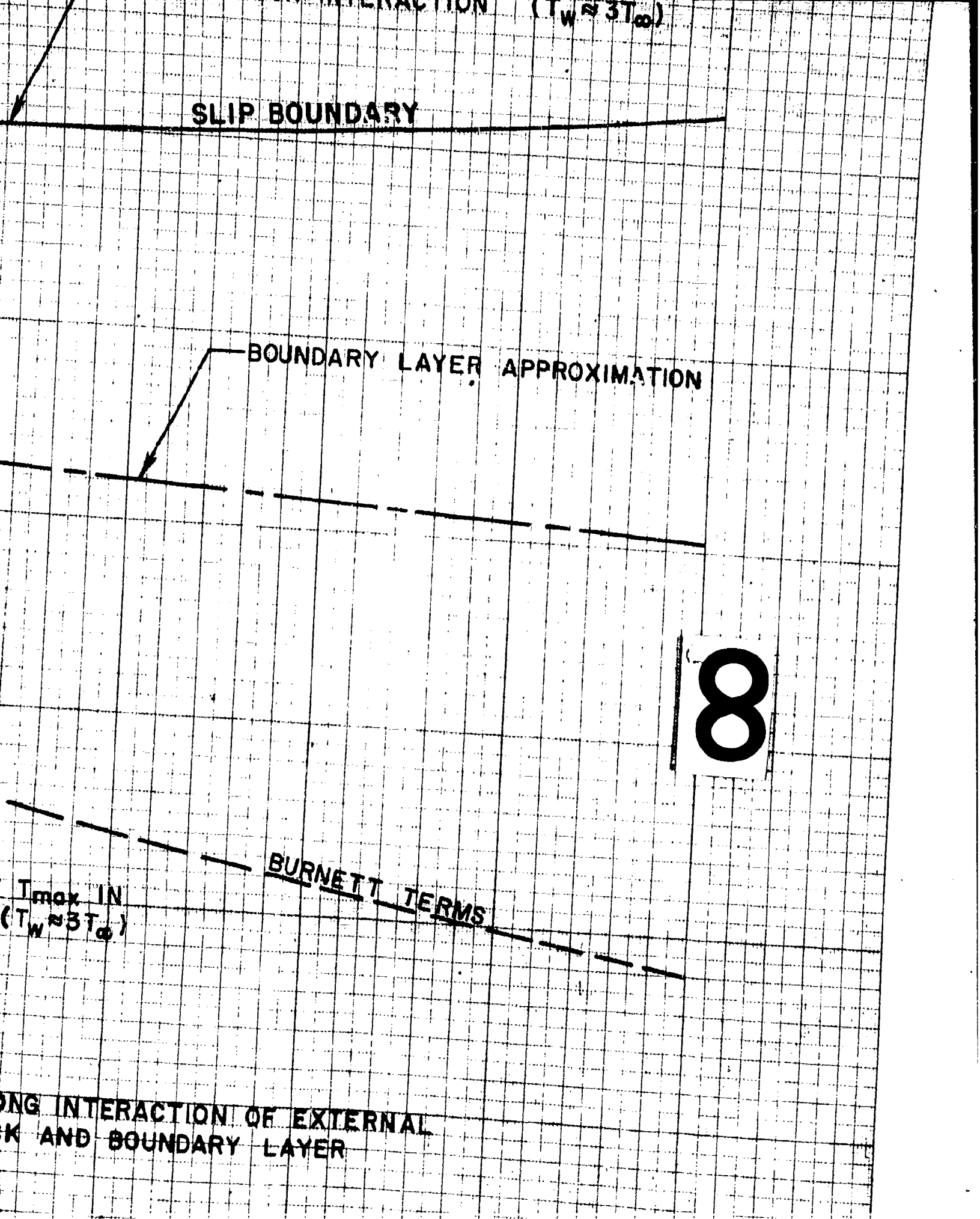
INTERACTION ($T_w \approx 3T_\infty$)
SLIP BOUNDARY
BOUNDARY LAYER APPROXIMATION
8
BURNETT TERMS
T_{max} IN
($T_w \approx 3T_\infty$)
ONG INTERACTION OF EXTERNAL
K AND BOUNDARY LAYER

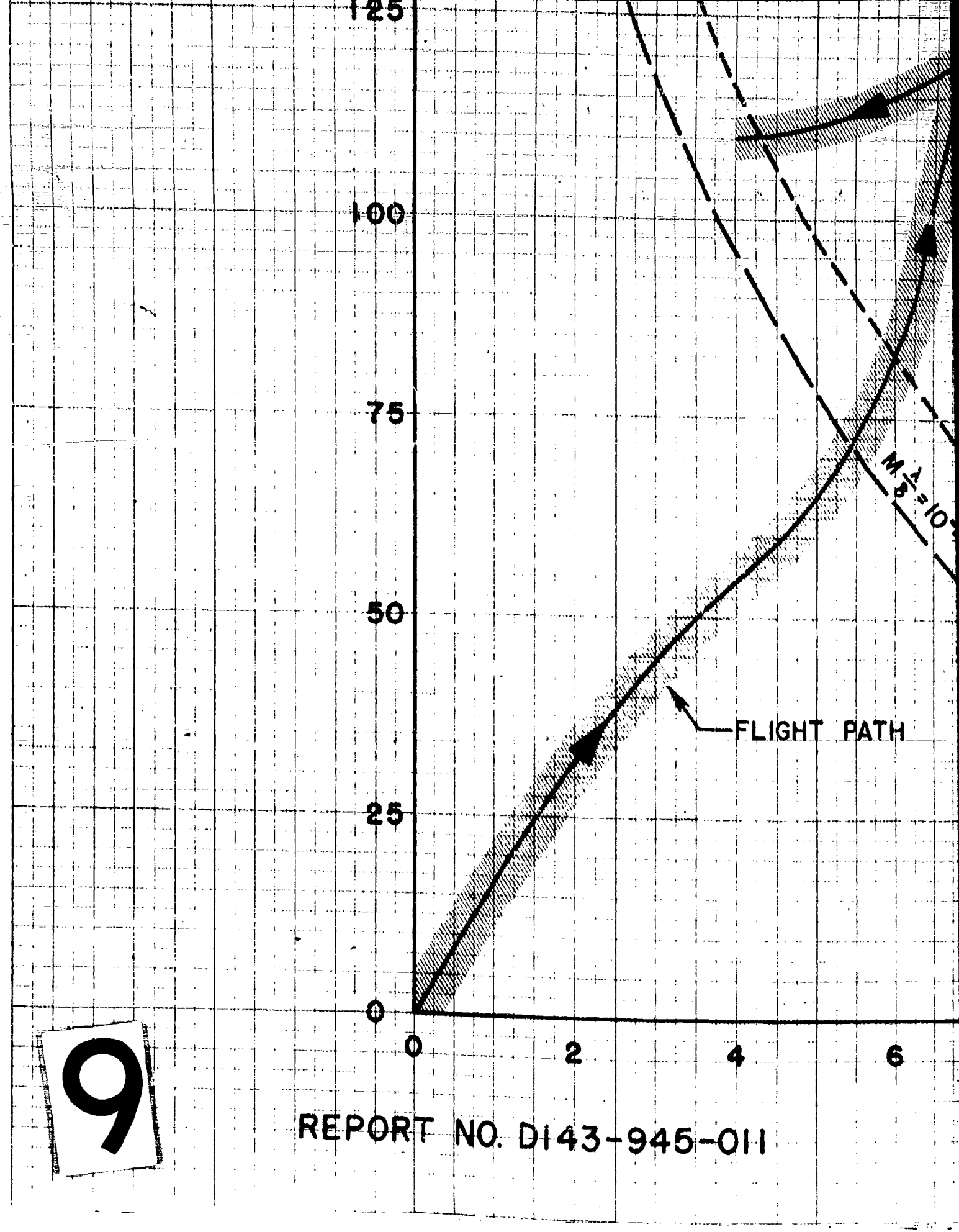
125
100
75
50
25
0
0
2
4
6
FLIGHT PATH

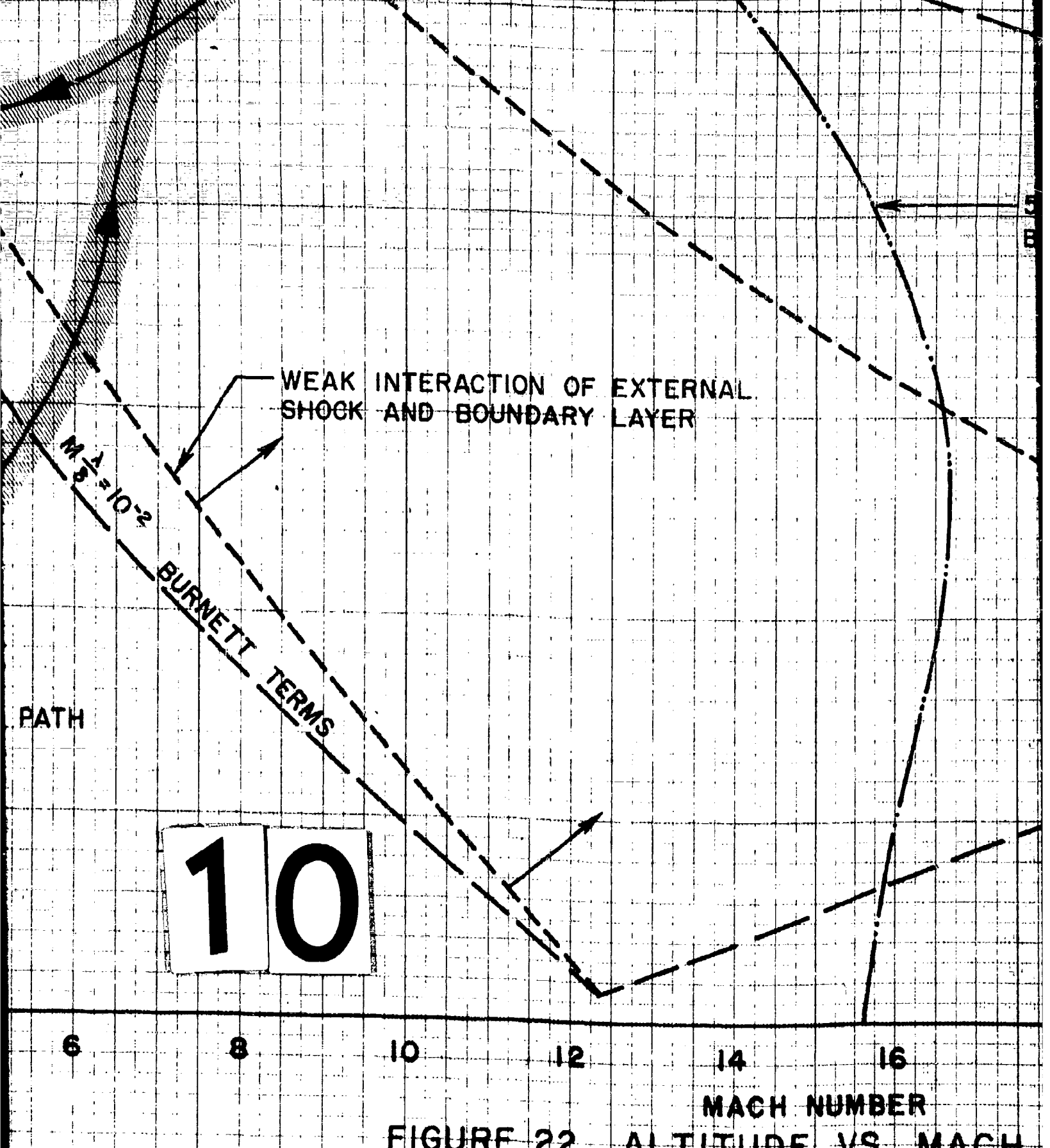

FIGURE 22. ALTITUDE VS MACH

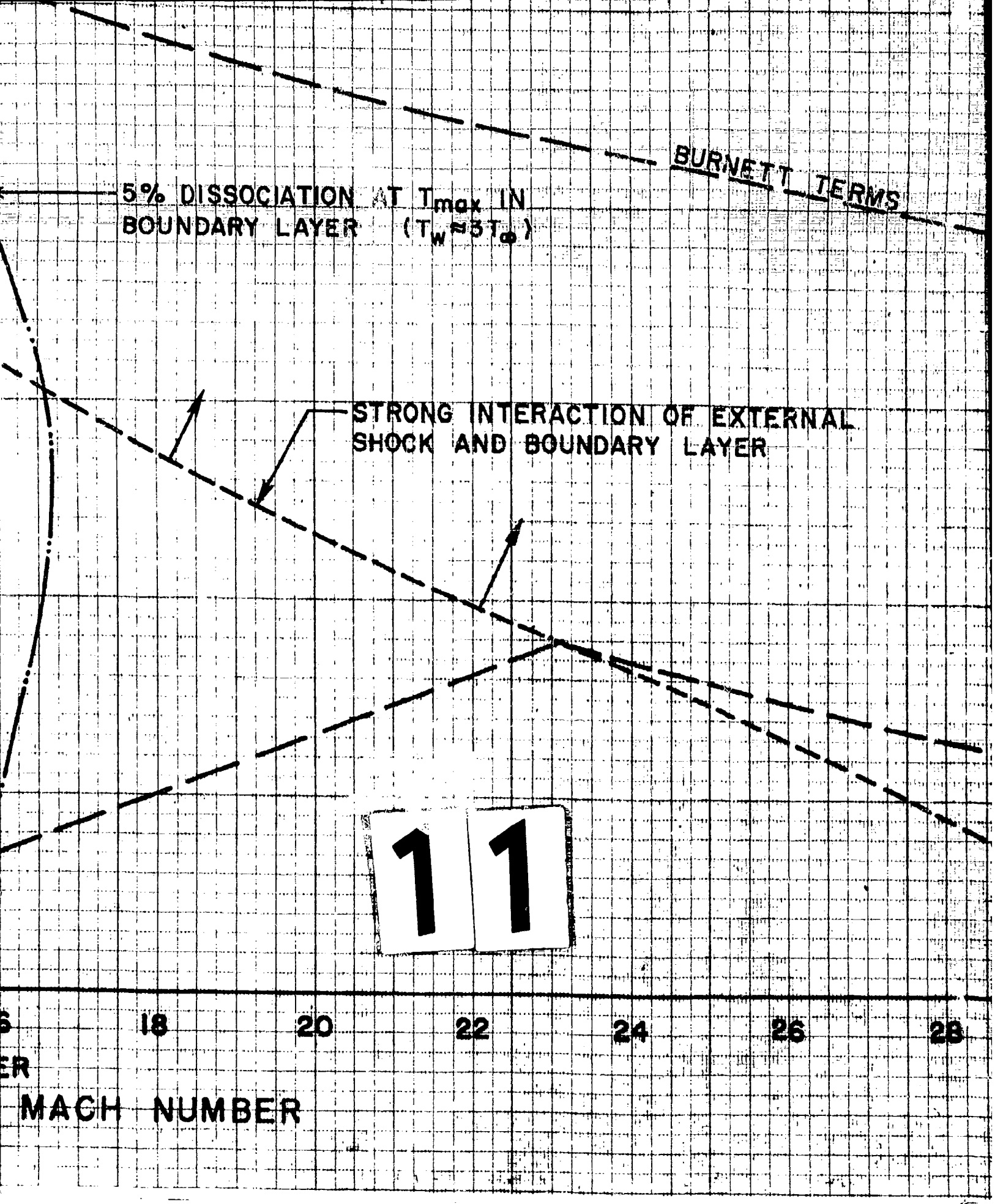
BURNETT TERMS
5% DISSOCIATION AT T_{max} IN BOUNDARY LAYER ($T_w \approx 5T_\infty$)
STRONG INTERACTION OF EXTERNAL SHOCK AND BOUNDARY LAYER
11
18
20
22
24
26
28
MACH NUMBER

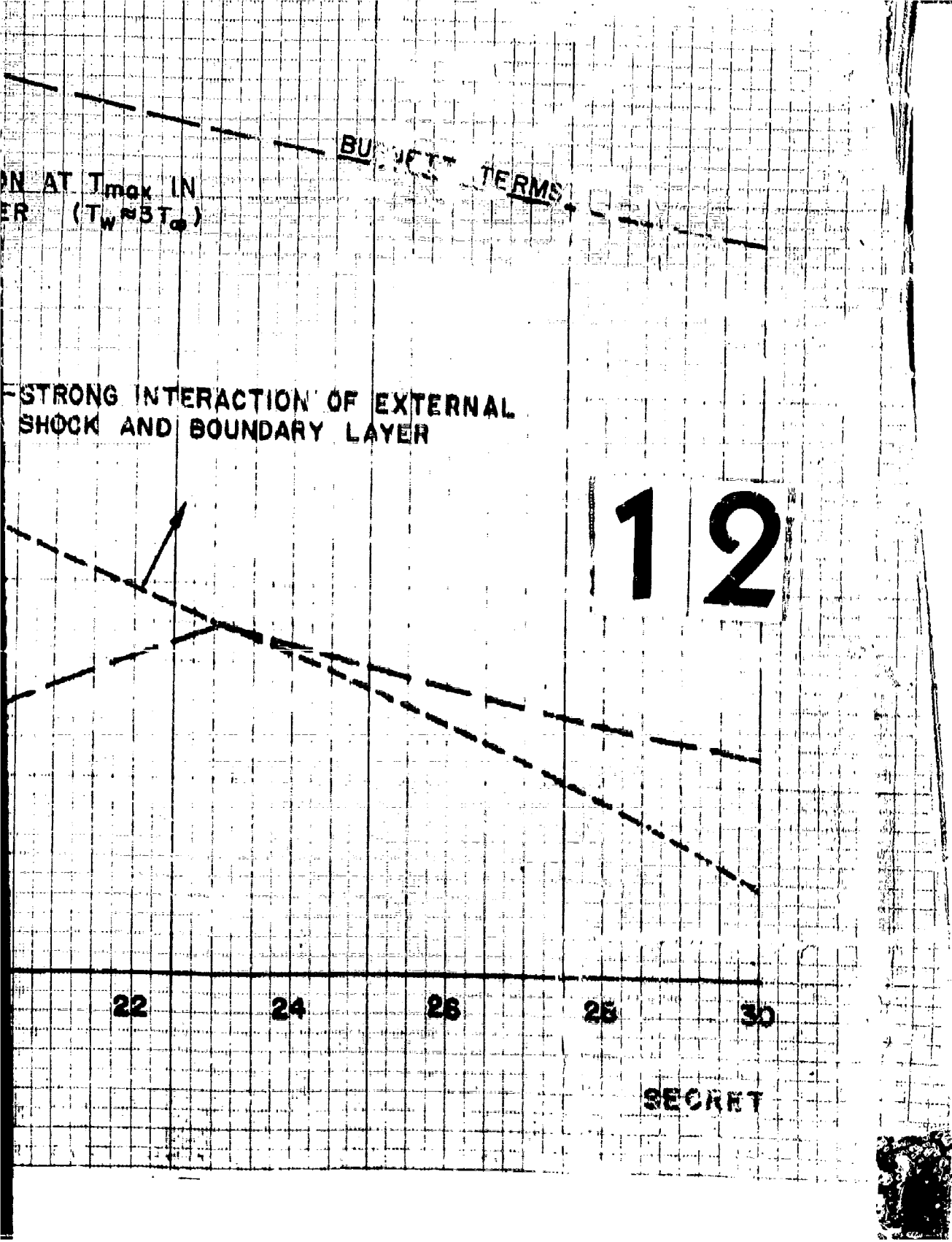
BU[illegible] TERMS
ON AT Tmax IN
ER (Tw≈3T∞)
-STRONG INTERACTION OF EXTERNAL
SHOCK AND BOUNDARY LAYER
12
22
24
26
28
30
SECRET

DEPARTMENT OF THE AIR FORCE
HEADQUARTERS 88TH AIR BASE WING (AFMC)
WRIGHT-PATTERSON AIR FORCE BASE OHIO

17 March 2006

88 CG/SCCMF
3810 Communications Blvd
Wright-Patterson AFB OH 45433-7802

Defense Technical Information Center
Attn: Ms. Kelly Akers (DTIC-R)
8725 John J. Kingman Rd, Suite 0944
Ft Belvoir VA 22060-6218

Dear Ms. Akers,

This concerns Technical Report AD161231, MX-2276 Advanced Strategic Weapon System, 25 Oct 1954. This technical report, previously Unclassified/Limited Distribution, is now releasable to the public. The attached AFMC Form 559 verifies that it was reviewed by release authorities at Air Force Research Lab Air Vehicles Directorate (AFRL/VA) and determined to be fully releasable to the public.

Please call me at (937) 522-3091 if you have any questions.

Sincerely

Lynn Kane

Lynn Kane
Freedom of Information Act Analyst
Management Services Branch
Base Information Management Division

Attachment
AFMC Form 559, RUSH – Freedom of Information Act